



Comportement hydromécanique d'un loess naturel

José Muñoz-Castelblanco

► To cite this version:

José Muñoz-Castelblanco. Comportement hydromécanique d'un loess naturel. Autre. Université Paris-Est, 2011. Français. NNT : 2011PEST1107 . pastel-00647891

HAL Id: pastel-00647891

<https://pastel.hal.science/pastel-00647891>

Submitted on 3 Dec 2011

HAL is a multi-disciplinary open access archive for the deposit and dissemination of scientific research documents, whether they are published or not. The documents may come from teaching and research institutions in France or abroad, or from public or private research centers.

L'archive ouverte pluridisciplinaire **HAL**, est destinée au dépôt et à la diffusion de documents scientifiques de niveau recherche, publiés ou non, émanant des établissements d'enseignement et de recherche français ou étrangers, des laboratoires publics ou privés.



UNIVERSITÉ —
— PARIS-EST

Laboratoire Navier-CERMES, Equipe Géotechnique

Comportement hydromécanique d'un lœss naturel non-saturé

Présentée par :

José Muñoz-Castelblanco

Supervisé par :

Pierre Delage

Directeur de thèse

Jean-Michel Pereira

Conseiller d'études

Yu-Jun Cui

Conseiller d'études

Février 2011

Résumé

Ce mémoire de thèse est consacré à l'étude expérimentale du comportement hydromécanique d'un lœss naturel non saturé effondrable provenant d'un site proche de la ville de Bapaume (nord de la France) dans une zone où des problèmes de tassement le long de la ligne nord du TGV ont été attribués à l'effondrement du lœss, du fait d'infiltrations d'eau. Un nouvel appareil triaxial permettant de mesurer localement l'ensemble des variables hydromécaniques du lœss non saturé (déformation, teneur en eau et succion) a été développé. La courbe de rétention d'eau, déterminée à l'aide d'un tensiomètre de haute capacité et de la méthode du papier filtre a fait l'objet d'une attention particulière : elle présente autour de la teneur en eau naturelle une zone sans hystérésis bordée par deux boucles d'hystérésis des côtés secs et humides. L'analyse de la courbe de rétention et du phénomène d'hystérésis a été approfondie grâce à une étude microstructurale réalisée à l'aide de la porosimétrie au mercure et de la microscopie électronique à balayage. Une structure assez complexe composée d'un arrangement métastable de grains de limon secs (probablement liés par la reprécipitation du calcaire) et d'une phase argileuse répartie de façon hétérogène a été mise en évidence. L'étude du comportement hydromécanique a compris une investigation de l'effondrement à partir de faibles valeurs de contraintes proches de la contrainte in-situ, à l'aide d'essais oedométriques à taux de déformation constant avec mesures de succion. Un maximum du potentiel d'effondrement et une dépendance du comportement mécanique vis-à-vis de la vitesse de chargement ont été identifiés. Une campagne d'essais triaxiaux à différentes teneurs en eau constantes avec mesure de succion a permis de déterminer l'allure de la surface de charge du limon naturel dans le plan (p,q), ainsi que ses variations avec la teneur en eau (ou la succion) et de confirmer l'écrouissage en succion. Les résultats expérimentaux montrent également que le potentiel plastique est distinct de la surface de charge.

Abstract

The hydromechanical behaviour of an unsaturated natural loess from Northern France is studied. Some stability problems detected on the loess foundations of the high speed train line that links Paris to Brussels have been detected. They have been attributed to collapse-upon-wetting phenomena under constant external load in the in-situ conditions. An experimental study is thus proposed in order to analyse the unsaturated behaviour of this loess, specially its collapse susceptibility and the couplings between its hydromechanical properties.

The studied loess is a natural deposit of aeolian origin, characterized by a complex structure that is mainly composed of an open and metastable silt grains arrangement. The inter-grains pores are filled of clay aggregates featured by an important volume change potential. Clay aggregates tend to swell or shrink into the inter-grains pores with negligible changes of the total volume of the loess specimens. These characteristics explain partly the particular hydromechanical behaviour of this loess.

The loess water retention properties were studied by using an in-house constructed high capacity tensiometer and the filter paper method. Further analysis of hysteresis phenomena and equilibration time of the Whatman No. 42 filter paper were conducted. A good agreement between suction measurements obtained by both techniques was observed. The evaluation of the loess water retention curve shows a hysteretic response, especially at low water contents. Changes on the water retention curve were observed after loading. Microstructure observations, performed by mercury intrusion porosimetry and scanning electron microscope, were used for the analysis of the water retention curve. This study lead to the proposal of a model for the hydraulic hysteresis phenomena. Furthermore, it has been observed that microstructure of loess varies with moisture changes due to the swelling-shrinking potential of the existing clay fraction.

A new triaxial apparatus for unsaturated soils with complete local monitoring was performed. The development of a new electrical resistivity probe to measure water content variations is highlighted. A series of triaxial tests at different hydric states was made in order to analyse the hydromechanical behaviour of loess. This study shows that compressibility, elastic stiffness and dilatancy increases with suction. A plastic potential distinct from the yield surface has been observed. The collapse-upon-wetting phenomena were studied by a series of suction-monitored oedometer tests. A maximum of collapse occurring at stress levels depending on the imposed stress conditions (oedometer, isotropic and K_0 triaxial tests) was observed.

Sommaire

Chapitre 1. Comportement des sols non saturés - Application aux lœss naturels	9
1.1 Introduction	9
1.2 Comportement des sols non saturés	11
1.2.1 Succion dans les sols	11
1.2.2 Courbe de rétention d'eau	15
1.2.3 Contraintes dans les sols non saturés	16
1.2.4 Points faibles du concept de contrainte effective	18
1.2.5 Variables d'état dans les sols partiellement saturés	23
1.2.6 Structure des sols partiellement saturés	26
1.2.7 Aspects du comportement mécanique des sols non saturés	29
1.2.8 Couplage hydromécanique	37
1.3 Le Lœss	40
1.3.1 Le lœss de Bapaume.....	42
1.4 Le phénomène d'effondrement	45
1.4.1 L'effondrement lié aux caractéristiques spéciales des dépôts lœssiques naturels	46
1.4.2 Caractéristiques de la structure	50
Chapitre 2. Propriétés de rétention d'eau.....	51
2.1 Introduction	51
2.2 La courbe de rétention d'eau	52
The water retention properties of a natural unsaturated loess from Northern France ..	54
Introduction	54
Results and discussions	62
Conclusions	76
2.3 Effet des cycles d'humidification et de séchage sur la microstructure	82
A microstructure analysis of the hysteresis of the water retention curve of a natural loess	84
Introduction	84
Tested material, equipment and procedures	85
Tests results	88
Discussion	96
Multiscale modelling of the water retention curve.....	98
Conclusions	106
Chapitre 3. Dispositifs expérimentaux	111
3.1 Introduction	111
3.2 Mesure de la teneur en eau: Nouvelle sonde de résistivité électrique.....	113

Measurement of the water content of a natural unsaturated loess by a new resistivity probe	115
Introduction	115
Elements of electrical resistivity in soils.....	116
Material and experimental setup	118
Experimental investigation on natural unsaturated loess	121
Analysis and discussion of the resistivity data.....	123
Conclusions	127
3.3 Dispositif triaxial pour les sols non saturés : mesure locale de la déformation, la succion et la teneur en eau.....	131
Triaxial testing of a natural unsaturated loess with complete local monitoring.....	133
Introduction	133
Tested loess	134
Triaxial apparatus	136
Testing procedures and results	146
Discussion	153
Conclusions	154
Chapitre 4. Comportement hydromécanique.....	158
4.1 Introduction	158
4.2 Caractérisation de la compressibilité et du phénomène d'effondrement	159
Some aspects of the compression and collapse behaviour of an unsaturated natural loess	161
Abstract	161
Introduction	161
Experimental programme	162
Time dependent behaviour	164
Collapse behaviour	166
Discussion	168
Conclusions	169
4.3 Caractérisation du comportement hydromécanique du Loess de Bapaume.....	172
Hydromechanical behaviour of a natural unsaturated loess	174
Introduction	174
Material and experimental setup	176
Experimental results	180
Effects of moisture changes on the mechanical behaviour	190
Impact of loading on microstructure and on water retention properties	197
Conclusions	201
Conclusion Générale	206
Références	210

Introduction

Les sols effondrables, comme les sols gonflants, attirent depuis longtemps l'attention des chercheurs de par les problèmes de stabilité qu'ils posent aux bâtiments, aux ouvrages géotechniques et aux infrastructures linéaires. D'après Dudley (1970), Terzaghi et Fröhlich (1936) avaient déjà observé la tendance que peuvent avoir certains sols non saturés à s'effondrer lorsqu'ils sont inondés. Les recherches menées jusqu'à présent sur ce thème et sur le thème plus général de la mécanique des sols non saturés ont permis l'élaboration de lois de comportement couplées hydromécaniques. Mais le développement de ces lois est dans la plupart des cas basé sur des résultats expérimentaux obtenus sur des échantillons reconstitués ou compactés et très peu de données concernent les sols naturels intacts.

La susceptibilité à l'effondrement peut concerter les dépôts alluviaux, colluviaux et les sols éoliens. Le lœss est un dépôt limoneux éolien, transporté dans des conditions périglaciaires et déposé dans des environnements froids de steppe, près des principales nappes glaciaires du Quaternaire, principalement autour du parallèle 50°N dans l'hémisphère Nord, mais aussi en Amérique du Sud. On les rencontre sur des plateaux, des pentes et des grands bassins alluviaux. En Chine, les épaisseurs de "lœss du Plateau" peuvent atteindre 300 m. Des dépôts existent aussi dans le plateau de la Sibérie en Russie, dans les bassins des rivières du Danube, du Rhin et du Mississippi (Amérique du Nord) ainsi que dans la Pampa (Argentine) (Pecsi 1990).

Des dépôts lœssiques ont été détectés en France suite à des problèmes d'effondrement sous les fondations de la ligne à grande vitesse (LGV Nord). Ces problèmes sont apparus lors de périodes de pluies intenses en hiver 2001 et au printemps 2002 en relation également avec des fuites d'un système d'écoulement d'eau. Au-delà des travaux de renforcement de sols, la Société Nationale des Chemins de Fer (SNCF) et l'équipe géotechnique (CERMES) du laboratoire Navier (Ecole des Ponts ParisTech) ont entamé une étude approfondie sur la problématique d'effondrement de ce lœss pour le compte du Réseau Ferré de France (RFF).

C'est dans ce contexte qu'il a été décidé de mener une étude du comportement hydromécanique du lœss naturel, non saturé. Pour ce faire, les blocs de lœss ont été extraits à

proximité du remblai de la ligne LGV nord sur un site proche de la ville de Bapaume. Un programme d'essais sur ces échantillons a été effectué à l'aide d'un nouvel appareil triaxial pour les sols non saturés, spécifiquement développé, et permettant le suivi local à mi-hauteur, pendant le chargement, de l'ensemble des variables caractéristiques de l'éprouvette non saturée : déformations axiales et radiales, teneur en eau et succion. Des observations complémentaires sur les propriétés de rétention d'eau et sur la microstructure ont été également réalisées ; elles ont permis la mise en évidence de certains couplages entre les propriétés hydrauliques et mécaniques.

Les résultats des travaux réalisés ont fait l'objet de plusieurs articles dans des revues de renom international. Un premier article sur les propriétés de rétention d'eau du loess a été accepté dans le journal *Géotechnique* et trois autres ont été soumis respectivement au *Geotechnical Testing Journal*, *Géotechnique Letters* et *Géotechnique*. Deux articles supplémentaires ont été finalisés et seront également soumis prochainement. Ainsi, dans l'organisation du mémoire de la thèse, les deuxième, troisième et quatrième chapitres sont composés d'un résumé en français et des manuscrits correspondants.

Dans le premier chapitre, on présente une étude bibliographique sur le comportement des sols non saturés et le phénomène d'effondrement. Les connaissances acquises à cette occasion ont été ensuite utilisées dans l'analyse des données expérimentales obtenues sur le comportement du loess.

Le deuxième chapitre, dédié à l'analyse des propriétés de rétention d'eau du loess, a fait l'objet de deux articles : le premier, accepté par *Géotechnique*, présente la courbe de rétention d'eau, quelques particularités de la méthode du papier filtre (dont une approche alternative avec un papier initialement humide, l'hystérésis du papier filtre et l'étude des temps d'équilibre), une description de la technique de mesure de succion par le tensiomètre de haute capacité (modèle développé au CERMES) et surtout une analyse de la courbe de rétention à partir de la microstructure du loess ; le deuxième article présente une étude plus approfondie des effets de la microstructure sur les propriétés de rétention d'eau, qui a débouché sur la modélisation de la courbe de rétention d'eau à partir du modèle d'hystérésis proposé par Rojas et Rojas (2005) et prenant en compte les différents éléments de la structure du loess.

Le troisième chapitre correspond aux résultats présentés dans deux articles : le premier présente le développement de la mesure de la teneur en eau à l'aide d'une nouvelle sonde de

résistivité électrique ; le deuxième décrit un nouvel appareil triaxial pour les sols non saturés avec suivi local, pendant le chargement, des déformations, de la teneur en eau et de la succion. Les courbes d'étalonnage de la résistivité électrique en fonction de la teneur en eau volumique ont été analysées à partir de la loi d'Archie et d'un modèle théorique proposé par Fukue *et al.* (1999). Trois essais triaxiaux d'étalonnage ont été effectués avec le nouveau dispositif afin de tester la précision et la fiabilité des tests. Grâce à ce nouvel appareillage, on a pu obtenir pour la première fois la détermination locale complète de l'état du sol non saturé (déformation, teneur en eau et succion) pendant un chargement triaxial.

Le quatrième et dernier chapitre, qui concerne le comportement couplé hydromécanique, a fait l'objet de deux articles : le premier présente une étude à l'oedomètre de l'effondrement au remouillage conduite à taux de déformation constant (CRS tests) à deux valeurs de contrainte nette verticale ; le second présente les résultats d'une campagne d'essais triaxiaux à différentes teneurs en eau selon plusieurs chemins de contraintes : compression isotrope, compression K_0 anisotrope et cisaillement triaxial à confinement constant. Les résultats obtenus mettent clairement en évidence les couplages des propriétés mécaniques (compressibilité, elasticité, comportement à la rupture, surface de charge) avec les caractéristiques hydrauliques (courbe de rétention d'eau). L'effet de la microstructure sur ces couplages est également analysé.

Chapitre 1. Comportement des sols non saturés - Application aux lœss naturels

Table de matière

1.1	Introduction	9
1.2	Comportement des sols non saturés	11
1.2.1	Succion dans les sols	11
1.2.2	Courbe de rétention d'eau	15
1.2.3	Contraintes dans les sols non saturés	16
1.2.4	Points faibles du concept de contrainte effective	18
1.2.5	Variables d'état dans les sols partiellement saturés	23
1.2.6	Structure des sols partiellement saturés	26
1.2.7	Aspects du comportement mécanique des sols non saturés	29
1.2.8	Couplage hydromécanique	37
1.3	Le Lœss	40
1.3.1	Le lœss de Bapaume	42
1.4	Le phénomène d'effondrement	45
1.4.1	L'effondrement lié aux caractéristiques spéciales des dépôts lœssiques naturels	46
1.4.2	Caractéristiques de la structure	50

1.1 Introduction

Pendant une longue période, l'étude du comportement des sols non saturés avait été mise à l'écart, au profit des études sur les sols saturés, alors même qu'il existe de grandes étendues de sols partiellement saturés dans le monde. D'après Dudley (1970), Terzaghi et Fröhlich (1936) avaient déjà remarqué la tendance qu'ont les sols partiellement saturés à s'effondrer lorsqu'ils sont inondés. Récemment, l'étude des conditions de non saturation en mécanique des sols a fait l'objet de nombreuses recherches, tant du point de vue expérimental que théorique. En particulier, de nombreux modèles constitutifs tenant compte des phénomènes de couplages entre les composantes mécaniques et hydrauliques du comportement de ces sols ont été développés. Du point de vue expérimental, bien qu'il existe un nombre important d'essais

réalisés sur divers types de sols (Maatouk *et al.* 1995 sur un limon compacté du Québec, Cui et Delage 1996 sur un limon compacté de Jossigny, France, Romero et Vaunat 2000 sur une argile compactée, Cunningham *et al.* 2003 sur une argile limoneuse reconstituée, Tarantino et De Col 2008 sur une argile compactée, Jotisankasa *et al.* 2009 sur un limon argileux compacté, entre autres) et faisant appel à des techniques de plus en plus avancées, les échantillons testés sont souvent préparés à partir de matériau reconstitué ou remanié. Ainsi, les données expérimentales sur des échantillons de sol naturels ou intacts sont relativement peu courantes. Les sols naturels non saturés sont pourtant très fréquents dans des régions arides ou semi-arides (Dudley 1970). Dans ces régions, il existe une grande variété de sols non saturés tels que les argiles gonflantes très plastiques (gonflement et retrait suite à des cycles d'humidification et séchage, respectivement), les dépôts alluviaux (risque d'effondrement s'ils présentent une structure très ouverte), les sols colluviaux ou encore les sols éoliens (dont le loess) entre autres.

Suite aux problèmes de tassement du terrain de fondation des voies ferrées du TGV Nord en France, certains phénomènes d'effondrement ont été détectés au niveau des dépôts loessiques traversés par cette ligne à grande vitesse. Ces phénomènes peuvent avoir pour origine des périodes de pluies intenses au cours de l'hiver 2001 et du printemps 2002 ainsi que des fuites accidentelles d'un canal de conduction d'eau. Faisant suite aux travaux précédents (Cui *et al.* 1995, 2004, Delage *et al.* 2005, Karam 2006, Yang *et al.* 2008, Karam *et al.* 2009) qui se sont attachés à l'étude de l'effondrement du loess sous sollicitations cycliques (simulant le passage des trains), ce travail concerne la caractérisation expérimentale du comportement hydromécanique du loess en conditions non saturées.

Ce chapitre présente une synthèse bibliographique du comportement hydromécanique des sols non saturés. Une fois le contexte général de cette étude établit, on poursuit avec le cas particulier des loess, en précisant les contextes géographique et géologique de ces sols, ainsi que la description des propriétés géotechniques de base du loess étudié. Finalement, on termine avec une description du phénomène d'effondrement caractéristique à ce matériau.

1.2 Comportement des sols non saturés

Les sols sont formés de particules de sable, de limon, d'argile, d'oxydes colloïdaux et, si le sol se situe à une profondeur faible, de matière organique (Pedro 1976). L'assemblage de ces particules comporte nécessairement des vides (pores). L'existence de cette porosité, qui peut être remplie par un ou plusieurs fluides, confère aux sols un comportement géomécanique particulier. L'eau coexiste avec l'air dans le cas des sols non saturés et l'interface entre l'air et l'eau est constituée de ménisques eau-air qui engendrent un état de succion (ou pression négative) de l'eau dans le sol. La distribution des ménisques dans l'ensemble des contacts n'est pas uniforme et la succion est une contrainte locale. Ainsi, lorsqu'on applique un chargement mécanique sur un échantillon de sol non saturé, il n'existe pas de relation directe entre la contrainte externe appliquée et celle qui se produit entre les particules. La succion matricielle correspond localement à une contrainte agissant sur la surface du ménisque, normale au contact entre les grains. L'action de "collage" de la succion matricielle sur les contacts provoque l'augmentation de la résistance du sol (Jennings et Burland 1962). Si le sol est alors saturé, il perd cette résistance additionnelle due à la succion et l'on observe, pour certains types de sols suffisamment lâches, le phénomène dit d'effondrement (Jennings et Burland 1962) et qui correspond à des déformations volumiques contractantes et irréversibles.

1.2.1 Suction dans les sols

Buckingham (1907) fut le premier à étudier la capillarité dans les sols partiellement saturés. Richards (1928) a défini le potentiel total de l'eau dans les pores du sol comme la somme des potentiels capillaire et gravitationnel. Dans un profil de sol non saturé au-dessus de la nappe phréatique, le potentiel capillaire augmente linéairement à partir de zéro au niveau de la nappe. Le terme *potentiel de l'eau*, ou *suction*, concerne toutes les forces capables de retenir l'eau dans la structure du sol. Le potentiel d'eau dans le sol joue un rôle important dans la compréhension du comportement mécanique des sols partiellement saturés et des sols saturés (Alonso *et al.* 1987).

Le potentiel total de l'eau Ψ_t est défini comme la somme de quatre éléments: le potentiel de pression externe Ψ_p , le potentiel gravitationnel Ψ_g , **les potentiels capillaire et d'adsorption dont la somme forme le potentiel matriciel Ψ_m** et, le potentiel osmotique Ψ_o (Aitchison 1965a, Alonso *et al.* 1987, Delage et Cui 2000a). Ce concept peut être représenté comme suit:

$$\psi_t = \psi_p + \psi_g + \psi_m + \psi_o \quad (1-1)$$

Le terme *potentiel* est plutôt associé au bilan d'énergie de l'eau dans le sol, tandis que le terme *suction* est lié à la pression de l'eau (pression négative). La *suction matricielle* est représentée par la différence ($u_a - u_w$) entre la pression de l'air et la pression de l'eau dans les pores du sol.

Les phénomènes de capillarité se produisent à l'interface entre deux fluides, car les molécules y sont soumises à un ensemble de forces d'interactions non-équilibrées, à la différence d'une molécule située au sein du fluide. Une molécule d'eau au sein d'une masse d'eau est soumise à des actions de même nature, alors que celle à l'interface entre deux fluides, eau-air par exemple, est soumise à des actions différentes : actions dues à l'eau et actions dues à l'air. Les molécules d'eau à l'interface eau-air sont ainsi attirées vers la masse d'eau et la surface de l'eau est soumise à une force perpendiculaire à la surface libre. Il est cette attraction qui engendre une tension de surface T à l'interface eau-air (Delage et Cui 2000a).

La capillarité est souvent illustrée par le schéma de la Figure 1-1, décrivant la remontée capillaire de l'eau dans un tube de rayon r petit plongé dans un récipient contenant de l'eau. La relation entre le rayon de courbure du ménisque sphérique eau-air dans le tube et la différence de pression entre l'air et l'eau est donnée par la loi de Laplace, qui se simplifie dans l'hypothèse de pores cylindriques et prend l'expression de la loi de Jurin :

$$(u_a - u_w) = \frac{4T \cos \theta}{D} \quad (1-2)$$

où $(u_a - u_w) = s$ est la *suction matricielle* due à la capillarité et θ est l'angle de mouillage de l'eau sur le solide (la paroi du tube dans la Figure 1-1). En supposant que l'eau est un fluide parfaitement mouillant, cet angle est alors nul.

La *suction osmotique* est due aux effets des sels dissous dans l'eau du sol. D'après Alonso *et al.* (1987), il est important de déterminer les composantes du potentiel hydraulique qui influencent le comportement mécanique des sols partiellement saturés. Généralement, la *suction matricielle* est l'élément principal mais la *suction osmotique* reste une composante à considérer.

La succion est mesurable à travers plusieurs méthodes expérimentales. Chacune couvre une gamme différente de succions. Une description des principales méthodes de mesure est présentée dans le Tableau 1-1.

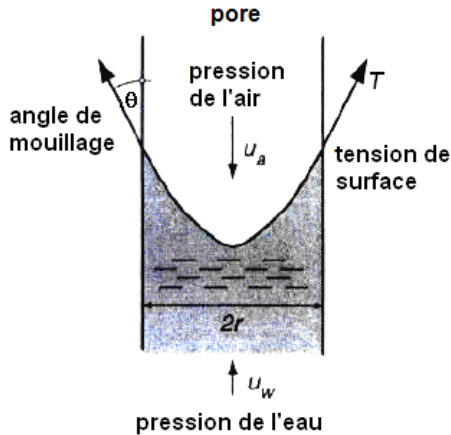


Figure 1-1. Représentation du phénomène de capillarité. Modifiée d'après Engel et al. (2004)

De nombreuses techniques de mesure reposent sur l'utilisation de pierres poreuses céramiques de haute valeur d'entrée d'air. Elles ne peuvent être désaturées que sous des succions beaucoup plus fortes que celles présentes dans le sol. Ces pierres doivent en effet rester saturées, même si elles sont soumises à des pressions négatives. Cela permet d'assurer le passage de l'eau entre la pierre et le sol (Fredlund and Rahardjo 1993, Delage et Cui 2000a). Ridley et Wray (1996) donnent une description complète de ces méthodes de mesure de succions. Le développement du tensiomètre de haute capacité par Ridley et Burland (1993) a représenté un avancement significatif dans la mesure des succions matricielles jusqu'à 1500 kPa. De nombreux capteurs similaires ont été développés à partir de ce premier concept avec quelques améliorations techniques (Tarantino 2004, Mahler et Diene 2007, Marinho *et al.* 2008). Ce dispositif est intermédiaire entre le tensiomètre classique (jusqu'à 80 kPa) et les psychromètres à miroir (1 - 60 MPa) ou du type SMI (1 - 70 MPa).

Technique	Principe	Ordre de grandeur de succions
Tensiomètre	Mesure de la pression engendrée dans un réservoir d'eau placé derrière une pierre poreuse céramique qui est en contact direct avec le sol	0 – 80 kPa: tensiomètres classiques (limite classique de 80 kPa, due à l'apparition de la cavitation) 0 – 1500 kPa: tensiomètres de haute capacité, composés d'une pierre poreuse de haute valeur d'entrée d'air et d'un réservoir d'eau de très petite taille

Technique	Principe	Ordre de grandeur de suctions
Méthode du papier filtre	Transfert d'eau entre le sol et une pièce de papier filtre standardisé. La succion est déduite de la teneur en eau du papier filtre à l'équilibre (7 jours) par rapport à une courbe d'étalonnage	0 – 30 MPa
Psychromètre à thermocouple	Mesure de l'humidité relative à proximité de l'eau interstitielle du sol à l'aide d'une thermocouple. On en déduit la succion par la loi de Kelvin	0,3 - 8 MPa
Hygromètre à point de rosée – psychromètre à miroir	Mesure de la température au point de rosée associé au début de la condensation. Ceci est réalisé par un miroir à température contrôlée, sur lequel est projeté un rayon optique dont on analyse la réflexion. L'humidité relative est déterminée par la mesure de la température du point de rosée de l'atmosphère considérée, qui est d'autant plus faible que l'air est sec	1 - 60 MPa
Psychromètre SMI	Mesure indirecte de l'humidité relative à partir de la différence des températures mesurées par un thermomètre "sec" et un autre "humide", lesquels sont en équilibre avec l'échantillon. L'évaporation du thermomètre "humide" fait descendre sa température	1 - 70 MPa
Sonde de conductivité thermique	La mesure de succion est réalisée de façon indirecte par une pierre poreuse céramique et un capteur de conductivité thermique inséré dans la pierre. La conductivité thermique est associé à la succion à partir d'une courbe d'étalonnage proposée par Zhang <i>et al.</i> (2001)	1 – 1500 kPa
Sonde de conductivité électrique	La mesure de succion est réalisée de façon indirecte par une pierre poreuse céramique et deux électrodes concentriques insérées dans la pierre. He (1999) a proposé une courbe d'étalonnage afin d'obtenir la succion à partir de l'intensité du courant électrique qui traverse l'espace poreux du sol. Néanmoins, il faut tenir compte l'effet de la salinité de l'eau dans la mesure de la intensité.	0 – 300 kPa; la sensibilité de la sonde devienne très basse lorsque la succion dépasse 300 kPa

Tableau 1-1. Techniques de mesure de succion. Adapté de Delage et Cui (2000a), Townend *et al.* (2000), Delage (2002), Tarantino *et al.* (2008) et Delage *et al.* (2008)

Les méthodes de contrôle se font par l'imposition et le maintien de la succion à une valeur fixée. Une description des principales méthodes de contrôle est présentée dans le Tableau 1-2.

Technique	Principe	Rang de succions
Plaque tensiométrique	Application d'une pression négative dans l'eau	0 – 10 kPa : (1m d'eau) 0 – 80 kPa : on applique une pression négative jusqu'à la limite imposée par la cavitation (80 kPa)

Technique	Principe	Rang de succions
Translation d'axes (cellule de Richards)	Application d'une pression positive du gaz, supérieure à la pression d'eau. Cette dernière est généralement égale à la pression atmosphérique, mais elle peut être contrôlée à une valeur donnée	Ces systèmes ont été étendus à succions aussi élevées que 12 MPa (Escario et Juca); ce qui impose la construction de cellules métalliques résistantes aux variations de la pression du gaz
Technique osmotique	Transfert d'eau par osmose. On utilise une membrane semi-perméable et une solution de molécules organiques de polyéthylène glycol (PEG)	0 – 12 MPa
Contrôle par phase vapeur	Contrôle de l'humidité relative par des solutions salines saturées (ou des solutions d'acide sulfuriques à diverses concentrations)	Succion maximale : 332 MPa , qui correspond à une humidité relative de 9% exercée par une solution saturée en KOH

Tableau 1-2. Techniques de contrôle de succion. Adapté de Delage et Cui (2000a), Townend *et al.* (2000), Delage (2002) et Delage *et al.* (2008)

1.2.2 Courbe de rétention d'eau

Le comportement des sols non saturés est fortement lié à la relation entre la succion et la teneur en eau, qui conditionne également les variations de la conductivité hydraulique non saturée avec la teneur en eau et, plus généralement, la réponse hydromécanique des sols non saturés. La relation entre la succion et la teneur en eau définit la courbe de rétention d'eau qui est caractérisée, entre autres choses, par les aspects suivants:

- Une zone aux forts degrés de saturation où la phase d'air n'est pas continue, la phase d'eau continue et le sol reste quasi-saturé. Les lois de comportement qui s'appliquent aux sols saturés peuvent être utilisées (Fredlund et Rahardjo 1993). Dans cette zone, le sol est soumis à des valeurs de succion inférieures à la pression d'entrée d'air ("air entry value", AEV) ;
- Une deuxième zone où les phases air et eau sont continues, rencontrée quand la succion devient supérieure à la pression d'entrée d'air et que la teneur en eau diminue significativement. L'air peut ainsi entrer dans les pores lors de l'augmentation de la succion. Les effets de l'hystérésis caractérisent cette section ;
- Une zone résiduelle où la phase d'eau est discontinue et où les transferts d'eau en phase gazeuse deviennent prépondérants. Dans cette région, de faibles variations de teneur en

eau peuvent correspondre à de forts changements de la succion (Croney et Coleman 1954).

1.2.3 Contraintes dans les sols non saturés

Les rôles de la contrainte totale et de la succion sur l'état de sollicitation auquel est soumis un sol non-saturé et la question de la validité de la notion de contrainte effective dans les sols non saturés sont des points encore largement débattus. La contrainte effective pour les sols saturés a été formulée par Terzaghi et Fröhlich (1936) :

“all the measurable effects of a change in stress, such as compression, distortion, and a change in shearing resistance are exclusively due to changes in the effective stress”. En français: “tous les effets mesurables d'un changement de contrainte, comme une compression, une distorsion, et un changement dans la résistance au cisaillement, sont dus exclusivement aux variations de la contrainte effective ”.

Bishop (1959) a souligné les implications les plus importantes du principe de contrainte effective :

“(1) that volume change and deformation in soils depend not on the total stress applied, but on the difference between the total stress and the pressure set up in the fluid in the pore space”. En français: “le changement de volume et la déformation dans les sols ne dépendent pas de la contrainte totale appliquée, mais de la différence entre la contrainte totale et la pression du fluide présent dans l'espace poreux ”.

“(2) that shear strength depends, not on the total normal stress on the plane considered, but on the effective stress”. En français: “la résistance au cisaillement ne dépend pas de la contrainte normale totale sur le plan envisagé, mais de la contrainte effective ”.

Ces concepts prennent en compte l'interaction entre la contrainte totale, la pression de l'eau et la contrainte intergranulaire. On considère que la contrainte effective agit sur le contact des particules du sol. Dans la Figure 1-2 (Engel et al. 2004), on présente un schéma détaillé des forces qui agissent sur les contacts des particules. L'équilibre des forces en direction verticale donne :

$$\sigma A = (f_H - f_C)A_s - f_w A + u_w A_w \quad (1-3)$$

- f_H est la force due à l'hydratation et la répulsion naturelle entre les particules,

- f_c est la force d'attraction due à la cimentation et aux liaisons chimiques,
- f_w est une force d'attraction due aux forces de van der Waals et aux contraintes électrostatiques,
- u_w est la pression du fluide (eau) dans les pores.

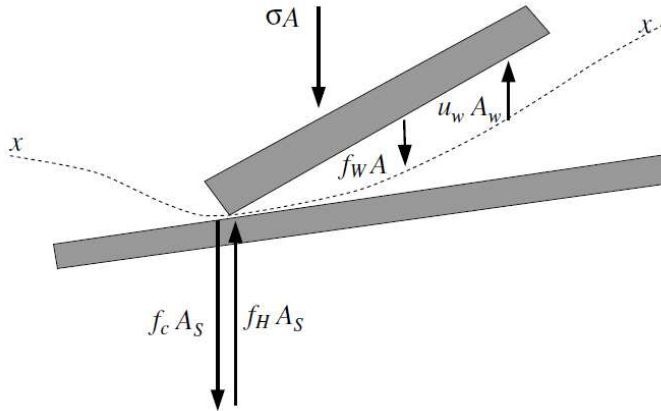


Figure 1-2. Schéma des forces agissant sur un contact entre particules (Engel *et al.* 2004)

On peut diviser la surface totale A en trois parties : la surface de contact A_s , la surface mouillée A_w et la surface sèche A_a . Ainsi, la contrainte effective pour les sols saturés est définie par :

$$\sigma' = \frac{(f_H - f_c)A_s}{A} = \sigma + f_w - u_w \quad (1-4)$$

Dans la plupart des cas, les forces de van der Waals et les contraintes électrostatiques peuvent être négligées. Ainsi, la contrainte effective proposée par Terzaghi est :

$$\sigma' = \sigma - u_w \quad (1-5)$$

Cette relation est valable dans le cas de sols saturés, où la pression de l'eau u_w est généralement positive ou nulle. Il existe des cas où la pression de l'eau u_w est négative, mais le sol reste saturé : dans ces conditions cette relation est également valable.

Dans les sols non saturés, la façon dont les contraintes existantes agissent sur chacune des trois phases (solide, fluide et gaz) dépend de différents facteurs. Dans les sols grenus non saturés, la capillarité engendre une attraction entre les grains qui n'agit que sur la surface mouillée des grains, qui diminue lorsque la succion augmente. Comme souligné par Jennings et Burland (1962), la succion est une contrainte locale et perpendiculaire aux contacts entre les grains qui dépend de la géométrie des contacts intergranulaires. Dans les sols fins non

saturés, en plus de la capillarité, on doit tenir compte des forces d'adsorption dans la phase argileuse.

Nombre d'auteurs (Croney *et al.* 1958, Bishop 1959, Aitchinson 1961, Jennings 1961, Bishop et Blight 1963) ont proposé des approches qui décrivent l'état de contraintes des sols non saturés afin de relier la contrainte totale, la succion et la contrainte effective. Bishop (1959) a proposé une approche de la contrainte effective pour les sols non saturés, basée sur le principe proposé par Terzaghi et Fröhlich (1936). En ajoutant la force qui agit sur la phase gazeuse (air) u_a dans l'équation (1-3) proposée par Bishop (1959), soit:

$$\sigma A = (f_H - f_C) A_S - f_W A - u_a A_a + u_w A_w \quad (1-6)$$

Cela donne finalement l'expression de Bishop (1959):

$$\sigma' = \sigma - u_a + \frac{A_w}{A} (u_a - u_w) = \sigma - u_a + \chi (u_a - u_w) \quad (1-7)$$

- σ' est la contrainte dite « effective »,
- $(\sigma - u_a)$ est la contrainte totale moins la pression dans l'air,
- $(u_a - u_w)$ est la succion matricielle dans l'eau du sol (différence entre les pressions d'air et d'eau),
- χ est un paramètre qui dépend du degré de saturation, égal à l'unité dans les sols saturés et zéro dans l'état sec.

D'après Bishop (1959), il suffit ainsi de trois grandeurs (la contrainte totale appliquée, la succion et le paramètre χ) pour décrire la résistance au cisaillement dans les sols non saturés. Néanmoins, le principe de contrainte effective semble inapplicable pour décrire le comportement contrainte - déformation des sols non saturés (Jennings et Burland 1962, Wheeler et Karube 1996, Alonso *et al.* 1987, Delage *et al.* 2000b).

1.2.4 Points faibles du concept de contrainte effective

Des analyses faites à partir de travaux expérimentaux réalisés par Jennings et Burland (1962), montrent un certain nombre de points faibles du concept de contrainte effective appliqué aux sols non saturés. On analyse maintenant le paramètre χ et on présente des anomalies liées à son utilisation dans la description du comportement hydromécanique des sols non saturés.

Analyse du paramètre χ

Donald (1960) et Aitchison (1961) ont proposé l'une des premières expressions qui décrit le paramètre χ . Elle est une fonction de la succion $s = (u_a - u_w)$ et du degré de saturation S_r :

$$\chi = S_r + \frac{1}{s_0} \int_0^s 0.3 s \Delta S_r \quad (1-8)$$

Dans la Figure 1-3, on présente des courbes du paramètre χ en fonction du degré de saturation (Donald 1960, Aitchison 1961, Bishop *et al.* 1960, Bishop et Donald 1961, Jennings et Burland 1962). Le paramètre χ a été calculé à partir des relations entre les contraintes appliquées et la succion, obtenues à des indices de vides constants, pour différents sols.

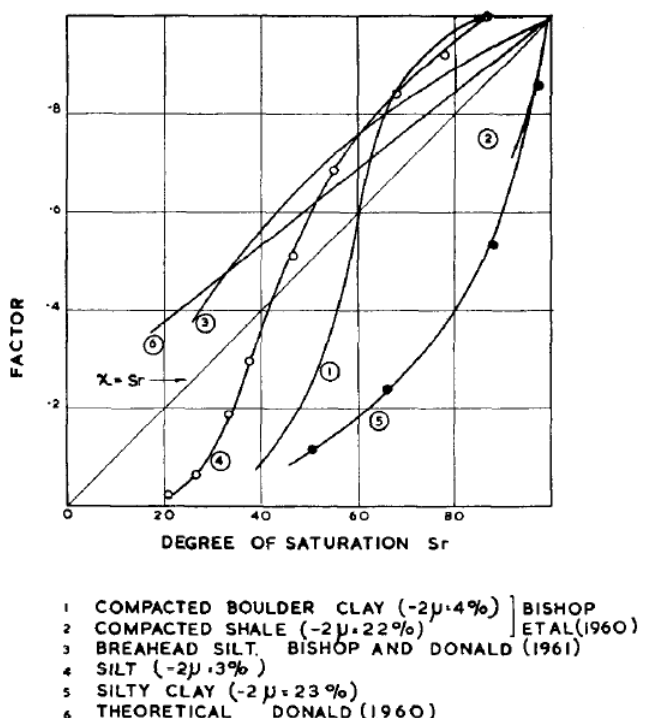


Figure 1-3. Variation du paramètre χ (FACTOR) en fonction du degré de saturation (Jennings et Burland 1962)

Les courbes $\chi(S_r)$ des sols granulaires ("BREAHEAD SILT" et "SILT") se rapprochent de l'expression théorique proposée par Donald (1960) et Aitchison (1961) à des degrés de saturation compris entre 40% et 60%. À propos des sols argileux, on souligne le grand écart entre les données expérimentales et l'expression théorique, surtout à des hautes valeurs de degré de saturation. Jennings et Burland (1962) ont suggéré d'adopter un degré de saturation critique, au-dessus duquel la notion de contrainte effective serait valable.

Bishop et Blight (1963) ont réétudié le concept de contrainte effective pour les sols saturés et non saturés dans laquelle l'expression proportionnelle à la succion est remplacée par une fonction plus complexe:

$$\sigma' = (\sigma - u_a) + f(u_a - u_w) \quad (1-9)$$

Bishop et Blight (1963) ont estimé cependant que l'expression $\chi(u_a - u_w)$ est une bonne approximation de $f(u_a - u_w)$ pour les sollicitations de cisaillement.

Analyse à partir de la "contrainte intergranulaire"

D'après Jennings et Burland (1962), on considère le principe de contrainte effective, plus comme une contrainte calculée à partir de la moyenne des forces intergranulaires, que comme une loi fondamentale du comportement mécanique des milieux poreux multiphasiques. Aitchison et Donald (1956) ont analysé les effets de changement de la teneur en eau dans la variation de la contrainte effective intergranulaire. Lors d'un processus de séchage, on estime que le réseau poreux du sol commence à drainer l'eau lorsque la succion dépasse la valeur de la pression d'entrée d'air, qui est associée à la géométrie des pores et au type de sol. La succion engendre l'apparition de ménisques, distribués de manière irrégulière au sein de l'arrangement de grains. Aitchison et Donald (1956) considèrent qu'à chaque étape du processus de séchage, il existe deux composantes de la contrainte intergranulaire: les forces existantes dans les ménisques du réseau drainé et la pression isotrope d'eau dans le réseau poreux toujours saturé. Pour eux, la somme de ces deux composants représente la contrainte effective intergranulaire. Aitchison et Donald (1956) ont aussi analysé expérimentalement la variation de la contrainte intergranulaire par rapport à la succion et à la teneur en eau, sur quatre sables ayant différentes compositions granulométriques. Alonso *et al.* (1987) ont redessiné les courbes originales en fonction de la contrainte effective intergranulaire et de la succion (Figure 1-4).

Ils ont remarqué une tendance linéaire pour les quatre sables aux faibles succions et une déviation de la relation initiale linéaire au moment où on dépasse la valeur d'entrée d'air de chaque sable. A partir de cette valeur, il n'existe pas de relation fixe entre la succion capillaire et la contrainte effective intergranulaire ; cette relation dépend de la valeur courante de succion et du type de sol.

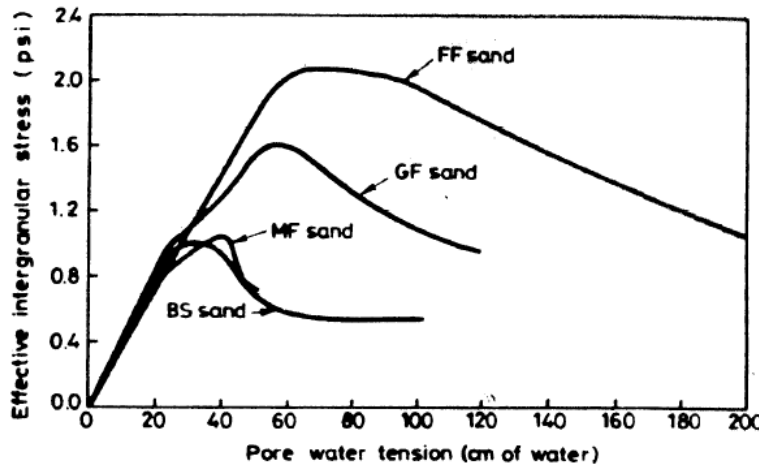


Figure 1-4. Relation entre la contrainte effective intergranulaire et la pression négative de l'eau (sucction) à partir du modèle capillaire. Modifié par Alonso et al. (1987) à partir des données d'Aitchison et Donald (1956)

Analyse à partir du comportement au changement volumique

Jennings et Burland (1962) ont réalisé une série d'essais oedométriques sur un limon d'après la méthode du double oedomètre (Jennings et Knight 1957) afin de caractériser le changement volumique en fonction des variations de succion sous différentes contraintes : i) la première éprouvette (test 1) a été initialement mouillée jusqu'à la saturation sans application de charge, et puis chargée par paliers jusqu'à une contrainte verticale de 16 tons/sq.ft. (1690 kPa); ii) en partant de l'état sec, la deuxième éprouvette (test 2) a été initialement chargée jusqu'à une contrainte verticale de 2 tons/sq.ft. (211 kPa) ; elle a ensuite été mouillée sous cette contrainte jusqu'à la saturation, et finalement chargée jusqu'à une contrainte verticale de 16 tons/sq.ft. (1690 kPa); iii) suivant la même procédure, trois éprouvettes additionnelles ont été testées (tests 3, 4 et 5) avec saturation à trois contraintes totales différentes de 4, 8 et 16 tons/sq.ft. (422, 845 et 1690 kPa).

Les résultats de ces tests ont permis de tirer les conclusions suivantes :

- La courbe du test 1 rejoint rapidement la *courbe de compression vierge*, obtenue lors du compactage d'un échantillon de limon remanié et saturé. Cette situation est typique pour les sols saturés normalement consolidés, car leur courbe de compression rejette une unique courbe de compression vierge ;
- Les échantillons des tests 2, 3, 4 et 5 ont une compressibilité plus faible qu'à l'état saturé. Avant la mise en saturation, leurs courbes de compression croisent la courbe de compression vierge, montrant l'augmentation de la contrainte de plastification avec l'incrément de succion ;

-
- Lors de la mise en saturation pendant les tests 2, 3, 4 et 5, on a observé du déplacement positif ou de compression. Cela semble *incohérent* avec le concept de contrainte effective pour les sols non saturés (proposée par Bishop 1959, eq. (1-7)) car une diminution de la succion (mise en saturation) engendre une réduction de la contrainte effective, et cela devrait générer le gonflement de l'échantillon ;
 - Après la saturation, les courbes des tests 2, 3, 4 et 5 rejoignent la courbe de compression vierge.

Sur la base du concept de contrainte effective, toute diminution de la contrainte effective est accompagnée d'une augmentation du volume du sol. Néanmoins, lorsqu'un sol partiellement saturé est mouillé sous une charge externe constante, il peut présenter une réduction de volume, de tassement ou "d'effondrement". Ceci est donc contraire au comportement prévu par le concept de contrainte effective. Jennings et Burland (1962) ont attribué ce comportement à des variations spéciales de la structure des sols non saturés. Les modifications dans l'arrangement des particules dues au retrait des ménisques dans la phase de mouillage sont différentes de celles générées par de variations de la contrainte externe (Delage et Cui 2000b).

Wheeler et Sivakumar (1995) ont montré la non-validité du principe de contrainte effective pour les sols non saturés en examinant l'évolution du volume spécifique v d'un échantillon de kaolinite compactée à l'état critique. Cela est expliqué avec les courbes déviateur de contrainte à la rupture q en fonction de la contrainte nette moyenne ($p - u_a$) et v en fonction de $(p - u_a)$, présentées dans la Figure 1-5. Sur cette figure, considérons deux points A et B situés sur les courbes de l'état critique de 0 et 200 kPa de succion respectivement. D'après le concept d'état critique, A et B correspondent à une même valeur de déviateur à la rupture q , ils doivent correspondre à la même contrainte effective et au même volume spécifique. La réponse en variation de volume indique que ce n'est pas le cas: le point B se trouve à une valeur de volume spécifique beaucoup plus petite que le point A . Un raisonnement inverse est également valable : les deux points A et C ont le même volume spécifique, mais des résistances au cisaillement à l'état critique très différentes.

Compte tenu des nombreuses difficultés pour décrire le comportement volumique sur la base d'une contrainte effective obtenue par la combinaison de la contrainte nette et de la succion dans une même équation (Jennings et Burland 1962, Bishop et Blight 1963, Aitchison 1965b,

Brackley 1971), plusieurs auteurs ont recommandé l'usage d'un jeu de deux contraintes indépendantes (Coleman 1962, Fredlund and Morgenstern 1977, Alonso *et al.* 1987).

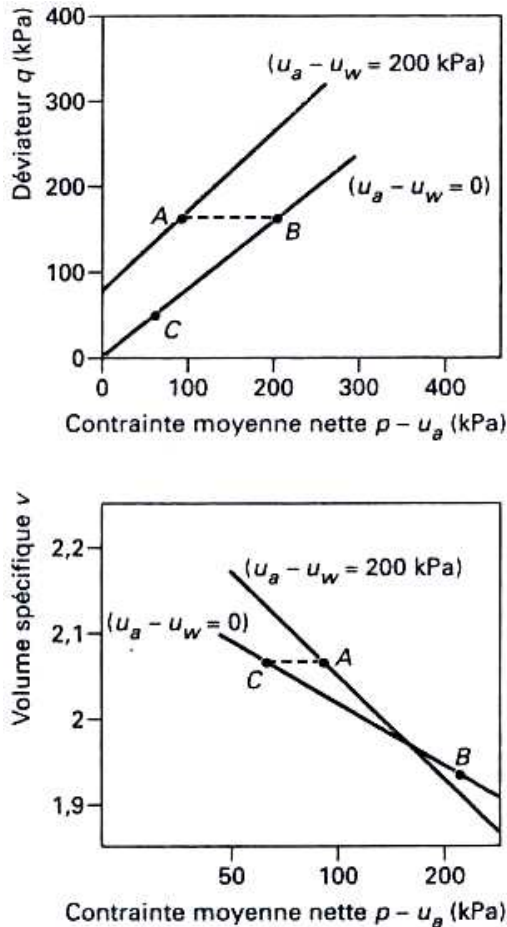


Figure 1-5. Représentation de l'état critique (après rupture) d'une kaolinite compactée (Wheeler et Sivakumar 1995).

1.2.5 Variables d'état dans les sols partiellement saturés

De nombreux auteurs ont cherché à définir les variables qui représentent le comportement hydromécanique des sols non saturés (Aitchison et Donald 1956, Bishop et Donald 1961, Bishop et Blight 1963, Burland 1965, Barden *et al.* 1969, Fredlund et Morgenstern 1977, Mongiovi et Tarantino 1998, Tarantino *et al.* 2000). En toute généralité, trois contraintes entrent en jeux dans le comportement mécanique des sols partiellement saturés : la contrainte totale σ_{ij} , la pression de l'eau dans le sol u_w et la pression de l'air dans le sol u_a ; les deux dernières sont isotropes (Fredlund et Morgenstern 1977, Alonso *et al.* 1987). Bishop et Donald (1961) et Coleman (1962) ont été les premiers à suggérer l'utilisation de la pression d'air comme composante de l'état de contraintes des sols non saturés. D'après des analyses théoriques (Bishop et Donald 1961, Coleman 1962, Matyas et Radhakrishna 1968) et des

observations expérimentales (Fredlund et Morgenstern 1977, Mongiovi et Tarantino 1998), il est maintenant accepté que deux combinaisons de ces trois contraintes permettent de décrire le comportement des sols partiellement saturés. La *contrainte nette* ($\sigma_{ij} - u_a \delta_{ij}$, où δ_{ij} est le symbole de Kronecker) et la *succion matricielle* ($u_a - u_w$) sont les deux combinaisons le plus largement utilisées en pratique.

Lors d'essais triaxiaux sur des échantillons de limon non saturé, Bishop et Donald (1961) ont imposé des variations de la contrainte de confinement σ_3 , de la pression d'eau u_w et de la pression d'air u_a , en gardant les combinaisons ($\sigma_3 - u_a$) et ($u_a - u_w$) constantes. D'après les résultats des essais, si ces deux combinaisons restent constantes, on n'observe presque pas de changement de la courbe contrainte – déformation, même si on impose des fortes variations aux variables individuelles. Au contraire, lorsqu'ils ont fait varier ($\sigma_3 - u_a$) ou ($u_a - u_w$), il y a eu un effet remarquable sur le comportement contrainte – déformation. Coleman (1962) a été le premier à considérer la contrainte nette ($\sigma_3 - u_a$) et la succion ($u_a - u_w$) comme variables indépendantes.

D'après les travaux expérimentaux de Mongiovi et Tarantino (1998), des incrémentations $\Delta\sigma$, Δu_a et Δu_w égaux et simultanés ne provoquent aucune déformation volumique si on maintient constants les champs de contrainte ($\sigma - u_a$) et ($u_a - u_w$). Dans un de leur tests, ils ont observé qu'une augmentation de la variable ($\sigma - u_a$) engendre la même variation de la succion ($u_a - u_w$) si on maintient constant le volume de l'échantillon de sol. D'après Delage et Cui (2000), il existe trois raisons qui expliquent l'utilisation du couple des variables d'état ($\sigma - u_a$) et ($u_a - u_w$):

- la variable ($u_a - u_w$), qui correspond à la succion matricielle, a une signification physique bien définie;
- la pression u_a est dans la plupart des cas prise égale à 0 (pression atmosphérique); ainsi, l'expression de la contrainte totale nette est simplifiée et la succion devient une pression d'eau négative;
- ce couple de variables est également bien adapté à l'analyse d'essais réalisés par la technique de translation d'axes, où une pression d'air positive u_a est appliquée.

Les variations indépendantes de la contrainte totale nette ($\sigma - u_a$) et de la succion matricielle ($u_a - u_w$) ont une influence directe sur le comportement des sols non saturés.

Bien que le principe de contraintes effectives de Bishop pour les sols non saturés comporte quelques points faibles dans la description de leur comportement, il a été repris par différents auteurs dans le développement de leurs modèles constitutifs (Kohgo *et al.* 1993, Modaressi et Abou-Bekr 1994, Bolzon *et al.* 1996, Loret et Khalili 2000, 2002, Gallipoli *et al.* 2003, Wheeler *et al.* 2003, Sheng *et al.* 2004, Ehlers *et al.* 2004, Santaguliana et Schrefler 2006, entre autres). Leur formulations varient beaucoup, mais se basent essentiellement sur deux contraintes indépendantes : la première, alternative à la contrainte nette moyenne, du type « Bishop », et la deuxième associée à la succion. Des exemples de modèles élasto-plastiques utilisant ce choix de contraintes sont donnés par Gens (1995). Jommi (2000) fait une discussion claire sur la sélection de ce choix de contraintes.

Certains de ces modèles ont été catalogués comme de « contrainte effective ». Ceci a généré une confusion par rapport aux points faibles qu'on a déjà décrits dans la section 1.2.4. Bien que ces modèles utilisent une « contrainte effective » dans leur formulation, ils considèrent de façon indépendante la succion. Cette interprétation est actuellement largement acceptée (Alonso *et al.* 2010). Des considérations thermodynamiques ont été invoquées par Gray et Schrefler (2001), Laloui *et al.* (2003) et Coussy (2004), entre autres, afin de proposer une équation de contrainte effective sous la forme :

$$\sigma' = \sigma - p_g 1 + S_r s 1 \quad (1-10)$$

Où σ' et σ sont les tenseurs effectif et total, p_g est la pression du gaz (air), et s est la succion égale à $= (p_g - p_l)$. Le degré de saturation doit être défini sur la surface réellement mouillée, et on ne doit pas le confondre avec le paramètre χ . Les dernières formulations d'une « contrainte effective » acceptable sont basées sur les relations existantes entre la contrainte total, la succion et dans certains cas le degré de saturation (comme décrit par Pereira *et al.* 2003 et Nuth et Laloui 2007) et peuvent être résumés par l'expression :

$$\sigma' = \sigma + \pi(p_g, p_l, S_r) 1 \quad (1-11)$$

où la fonction $\pi(p_g, p_l, S_r)$ peut être considérée comme une pression de pore équivalente, correspondant à la pression d'un fluide saturant l'espace poreux et entraînant le même comportement d'ensemble que celui observé dans un sol non saturé (Alonso *et al.* 2010).

1.2.6 Structure des sols partiellement saturés

L'étude de la structure du sol a un rôle majeur dans la compréhension de son comportement mécanique et pour la prédiction qualitative de l'effet des variables environnementales. Dans les sols non saturés, l'analyse de la structure a une importance particulière dans la mesure où la structure contrôle en grande partie l'état de l'eau dans le sol et donc la succion. D'après Alonso *et al.* (1987), une meilleure compréhension de la structure permet également d'analyser l'effet de l'eau adsorbée sur les argiles sur la valeur de la succion matricielle et l'influence de la géométrie interne sur la capillarité.

Les deux méthodes les plus utilisées pour les analyses de la structure des sols sont la microscopie électronique à balayage (MEB) et la porosimétrie par intrusion de mercure. A partir d'observations expérimentales, McGown et Collins (1975) et Collins (1984) ont proposé une classification des sols naturels par rapport à leur comportement gonflant ou effondrable. Cette classification est conçue à partir de trois niveaux d'arrangements entre les particules du sol: l'espace poreux, l'arrangement des particules individuelles (comme dans une sable propre ou dans une argile pure), et les arrangements complexes entre les grains (sable, limon) et les particules argileuses (comme dans le loess). Par exemple, les sols gonflants sont généralement caractérisés par des arrangements simples entre particules argileuses. Les sols effondrables ont des organisations plus complexes avec des arrangements des grains liés par des agrégations argileuses ou des agents cimentants.

D'après Alonso *et al.* (1987), la structure du sol peut être caractérisée par l'identification de différents éléments simples (Figure 1-6) :

- grains ou particules individuelles ;
- matrice ou volume de sol composé par des particules distribuées de façon relativement homogène ;
- agrégations entre particules individuelles ;
- assemblages entre agrégations argileuses et grains de limon ou sable ;
- connecteurs entre les grains de limon ou sable ; ils peuvent être composés d'agrégations argileuses ou d'autres agents cimentants.

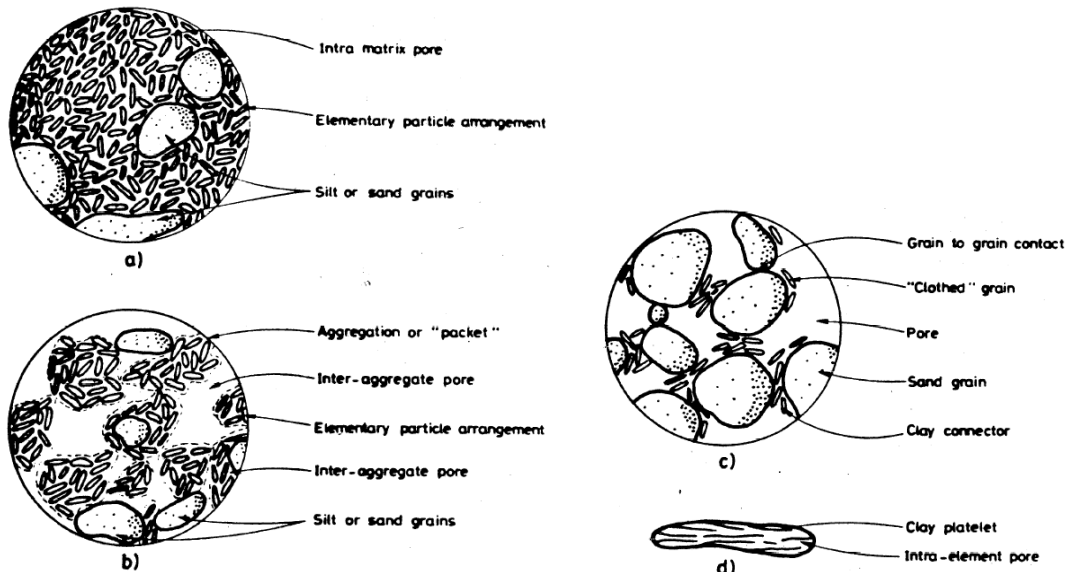


Figure 1-6. Eléments de la structure du sol (Alonso *et al.* 1987): a) matrice argileuse composée par l’agrégations de particules argileuses et par quelques grains de limon ou sable; b) structure composée par des assemblages entre agrégations argileuses et grains de limon ou sable; c) matrice de sable ou limon avec des connecteurs d’argile entre les grains individuels; d) agrégation simple d’éléments argileux

Cette analyse est conforme aux travaux menés en porosimétrie au mercure par Ahmed *et al.* (1974) et Delage *et al.* (1996). On présente en Figure 1-7 des photographies au MEB obtenues sur un échantillon de limon de Jossigny compacté des côtés sec et humide de l’optimum Proctor, tirées de Delage *et al.* (1996). Dans la photographie de l’échantillon compacté du côté sec (Figure 1-7a), on observe un agrégat de 100 µm de diamètre composé de grains de limon angulaires de rayon moyen 20 µm. Des agrégats argileux, sous la forme de plaquettes de kaolinite, couvrent la surface des grains de limon. Il semble que les agrégats argileux agissent comme de liaisons entre les grains. Le rayon d'accès des pores intergranulaires est d'environ 4 µm. Il existe des pores inter-agrégats de diamètre 40 µm. Cette structure correspond aux types b et c de la Figure 1-6. Il apparaît que le processus de compactage ne modifie pas la structure des agrégats, lesquels ont été initialement formés à partir d'une poudre passée par un tamis de 400 µm puis humidifiée. Aux faibles teneurs en eau (côté sec), en raison de valeurs relativement élevées de la succion, leur cohésion apparente augmente et le compactage ne peut pas les détruire entièrement. Cela explique l'existence d'agrégats et de gros pores entre eux et évite que l'échantillon atteigne la densité maximale au Proctor (Delage *et al.* 1996).

Au contraire, la structure du même limon compacté (avec la même fraction d'argile) change s'il a été initialement humidifié. Dans la Figure 1-7b, on observe l'augmentation du volume

des agrégats argileux, lesquels forment une matrice argileuse autour des grains de limon. Cet assemblage correspond à une structure du type a) dans la Figure 1-6.

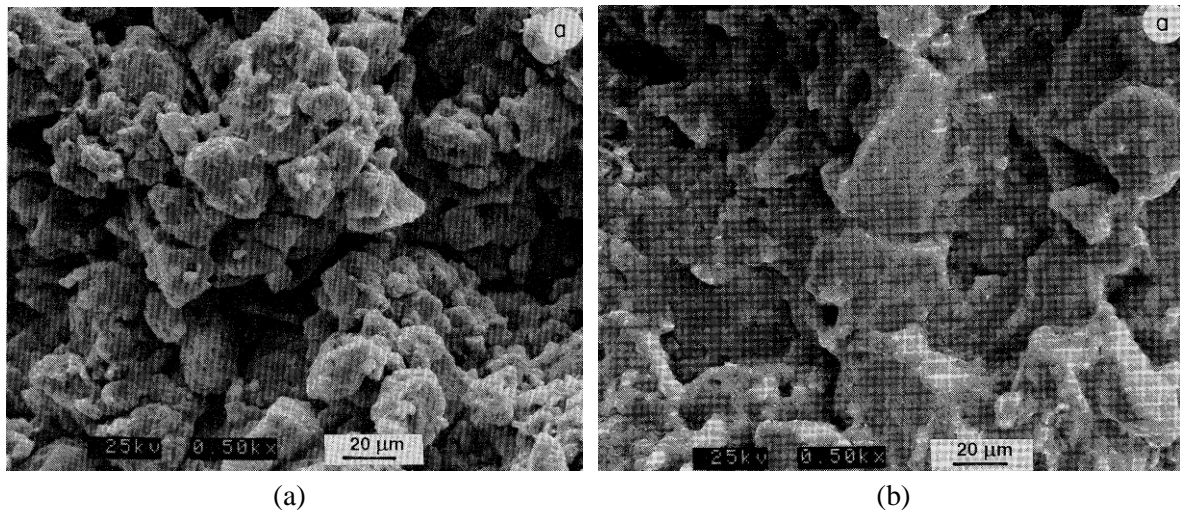


Figure 1-7. Observation au MEB de la structure d'un limon compacté: a) du coté sec de l'optimum; b) du côté humide (Delage et al. 1996)

Dans la Figure 1-8, on présente une observation au microscope électronique à balayage de la structure d'un échantillon de lœss provenant du Nord de la France. Ce matériau comporte des grosses agrégations des grains de limon liés par des agrégations argileuses, caractéristique d'une structure de type b) selon la Figure 1-6. Sur cette figure, on observe aussi de zones composées par des grains propres de limon avec quelques liaisons argileuses, distribuées de manière aléatoire (structure du type (c) dans la Figure 1-6). Ce lœss présente aussi de gros pores entre les agrégations ayant un diamètre supérieur à 100 µm. Cette type de structure est caractéristique des sols effondrables. Ce phénomène d'effondrement peut se produire à la suite de deux scénarios typiques : 1) on humidifie le sol (sous charge externe constante) et ceci entraîne la disparition des effets de la succion (qui augmentaient sa résistance) entraînant un effondrement, lié à la présence des zones composées par de grains propres de limon et faiblement cimentées; ou 2) on applique une charge externe (en condition saturée par exemple) et les agrégations de limon-argile s'effondrent et remplissent les gros pores qu'on observe à l'état intact.

Alonso *et al.* (1987) ont présenté une analyse des phénomènes de gonflement et d'effondrement des sols à partir de l'analyse de leur structure. Sous basse contrainte et lors du mouillage, on observe généralement une augmentation macroscopique du volume du sol, liée au gonflement des agrégations simples d'argiles ; son intensité dépend de la minéralogie de l'argile. Ces agrégations tendent à conserver leur structure tant qu'on n'augmente pas de manière significative la contrainte externe. Si elle augmente, les connecteurs ou les

agrégations d'argiles s'écrasent, les particules glissent aux contacts et les pores qui existaient entre particules sont emplis par les agrégations déformées ou par les grains de limon ou sable. Cette réorganisation engendre une réduction de volume macroscopique du sol qui, selon son intensité, peut être qualifiée d'un effondrement.

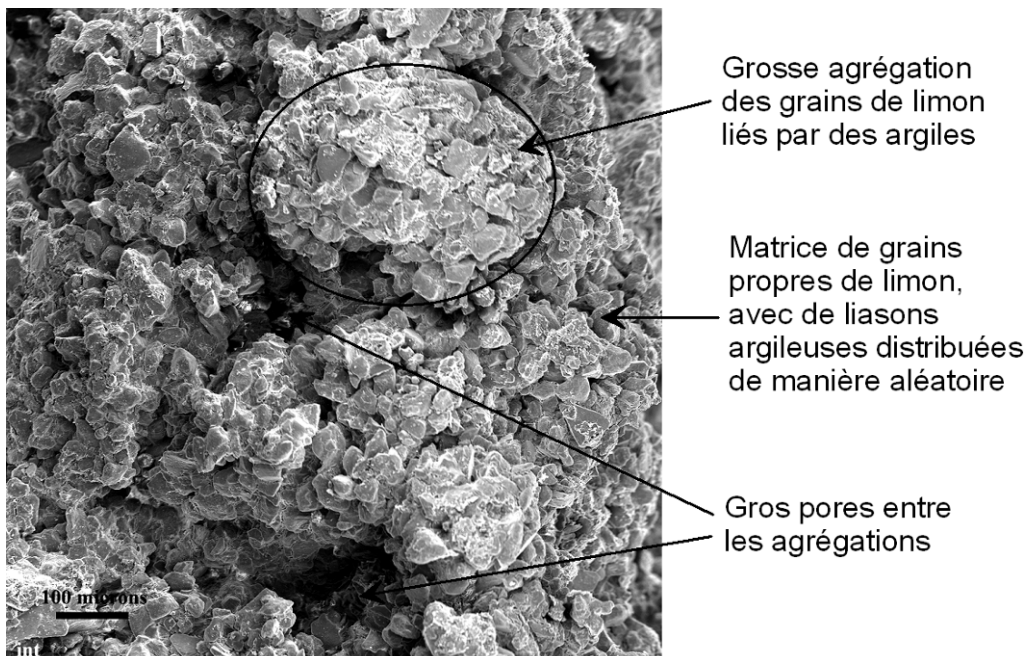


Figure 1-8. Structure d'un échantillon de loess du Nord de la France

1.2.7 Aspects du comportement mécanique des sols non saturés

Le comportement des sols non saturés est complexe. D'une part, il dépend de façon très importante de la nature du sol, en raison de sa structure, comme évoqué plus haut. D'autre part, la prépondérance de couplages d'origine hydro-mécanique rend une identification complète du comportement plus longue et plus difficile à réaliser. Afin de caractériser précisément ce comportement, il est nécessaire d'obtenir un ensemble complet de résultats expérimentaux sur différents types de sol, en considérant des tests de compression et de cisaillement le long de différentes trajectoires de contrainte (Maatouk *et al.* 1995) à différents degrés de saturation. Dans cette section, on résume les principaux aspects du comportement mécanique des sols non saturés en insistant sur l'analyse des effets de l'état hydrique (teneur en eau, succion) sur les propriétés mécaniques (déformabilité, résistance).

Comportement volumique

La réponse volumique des sols non saturés ne dépend pas seulement des valeurs initiales et finales de la contrainte nette et de la succion matricielle ; elle est fortement influencée par les

chemins intermédiaires de contrainte ou succion (Alonso *et al.* 1990). Des variations de la succion peuvent provoquer de déformations volumiques irréversibles (Josa 1988, Alonso *et al.* 1990). Yong *et al.* (1971) ont observé de déformations plastiques lors du séchage d'une argile naturelle de faible activité. Josa *et al.* (1987) ont détecté le même phénomène sur une kaolinite légèrement plastique. Certains sols non saturés peuvent présenter du gonflement ou de l'effondrement suite aux variations de son état hydrique (Maswoswe 1985 sur une argile sableuse compactée, Justo *et al.* 1984 sur des échantillons compactés d'argile gonflante, entre autres).

La Figure 1-9 (Matyas et Radhakrishna 1968), obtenue par mesures de variations volumiques d'échantillons compactés au laboratoire et soumis à des contraintes isotropes dans une cellule triaxiale, montre les résultats obtenus quand les chemins ($\sigma - u_a$, $u_a - u_w$) sont tels que le degré de saturation S_r est toujours croissant. Elle fournit une bonne synthèse sur l'influence des variations de contraintes totales nettes et de succion sur l'indice des vides d'un sol non saturé, qui est défini dans ces conditions par une surface d'état :

$$e = F(\sigma - u_a, u_a - u_w) \quad (1-12)$$

Ces points se résument de la manière suivante (Delage et Cui 2000b) :

- l'allure de la surface montre, en comparant le chemin de consolidation du sol saturé (1) à celui à succion non nulle constante (2), dont la pente moyenne est moins forte, que la compressibilité diminue quand la succion augmente, c'est-à-dire quand le sol est plus sec ;
- le chemin (3) à contrainte constante avec diminution de la succion correspond à un remouillage sous charge constante et la figure présente un cas d'*effondrement* (cet aspect est traité plus amplement dans une prochaine section) ;
- le chemin (4) est caractéristique d'un remouillage sous contrainte nulle, qui se produit avec augmentation de l'indice des vides et présente un léger *gonflement*, que l'on peut relier au relâchement de l'attraction exercée entre les particules du sol du fait de la diminution de la succion. Ce léger gonflement se produit également pour des contraintes faibles ;
- le chemin (5) est obtenu quand le relâchement de la succion se fait à volume constant et son intersection avec le plan ($\sigma - u_a$, e) donne la valeur de la contrainte de gonflement dans ces conditions. En dessous de cette valeur, le remouillage sous charge constante

engendre un gonflement du sol (cf. chemin (4)) : au-dessus, il engendre son effondrement (cf. chemin (3)) ;

- un essai de compression à teneur en eau constante de sol compacté (chemin (6)) suffisamment sec voit la valeur de la succion ($u_a - u_w$) qui diminue tout en restant positive, avec augmentation du degré de saturation (mais pas d'expulsion d'eau) ;
- si cet essai est prolongé, il est possible d'atteindre la saturation avec passage de l'état de succion à celui de pression positive avec expulsion ou mise en pression de l'eau, dans des conditions de drainage nul ou imparfait.

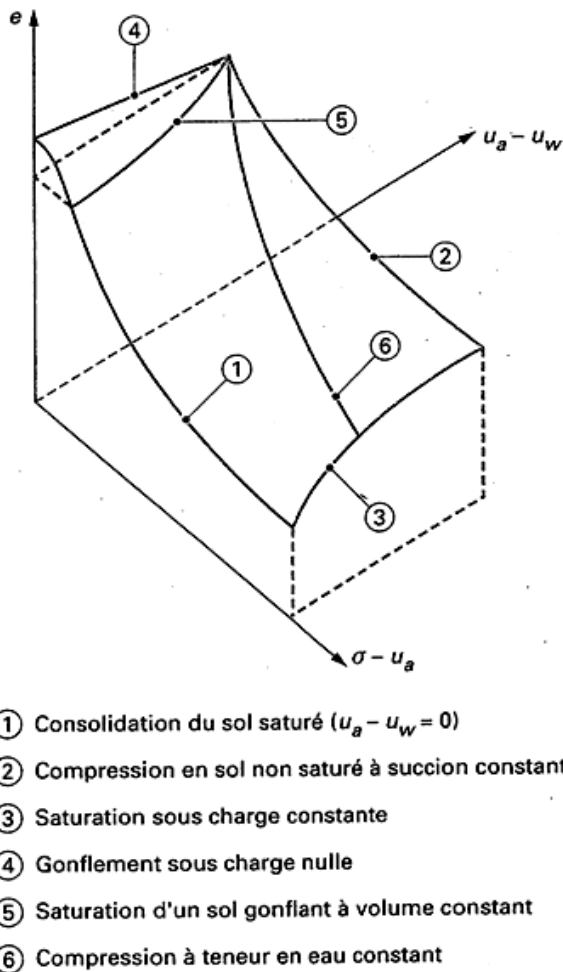


Figure 1-9. Surface d'état $e = F(\sigma - u_a, u_a - u_w)$ (Matyas et Radhakrishna 1968)

Les résultats des essais oedométriques réalisés par Barden *et al.* (1969) montrent ce comportement sur des échantillons d'argile de faible plasticité. Rico et Del Castillo (1976) ont observé l'influence de la succion à l'aide des résultats de tests de compression à l'oedomètre, réalisés par Wilson (1952) sur des échantillons de sable argileux compactés des cotés sec et humide de l'optimum Proctor. Ces résultats montrent une compressibilité plus importante

pour les échantillons humides que pour les échantillons secs, bien que ces derniers soient plus fragiles et se fissurent plus rapidement.

Effondrement et gonflement

L'augmentation du degré de saturation du sol non saturé, suite à des variations des conditions environnementales par exemple, peut produire une réduction volumique irréversible sans variation du niveau de la contrainte externe appliquée. Ce phénomène est connu comme *effondrement* du sol. Il est décrit plus en détail dans la section 1.4 sur l'effondrement de sols non saturés et spécialement du lœss.

Certains sols (gonflants) peuvent subir un processus de *gonflement* d'un ordre de grandeur relativement grand lorsqu'on augmente sa teneur en eau. Ce phénomène correspond à l'incrément du volume du sol dû au remouillage sous contrainte externe constante. En général, on observe un gonflement dans les sols argileux ayant une forte plasticité et une densité sèche importante lorsqu'ils sont soumis à des contraintes externes faibles. Ce comportement est lié principalement à la minéralogie du sol. Les sols contenant des minéraux argileux tels que l'illite, la kaolinite, la montmorillonite (dont la smectite) ont une tendance à gonfler, ceci étant beaucoup plus important pour la smectite, lorsqu'on les met en contact avec de l'eau (Lambe et Whitman 1959).

Le potentiel de gonflement dépend, entre autres (Barrera 2002), des caractéristiques des minéraux argileux (telles que la structure des cristaux et leur capacité d'échange cationique), de la densité du sol (une densité sèche plus forte donnera lieu à un gonflement plus important), de l'état de contraintes (le gonflement est plus grand sous faible contrainte), de la structure du sol (une structure flokulée a une tendance plus grande à gonfler qu'une structure disperse (Seed et Chan 1959)), du temps (les sols argileux sont très peu perméables, ainsi le processus d'humidification – gonflement peut durer de semaines voire des années), de la présence de sels qui diminuent la capacité d'échanges cationiques et ainsi le gonflement, et de la teneur en eau (une humidité plus faible implique un potentiel de gonflement plus grand).

La contrainte externe contrôle l'ordre de grandeur du gonflement lorsqu'on soumet le sol à une diminution de la succion..Pour les sols gonflants, les cycles d'humidification et de séchage produisent un gonflement irréversible (déformation plastique) dans le premier cycle d'humidification ; le comportement peut être considéré comme élastique pour les cycles suivants (Yuk 1994).

Influence de la succion sur le comportement avant rupture

La succion augmente la rigidité et la résistance des sols, comme le rappellent Alonso *et al.* (1987). En réalisant des essais oedométriques sous différentes conditions d'humidité, Dudley (1970) a observé l'augmentation de la contrainte de plastification avec la succion. Plus récemment, différents programmes expérimentaux réalisés à l'appareil triaxial (dont Cui et Delage 1996 et Geiser *et al.* 2000) ont généralisé ces observations en mettant en évidence un élargissement de la zone élastique avec la succion (écrouissage apparent lié à l'augmentation de la succion) conforme avec les principales hypothèses du modèle BBM (Alonso *et al.* 1990).

D'après les résultats de compression isotrope à succion contrôlée obtenus par Cui et Delage (1996) sur le limon de Jossigny (France) compacté, le comportement volumique des sols compactés est marqué par deux caractéristiques principales (Delage et Cui 2000b) :

- un comportement de type surconsolidé, avec une contrainte limite (analogue à la pression de préconsolidation) séparant un comportement pseudoélastique raisonnablement réversible d'un comportement plastique, dont la valeur augmente avec la succion. Cette contrainte limite est fonction de la contrainte de compactage et de la succion appliquée ensuite ;
- un raidissement avec l'augmentation de la succion, particulièrement dans la zone où le comportement est plastique, qui engendre une diminution des coefficients de compression avec l'augmentation de la succion.

Dans la Figure 1-10, on présente les résultats obtenus au triaxial à succion contrôlée sur le limon de Jossigny par Cui et Delage (1996). Les échantillons ont été compactés à l'optimum ($w_{opt.} = 18\%$). Les tests ont été faits pour quatre succions différentes (200, 400, 800 et 1500 kPa) sous 50 kPa de contrainte de confinement. On observe sur la Figure 1-10a que le module de rigidité initial augmente avec la succion. Cette tendance exprime le raidissement de la structure avec l'augmentation de succion et la désaturation. Pour les succions supérieures à 400 kPa, des pics de plus en plus prononcés sont observés, illustrant l'augmentation de la fragilité du matériau avec la succion. Le comportement volumique est initialement contractant, puis d'autant plus dilatant que la succion est élevée (Figure 1-10b)

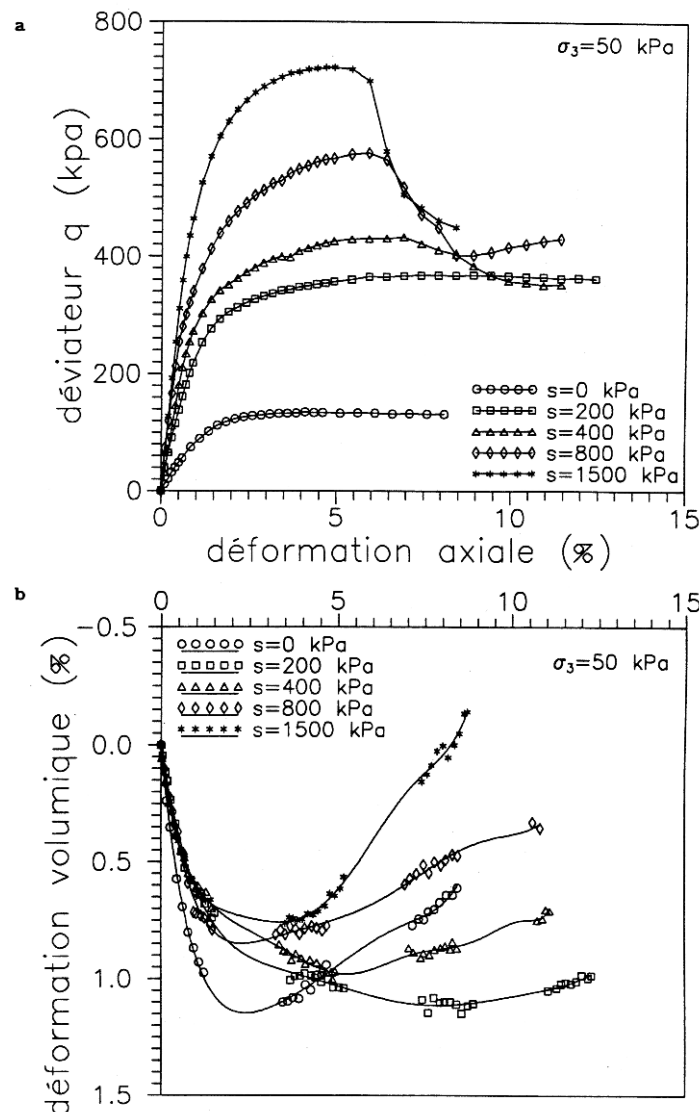


Figure 1-10. Courbes de cisaillement à une contrainte de confinement de 50 kPa sur le limon de Jossigny. a) Effort-déformation; b) variations volumiques (Cui 1993)

D'après Geiser *et al.* (2000), on peut analyser le comportement mécanique des sols non saturés à partir des chemins de chargement isotrope ou anisotrope (cisaillement). Lors de trajectoires de chargement isotrope, l'incrément de la succion génère l'augmentation de la contrainte de préconsolidation et la diminution de la compressibilité. Dans ce cas, l'augmentation de la résistance ne commence que lorsqu'on dépasse la succion d'entrée d'air, même si cela doit être confirmé par des essais expérimentaux.

Lors de trajectoires de cisaillement (chargement anisotrope) Geiser *et al.* (2000) ont remarqué les aspects suivants du comportement :

- la résistance de pic augmente avec la succion (Delage et Graham 1995, Geiser 1999); ceci peut être interprété comme un incrément de la cohésion apparente en gardant constant l'angle de frottement ;

- l'augmentation de la succion pourrait engendrer une légère augmentation de la rigidité élastique ;
- aux fortes succions, on pourrait observer des pertes significatives de la résistance (rupture fragile) ;
- pour chaque niveau de succion, on devrait observer une seule surface d'état critique dans l'espace de contraintes $p_{nette} - q$.

Résistance au cisaillement et comportement à la rupture

Bien que l'approche de Bishop présente différents points faibles dans la définition d'un état de contraintes effectives dans les sols non saturés, il permet une interprétation du critère de Mohr-Colomb en conditions non saturées :

$$\begin{aligned}\tau &= \sigma' \tan \varphi' + c' = [\sigma - u_a + \chi(u_a - u_w)] \tan \varphi' + c' = \\ &= (\sigma - u_a) \tan \varphi' + \chi(u_a - u_w) \tan \varphi' + c'\end{aligned}\tag{1-13}$$

Khalili et Khabbaz (1998) ont proposé une formule pour le paramètre χ en analysant une quantité importante de données de résistance au cisaillement pour différents niveaux de succion et différents types de sols ($(u_a - u_w)_b$ représente la succion d'entrée d'air) :

$$\chi = \left(\frac{(u_a - u_w)}{(u_a - u_w)_b} \right)^{-0.55}\tag{1-14}$$

Fredlund *et al.* (1978) ont proposé un critère de cisaillement modifié, basé sur l'hypothèse d'une enveloppe de rupture plane dans l'espace $\tau, (\sigma - u_a), (u_a - u_w)$:

$$\tau = c' + (\sigma - u_a) \tan \varphi' + (u_a - u_w) \tan \varphi^b\tag{1-15}$$

Cette expression implique que l'angle de frottement φ' est constant et indépendant de la succion. Cette hypothèse, souvent vérifiée, n'est cependant pas toujours vraie. On voit sur la Figure 1-11 que l'angle de frottement n'augmente pas toujours avec la succion, comme le montre le diagramme de la figure, qui regroupe les résultats obtenus par différents auteurs sur divers sols : argile de Guadalix ($w_L = 33\%$, $I_P = 13,6$) (Escario et Saez 1986), sable argileux de Madrid ($w_L = 32\%$, $I_P = 15$) (Escario et Saez 1986), limon de Jossigny compacté à $w = 15,5\%$ ($w_L = 37\%$, $I_P = 18$) (Delage *et al.* 1987), limon faiblement compacté de Trois-Rivières

($I_P = 7$, $e_i = 1$) (Maatouk *et al.* 1995). On observe une augmentation de l'angle de frottement pour les argiles et une diminution pour le limon.

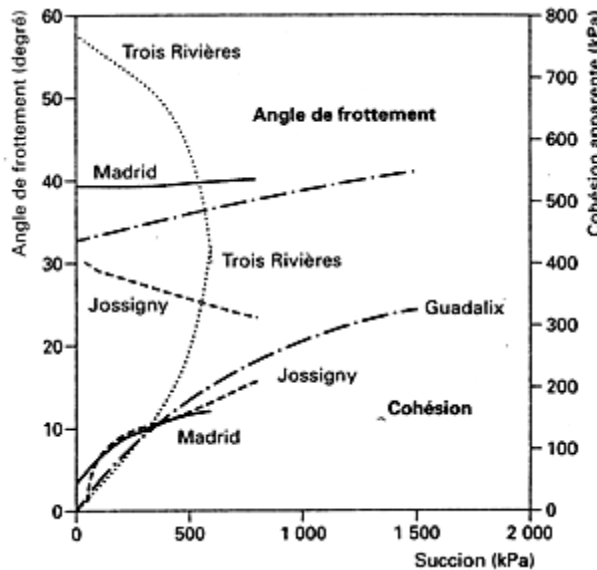


Figure 1-11. Variations de l'angle de frottement avec la succion

Dans la Figure 1-12, on observe que l'augmentation de la succion de 0 à 500 kPa renforce le sol, avec augmentation de la cohésion apparente et de l'angle de frottement pour une argile rouge de Guadalix de la Sierra (Escario et Saez 1986). Cette augmentation de la cohésion apparente a été aussi observée pour autres sols comme on le présente dans la Figure 1-11. D'après les résultats des essais de cisaillement réalisés par plusieurs auteurs (Fredlund *et al.* 1978, Gulhati et Satija 1981, Ho et Fredlund 1982, Fredlund et Rahardjo 1985), l'augmentation de la succion génère une augmentation de la résistance au cisaillement, de la cohésion apparente, et dans quelques cas, de l'angle de frottement.

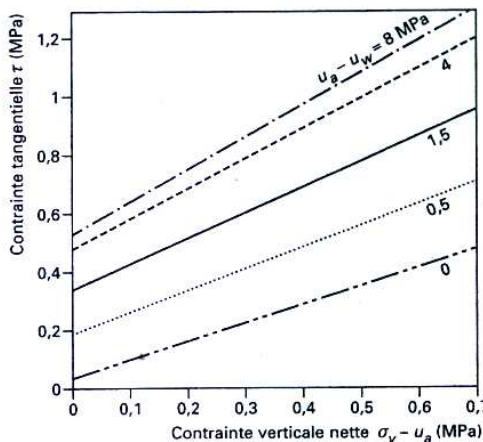


Figure 1-12. Résistance au cisaillement d'une argile rouge de Guadalix de la Sierra (Escario et Saez 1986)

L'angle ϕ' quantifie l'augmentation de résistance avec la succion sous contrainte nette constante et correspond à l'intersection de la surface plane caractérisant la rupture avec le plan $(\sigma - u_a) = 0$. La Figure 1-13 (Escario et Juca 1989) présente les contraintes de cisaillement obtenues à la rupture sur l'argile de Guadalix en fonction de la succion, chaque ensemble de points correspondant à une contrainte nette donnée. On observe que les enveloppes de rupture sont non linéaires, et qu'il y a une décroissance progressive de la pente des courbes jusqu'à une valeur stable, atteinte aux fortes valeurs de succion (> 8 MPa). La résistance peut atteindre une valeur maximale à une valeur de succion déterminée et puis rester constante ou descendre à des succions plus fortes. Ces variations de l'angle ϕ' avec la succion sont illustrées par la Figure 1-13 (Escario et Juca 1989). L'angle des courbes avec l'axe vertical, à succion nulle, est égal à l'angle de frottement à l'état saturé φ' . On note que ϕ' doit théoriquement être égal à φ' à succion nulle.

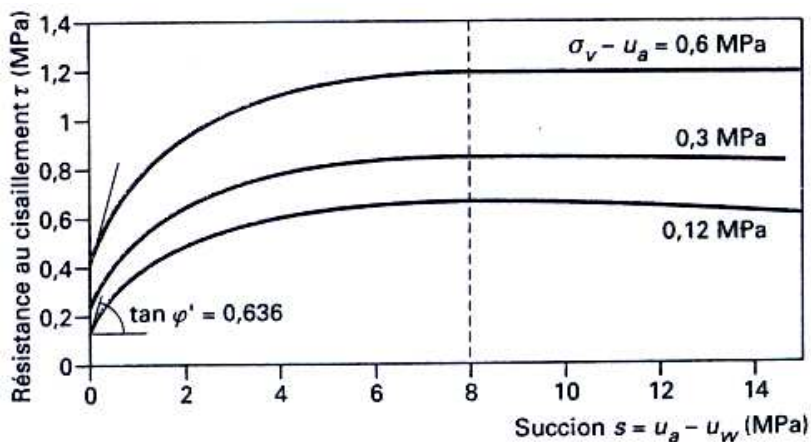


Figure 1-13. Lieux des points de rupture dans le plan $(u_a - u_w, \tau_{max})$. Tests sur l'argile rouge de Guadalix (Escario et Juca 1989).

1.2.8 Couplage hydromécanique

Pour décrire complètement le comportement des sols non saturés, différentes variables et relations entre celles-ci doivent être identifiées. Du côté *hydraulique*, on a la courbe de rétention d'eau qui relie la teneur en eau w à la succion s dans le sol. Cette courbe peut changer avec des variations de volume qu'on mesure plutôt à l'aide de l'indice des vides e . Du côté *mécanique*, les variations du degré de saturation peuvent engendrer de grands changements dans la réponse mécanique, dont la compressibilité et les comportements avant et après la rupture. D'après Jotisankasa *et al.* (2009), la majorité des études théoriques sur le comportement de sols non saturés ont évolué à partir du cadre élastoplastique proposé par

Alonso *et al.* (1987), et développé d'avantage par les travaux d'Alonso *et al.* (1990), Wheeler et Sivakumar (1995), Maatouk *et al.* (1995) et Cui et Delage (1996). L'idée centrale de ce modèle constitutif consiste en la définition d'une surface de charge appelée "loading collapse" (LC), qu'on peut obtenir à partir d'une série d'essais de compression obtenues à succion constante, et représentées dans un espace du volume spécifique en fonction de la contrainte moyenne nette et de la succion. Dans ce contexte, on suppose que la compression plastique associée à l'effondrement par remouillage et celle liée à l'application d'une contrainte externe sont des processus similaires. Ainsi, ces processus peuvent être décrits avec une unique surface de charge (LC). Cette hypothèse a été largement confirmée par la suite. On peut citer les résultats récents de tests oedométriques avec suivi de la succion sur une argile limoneuse compactée, réalisés par Jotisankasa *et al.* (2007).

D'autre part, la relation entre la succion et la teneur en eau (appelée *courbe de rétention d'eau*) a d'abord été ignorée en mécanique des sols non saturés, que ce soit au niveau des recherches expérimentales ou de la modélisation constitutive. En effet, seul l'effet de la succion dans la réponse mécanique avait été pris en compte pendant une longue période (Vaunat *et al.* 2000). On supposait que la courbe de rétention n'était nécessaire que pour la modélisation des phénomènes d'écoulement (de l'eau et de l'air) dans le réseau poreux du sol. Il est ainsi regrettable que la courbe de rétention soit considérée comme une partie complémentaire de l'étude du comportement mécanique, car elle contient des informations précieuses sur l'influence de la distribution du réseau poreux dans le comportement du sol. D'ailleurs, la courbe de rétention d'eau est clairement dépendante de la trajectoire des contraintes appliquées, montrant une réponse hystérotique importante. Ce phénomène d'hystérosis a une grande influence dans le comportement mécanique, car il est lié à la distribution de l'eau dans les pores du sol, et ceci affecte directement la réponse mécanique du sol (Wheeler et Karube 1996).

Les premiers efforts vers des descriptions plus complètes du comportement des sols non saturés ont démarré dans les années 70 (regarder le récapitulatif réalisé par Wheeler et Karube 1996). En adoptant la contrainte moyenne nette ($\sigma - u_a$) et la succion matricielle ($u_a - u_w$) comme variables d'état, il a été proposé de décrire le comportement hydromécanique à partir des *surfaces d'état* pour les sols non saturés. Celles-ci décrivent l'évolution de l'indice de vides e et du degré de saturation S_r (ou la teneur en eau w) avec la contrainte moyenne nette et la succion matricielle (Vaunat *et al.* 2000). Le premier modèle capable de décrire les aspects

irréversibles de la réponse volumique des sols non saturés a été formulé par Alonso *et al.* (1990) dans le cadre de l'élastoplasticité. Ensuite, Wheeler et Sivakumar (1995) et Wheeler (1996) ont proposé un modèle élastoplastique amélioré, lequel prend en considération les variations de la teneur en eau. Dans le même temps, Barbour (1998) a proposé des relations entre la courbe de rétention et d'autres propriétés du sol (résistance au cisaillement, perméabilité et conductivité thermique).

Le développement des nouvelles techniques expérimentales a permis la validation d'autres analyses constitutives à partir des données obtenues au laboratoire. Ces avancées expérimentales ont permis une mesure plus précise des échanges d'eau pendant le chargement (e.g. Rampino *et al.* 1999). Des études expérimentales ont également été réalisées afin d'analyser la dépendance de la courbe de rétention d'eau sur la structure du sol, le niveau de contraintes et l'histoire de contraintes (e.g. Vanapalli *et al.* 1999).

Différents ensembles relativement complets de résultats expérimentaux décrivant les couplages hydromécaniques dans les sols non saturés ont été présentés, entre autres, par Wheeler (1996) à partir d'essais de chargement isotrope, par Rampino *et al.* (1999) à l'aide de tests de compression et cisaillement au triaxial, par Chen *et al.* (1999) sur la base de tests de compression isotrope et du retrait, et par Ng et Pang (2000) à partir de cycles de remouillage et de séchage à l'oedomètre. Romero (1999) a présenté des cycles de remouillage et de séchage, faits en parallèle avec de trajectoires de chargement et déchargement à l'oedomètre. Ces résultats ont montré un comportement couplé de la réponse volumique avec les variations de la teneur en eau dans des argiles non saturés.

Babour (1998), Romero (1999) et Vanapalli *et al.* (1999) ont souligné deux mécanismes contrôlant le stockage de l'eau dans un sol. Le premier mécanisme est principalement associé à l'écoulement d'eau libre à l'intérieur des macropores. Le deuxième est lié à l'adsorption de l'eau au niveau intra-agrégat, quand il existe. Tandis que le deuxième mécanisme est considéré comme indépendant de la structure au niveau macroscopique, le premier est couplé avec la réponse du sol lors de sollicitations mécaniques. Les résultats expérimentaux, obtenus par Wheeler (1996), Rampino *et al.* (1999) et Romero (1999), montrent que les changements volumiques irréversibles de la teneur en eau sont une conséquence de la déformation volumique du squelette du sol. En parallèle, l'histoire des cycles de remouillage et de séchage du sol peut affecter l'évolution des déformations irréversibles (Chen *et al.* 1999).

1.3 Le Lœss

Le lœss est un dépôt limoneux éolien, transporté dans des conditions périglaciaires et déposé dans des environnements froids de steppe, aux marges des nappes glaciaires importantes du Quaternaire, principalement autour du parallèle 50°N à l'hémisphère Nord. Il existe quelques dépôts aussi en Amérique du Sud. La Figure 1-14 (Pécsi 1990) présente la localisation des dépôts de lœss dans le monde; les régions en noir (1) correspondent aux dépôts lœssiques et celles éoliennes du type lœssique en gris (2). On les trouve sur des plateaux, des pentes et de grands bassins alluviaux. Des épaisseurs jusqu'à 300 m ont été observées en Chine dans le "Plateau de Lœss". Des dépôts existent aussi dans le plateau de Sibérie (Russie), dans les bassins des rivières du Danube, du Rhin et du Mississippi (Amérique du Nord) et aussi dans la Pampa (Argentine) (Delage *et al.* 2005).

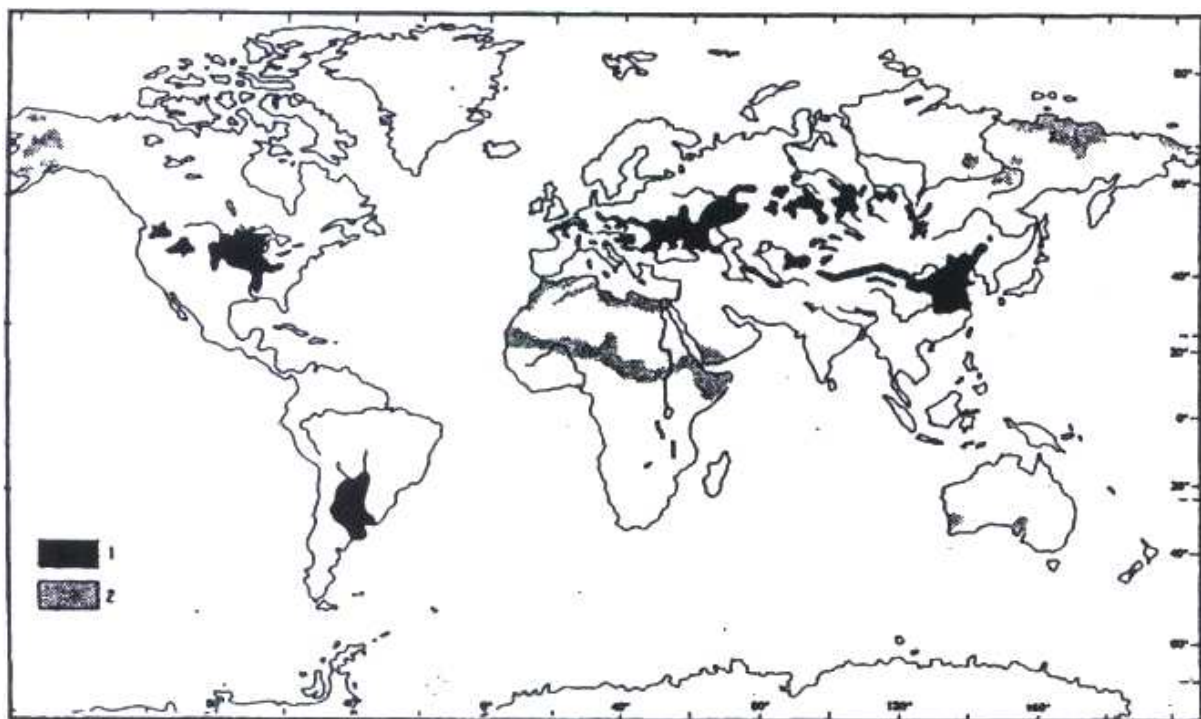


Figure 1-14. Dépôts lœssiques dans le monde (Pécsi 1990)

Le processus typique de formation d'un dépôt lœssique éolien est résumé dans la Figure 1-15. D'abord, des particules fines produites par abrasion glaciaire sont lavées, transportées par des courants proglaciaires et redéposées près des dépôts préexistants de moraine (plaines alluviales proglaciaires). Ensuite, des particules de sable, limon et argile sont soumises aux cycles de gel et dégel. Elles sont érodées et transportées par l'action permanente des vents froids et secs. Ces vents sont créés par les hautes pressions existant au-dessus des calottes

glaciaires. Puis, les particules de sable, plus grandes et lourdes, sont déposées en premier sous la forme de dunes et en couches superficielles. Ensuite, les particules de limon et d'argile sont transportées vers des zones de basses pressions et en haute atmosphère. Finalement, ces particules fines sont déposées suite aux changements climatiques : décroissance de la vitesse du vent, présence d'un obstacle, capture par la végétation herbacée ou couverture de neige (Antoine 2002).

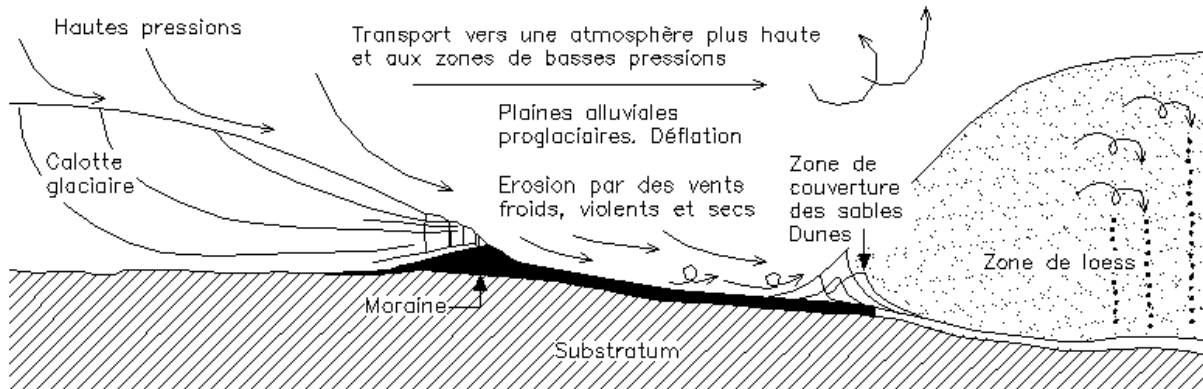


Figure 1-15. Processus de formation des lœss (d'après Andersen et Borns 1997 cité par Antoine 2002)

Le lœss est principalement composé de particules de limon de taille d'environ 5 à 80 microns et d'une fraction assez importante d'argile. On trouve des minéraux argileux tels que la smectite, la vermiculite, la kaolinite et une faible proportion d'illite et chlorite (Lautridou 1985). La fraction des composants biologiques (pollens, mollusques, restes de microorganismes) montre l'action d'une ambiance froide de steppe (Antoine 2002). D'après différents chercheurs (Smalley 1971, Jamagne *et al.* 1981, Lautridou 1985, Pécsi 1990) le lœss est caractérisé par :

- une structure homogène et poreuse,
- l'absence de stratification,
- une abondance de particules limoneuses d'environ 30 µm, d'argile (15 – 18%), et de sable (< 2%),
- la présence de carbonates,
- une prédominance de minéraux comme des grains de quartz (=70%), de fer (1,5 - 2%) et de carbone d'origine organique (0,2%).

D'après Pécsi (1990), "Loess is not just the accumulation of dust". Les dépôts lœssiques ont été soumis à des transformations diagénétiques après le dépôt initial, avec en particulier une cimentation due à la dissolution et à la reprécipitation des particules calcaires primaires et un

phénomène d'illuviation de la couche superficielle qui, en devenant plus argileuse dû à l'action de la pluie et au transport de particules fines en surface, empêche l'écoulement de l'eau de pluie depuis la surface jusqu'aux couches effondrables et non saturées. D'après Becze-Deack *et al.* (1997), d'autres caractéristiques importantes du lœss sont :

- l'orientation aléatoire des grains,
- la présence de liens argileux entre les particules limoneuses,
- la distribution hétérogène de revêtements argileux sur les grains de limon.

1.3.1 Le lœss de Bapaume

Des grandes étendues de dépôts lœssiques sont localisées au Nord de la France. Certains niveaux de ces dépôts sont non saturés *in situ* car protégés des actions climatiques par une couche supérieure rendue imperméable par illuviation et contenant une plus forte quantité d'argile, elle-même recouverte de sol végétal. Généralement, ils ne présentent pas de problèmes de stabilité. Néanmoins, certains sites présentent des caractéristiques particulières telles qu'une grande fraction de carbonates et de faibles densité et plasticité. Ces caractéristiques rendent le lœss sensible à l'effondrement lorsqu'on change son état hydrique (Delage *et al.* 2005). Il existe plusieurs sites dans le Nord de la France où l'on trouve à quelques mètres de profondeur des couches horizontales de grande extension ayant ces particularités (Antoine 2002). Lors d'une exploration réalisée dans la région de Bapaume (Picardie) en octobre 2007, on n'a toutefois pas observé de nappe phréatique dans une excavation de 5 mètres de profondeur, malgré les fortes précipitations caractéristiques de ces régions.

Des problèmes de tassement le long de la ligne Nord du Train à Grande Vitesse (TGV), qui relie Paris à Bruxelles et à Londres, ont été observés lors de périodes de pluie intense (Cui *et al.* 1995, Cui *et al.* 2004). Cette ligne traverse de grandes extensions de lœss. Il semble que lors des travaux de construction, des couches de lœss sensibles à l'effondrement aient été exposées aux conditions climatiques externes (évaporation, séchage, infiltration d'eau), après le retrait de la couche végétale superficielle. Mis à part l'effet possible des cavités souterraines artificielles et de tranchées construites pendant la première guerre mondiale, la sensibilité à l'effondrement du lœss dans cette région est apparemment une des causes privilégiées des problèmes de stabilité observées le long de cette ligne (Cui *et al.* 1995, Cui *et al.* 2004, Delage *et al.* 2005).

Les dépôts lœssiques du Nord de la France ont été formés sous des conditions périglaciaires pendant la période Quaternaire (25 000 - 15 000 ans avant J.C.). Ils ont été déposés sur des formations de craie et dépôts alluviaux, suite aux processus de transport éolien de particules de limon, provenant du front glaciaire situé à l'époque dans le Canal de la Manche (Antoine 2002, Antoine *et al.* 2003, Delage *et al.* 2005). Les principales formations calcaires dans la région correspondent à la période Pléniglaciaire Weichsel Supérieur. La région est ainsi caractérisée par une couverture lœssique continue et subcontinue ayant une épaisseur comprise entre 3 et 8 mètres et une relative homogénéité. Les dépôts plus importants de lœss se localisent dans la vallée de la Basse-Seine, dans le bassin de la Somme et au nord entre Lille et Bruxelles (Antoine 2002, Antoine *et al.* 2003).

La Figure 1-16 (Antoine 2002) montre l'extension des dépôts lœssiques dans le Nord de la France.

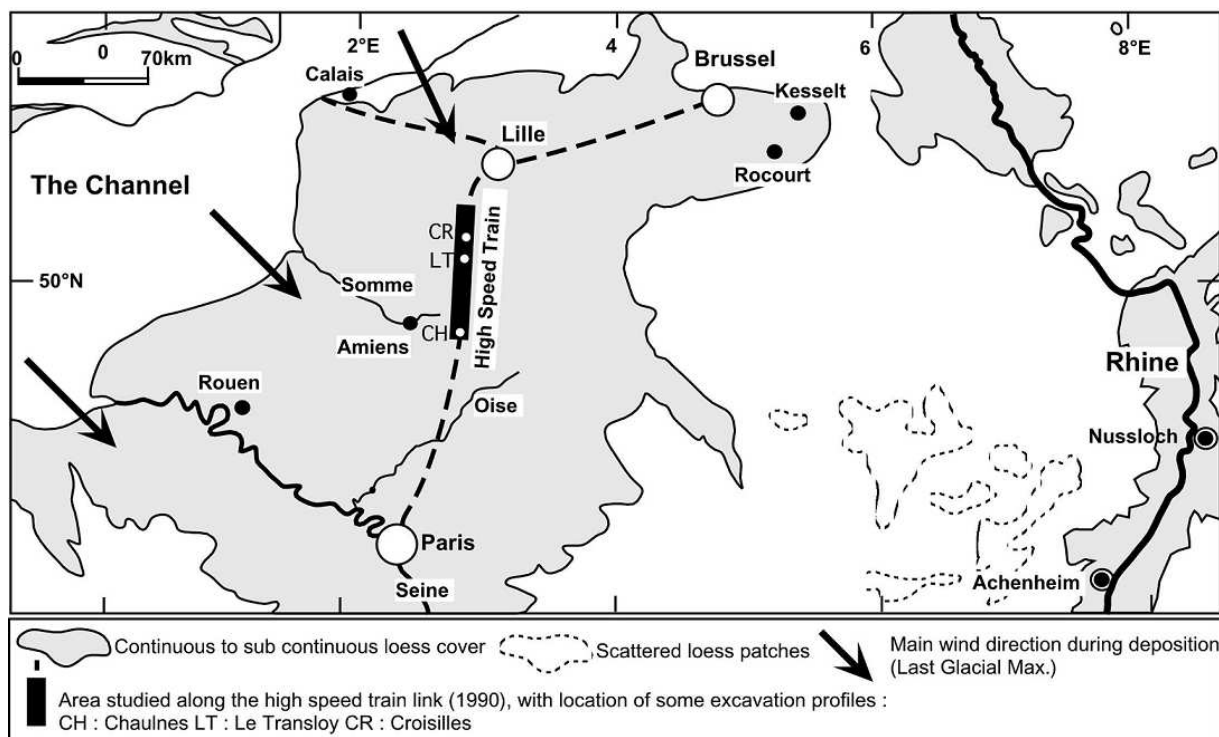


Figure 1-16. Localisation des dépôts lœssiques dans le nord de la France (d'après Antoine 2002)

Les flèches dans la Figure montrent la direction des fronts de vent en direction Sud-Ouest et Nord-Ouest qui ont été à l'origine de la formation des dépôts actuels. La ligne du TGV Nord est représentée dans la figure par la ligne à discontinue. Le rectangle en noir sur la ligne de TGV, entre Amiens et Lille, représente la zone où on a observé les problèmes de stabilité les plus importants. Les dépôts de lœss sont localisés entre la Normandie (France) et la région de Bruxelles (Belgique). On les trouve aussi dans l'est de la région parisienne sous l'appellation

“Limons des plateaux” (Audric 1973). Dans la plupart des cas, ces dépôts sont naturellement non saturés et très favorables pour l’exploitation agricole. Les aéroports d’Orly et Roissy - Charles de Gaulle, au sud et au nord de Paris respectivement, sont aussi situés sur ces dépôts lœssiques (Audric 1973).

Description du matériau

Le site considéré est situé dans la vallée de la Somme à 11 km de la rivière, dans un endroit proche de la ville de Bapaume (Pas-de-Calais, France). Lors de la visite effectuée en octobre 2007, on a localisé un terrain adjacent à la ligne du TGV. Afin de caractériser les propriétés physiques et mécaniques du matériau, plusieurs blocs intacts de lœss ont été prélevés à 4 profondeurs (1,0 m, 2,1 m, 3,3 m et 4,7 m) lors de la réalisation d’une excavation de 5 mètres de profondeur. Ensuite, ces blocs ont été isolés, protégés de l’évaporation par application d’une couche de paraffine et enveloppés dans un film plastique. A partir des échantillons taillés dans les blocs intacts, on a obtenu les propriétés physiques et géotechniques du matériau (Tableau 1-3).

Profondeur	1 m	2,1 m	3,3 m	4,7 m
Teneur en eau naturelle, w (%)	14,0	14,9	17,0	20,4
Indice de vides naturel, e	0,84	0,79	0,60	0,60
Masse volumique sèche, ρ_d (Mg/m ³)	1,45	1,50	1,67	1,66
Degré de saturation naturel S_r (%)	46	50	76	87
Succion naturelle (HTC) (kPa)	40	-	49	-
Pourcentage d’argiles (% < 2 µm)	16	18	25	25
Limite de plasticité, w_p	19	21	21	21
Limite de liquidité, w_l	28	30	30	30
Indice de plasticité, I_p	9	9	9	9
Teneur en carbonates, (%)	6	9	5	5
Contrainte verticale totale in situ, σ'_{v0} (kPa)	16	42	70	95
Effondrement (%) sous σ'_{v0}	7,5	-	6,3	-

Tableau 1-3. Caractéristiques géotechniques du profil du lœss de Bapaume

Le lœss étudié a une composition relativement homogène, avec une couleur jaune grisâtre. Il s’agit d’un matériau très poreux ayant une fraction importante de carbonates (jusqu’à 18% de CaCO₃) ; il peut aussi exister localement des granules calcaires (Delage *et al.* 2005). L’indice de plasticité I_p est constant dans tout le profil et égal à 9. Les couches supérieures sont en

condition non saturée ($S_r = 46\%$ à 1,0 m et 50% et 2,1 m). Les couches plus profondes sont proches de la saturation. Dans ce travail, on a utilisé des échantillons de lœss de la couche 1 (1,0 m), car celui-ci s'est révélé présenter la plus grande susceptibilité à l'effondrement d'après des observations expérimentales initiales. Des études sur la totalité du profil ont également été menées, avec notamment une analyse du risque d'effondrement sous sollicitations cycliques (Karam 2006, Yang *et al.* 2008, Karam *et al.* 2009).

La distribution granulométrique du lœss étudié (1,0 m) est présentée dans la Figure 1-17. Les fractions de sable, de limon et d'argile sont de 2, 82 et 16% respectivement. D'après la classification de Casagrande, le lœss est classé comme CL ou limon argileux.

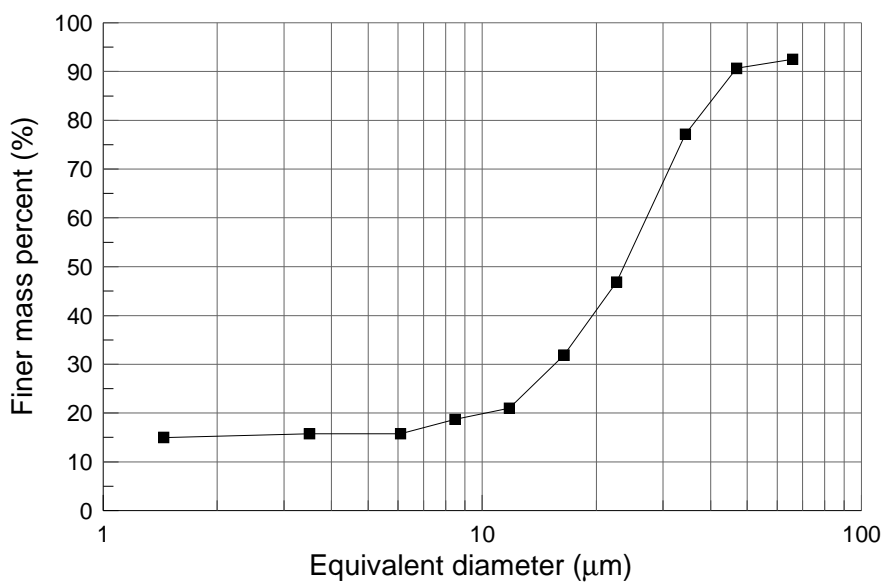


Figure 1-17. Distribution granulométrique du lœss de Bapaume (France)

Les minéraux argileux dominants dans le lœss sont la kaolinite, l'illite et un ensemble interstratifié d'illite et de smectite (Cui et Marcial 2003).

1.4 Le phénomène d'effondrement

Le phénomène d'effondrement est typiquement associé aux sols de faible plasticité et non saturés, bien qu'il puisse être aussi observé dans de sols saturés soumis à de sollicitations mécaniques. Le lœss a tendance à subir ce phénomène du fait de ses caractéristiques spéciales telles qu'une condition *in situ* non saturée, une faible densité totale, une cimentation faible composée de carbonates ainsi qu'une structure particulière. La structure du lœss est caractérisée par un indice des vides élevé et un arrangement instable des particules (Cui *et al.*

2004, Delage *et al.* 2005). L'une des causes principales de l'effondrement dans les sols lœssiques est l'humidification subite du sol sous la contrainte naturelle *in situ*. Ce phénomène a été décrit depuis longtemps dans les régions arides (Dudley 1970).

Les sols non saturés ayant une structure naturelle lâche ont tendance à s'effondrer lorsqu'ils sont soumis à une augmentation du degré de saturation (Holtz 1948, Jennings and Knight 1957, Burland 1961, Jennings 1961, Knight 1961, Wagener 1961, Jennings et Burland 1962, Lucas *et al.* 1964, Jennings 1965). Ce processus entraîne la diminution de la valeur de la succion initiale et une compression volumique irréversible. Le risque et l'intensité de l'effondrement sont associés à l'amplitude des contraintes appliquées et à la valeur de la succion initiale. Ces conditions changent d'un sol à l'autre.

Typiquement, l'intensité de l'effondrement augmente lorsque la contrainte de confinement croît (Jennings et Knight 1957, Blight 1965, Barden *et al.* 1969, Dudley 1970, Erol et El Ruwaih 1982, Yudhbir 1982). Néanmoins, Yudhbir (1982) a observé que l'intensité de l'effondrement atteint sa valeur maximale à une contrainte donnée, puis cette intensité décroît même si la contrainte continue à augmenter. Cette valeur maximale varie par rapport au type de sol et aux conditions initiales. Une fois saturé, l'échantillon effondré suit, de manière approximative, la trajectoire contrainte-déformation d'un échantillon initialement saturé sous compression (Jennings et Knight 1957, Erol et El Ruwaih 1982, Maswoswe 1985).

1.4.1 L'effondrement lié aux caractéristiques spéciales des dépôts lœssiques naturels

Des problèmes d'instabilité des dépôts lœssiques ont été observés par divers auteurs dans différentes parties du monde (Li 1995, Huang 2008, Meier 2008, Nouaouria *et al.* 2008, Punrattanasin 2008, Whithall et Duffy 2008, Yuan et Wang 2009). L'effondrement des dépôts lœssiques est principalement dû à l'humidification des dépôts et la chute correspondante de la succion, mais on cite également divers phénomènes tels que les mouvements sismiques (Yuan et Wang 2009), le chargement statique dû aux constructions (Meier 2008), le chargement dynamique dû au passage des trains (Cui *et al.* 1995, Karam 2006) et la décongélation des dépôts lœssiques (Huang 2008) localisés en zones de pergélisol.

La difficulté de prévoir l'effondrement est liée principalement à la connaissance insuffisante des propriétés du lœss dans l'état naturel. Dans la plupart des cas, le lœss a une très faible

résistance associée à une structure métastable (Yuan et Wang 2009). Il y a aussi une faible connaissance de la relation entre les variations de la teneur en eau et le comportement mécanique.

Houston (1995) a observé de nombreuses causes d'humidification telles que, la rupture des conductions de réseaux résidentiels, canaux ou systèmes d'arrosage (Walsh *et al.* 1993), l'écoulement superficiel et les systèmes déficients de drainage (Walsh *et al.* 1993), les recharges de l'eau intentionnelles ou non (Shmuelyan 1995), l'ascension du niveau de la nappe phréatique (El Nimr *et al.* 1995), l'endiguement de l'eau dû aux chantiers de constructions (Kropp *et al.* 1994, Noorany et Stanley 1990), et les processus de transfert d'eau dus à la capillarité ou aux isolations thermiques (Jimenez-Salas 1995). Li (1995) a observé des phénomènes d'effondrement sur des dépôts lœssiques en Chine lors du remplissage des retenues d'eau.

D'après plusieurs auteurs, le risque d'effondrement du lœss est lié aux conditions suivantes :

- les propriétés de base, y compris la minéralogie, la teneur en argile, la forme et la distribution des pores dans le sol, la cimentation intergranulaire et les propriétés électromagnétiques de l'argile (Cui *et al.* 2004) ;
- un indice de plasticité faible (Delage *et al.* 2005) ;
- une porosité importante qui correspond à une structure ouverte (Barden *et al.* 1973) ;
- une condition non saturée liée à une valeur élevée de succion (Barden *et al.* 1973) ;
- une structure spéciale susceptible de se dégrader (Shao *et al.* 2007), caractérisée par une densité faible et une cimentation peu importante entre grains limoneux (Barden *et al.* 1973, Pereira *et al.* 2008) ;
- une sensibilité à l'humidification : dès qu'un dépôt de lœss est sec, sa résistance est plus importante, mais suite à une saturation subite sous charge, le sol peut perdre sa stabilité et s'effondrer (Mitchell et Soga 2005, Hormdee 2008).

Différents auteurs ont proposé des études expérimentales afin d'analyser l'effondrement des dépôts lœssiques dans de nombreux sites dans le monde par le biais d'essais d'effondrement à l'oedomètre (Jennings et Knight 1957, Cui et Marcial 2003, Nouaouria 2008, Whithall et Duffy 2008), de tests de caractérisation du risque d'effondrement (Hormdee 2008, Meier 2008, Punrattanasin 2008, Whithall et Duffy 2008), de la caractérisation microscopique (Cui

et Marcial 2003, Meier 2008) et d'essais plus sophistiqués comme l'essai triaxial statique (Shao *et al.* 2007) ou des essais triaxiaux cycliques (Karam 2006).

Karam (2006) a effectué des essais de chargement triaxial cyclique sur un profil de lœss prélevé à quatre profondeurs différentes (1,2 m ; 2,2 m ; 3,5 m et 4,9 m) dans un site proche de la ligne nord du TGV à Beugnâtre, en France. Il a observé le phénomène de liquéfaction dû au chargement cyclique sur des échantillons saturés, provenant de toutes les profondeurs étudiées. De plus, il a observé que le sol à 2,20 m a le taux de résistance cyclique (τ_{cyc}/σ'_c) le plus faible, de l'ordre de 0,3, qui est inférieur au taux de chargement cyclique appliqué par le train, qui est de 0,4, ce qui signifie que si le sol à 2,20 m se trouve dans un état saturé, la fréquence de circulation normale du TGV nord suffit pour le liquéfier. Mitchell et Soga (2005) ont remarqué la possibilité de liquéfaction des dépôts saturés de lœss pendant des tremblements de terre.

Jennings et Knight (1957) ont proposé le "test du double oedomètre" pour étudier le risque d'effondrement des sols non saturés. Celui-ci est basé sur deux types d'essais oedométriques. Le premier test est réalisé à la teneur en eau initiale en condition non saturée. Pour le deuxième, on humidifie l'échantillon sous une charge fixe et on suit le chargement en condition saturée. Dans certains cas, l'humidification du sol produit des changements importants du volume total. Ce processus implique une perte de la résistance du sol, car pour la plupart des sols non saturés, la résistance augmente lorsque le niveau de saturation diminue et la valeur de succion augmente. Matyas et Radhakrisna (1968) ont élargi les essais à différents niveaux de succion en observant des comportements similaires sur des échantillons de limon compacté.

Knight (1963) a proposé une méthode pour analyser le risque d'effondrement basée sur l'humidification sous une contrainte verticale de 200 kPa d'un échantillon de sol préalablement chargé à sa teneur en eau naturelle. Le critère est basé sur le pourcentage de déformation verticale obtenu. La susceptibilité à l'effondrement est présentée dans le Tableau 1-4.

D'autres méthodes pour analyser la susceptibilité à l'effondrement ont été développées par divers auteurs à partir des propriétés géotechniques de base. Gibbs et Bara (1962) ont proposé un critère basé sur les valeurs de la masse volumique sèche ρ_d et de la limite de liquidité w_L . D'après ce concept, les sols ayant une densité faible et une limite de liquidité basse sont

susceptibles de s'effondrer. Ce concept est présenté dans la Figure 1-18. Huergo *et al.* (1989) ont présenté divers critères d'évaluation de l'effondrement. Ils sont décrits dans le Tableau 1-5.

Déformation d'effondrement (%) sous $\sigma_v = 200$ kPa	Risque
0 – 1	Non Effondrable
1 – 5	Légèrement Effondrable
5 – 10	Effondrable
10 – 20	Très Effondrable

Tableau 1-4. Critère de Knight (1963)

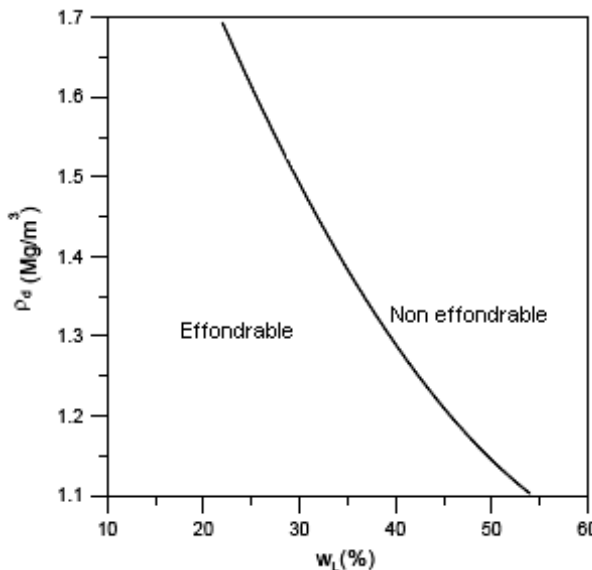


Figure 1-18. Critère d'évaluation du risque d'effondrement proposé par Gibbs et Bara (1962)

Auteur	Critère	Expression
Denisov (1951)	$K_e < 0,75$	$K_e = \frac{e_{(w_L)}}{e_{nat}}$
Prikłonskij (1952)	$w_p - w_{nat} < 0$	
Feda (1966)	$K_L > 0,85$ et $S_{r(nat)} > 0,6$	$K_L = \frac{(w_{nat}/S_{r(nat)}) - w_p}{I_p}$
Stephanokk et Kremakova (1960)	Estimation quantitative de l'effondrement	$\delta = K(n - 40)(30 - w_{nat})$, où : $K = 0,08$ pour lœss argileux ; $K = 0,05$ pour lœss avec une faible fraction d'argile

$e_{(w_L)}$: indice des vides correspondant à la limite de liquidité ; e_{nat} : indice naturel des vides ;
 w_p : limite de plasticité ; w_{nat} : teneur naturelle en eau ; $S_{r(nat)}$: degré naturel de saturation ;
 I_p : indice de plasticité ; n : porosité

Tableau 1-5. Critères d'évaluation du risque d'effondrement

1.4.2 Caractéristiques de la structure

Le sol, généralement assimilé à un milieu continu lorsqu'il est étudié à l'échelle macroscopique, est composé de trois phases : l'air, l'eau et la phase solide constituée de particules de tailles variables. La résistance, la perméabilité et la compressibilité du sol sont étroitement liées à la taille et la forme des particules, à leur organisation et aux forces agissant entre elles. Le terme anglais *fabric* est défini comme l'assemblage des particules individuelles, des groupes de particules et du milieu poreux. Quand on considère également les forces inter particulières (forces d'interaction physico-chimiques dont la cohésion apparente, la frottement, la dilatance, la cémentation ou l'endurcissement dû à la succion), on parle de *structure* du sol (Mitchell et Soga 2005).

A partir d'observations au microscope électronique à balayage (MEB) sur des échantillons de *laess*, Cui *et al.* (2004), Delage *et al.* (2005), Yang *et al.* (2008) et Karam *et al.* (2009) ont remarqué que la structure est composée d'agrégations argileuses avec un assemblage principal de grains limoneux (environ 20 – 30 µm de diamètre). Cette organisation est irrégulière, car il y a des domaines dans lesquels les grains limoneux sont propres, c'est-à-dire sans présence d'argile. De cette façon, l'effondrement pourrait être dû à la présence de domaines avec une structure ouverte, pauvrement cimentée et avec de grands pores (environ 20 µm de diamètre moyenne).

D'après Dudley (1970), les grains de limon sont assemblés avec des matériaux de contact, tels que l'argile, ou avec des forces de liaison importantes dues à la succion ou à la cimentation. Lorsque le phénomène d'humidification se produit, les matériaux de contact absorberont de l'eau, menant à leur affaiblissement mécanique car la succion dans les matériaux de contact va diminuer (éventuellement jusqu'à zéro). Néanmoins, l'effondrement peut être dû aussi à la rupture des liaisons cimentées, lesquelles peuvent être affaiblies par l'humidification et brisées si la contrainte mécanique est suffisamment grande.

Chapitre 2. Propriétés de rétention d'eau

Table de matière

2.1	Introduction	51
2.2	La courbe de rétention d'eau	52
	Article 1. The water retention properties of a natural unsaturated loess from Northern France	54
	Introduction	54
	Results and discussions	62
	Conclusions	76
2.3	Effet des cycles d'humidification et de séchage sur la microstructure	82
	Article 2. A microstructure analysis of the hysteresis of the water retention curve of a natural loess	84
	Introduction	84
	Tested material, equipment and procedures	85
	Tests results	88
	Discussion	96
	Multiscale modelling of the water retention curve.....	98
	Conclusions	106

2.1 Introduction

Les propriétés de rétention d'eau peuvent être analysées par des méthodes expérimentales de contrôle ou de mesure de la succion. Dans ce travail, on a utilisé deux techniques de *mesure* de la succion : la méthode du papier filtre et le tensiomètre de haute capacité développé au laboratoire CERMES et décrit dans Mantho (2005) et Cui *et al.* (2008). Les mesures ont été faites sur des échantillons intacts du lœss de Bapaume, extraites manuellement sous la forme de blocs, lesquels ont été soigneusement encaissées dans de boîtes plastiques, couverts par une couche de paraffine et finalement enveloppés avec de film plastique. Ceci a été fait afin d'éviter l'évaporation et ainsi de changements indésirables dans l'état hydrique in-situ.. A l'issu des nombreuses mesures de la succion obtenues à travers de plusieurs cycles de séchage - remouillage, on a obtenu la courbe de rétention d'eau du lœss. La description des techniques expérimentales ainsi que l'analyse de la courbe de rétention d'eau à partir des études

préliminaires de la microstructure (porosimétrie par intrusion de mercure, observations au microscope électronique à balayage) constituent la *première partie* du chapitre. Cette étude a été publiée dans la revue *Géotechnique*, l'article étant reproduit ici dans sa version originale en anglais.

Une analyse plus approfondie de la relation entre les propriétés de rétention d'eau et la microstructure du lœss est exposée dans la *deuxième partie* du chapitre. Cette seconde partie correspond à un article en anglais prêt à soumettre dans un journal international. Cette étude est basée sur des observations microstructurales réalisées sur des échantillons intacts de lœss, extraits à différents points d'une trajectoire de séchage -remouillage et à différentes teneurs en eau. Les résultats de ces analyses ont permis de proposer une approche théorique permettant de modéliser les branches de séchage et humidification de la courbe de rétention d'eau. Cette approche est basée sur le modèle d'hystérésis proposé par Rojas et Rojas (2005).

2.2 La courbe de rétention d'eau

L'étude des propriétés de rétention d'eau du lœss de Bapaume fait suite aux problèmes de tassement des dépôts de fondation de la ligne à grande vitesse (LGV Nord), observés lors de périodes de pluie intense. De nombreuses mesures de succion ont été faites à l'aide de la méthode de papier filtre et d'un tensiomètre de haute capacité, développé lors de précédents travaux au laboratoire UR Navier – CERMES. Ces mesures ont permis de caractériser la *courbe de rétention d'eau* du loess de Bapaume. Du point de vue des méthodes expérimentales, et de la méthode du papier filtre en particulier, les résultats montrent qu'une méthode alternative, proposée par Parcevaux (1980) et consistant à utiliser une pièce de papier filtre initialement humidifiée, peut être mise en œuvre avec des résultats comparables à ceux obtenus par la méthode classique du papier filtre (standardisée par l'ASTM (2003)) et ceux mesurés par le tensiomètre de haute capacité.

La courbe de rétention d'eau obtenue montre une forme particulière, caractérisée par l'absence d'hystérésis autour de la teneur en eau naturelle ($w = 14.4\%$) et par deux boucles d'hystérésis de part et d'autre de la teneur en eau naturelle. On suppose que cette zone sans hystérésis correspond à la plage des variations naturelles de la teneur en eau liées aux changements saisonniers et correspondant à une gamme de succions naturelles variant entre 20 et 80 kPa, bien que ceci doive être vérifié par des mesures in-situ. On a étudié la

microstructure du lœss à partir d'observations au microscope électronique à balayage et de porosimétries par intrusion de mercure. La fraction argileuse (16%) semble être distribuée de façon hétérogène, avec notamment des zones composées de grains de limon propres et d'un réseau de pores intergranulaires bien hiérarchisé. A contrario, les agrégats argileux sont caractérisés par de pores de plus petite taille.

D'après la courbe de rétention calculée à partir de la courbe porosimétrique (obtenue par intrusion de mercure), on observe que les propriétés de rétention d'eau sont principalement gouvernée par des phénomènes capillaires dans les plus grands pores, tandis que les phénomènes d'adsorption dans les argiles deviennent plus importants dans les plus petits pores. Il semble que cette dernière zone soit plus sensible à des changements de teneur en eau.

Certains aspects de la microstructure et leurs relations avec les propriétés de rétention d'eau pourraient être utilisés dans la modélisation de la courbe de rétention d'eau du lœss. Cela devrait inclure:

- i) les effets indépendants (1) des pores intergranulaires et inter-agrégats et (2) des pores intra-agrégats dans la fraction argileuse ;
- ii) les changements de la microstructure pendant les cycles d'humidification et séchage, ou, plus largement, lors de changements hydromécaniques ;
- iii) les mécanismes qui contrôlent le transfert d'eau à travers les réseaux complexes de pores qui caractérisent les sols naturels.

Ces études ont été publiées dans un article dans la revue *Géotechnique*, qu'on présente ensuite dans sa version originale en anglais.

Muñoz-Castelblanco, J., Pereira, J.M., Delage, P. & Cui Y.J. (2011). *Géotechnique* (Accepted for publication)

The water retention properties of a natural unsaturated loess from Northern France

J. A. Muñoz-Castelblanco*, J. M. Pereira¹, P. Delage* and Y. J. Cui*

The water retention properties of a natural loess from Northern France were investigated on intact block samples that were excavated along a high speed train line (TGV) that experienced stability problems during heavy rain episodes. Suction measurements were made by using the filter paper method and an in-house constructed high capacity tensiometer (HCT) so as to determine the water retention curve of the loess. The results showed that an alternative approach using a previously wetted filter paper could fruitfully be used with suction values reasonably compatible with the HCT measurements.

The water retention curve obtained exhibited a peculiar form with no hysteresis observed around the natural water content (14.4%) and two hysteresis loops on both the wet and dry sides of the curve. It is hypothesized that this zone with no hysteresis corresponds to the natural variations of the water content under seasonal changes, providing a range of natural suction between 20 and 80 KPa and noted that this should be checked by in-situ measurements. The loess microstructure was investigated by using scanning electron microscope and mercury intrusion porosimetry. It appeared that the clay fraction (16%) was not uniformly distributed with some areas composed of clean grains and a well graded corresponding inter-grains pore population. Conversely, the clay aggregations define a smaller sized porosity. The calculation of a water retention curve derived from the pore size distribution curve showed that water retention is governed by capillarity in the largest pores between clean grains whereas clay adsorption becomes dominant in smallest pores, a zone where the microstructure is sensitive to change in water content.

KEYWORDS: Loess; water retention; microstructure

Introduction

Widespread aeolian loess deposits are located in Northern France (Antoine *et al.* 2003, Cui *et al.* 2004, Delage *et al.* 2005). In most areas, they are naturally unsaturated and characterised by satisfactory geotechnical properties with no particular problematic behaviour. In some areas however, some layers of loess are characterised by a significant calcareous content, a higher porosity and a low plasticity. These features lead to a metastable structure that is strengthened by suction when the soil is partially saturated. Subsequent soil saturation may thus induce a loss of stability of the structure with relatively large volumetric deformations due to the collapse of the open structure of the soil. This collapse behaviour of loose unsaturated soils has been observed by many authors including Barden *et al.* (1973), Yudhbir

* Ecole des Ponts ParisTech, Laboratoire Navier – CERMES, Université Paris-Est

(1982), Alonso *et al.* (1987), Cui *et al.* (2004), Delage *et al.* (2005), Hormdee (2008), Punrattanasin (2008), Yuan and Wang (2009).

A geological survey of the area showed that collapsible loess layers are protected from the interactions with the atmosphere and from rain by shallow layers of higher clay content and density. Since the water table appears to be deep enough (more than 5m depth as observed during various excavation works), some of these deposits may remain unsaturated in spite of being located in a quite rainy region.

Stability problems must be considered when the collapsible layers become exposed to atmosphere and rain due to excavation. Up to now the main regions of concern have been met along the North line of the high speed train (TGV) that links Paris to Brussels and London, in cut areas where the line went through collapsible layers. Besides other reasons, like for instance the presence of remaining trenches from World War I in the Somme Battle region, the collapse susceptibility of loess is thought to be one of the reasons of some instabilities observed along the line and described in Cui *et al.* (1995).

In this paper, an investigation of the water retention properties of an unsaturated natural loess of Northern France is presented. This study is part of a wider on-going research program (Cui *et al.* 2004, Delage *et al.*, 2005, Yang *et al.*, 2008) on the hydro-mechanical behaviour of the loess that is conducted in collaboration with the French Railways company (SNCF).

In spite of the impressive interest towards unsaturated soils developed in the last decades, relatively few data on natural unsaturated soils have been published up to now. The data presented in this work aim at complementing existing data on the water retention properties of unsaturated soils by further investigating the peculiar hydraulic behaviour of this natural unsaturated loess.

Up to now, water retention properties have been more often investigated by using methods of controlling suction. Here, two methods of measuring suction, the filter paper method and the high capacity tensiometer (HCT), respectively, are used on intact samples in which the water content is varied. The filter paper method provides suction measurements between 0.01 and about 10 MPa whereas the suction range covered by HCT is between 0 and 1 MPa. The water retention curve obtained in this work is also interpreted by using microstructure data from scanning electron microscopy (SEM) and mercury intrusion pore size distribution measurements.

The loess of Northern France

Loess deposits in Northern France were formed under periglacial conditions during the Quaternary period (15 000– 25 000 years BP). At that time of low sea level that preceded ice melting, coastlines had a different shape than presently. The presence of a glacial front at the North-West of the area and the temperature and pressure gradients induced in the atmosphere above the ice mass resulted in constant and strong North-West winds, typical of cold and arid steppic climates (Antoine 2002, 2003). Winds eroded the ground exposed in the area, now corresponding to the Channel, close to the ice front and transported silt sized particles that were further deposited on the sedimentary deposits in widespread cover deposits. The thickness of loess deposit in the area ranges between 3 and 8 metres with a relative homogeneity. Loess deposits are homogenous in terms of composition and structure when considering a given horizon. However, these characteristics may vary with depth depending on the geological depositional conditions.

Figure 1 shows that the loess deposits are located along the Channel seashore from Normandy up to the Brussels area. They also include the Paris area where they are known under the term of “Limon des plateaux” (East of Paris). In most cases, loess deposits are unsaturated, a favourable condition in terms of agricultural potential that explains the prosperous wheat cultures that are found in the Eastern Paris area. The Orly and Roissy CDG airports, respectively south and north of Paris, are also located on loess deposits (Audric 1973).

As commented above, some loess layers are characterised by a low plasticity, a high porosity, a high calcareous content and an open structure that might give rise to collapse under wetting. These collapsible layers can be found in particular close to the city of Amiens in the Picardie region.

As quoted from Pecsi (1990) in Antoine (2002), “loess is not only dust accumulation”. Diagenetic transformation includes clay illuviation from the surface that explains the higher density and plasticity and the lower permeability of the surface layer (about 20 cm in depth from the surface) that protects lower layers from rain water infiltration. Aeolian deposits are also affected by the subsequent chemical dissolution/re-precipitation of primary calcareous particles that change into a cementing agent. In this regard, the loess considered here falls into the category of cemented unsaturated soils with inter-grains bonding due to the combined action of calcareous cement and clay bonding. Whereas clay bonding is directly affected by

changes in water content and suction, changes in calcareous bonding with suction is probably less significant. This combined effect has been investigated by various researchers including the theoretical considerations of Gens and Nova (1993) and the experimental investigations carried out on artificial soils by Leroueil and Barbosa (2000) and Koliji *et al.* (2010).

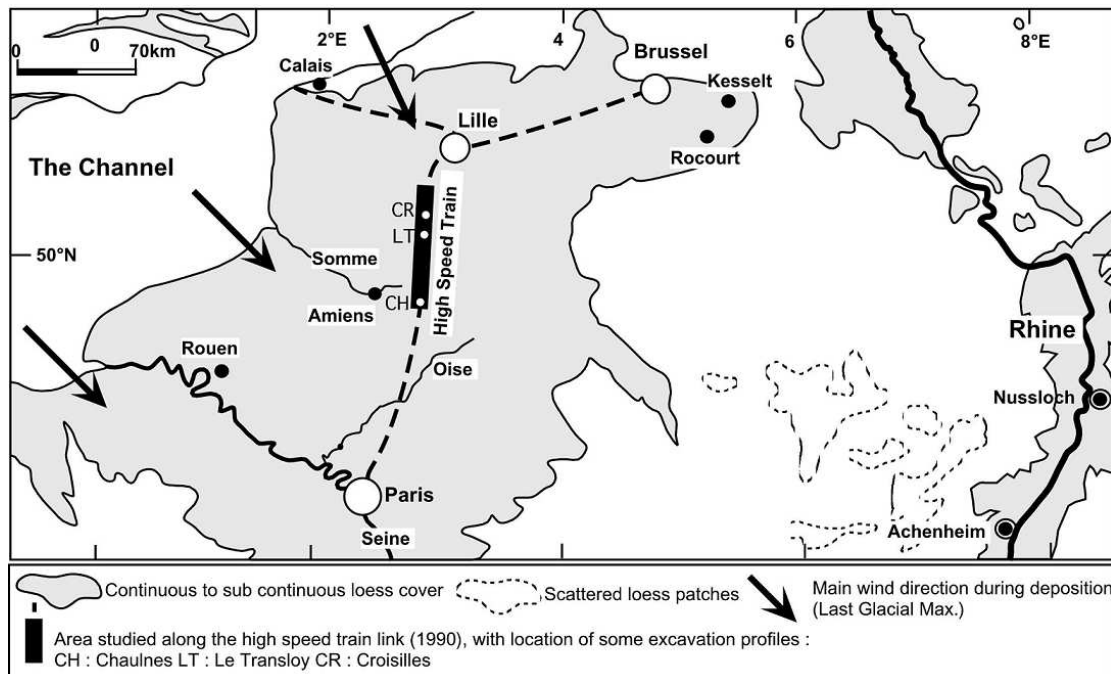


Figure 1. Extension of the Last Glacial loess in Northern France (after Antoine 2002)

To obtain good quality specimens in a rather fragile material, intact block samples have been manually extracted using plastic cubic boxes of 300 mm side at different depths from a 5 m excavation in the area of Bapaume (Picardie). The geotechnical profile of the excavation is presented in Table 1. One can observe that the plasticity index is constant along the profile and equal to 9. Upper layers are unsaturated (layer 1: $S_r = 0.44$ at depth 1m, and layer 2: $S_r = 0.50$ at depth 2.1 m) compared to deeper layers that are closer to saturation. Layer 1 (1 m) is the loosest one ($e = 0.85$, $w = 14.4\%$, $S_r = 44\%$, 6% carbonate content) and layer 2 (2.1 m) has the highest calcareous content (9%). It is worth noting that, since the samples have been extracted at the end of the summer period, the water content and degree of saturation of the samples should correspond to relatively low values with respect to natural cycling changes. According to Cui *et al.* (2008) who monitored in situ suction and water content variations of a "Limons des plateaux" (an aeolian silt from same origin) located near Paris, shallow layers (upper than 50cm depth) experienced suction changes between 10 kPa (during winter) and 200 kPa (during summer). Since this study concerns deeper layers protected by more clayey top layers, smaller suction variations are expected. The initial water content ($w = 14.4\%$)

value at 1m depth should be smaller than the annual average value and the suction value (40 kPa) close to the upper boundary.

No.	Depth (m)	w_0 (%)	S_{r0}	ρ_s (Mg/m ³)	e_0	w_L (%)	I_P	CaCO ₃ (%)	Clay content (%)
1	1.0	14.4	0.44	2.67	0.85	28	9	6	16
2	2.1	14.9	0.50	2.68	0.79	30	9	9	18
3	3.3	21.2	0.91	2.66	0.63	30	9	5	25
4	4.7	20.4	0.87	2.66	0.60	30	9	5	25

Table 1. Geotechnical profile of the loess deposit

The samples investigated here come from layer 1 that present the highest collapse potential. The grain size distribution of the sample investigated is given in Figure 2. The sand, silt and clay fractions are equal to 2, 82 and 16% respectively. The dominant clay minerals are kaolinite, illite and interstratified illite-smectite (Karam 2006). The Casagrande classification of the loess is CL.

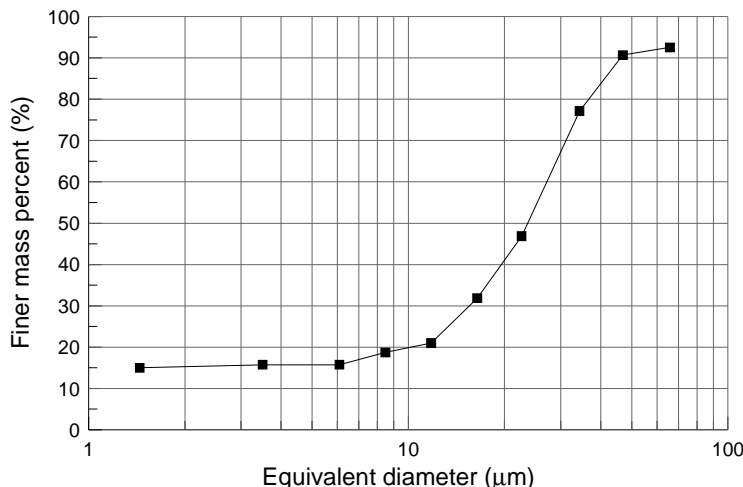


Figure 2. Grain size distribution of the loess from Bapaume (France)

Filter paper measurements

The filter paper method, developed several decades ago by Gardner (1937) to measure soil suction over a wide range, has been further investigated and used by many researchers (including Fawcett and Collis-George 1967, McQueen and Miller 1968, Al Khafaf and Hanks 1974, Hamblin 1981, Chandler and Gutierrez 1986, Houston *et al.* 1994, Swarbrick 1995, Bulut *et al.* 2002) prior to be standardized by the ASTM (2003, D 5298-03). Recent contributions also include papers by Patrick *et al.* (2007) and Kenton *et al.* (2008).

Parcevaux (1980) proposed an approach based on using an initially wet filter paper and provided the corresponding calibration curve. Since the “dry” approach (initially dry paper)

recommended by ASTM and the “wet” one start from different initial water contents, hysteretic effects in the filter paper calibration curve are to be considered, as done by Leong *et al.* (2002) based on the compilation of data by several researchers (Fawcett and Collis-George 1967, Hamblin 1981, Greacen *et al.* 1987, Ridley 1995, Harrison and Blight 1998).

The equilibration time of both methods might be different when considering either a drying or a wetting process since the water infiltration rate depends on the permeability to liquid water that is largely influenced by the degree of saturation of water (both in sample and paper). Equilibration time should also vary with the amount of water to be transferred to reach equilibrium and hence depend on the suction to measure.

Figure 3 presents a compilation of filter paper calibration curves obtained on the Whatman No. 42 filter paper by various authors using either drying or wetting processes. Data below 1 MPa (calibrated by techniques involving liquid transfers) concern matrix suction measurements whereas highest (total) suctions were determined with the vapour equilibrium technique. Quite a good agreement is observed between the data obtained independently by different authors with different techniques at different times. The data also provide a satisfactory insight into the hysteresis of the water retention curve of the filter paper.

In this work, a Whatman No. 42 filter paper was employed. The initial water content under ambient laboratory conditions of the Whatman No. 42 filter paper in original boxes is around $w = 6.0\%$ that corresponds to a suction of 29 MPa that is almost the upper limit for measuring suction with the method (Marinho and Oliveira 2006). The testing procedure adopted here is described below.

Tests were performed on specimens of 70 mm diameter and 19 mm height. Specimens were carefully cut to get a surface as planar as possible thus ensuring a good contact with the filter paper piece. With respect to the ASTM procedure, it was preferred to place a set of three circular pieces of filter paper of 50 mm diameter between two pieces of soil so as to allow drainage on both faces of the paper and to ensure faster water transfer and better contact. The central piece of filter paper was cut smaller than the two other ones so as to keep it clean with no perturbation of the water mass measurement that would be caused by soil fragments. The overall set was then covered with paraffin wax, enveloped in a plastic film to avoid evaporation during the equilibration time and put in an insulated plastic box so as to reduce any temperature perturbation. After seven days, the set was opened, both soil samples and the

central piece of filter paper were carefully weighed with a high precision balance (1/10 000 g). Weighing was as quick as possible to minimize evaporation. Finally, suction was calculated from the filter paper water content using the appropriate calibration curve, depending upon the initial state of the filter paper.

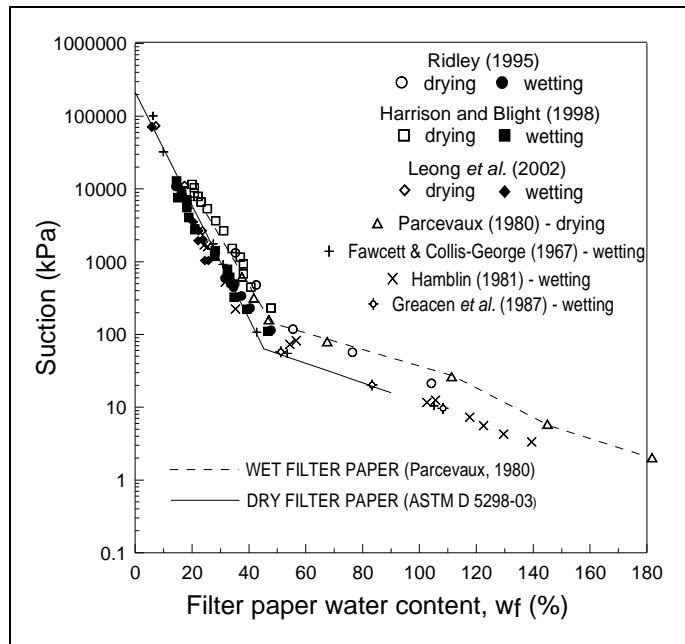


Figure 3. Calibration curves of Whatman No. 42 filter paper

Suction measurements were performed by using both the dry and wet filter paper methods to compare obtained values and equilibration times. Equilibration was monitored by weighing the filter paper at various periods of time varying from 1 to 12 days.

Samples were prepared starting from the natural water content ($w = 14.4\%$) after either drying or wetting stages. Drying was performed by allowing evaporation of the sample under laboratory conditions for periods of time comprised between 1 and 4 hours. Wetting was achieved by adding small quantities of water to the soil sample. To do so, a piece of filter paper was placed on top of the sample and water drops were uniformly distributed over the surface using a syringe in order to ensure homogeneous wetting. Once the target water content was reached, a new filter paper was placed and the measurement was restarted. Target water contents were checked by weighing the samples while minimizing evaporation. The time period necessary to ensure a uniform water distribution within the sample has been estimated by using tensiometer measurements. Once suction was stabilized, water was assumed to be uniformly distributed within the soil matrix. The maximum equilibration time was estimated to 4 hours for both drying and wetting processes. The target values of water content were the following: $w = 23.8, 13.3, 7.9$ and 7.2% .

The high capacity tensiometer

Suction measurements by an in-house constructed high capacity tensiometer (CERMES HCT) based on the principle proposed by Ridley and Burland (1993, 1995) and already described in Manthro (2005) and Cui *et al.* (2008) were compared to those obtained by the filter paper technique. The suction values obtained by both methods were then used to determine the water retention curve of the loess. As seen in Figure 4, the CERMES HCT is an integral strain gauge tensiometer (Tarantino 2004, Delage *et al.* 2008) composed of a porous high air entry value (1.5 MPa) ceramic disk with strain gauges glued to a metallic diaphragm and a water reservoir of 0.1 mm thickness. The HCT allows suction measurements ranging from 0 to about 1 MPa. As suggested by Tarantino and Mongiovi (2001), the HCT has first been saturated at a 4 MPa positive water pressure to get rid of any air trapped in the system. Manthro (2005) proposed to resubmit the tensiometer to a water pressure of 2 MPa after each cavitation of the water contained in the tensiometer reservoir. Performing such cycles of cavitation – saturation is suggested to improve the tensiometer performance in terms of range of measurement (Manthro, 2005) and measurement duration (Tarantino and Mongiovi 2001).

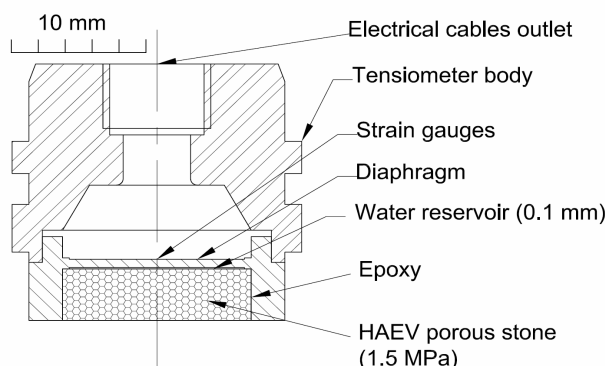


Figure 4. CERMES high capacity tensiometer (Cui *et al.* 2008)

As seen in Figure 5, the HCT was inserted in the base of a modified oedometer cell already used to perform oedometer compression tests with suction measurements (Delage *et al.* 2008, Tarantino and De Col 2008). The oedometer base was placed on a precision balance to register weight changes with time. A loess specimen of 70 mm diameter and 19 mm height was inserted into a metallic ring and placed over the oedometer base. In order to improve the contact between the tensiometer and the soil sample and thus to avoid early cavitation, a fine layer of slurry made from the tested soil was placed on the tensiometer surface. To the same aim, a vertical stress of 1.5 kPa corresponding to the piston weight has been applied to the sample. The vertical settlement induced by the piston is smaller than 0.04% and remains within the domain of elastic behaviour.

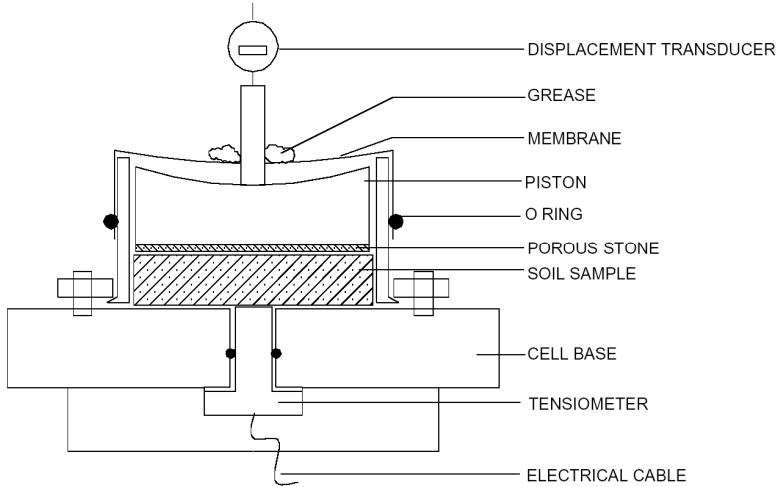


Figure 5. HCT measurement inside an oedometer cell (Delage *et al.* 2008)

Like in the filter paper test, the wetting process was carried out by removing the oedometer piston (loading-unloading cycles do not imply significant volume changes) and by carefully dropping, with a syringe, small amounts of water over a filter paper in contact with the upper face of the sample. Once the desired water content reached, the piston was placed back and a membrane was installed so as to avoid evaporation as shown in Figure 5. The drying process was performed by free drying after having removed the oedometer piston. Once the desired water content was reached (indicated by the balance measurement), water content equilibration was waited for after placement of both piston and membrane. After each change in water content, an equilibration time of 1 hour was waited for before measuring suction with the HCT.

Results and discussions

Filter paper measurements

Filter paper measurements were performed on four samples, starting from different water contents ($w = 23.8, 13.3, 7.9$ and 7.2%). Suction measures for both dry and wet filter paper methods are presented later together with the overall experimental data. As an illustration of the suction equilibration process between the sample and the filter paper, Figure 6 presents the evolution in suction measurement with time for the test corresponding to an initial water content $w = 13.3\%$. Each point corresponds to the measurement of the water content of the filter paper at a given time (between 1 and 12 days) once the contact between the filter paper and the soil has been ensured. After each weighing, a new filter paper was inserted into the soil sample to perform the subsequent measurement. In the dry method, the filter paper

extracted water from the soil whereas it released water to the soil in the wet method. The corresponding wetting or drying branch of the filter paper calibration curve (Figure 3) was used accordingly.

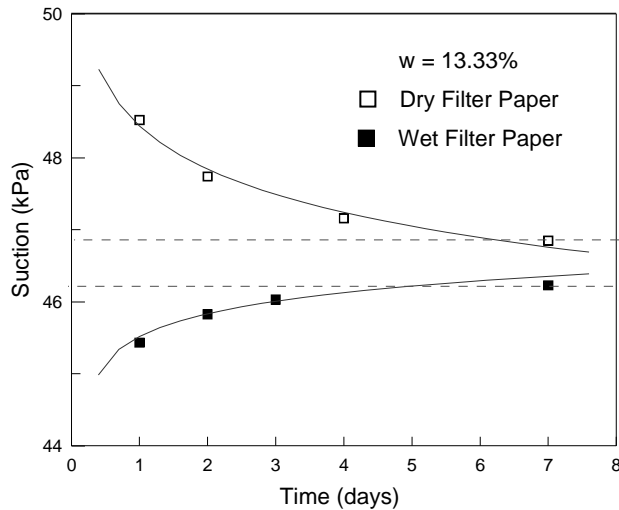


Figure 6. Evolution of suction measurement with time obtained by the filter paper techniques

Figure 6 shows that monotonic changes in water content are observed. The two curves tend to converge with a difference in final suction value around 0.5 kPa after 7 days, providing an average final value of 46.5 kPa. In all tests, water transfers tend to stabilize after a few days, generally before the seven days period recommended by ASTM.

An overall good agreement between the results obtained by the two protocols (wet and dry paper) is observed. It has also been checked that the water exchanges due to the presence of the filter paper itself had a negligible influence on the measured suction. This influence is estimated for all tests in Table 2 in which the ratio $\Delta M_w^{FP} / M_w^{soil}$ between the change of mass of water in the filter paper (ΔM_w^{FP}) and the total mass of water in the soil sample (M_w^{soil}) is given at all final water contents for both techniques. Obtained data shows that water exchanges are quite small, confirming that the filter paper does not significantly affect the hydric state of the sample. This confirms that both protocols provide comparable results in terms of measured values.

w_i (%)	Wet Filter Paper	Dry Filter Paper
23.8	0.74‰	2.04‰
13.33	2.86‰	1.93‰
7.88	9.89‰	2.58‰
7.19	10.02‰	2.15‰

Table 2. Ratio of water exchange between filter paper and soil

The water retention properties of the natural loess obtained with both dry and wet filter paper methods are presented in Figure 7 in a suction/water content diagram. The values of the degree of saturation are also presented in the top x axis under the hypothesis of no volume change, showing that a degree of saturation of 1 theoretically corresponds to a water content of $w = 31.8\%$. Since the degree of saturation under the lowest 3 kPa suction is $w = 26.5\%$, it is very probable that the sample is not fully saturated when put under zero suction by infiltrating liquid water. However, total saturation has not been possible since the material became very soft and difficult to handle in such conditions.

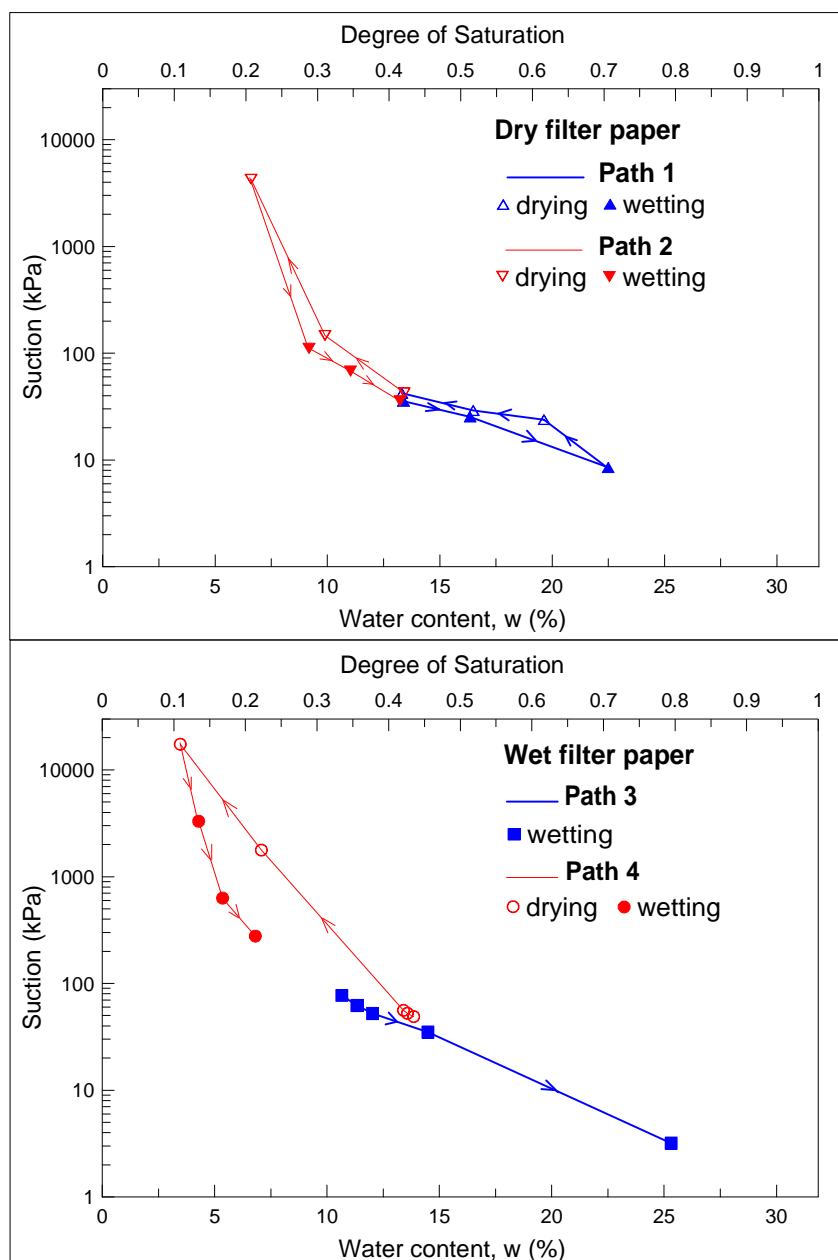


Figure 7. Hydraulic paths by the filter paper technique on Bapaume loess

The data presented in Figure 7a) were obtained along two hydric paths imposed to two distinct specimens starting from the same initial point ($w = 13.2\%$, $s = 35.8 \text{ kPa}$). A wetting path was imposed with values of water content successively equal to 16.5% and 22.5% (the last value corresponding to $s = 8.6 \text{ kPa}$ and $S_r = 0.71$). The specimen was subsequently dried at $w = 19.7\%$ ($s = 23.9 \text{ kPa}$, $S_r = 0.60$) and wetted back to a point that appeared to be very close to the initial one at $w = 13.3\%$ ($s = 42.2 \text{ kPa}$, $S_r = 0.41$). Whereas some hysteresis is observed above $w = 16.2\%$, hysteresis becomes quite slight between $w = 14$ and $w = 16\%$ with two close parallel sections of the water retention curve. Starting from the same initial point ($w = 13.4\%$, $s = 42.3$), another specimen was dried in 3 steps down to $w = 6.6\%$ ($s = 4250 \text{ kPa}$, $S_r = 0.20$) prior to be wetted back in 3 steps up to $w = 13.2\%$ ($s = 35.8 \text{ kPa}$, $S_r = 0.41$) to finally reach a point very close to the initial state. Again, a small hysteresis is observed along the cycle.

The data of the test carried out with the wet filter technique are presented in Figure 7b. A drying phase was imposed in two steps down to a water content $w = 3.5\%$ ($s = 17.3 \text{ MPa}$, $S_r = 0.11$) prior to rewetting the specimen in 3 steps up to $w = 6.8\%$ ($s = 277 \text{ kPa}$, $S_r = 0.21$), a point at which the test was ended. The other path starting by an unplanned drying phase down to $w = 10.8\%$ ($s = 78 \text{ kPa}$, $S_r = 0.33$) followed by a wetting phase up to $w = 25.6\%$ ($s = 3.2 \text{ kPa}$, $S_r = 0.79$). All the points obtained with both the dry and wet filter paper methods are presented in Figure 8. The figure shows excellent agreement between the results obtained by the two methods on 4 different samples, showing both the quality of the technique and the homogeneity of the samples.

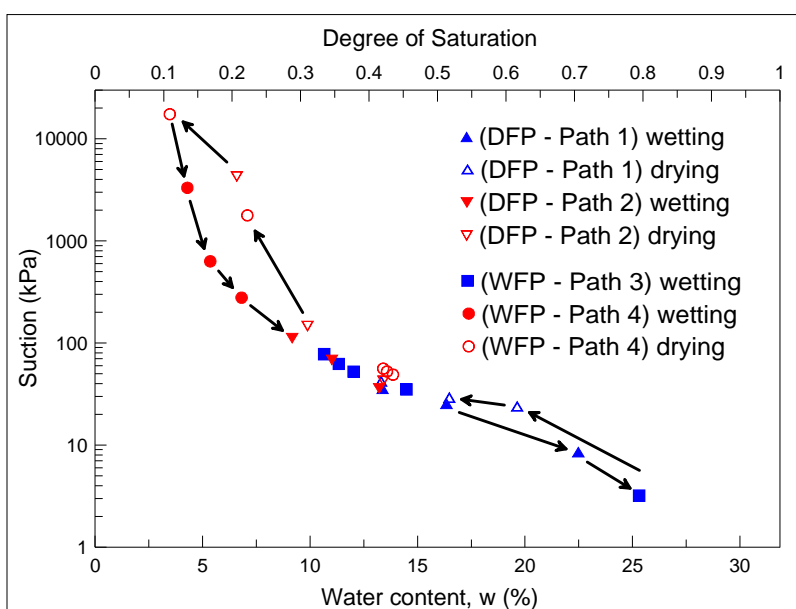


Figure 8. Summary of all the data obtained with both the wet and dry filter paper methods

HCT measurements

The water retention curve of the intact loess from Bapaume was obtained by performing various hydric paths and by measuring suction using on one hand the HCT and on the other hand the wet and the dry filter paper methods described above. Hydric paths were started from the natural loess water content of 14.2% that corresponds to an initial degree of saturation of 0.44 and a suction of 40 kPa as measured by the filter paper (wet or dry).

As commented above, HCT measurements were conducted in an oedometer cell (see Figure 5). Some examples of the response of the HCT with time along both a wetting (top) and a drying phase (bottom) are presented in Figure 9.

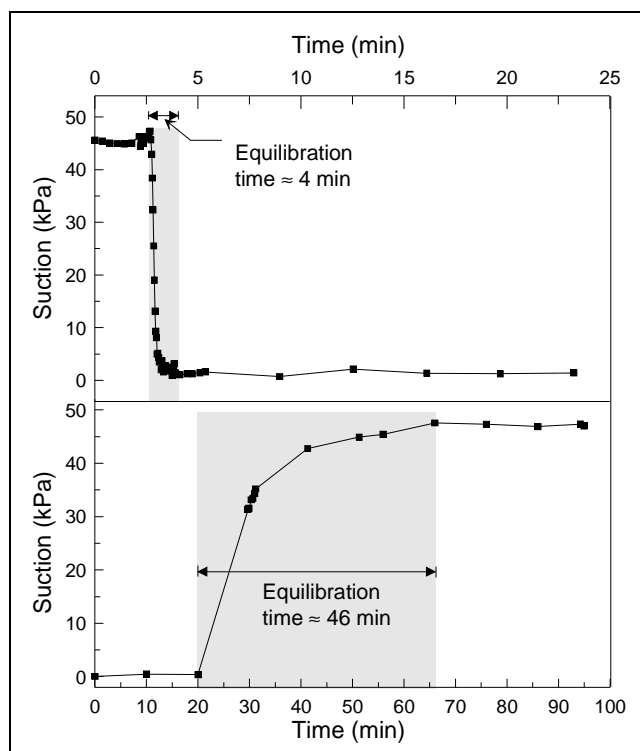


Figure 9. Response of the HCT with time for both a wetting (top) and a drying (bottom) path

HCT readings in the wetting phase (suction reduced from 45 kPa to 0 kPa) indicate that quite a short period of time comprised between 3 and 10 min was necessary to reach equilibrium. For a drying phase (suction increase from zero to 45 kPa), a longer period of time comprised between 30 mn and 1h was observed. Longer equilibration times were observed with higher suctions, in accordance with previous results in the literature (Ridley and Burland 1999, Delage *et al.* 2008). The difference in kinetics observed in Figure 9 is due to a faster liquid transfer in the case of wetting compared to phase change and vapour transfer (evaporation) in the case of drying. It also corresponds to the differences observed in permeability changes

during drying and wetting processes, favourable to faster equilibrium during wetting. Note that the wettest states obtained correspond to a water content $w = 27.0\%$ ($S_r = 0.84$) with a calculated water content at saturation equal to $w = 31.9\%$ (assuming a rigid skeleton). It indeed appeared practically impossible to wet samples at higher water content than 27.0% with the technique adopted here since further wetting made the samples quite soft, sticky and impossible to handle.

Four hydraulic paths (2 wetting and 2 drying paths) carried out on 4 distinct samples were performed using the HCT technique in the oedometer (Figure 10).

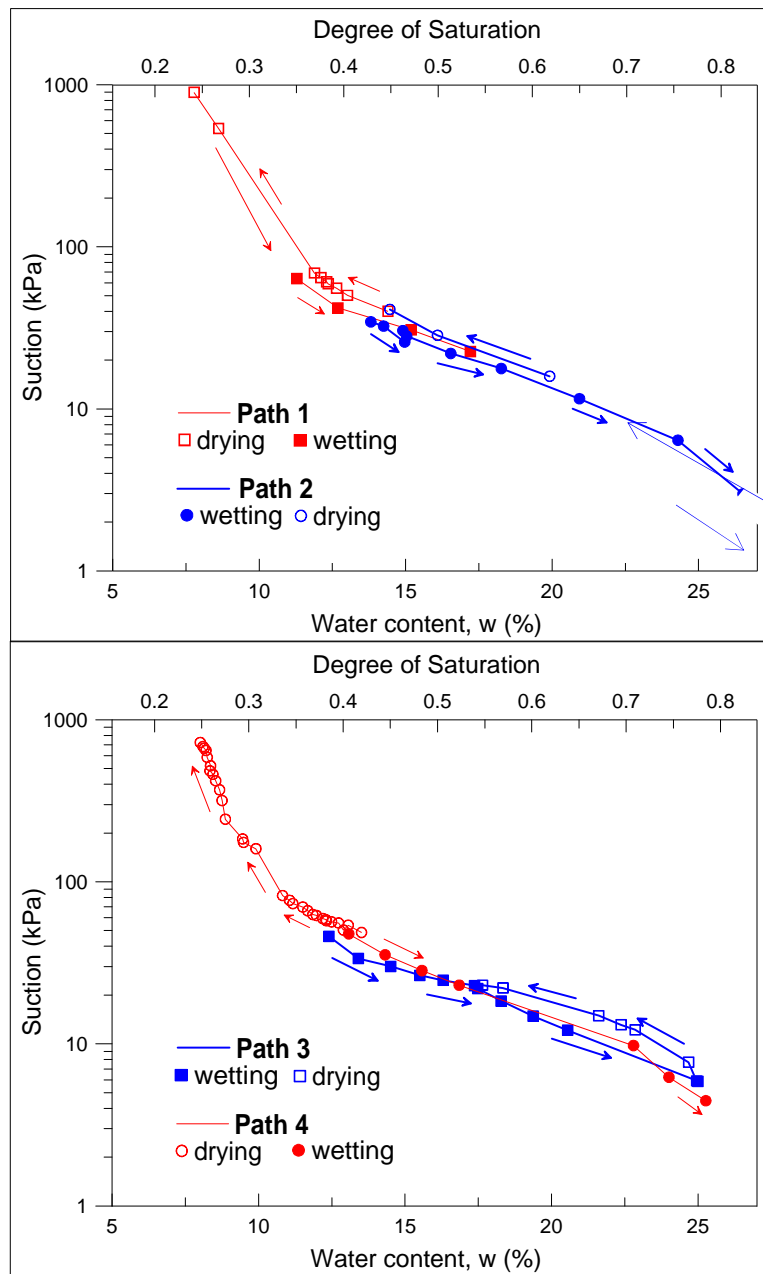


Figure 10. Hydraulic paths by the tensiometer on Bapaume loess

As seen in the figure, the maximum suction measured was equal to 898 kPa, a suction value at which the HCT satisfactorily behaved. An advantage of the technique is that there is neither any manipulation nor any weighing of the sample making it easier to obtain a large number of measurement points. The drying and wetting paths presented on top of Figure 10 (paths 1 and 2) again exhibit a rather slight hysteresis with parallel wetting and drying curves close one to the other, particularly in the area of the initial water content. A quite good correspondence is observed between the data that come from two distinct samples. Path 3 presented in the bottom graph exhibits a trend similar to the previous paths in the same area with a closed cycle ending at a point with $w = 14.5\%$ and $s = 23$ kPa. The wetting stage of path 4 also lies close to that obtained during path 3 on another sample.

Microstructural observation

The microstructure of the intact loess has been investigated by using both mercury intrusion pore size distribution (PSD) measurements and scanning electron microscope (SEM) observations. Both techniques must be carried out on dry samples. To preserve the microstructure during dehydration, samples were dehydrated by freeze drying (Delage et al. 1982). To ensure instantaneous freezing, small sticks were plunged in liquid nitrogen (-196°C) that was frozen down to its cooling point (-210°C) by applying vacuum to nitrogen prior to sample immersion (Delage et al. 2006). In such conditions, the heat quantity brought by the small soil sticks when plunged into nitrogen is not enough to heat nitrogen up to its boiling point. The water transfer occurs in liquid phase and is not slowed down by nitrogen bubbling as when directly plunging sample in liquid nitrogen. The heat transfer during freezing is instantaneous and generates amorphous ice with no volume expansion (Delage and Pellerin 1984).

Figure 11 presents the PSD curve of an intact sample of Bapaume loess in a diagram in which the intruded pore volume (y axis) is expressed in terms of a void ratio e_m , i.e. by using the ratio of the intruded volume divided by the volume of the solid phase (V_{Hg}/V_s). In the test presented, mercury intrusion was started at a pressure of 3.4 kPa (0.033 atm) quite below the atmospheric pressure, corresponding to an equivalent entrance pore diameter of 363 µm. Actually, the total volume of intruded mercury ($e_m = 0.70$) appeared to be smaller than the total pore volume of the sample determined in a standard way (void ratio $e = 0.85$). This difference may be due to the fact that, as seen by visual inspection, pores larger than 363 µm diameter exist in the loess. Since the clay fraction of the loess is small and based on previous

experience on Eastern Canada sensitive clays (Delage and Lefebvre 1984, Delage 2010), compacted low plasticity silt (Delage *et al.* 1996) and compacted kaolinite (Sridharan *et al.* 1971), it is believed that most of the pore volume is intruded when reaching the maximum mercury pressure (200 MPa) (soils that are not fully intruded by mercury at 200 MPa often contain a significant fraction of smectite as observed by Lloret *et al.* 2003 and Delage *et al.* 2006). This statement is also in agreement with the fact that the PSD curve becomes tangential to horizontal in the area of smallest pores whereas it remains inclined in that of largest pores, showing that pores with an entrance diameter larger than 0.363 mm probably exist. For this reason, the intrusion curve has been fitted with the total pore volume in the area of small pores.

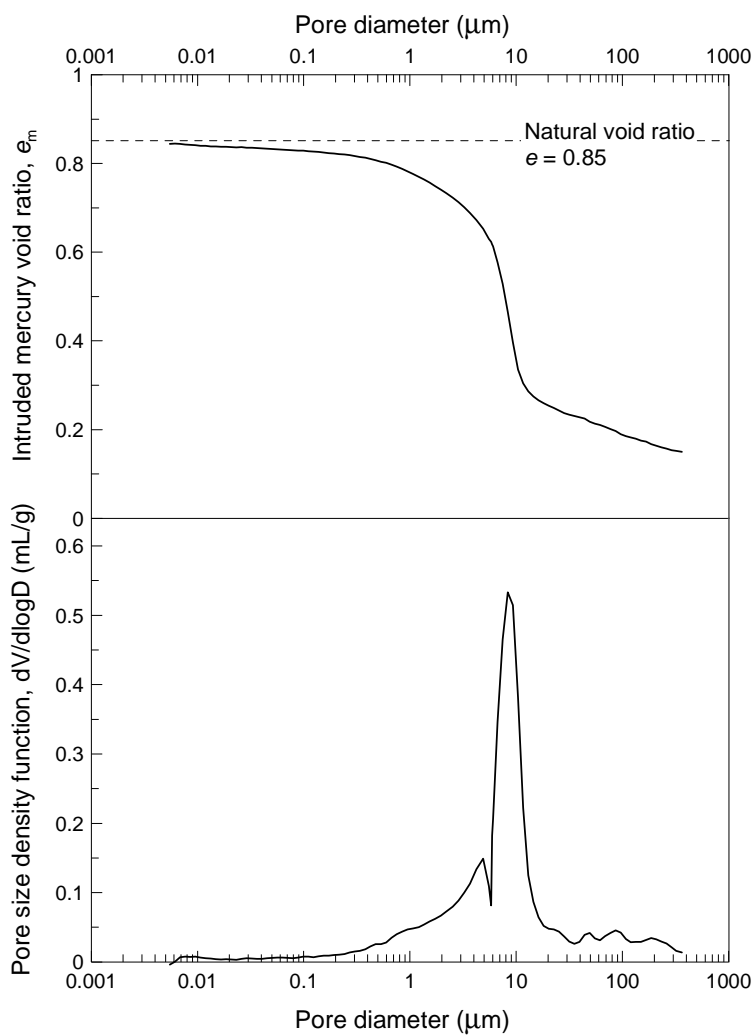


Figure 11. Pore size distribution of Bapaume loess

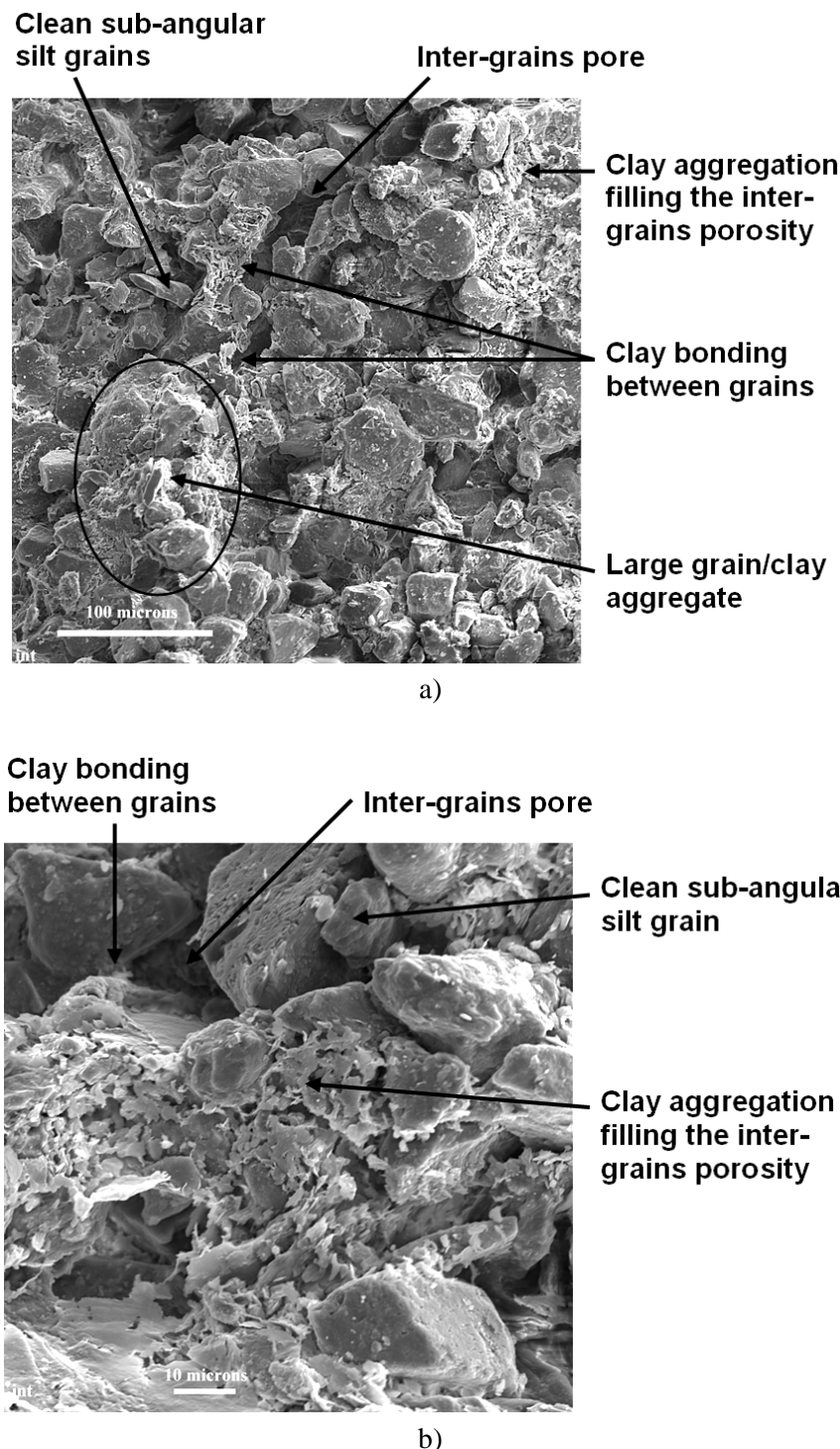
The data of Figure 11 show the existence of a main pore population with an average entrance diameter of 8.3 μm that represent 49% of the total porosity (if taken between 3 and 11 μm). Smaller pores correspond to 15%, whereas largest pores represent 36% of the total porosity.

The inclined linear section of the curve in the largest pores area indicates a poorly graded PSD, with some largest pores of 0.5 mm diameter that are visually observable, as commented before.

SEM observation was carried out on surfaces that were obtained by fracturing the frozen soil sticks prior to placing them under vacuum in the freeze dryer apparatus in which ice is sublimated (Delage *et al.* 1982). In such condition, the observation surface is not defined, as in ESEM, by any weakness plane of the wet soil microstructure and no deformation occurs when fracturing. The observation surface is plane indeed, well defined and it does cross the various levels of microstructure, allowing better observation. Examination of the SEM photos presented in Figure 12 at two magnitudes (see the bars giving lengths in micrometers) clearly show (Figure 12a, Figure 12c) a dominant proportion of subangular silt grains with diameters of several tens of micrometers. The figure also shows that the clay fraction is not regularly scattered among the grains. Whereas some grains are quite clean, some others appear to be strongly linked together by clay aggregations that seem to be firmly stuck to the grains. The figure also shows a “grain/clay aggregate” made up of various grains completely embedded in a clay matrix. Clay aggregations locally fill the inter-grains porosity. This is observed in more details in Figure 12b in which clay aggregations appear to be frankly cut by the freeze fractured observation plane. Here also, clean grains stuck together by clay aggregations (Figure 12d) are visible with also some clay bridges linking clean grains together. Observation of the SEM photos suggest that the resistance of the microstructure should not be homogeneous based on the irregular position of the clay aggregations. Clearly, collapse under wetting should occur by the densification of the areas where grains are clean with large pores around them. The zones in which the porosity is filled by clay aggregation should be more resistant and locally less sensitive to collapse.

SEM observations help to interpret the PSD curve of Figure 11 in more details. A large inter-aggregate pore with a diameter close to 100 μm that belongs to the poorly graded large pore population evidenced by the PSD curve of Figure 11 is observed in Figure 12c. Figure 12b shows an inter-grain pore of a diameter close to 10 μm , compatible with the main pore population with a 8.3 μm average diameter. Inspection of the clay aggregations (Figure 12b) shows that the largest intra-aggregate pores should be close to 1-2 μm , in accordance with the smallest pore population of Figure 11.

The process of mercury penetration can hence be described based on the SEM photos. In a first stage at lowest pressures, mercury penetrates the largest inter-grains porosity and embeds all clean grains prior to penetrate the smallest clay intra-aggregate porosity. Once the pressure corresponding to $2 - 3 \mu\text{m}$ is reached, the penetration of mercury in the clay aggregates starts.



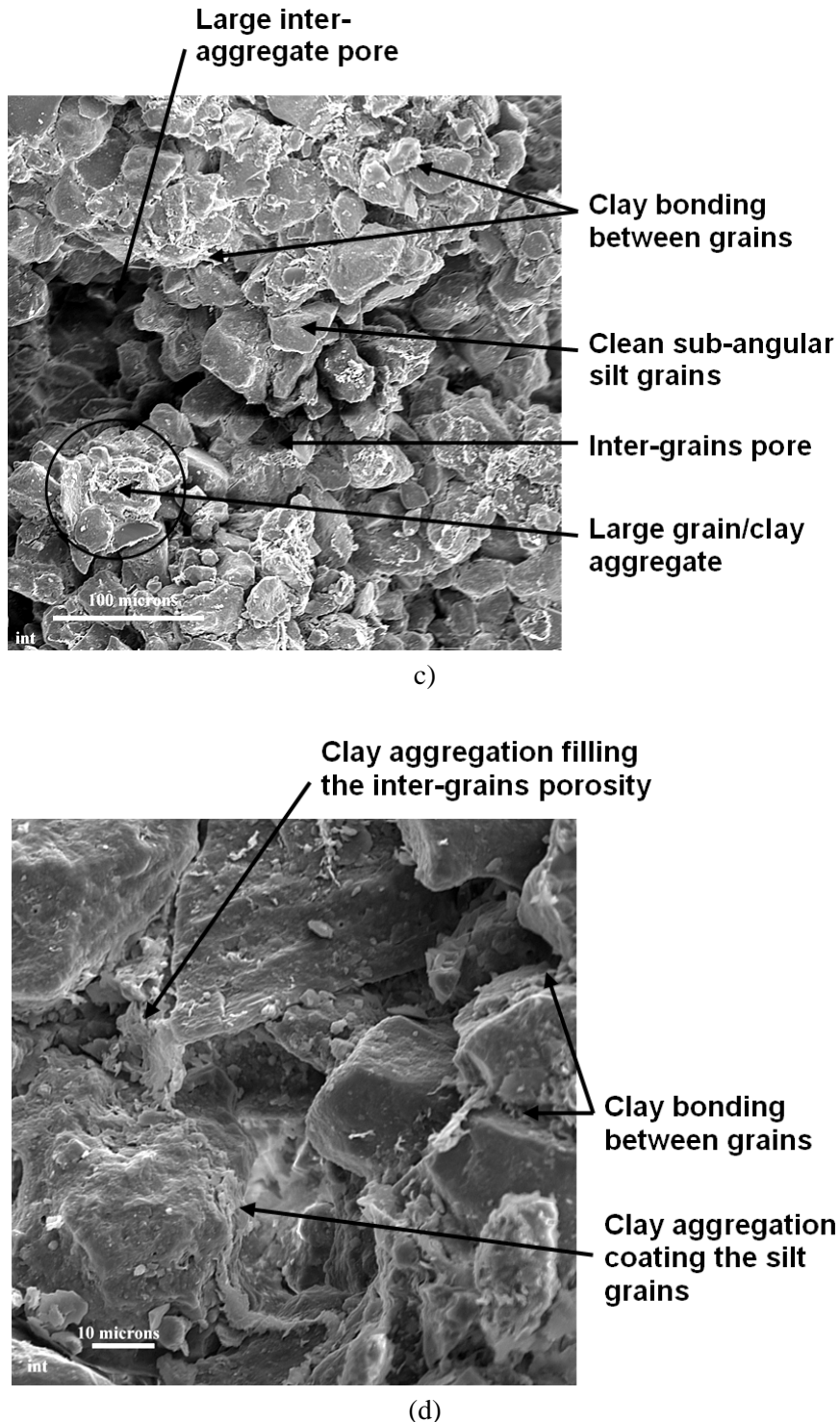


Figure 12. SEM observations of the Bapaume loess

Discussion

All data obtained with the two filter paper methods and the HCT technique are now plotted in Figure 13 together with a curve obtained from the PSD curve that will be further commented later. The filter paper measurements performed to study the changes in suction with time from different water contents ($w = 23.8, 13.3, 7.9$ and 7.2%) are also presented and referred to as

“DFP/WFP equilibration time data” (Dry Filter Paper/Wet Filter Paper). The data show a good global agreement between the various methods used on distinct samples. It confirms the validity and the quality of both suction measurements and highlights the homogeneity of the various samples tested. The results provide a detailed description of the water retention curve of the natural loess.

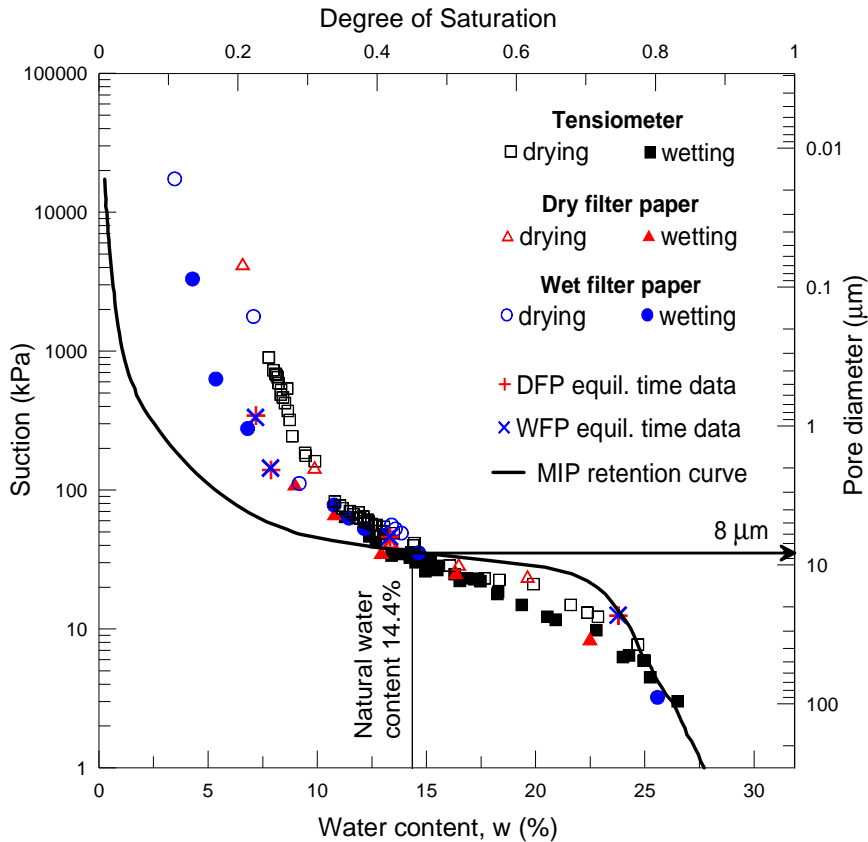


Figure 13. Retention curve of the intact loess from the different approaches used

Compared to existing published data in which the hysteresis of water retention curves (Hillel 1971, Pham *et al.* 2005) is clearly apparent (see for instance recent experimental data concerning natural soils from Konyai *et al.* 2006 in a saline sandy loam, Le *et al.* 2008 in Boom clay, Askarinejad *et al.* 2011 in a natural silty sand and Vasquez *et al.* 2011 in a red clay of high plasticity), the water retention curve obtained here exhibits a distinctive shape, with no apparent hysteresis observed in the area of the initial water content (between $w = 11.0$ and 16.0%). With an initial natural water content close to $w = 14.4\%$, one can conclude that little hysteresis affects the soil when submitted to change in water content imposed by climatic changes around this value. Under this hypothesis, water changes could be included between $w = 11.0\%$ in summer and $w = 16.0\%$ in winter with corresponding suctions of 20 and 80 kPa respectively. These ranges would of course need to be checked by direct in-situ

suction measurements. Conversely, hysteresis appears to be quite apparent on both the wet ($w > 16\%$) and dry ($w < 10\%$) sides of the curve.

It is well known that there are close links between the water retention curve of a soil and its pore size distribution, provided water-soil interactions in the soil are mainly governed by capillarity. Indeed, mercury intrusion porosimetry (MIP) is currently used in petroleum engineering to characterize more rapidly the capillary curve (another name of the water retention curve) of reservoir rocks like chalks or sandstones (with negligible clay fraction). In this regard, the mercury intrusion process, in which a non wetting fluid (liquid mercury) is penetrating a porous medium full of a wetting fluid (mercury vapour under vacuum) is assimilated to a drying process. In other words, the pore size distribution cumulative curve can be used to extrapolate a drying curve (see for instance Prapaharan *et al.* 1985, Delage *et al.* 1995, Romero 1999, Aung *et al.* 2001, Simms and Yanful 2001, 2002). To do so, one considers the Laplace's capillary equation applied to a capillary cylindrical tube (Jurin's law, sometimes called Wahsburn's equation) that is the base of MIP interpretation. Laplace's equation links the capillary pressure (difference in fluids pressure on both sides of a capillary meniscus) to the interfacial properties of the fluids-solid system together with the diameter of the cylindrical tube as follows:

$$u_{nw} - u_w = \frac{4T \cos \theta}{D} \quad \text{Eq. 1}$$

in which:

- u_{nw} and u_w are the pressure of the non wetting (mercury or air) and wetting (mercury vapour under vacuum or water) fluids respectively;
- T is the non-wetting–wetting surface tension (at 20°C, $T_w = 72.75 \times 10^{-3}$ N/m for air–water interface and $T_{Hg} = 485 \times 10^{-3}$ N/m for liquid mercury–vapour mercury interface);
- θ is the wetting fluid/solid contact angle (0° for water and 140° for mercury in clays according to Diamond 1970).

Under the hypothesis of a cylindrical shape, an indirect estimation of the pore diameter can hence be obtained through Laplace's equation with the two fluids/solid systems, giving:

$$D = \frac{4T_w}{(u_a - u_w)} = -\frac{4T_{Hg} \cos \theta}{(u_{Hg} - u_{VHg})} \quad \text{Eq. 2}$$

where u_{Hg} and u_{vHg} are the liquid mercury (non wetting fluid) and the vapour mercury (wetting fluid) pressures respectively. Matrix suction ($u_a - u_w$) can then be related to the mercury intrusion pressure ($u_{Hg} - u_{vHg}$) as follows:

$$u_a - u_w = -\frac{T_w}{T_{Hg} \cos \theta} (u_{Hg} - u_{vHg}) \approx 0.196 (u_{Hg} - u_{vHg}) \quad \text{Eq. 3}$$

A water retention curve can hence be extrapolated from the mercury intrusion curve by using Eq. 3.

The curve derived from the PSD curve plotted in Figure 13 (in which the entrance pore diameter from the MIP analysis are also plotted on the right y axis) significantly differs from the drying branch of the water retention curve, particularly in the area of small pores. However, it should be noticed that the curve is exactly passing through the point at natural state. The correspondence is also better in the zone of largest pores, with however a bend in the PSD derived curve that is not observed in the WRC curve.

The differences between the WRC and curves derived from PSD have been discussed in the literature and for instance Simms and Yanful (2001, 2002) mentioned the possible effects of the pore trapping effect (mercury intrusion only gives the entrance pore radius thus somewhat surestimating the porous volume associated to the estimated diameter). There are other reasons why the two curves should not be the same in soils containing some clay fraction whereas they compare favourably in granular soils and rocks. Mainly, the microstructure of the former is sensitive to changes in water content whereas the latter have a stable microstructure at all water contents. This stable microstructure governs in a constant way the response of both mercury intrusion and water drainage, giving comparable results. The WRC of a fine-grained soil results from a microstructure that changes with the water content changes whereas the PSD curve is obtained at the microstructure that corresponds to the water content at which it has been performed. In this regard, the good correspondence observed at natural water content in Figure 13 is interesting.

Under the hypothesis of having water located in the smaller pores due to both capillary action and water adsorption on clay particles, all pores located in pores with a diameter ($8 \mu\text{m}$) smaller than that corresponding to the natural water content (14.4%) should be saturated whereas pores of higher diameter should be dry. Referring to SEM observations, this means that the largest porosity between clean grains should be dry whereas the clay aggregations

should be water saturated. Then, the almost satisfactory correspondence observed on the right side of the drying curve concerns capillary effects in a dry granular assembly, compatible with observations in dry samples or sandstones.

On the left side of the natural water content, the significant difference between the curves concerns the saturated smaller porosity that is prone to significant microstructure changes under drying. On a compacted silt form the same aeolian origin, Delage *et al.* (1996) observed that drier samples were characterised by the coating of the clay particles along the grain surface, whereas in wetter samples, hydrated clay particles appeared to be quite more voluminous and able to fill the inter-grains pores. On the left side of the natural water content, the curve derived from the PSD curve indicates, at a given suction value, a significantly smaller water content (with only water capillary retention derived from the PSD of the microstructure at $w = 14.4\%$) than the real one (with capillarity and water adsorption in the clay aggregates observed in Figure 12, but in the shrunk configuration that they should have under the given suction). Under a suction of 1 MPa, the PSD derived curve indicates a water content close to $w = 1\%$ compared to $w = 7.5\%$ of water content remaining in the soil. The strong effect of clay water adsorption (with a 16% clay fraction) is compatible with the $w = 3.5\%$ water content that the soil is able to retain at a suction as high as 20 MPa (driest point obtained with the wet filter paper).

Conclusions

The water retention properties of a natural loess of Northern France have been investigated. This study is part of a wider research program on the hydro-mechanical behaviour of the loess of Northern France conducted with the French Railways company (SNCF) and devoted to the study of stability problems along the North high speed line in collapsible loess.

A high capacity tensiometer (HCT) and the filter paper method were used to obtain the water retention curve of the loess between 10 kPa to about 10 MPa with the filter paper and 0 to 1MPa with the HCT. The ASTM filter paper method that uses an initially dry filter paper has been complemented by an alternative method in which the filter paper is initially wet. The analysis of the drying branch of the water retention curve of the filter paper suggested that the wet filter paper method allowed to measure a wider range of soil suctions (between 2 kPa and about 10 MPa). The results confirmed that seven days were sufficient to reach equilibrium for both methods. A good agreement of the suction measurements obtained with the tensiometer

and the two filter paper methods was observed and a complete and coherent water retention curve could be obtained.

A microstructural analysis of the natural loess was performed based on Scanning Electron Microscopy and Mercury Intrusion Porosimetry. Both methods provided compatible results evidencing a well graded main pore population with an entrance diameter of around 8 µm that characterised the pores between the grains of loess. It was also observed that the 16% clay fraction was not heterogeneously distributed among the silt grains, with some local aggregations of grains and clay particles.

The shape of the water retention curve appeared to be somewhat specific with a central zone bordering the natural water content ($w = 14.4\%$) between $w = 11\%$ and 16% in which no hysteresis was observed. Two hysteretic loops were observed on the dry side ($w < 11\%$) and the wet side ($w > 16\%$). The section with no hysteresis is supposed to be related to the natural variations of the water content due to climatic changes. The corresponding estimated maximum and minimum suction values (20 and 80 kPa) that can be derived should of course be checked by in-situ direct tension measurements.

When comparing the drying path of the experimental WRC with a WRC derived from the PSD curve, a reasonable correspondence was observed at higher water contents in the large pore spaces existing between clean grains, confirming the predominance of capillary effects in this area of the WRC. Conversely, the correspondence was no longer observed at lower water contents and higher suctions, showing the effects of changes in microstructure occurring at the level of clay aggregations and the growing importance of the adsorption of water in the clay fraction at higher suctions.

Some of the microstructure features evidenced in this work in relation with the water retention properties of the loess could be used in further modelling the loess WRC. This could include for instance i) the separate roles played on the one hand by the inter-grains and inter-aggregate pores and on the other hand by the intra-aggregate pores inside the clay fraction; (ii) the changes in microstructure during the drying and wetting processes or, more largely, when submitted to hydro-mechanical changes and (iii) the mechanisms that control the water transfers within the complex pore networks that characterise natural soils.

Acknowledgments

The present study is part of the first author PhD work. It was mainly supported by the European Alþan Program of high level scholarships for Latin America (scholarship N° E07D402297CO), through grants to Mr. J. Muñoz. The complementary support of the French Railways Company SNCF is also acknowledged.

References

- Al-Khafaf S. and Hanks R.J. (1974). Evaluation of the Filter Paper Method for Estimating Soil Water Potential. *Soil Science* **117** (4). 200-204.
- Alonso E., Gens A. and Hight A. (1987). Special problems soils. General Report, *Proc. 9th European Conf. on Soil Mechanics and Foundation Engineering*, Dublin (3), Balkema. 1087-1146.
- Antoine P. (2002). Les loess en France et dans le Nord-Ouest européen. *Revue Française de Géotechnique* **99**. 3-21.
- Antoine P., Catt J. and Sommè J. (2003). The Loess and Coversands of Northern France and Southern England. *Journal of Quaternary Science* **18**. 309-318.
- Askarinejad A., Casini F., Kienzler P. and Springman S.M. (2011). Comparison between the in situ and laboratory water retention curves for a silty sand. In *Proc. 5th Int. Conf. on Unsaturated Soils*, Barcelona, CRC Press. 423-428.
- ASTM International. (2003). Standard Test Method for Measurement of Soil Potential (Suction) Using Filter Paper, D 5298-03. ©ASTM International.
- Audric T. (1973). Etude Géologique Et Geotechnique Des Limons De Plateau De La Region Parisienne. *Bulletin of Engineering Geology and the Environment* **8** (1). 49-59.
- Aung K.K., Rahardjo H., Leong E.C. and Toll D.G. (2001). Relationship between porosimetry measurement and soil-water characteristic curve for an unsaturated residual soil. *Geotechnical and Geological Engineering* **19**. 401-416.
- Barden L., Mc Gown A. and Collins K. (1973). The collapse mechanism in partly saturated soil. *Eng. Geol.* **7**. 49-60.
- Bulut R., Hineidi S.M. and Bailey B. (2002). Suction Measurements-Filter Paper and Chilled-Mirror Psychrometer. *Proceedings of the Texas Section of the American Society of Civil Engineers Fall 2002 Meeting*. Waco, TX., October 2-5, 2002.
- Chandler R.J. and Gutierrez, C.I. (1986). The filter-paper method of suction measurement. *Geotechnique* **36** (2). 265-268.
- Cui Y.J., Delage P., Durand F., Schlosser F. and Wojnarowicz M. (1995). Comportement mécanique des loess sur le tracé du TGV Nord. *XIème Conférence Européenne de Mécanique des Sols et des Travaux de Fondations*, Copenhague, vol. 7.45-50.
- Cui Y.J., Marcial M., Terpereau J.M., Delage P., Antoine P., Marchadier G. and Ye W.M. (2004). A geological and geotechnical characterisation of the loess of Northern France. *A.W. Skempton Memorial Conference*, vol. 1. 417-428.
- Cui Y.J., Tang A., Mantho A. and De Laure E. (2008). Monitoring Field Soil Suction Using a Miniature Tensiometer. *Geotechnical Testing Journal* **31** (1). 95-100.
- Delage P. (2010). A microstructure approach of the sensitivity and compressibility of some Eastern Canada sensitive clays. *Géotechnique* **60** (5). 353-368.
- Delage P., Audiguier M., Cui Y.J. and Howat M.D. (1996). Microstructure of a compacted silt. *Can. Geotch. J.* **33**. 150-158.

- Delage P., Tessier D. and Audiguier M. (1982). Use of the Cryoscan apparatus for observation of freeze-fractured planes of a sensitive Quebec clay in scanning electron microscopy. *Canadian Geotechnical Journal* 19 (1). 111-114.
- Delage P. and Lefebvre G. (1984). Study of the structure of a sensitive Champlain clay and of its evolution during consolidation. *Canadian Geotechnical Journal* 21 (1). 21-35.
- Delage P. and Pellerin F.M. (1984). Influence de la lyophilisation sur la structure d'une argile sensible du Québec. *Clay Minerals* 19. 151-160.
- Delage P., Audiguier M., Cui Y.J. and Deveughele M. (1995). Propriétés de rétention d'eau et microstructure de différents géomatériaux. *XIème Conférence Européenne de Mécanique des Sols et des Travaux de Fondations*, Copenhague, Vol. 3. 43-48.
- Delage P., Cui Y.J. and Antoine P. (2005). Geotechnical Problems related with Loess deposits in Northern France. *Proceedings of International Conference on Problematic Soils*. 517-540.
- Delage P., Marcial D., Cui Y J and Ruiz X. (2006). Ageing effects in a compacted bentonite: a microstructure approach. *Géotechnique* 56 (5), 291-304.
- Delage P., Romero E. and Tarantino S. (2008). Recent developments in the techniques of controlling and measuring suction in unsaturated soils. *Keynote Lecture, Proc. 1st Eur. Conf. on Unsaturated Soils*, Durham, CRC Press. 33-52.
- Diamond S. (1970). Pore size distribution in clays. *Clays and clay minerals* 18. 7-23.
- Fawcett R. and Collis-George N. (1967). A Filter paper Method for Determining the Moisture Characteristics of Soil. *Australian Journal of Experimental Agriculture and Animal Husbandry* 7. 162-167.
- Gardner R. (1937). A Method of Measuring the Capillary Tension of Soil Moisture Over a Wide Moisture Range. *Soil Sci.* 43. 277-283.
- Gens A. and Nova R. (1993). Conceptual bases for a constitutive model for bonded soils and weak rocks. *Proc. Int. Symp. on Hard Soils & Soft Rocks* 1, Athens. 485-494.
- Greacen E.L., Walker G.R., and Cook P.G. (1987). Evaluation of the Filter Paper Method for Measuring Soil Water Suction. *International Conference on Measurement of Soil and Plant Water Status*. 137-143.
- Hamblin A.P. (1981). Filter Paper Method for Routine Measurement of Field Water Potential. *J. Hydrol.* 53. 355-360.
- Harrison B. and Blight G. (1998). The Effect of Filter Paper and Psychrometer Calibration Techniques on Soil Suction Measurements. *Proceedings of the Second International Conference on Unsaturated Soils* 1. Beijing: International Academic Publishers. 362-367.
- Hillel, D. (1971). Soil and water: Physical principles and processes. Academic, New York
- Hormdee D. (2008). Investigation on Collapse Potential of Loess Soil. *Proceedings of the 18th International Offshore and Polar Engineering Conference*, Vol. 2. Fontaine E., Uchida K., Chung J.S. et Moshagen H. (Eds.). 579-583.
- Houston S.L., Houston W.N. and Wagner A.M. (1994). Laboratory filter-paper suction measurements. *Geotechnical Testing Journal* 17 (2). 185-194.
- Karam J.P. (2006). Etude de la rhéologie des loess du Nord de la France. Application à l'évaluation de leur risque de liquéfaction. PhD thesis. École Nationale des Ponts et Chaussées. Paris.
- Kenton C.P., Vanapalli S.K. and Garga V.K. (2008). A Revised Contact Filter Paper Method. *Geotechnical Testing Journal* 31 (6). 461-469.

- Konyai S., Sriboonlue V., Trelo-ges V. and Muangson N. (2006). Hysteresis of water retention curve of saline soil. In *Proceedings of the Fourth International Conference on Unsaturated Soils*, Carefree, ASCE. 1394-1404.
- Koliji A., Vulliet L. and Laloui L. (2010). Structural characterization of unsaturated aggregated soil. *Canadian Geotechnical Journal* **47** (3). 297-311
- Le T.T., Delage P., Cui Y.J., Tang A.M., Lima A., Romero E., Gens A. and Li X.L. (2008). Water retention properties of Boom Clay: A comparison between different experimental techniques. In *Proc. 1st Eur. Conf. on Unsaturated Soils*, Durham, CRC Press. 229-234.
- Leong E., He L. and Rahardjo, H. (2002). Factors Affecting the Filter Paper Method for Total and Matric Suction Measurements. *Geotechnical Testing Journal* **25** (3). 322-333.
- Leroueil S. and Barbosa A. (2000). Combined effect of fabric, bonding and partial saturation on yielding of soils. In *Asian Conference on Unsaturated Soils*. 527-532.
- LLoret A., Villar M.V., Sanchez M., Gens A., Pintado X. and Alonso E.E. (2003). Mechanical behaviour of heavily compacted bentonite under high suction changes. *Géotechnique* **53** (1). 27-40.
- Manthro A. (2005). Echanges sol – atmosphère: application à la sécheresse. PhD thesis. *École Nationale des Ponts et Chaussées*. Paris.
- Marinho F. and Oliveira O. (2006). The Filter Paper Method Revisited. *Geotechnical Testing Journal* **29** (3). 250-258.
- McQueen I.S. and Miller R.F. (1968). Calibration and Evaluation of a wide-range gravimetric method for measuring moisture stress. *Soil Science* **106** (3). 225-231.
- Parcevaux P. (1980). Étude microscopique et macroscopique du gonflement de sols argileux. PhD thesis. *École Nationale Supérieure des Mines de Paris*.
- Patrick P.K., Olsen H.W. and Higgins J.D. (2007). Comparison of Chilled-Mirror Measurements and Filter Paper Estimates of Total Suction. *Geotechnical Testing Journal* **30** (5). 360-367.
- Pécsi M. (1990). Loess is not just the accumulation of dust. *Quaternary International* **7/8**. 1-21.
- Pham H.Q., Fredlund D.G., and Barbour S. L. (2005). A study of hysteresis models for soil-water characteristic curves. *Can. Geotech. J.* **42**. 1548–1568
- Prapaharan S., Altschaeffl A.G. and Dempsey B.J. (1985). Moisture Curve of Compacted Clay - Mercury Intrusion Method. *Journal of Geotechnical Engineering - ASCE* **111** (9). 1139-1146.
- Punrattanasin P. (2008). The capacity of improved Khon Kaen Loess as a road construction material. *1st International Conference on Transportation Geotechnics*, Nottingham, England, Aug. 25-27, 2008. In: Advances in Transportation Geotechnics, Ellis E., Yu H.S., McDowell G. Dawson A. et Thom N. (eds.). 535-540.
- Ridley A. (1995). Discussion on ‘Laboratory Filter Paper Suction Measurements’ by Sandra L. Houston, William N. Houston, and Anne-Marie Wagner. *Geotechnical Testing Journal* **18** (3). 391-396.
- Ridley A. and Burland J. (1993). A new instrument for the measurement of soil moisture suction. *Géotechnique* **43** (2). 321 – 324.
- Ridley A. and Burland J. (1995). Measurement of suction in materials which swell. *Applied Mechanics Reviews* **48** (9). 727-732.
- Ridley, A.M. and Burland, J.B. (1999). Discussion: Use of tensile strength of water for the direct measurement of high soil suction. *Canadian Geotechnical Journal* **36**. 178–180.

-
- Romero E. (1999). Characterisation and thermo-hydro-mechanical behaviour of unsaturated Boom clay: an experimental study. PhD thesis. *Universitat Politècnica de Catalunya*. Barcelone.
- Simms P.H. and Yanful E.K. (2001). Measurement and estimation of pore shrinkage and pore distribution in a clayey till during soil-water characteristic curve tests. *Canadian Geotechnical Journal* **38** (4). 741–754.
- Simms P.H. and Yanful E.K. (2002). Predicting soil-water characteristic curves of compacted plastic soils from measured pore-size distribution. *Géotechnique* **52** (4). 269–278.
- Sridharan A. Altschaeffl A.G. and Diamond S. (1971). Pore size distribution studies. *Journal of the Soil Mechanics and Foundation Division, ASCE* **97**. 771-787.
- Swarbrick G.E. (1995). Measurement of soil suction using the filter paper method. *First International Conference on Unsaturated Soils*, E.E. Alonso and P. Delage (eds), Vol. 2, Paris. 701-708.
- Tarantino A. (2004). Direct measurement of soil water tension. *Unsaturated Soils*, Jucá, de Campos & Marinho (eds). Swets & Zeitlinger, Lisse, ISBN 90 5809 371 9.
- Tarantino A. and De Col E. (2008). Compaction behaviour of clay. *Géotechnique* **58**(3). 199-213.
- Tarantino A. and Mongiovì L. (2001). Experimental procedures and cavitation mechanisms in tensiometer measurements. *Geotechnical and Geological Engineering* **19**. 189-210.
- Vázquez M., Durand P. and Justo J.L. 2011). Soil-Water Characteristic Curve (SWCC) and volumetric deformation law for a plastic clay under high suction. In *Proc. 5th Int. Conf. on Unsaturated Soils*, Barcelona, CRC Press. 509-512.
- Yang C., Cui Y.J., Pereira J.M. and Huang M.S. (2008). A constitutive model for unsaturated cemented soils under cyclic loading. *Computers and Geotechnics* **35**(6). 853-859.
- Yuan Z.X. and Wang L.M. (2009). Collapsibility and seismic settlement of loess. *Engineering Geology* **105** (1)-(2). 119-123.
- Yudhbir (1982). Collapsing behaviour of residual soils. *Proc. 7th Southeast Asian Geotech. Conf., Hong-Kong* **1**. 915-930.

2.3 Effet des cycles d'humidification et de séchage sur la microstructure

Il a été montré plus tôt que la courbe de rétention d'eau du lœss de Bapaume était caractérisée par le phénomène d'hystérésis hydrique, qui se traduit par l'écart entre les branches d'humidification et séchage. Ce phénomène montre la complexité de la microstructure de ce sol, composé par un squelette de grains de limon, ces derniers pouvant être entourés d'agrégats argileux. L'analyse de la relation entre la microstructure et les propriétés de rétention d'eau présentée dans Muñoz-Castelblanco *et al.* (2011) est maintenant approfondie sur la base d'observations microstructurales sur des échantillons obtenus à différents teneurs en eau sur les branches de séchage ou d'humidification de la courbe de rétention.

On a analysé neuf échantillons de lœss obtenus en différents points lors d'un cycle hydrique de séchage-humidification-séchage. La succion a été mesurée à l'aide d'un tensiomètre de haute capacité, développé au laboratoire Navier – CERMES (Manthro 2005, Cui *et al.* 2008). Les observations microstructurales (microscope électronique à balayage, porosimétrie par intrusion de mercure) montrent un espace poral marqué par quatre familles de pores : des macropores (diamètre moyen $D_{moyen} = 200 \mu\text{m}$), des pores intergranulaires ($D_{moyen} = 6 \mu\text{m}$), des pores intra-agrégats dans la fraction argileuse ($D_{moyen} = 1 \mu\text{m}$) et du volume associé aux espaces de séparation entre les feuilles d'argile (taille moyenne = $0.01 \mu\text{m}$). L'analyse montre le gonflement des agrégats argileux pendant l'humidification et leur contraction lors du séchage. Ceci affecte les propriétés de rétention d'eau du lœss. Les principales observations peuvent être résumées comme suit :

- la diminution de la taille moyenne des pores intergranulaires pendant l'humidification ;
- l'augmentation de la taille des pores à l'intérieur des agrégats argileux pendant l'humidification ;
- l'augmentation de la taille et du nombre des macropores piégés dans la matrice grains – agrégats argileux.

On a calculé les courbes de rétention à partir des neuf porosimétries obtenues par intrusion de mercure, à l'aide de la loi de Jurin. L'écart observé entre ces résultats et la courbe expérimentale de rétention d'eau semble être lié à l'existence d'eau adsorbée au niveau des feuillets d'argile, à la présence de macropores piégés et à la surestimation du volume de pores

d'entrée (en dépit de pores piégés dans une matrice par exemple) dans la technique d'intrusion de mercure.

Afin d'analyser l'effet des changements de la microstructure dus aux processus de séchage et d'humidification sur la courbe de rétention d'eau, on utilise le modèle d'hystéresis hydrique proposé par Rojas et Rojas (2005). Ces auteurs ont proposé une organisation simplifiée du réseau poreux, divisée en deux éléments: les *sites* ou cavités et les *liaisons* ou pores d'entrée. Sur la base des expressions théoriques donnant les courbes de séchage et d'humidification, une première modélisation de la courbe de rétention a été faite, montrant un grand écart entre la courbe calculée et les données expérimentales. L'application directe du modèle néglige la présence des macropores piégés, le grand changement de volume de pores à l'intérieur des agrégats argileux pendant les cycles de séchage-humidification, et les effets de l'eau adsorbée par la fraction argileuse (avec une proportion importante de smectite).

Ainsi, une réinterprétation du modèle est proposée en tenant compte de l'existence de différents niveaux de porosité. Cette approche est basée sur l'analyse qualitative et quantitative de la microstructure du lœss à partir des observations au microscope électronique à balayage et des porosimétries par intrusion de mercure. Les courbes obtenues par cette approche sont en conformité avec la courbe expérimentale de rétention d'eau. Les résultats de cette étude confirment l'existence d'au moins 4 niveaux de porosité:

- le volume associé aux espaces qui séparent les feuilles d'argile, observé par les cycles de relâchement du mercure après l'intrusion (8% de la porosité totale) ;
- le réseau de pores à l'intérieur des agrégations argileuses (17% de la porosité totale) ;
- les pores entre les grains de limon (28% de la porosité totale) ;
- les macropores piégés dans la matrice du sol (grains de limon – agrégations argileuses) (17% de la porosité totale).

On recommande la validation de ces concepts avec l'analyse des propriétés de rétention d'autres sols naturels ayant également plusieurs niveaux de microstructure. Les résultats de cette étude ont été rédigés en anglais sous la forme d'un article scientifique, soumis pour publication dans une revue internationale.

A microstructure analysis of the hysteresis of the water retention curve of a natural loess

J. A. Muñoz-Castelblanco*, P. Delage*, J. M. Pereira*, and Y. J. Cui*

The main wetting and drying branches of the water retention curve of a natural loess from Northern France already investigated by Muñoz-Castelblanco *et al.* (2011) are related to the microstructure of the soil, composed of a loose skeleton made up of silt-grains and of a clay fraction irregularly scattered among the grains. A detailed microstructure analysis was conducted by means of mercury intrusion porosimetry and scanning electron microscope observations carried out on different points along the main drying and wetting branches. The conclusions drawn from this investigation evidenced (i) the key role of the swelling-shrinking behaviour of clay aggregations within the grain skeleton, (ii) the role of large pores that remained unaffected by the drying-wetting cycle, (iii) the effects of the water adsorbed on the clay platelets and (iv) some limitations when using the mercury intrusion technique to characterize soil porosity and water retention properties. On the basis of this analysis a hysteresis model of the water retention curve proposed by Rojas and Rojas (2005) has been adapted based on the microstructure features evidence, providing a satisfactory prediction of the water retention properties of the loess.

KEYWORDS: water retention properties, hysteresis, loess, microstructure, drying-wetting processes

Introduction

The detailed investigation of the water retention properties of unsaturated soils is necessary for a better understanding of their hydro-mechanical behaviour. Water retention curves are characterised by a typical hysteresis (see for instance Croney and Coleman 1954, Hillel 1971) that is clearly apparent in natural soils (see for instance recent experimental data from Konyai *et al.* 2006 in a saline sandy loam, Le *et al.* 2008 in Boom clay, Askarinejad *et al.* 2011 in a natural silty sand and Vasquez *et al.* 2011 in a red clay of high plasticity). There are many models that simulate the hysteretic behaviour of the water retention properties of unsaturated soils (Haines 1929, Everet 1967, Hanks *et al.* 1969, Dane and Wierenga 1975, Hogarth *et al.* 1988, Nimmo 1992, Kawai *et al.* 2000, Pham *et al.* 2003).

This paper is devoted to the detailed analysis of the microstructure changes that occur in a loess along the drying and wetting paths of the water retention curve. The natural loess was manually extracted by blocks in an excavation located close to the city of Bapaume (Picardy, Northern France). Its hydromechanical properties have been studied in details for some time

* Ecole des Ponts ParisTech, Laboratoire Navier – CERMES, Université Paris-Est

(Cui *et al.* 1995, 2004, Delage *et al.* 2005, Yang *et al.* 2008, Karam *et al.* 2009, Muñoz-Castelblanco *et al.* 2011) because of a significant collapse susceptibility that may affect in some places the stability of the high speed railways between Paris and Northern Europe through the Picardy region (LGV Nord). According to the results of a previous study on the same material (Muñoz-Castelblanco *et al.* 2011), the water retention curve of the Bapaume loess exhibits a particular shape with no hysteresis around the natural water content and two hysteresis loops on both the wet side and the dry side.

In this paper, the relationship between the microstructure and the water retention properties of the Bapaume loess is further investigated based on the combined used of mercury intrusion porosimetry (MIP) and scanning electron microscope (SEM) observations. A model proposed by Rojas and Rojas (2005) is then adapted to model the main drying and wetting branches of the water retention curve. An accurate interpretation of the specific behaviour of the studied loess was found by extending the initial model to account for several levels of porosity.

Tested material, equipment and procedures

The material used has been taken from an intact block that was manually extracted at a depth of 1m from an excavation in a site near to the city of Bapaume in Northern France. The initial state of the loess was carefully preserved by protecting the block just after extraction with a plastic film and paraffin wax and by storing the protected sample in a temperature controlled room. The Bapaume loess is a silty soil with a relative low clay fraction of 16%, and a carbonate content of 6% assumed to be responsible of bonding between the silt grains (Pécsi 1990, Antoine 2002, Delage *et al.* 2005). The loess has a low plasticity index of 9% and does not present any significant swelling behaviour. Its main geotechnical properties are presented in Table 1.

Sample depth	1 m		
Water content w (%)	14.0	Plastic limit w_p	19
Void ratio e	0.84	Liquid limit w_l	28
Dry unit mass ρ_d (Mg/m ³)	1.45	Plasticity index I_p	9
Degree of saturation S_r	0.46	Carbonate content (%)	6
Suction (kPa)	40	In situ total vertical stress σ'_{v0} (kPa)	15.47
Clay fraction (% < 2 µm)	16	Collapse (%) under σ'_{v0}	7.5

Table 1. Geotechnical characteristics of the Bapaume loess as sampled (natural state)

Aeolian depositional conditions of silt size particles in a cold and arid steppic climate during the last glaciation (20-25000 BP) (Antoine 2002, Antoine *et al.* 2003) have given to the loess deposit an open fabric characterized by a low dry mass unit weight of 1.45 and a high void ratio of $e = 0.84$ (porosity $n = 45.7\%$). The natural degree of saturation at the date of sampling (Oct. 2007) was 0.46 and the suction (measured by using both a high capacity transducer and the filter paper method, Munoz-Castelblanco *et al.* 2011) was 40 kPa. The collapse susceptibility of the loess has been investigated by performing a series of double oedometer tests (Jennings and Knight 1957) and a value of 7.5% of collapse (soaking from an initial water content of $w_i = 11\% - S_r = 0.38$, upon an applied vertical stress of $\sigma_v = 200$ kPa) was obtained, indicating a collapsible susceptibility according to the Knight (1963) criterion.

To further investigate the relationship between microstructure and the water retention properties of the loess starting from its initial intact state, a series of microstructure investigations including MIP and SEM observations was conducted at various points along the water retention curve determined by Munoz-Castelblanco *et al.* (2011) and represented later in Figure 2. To do so, a 70 mm diameter and 19 mm high oedometric sample was placed in a oedometer cell equipped at its base with an in-house constructed high capacity tensiometer (HCT, Ridley and Burland 1993, Mantho 2005, Cui *et al.* 2008) as shown in Figure 1 (Delage *et al.* 2007, Munoz-Castelblanco *et al.* 2011). In order to improve the contact between the tensiometer and the soil sample and thus to avoid the early cavitation of the tensiometer, a fine layer of slurry made from the tested soil was placed over the tensiometer surface prior to inserting the sample in the oedometer ring. To the same end, a vertical load of 1.5 kPa (the piston weight) was applied to the sample. The oedometer cell was then placed on a precision balance to register water weight changes with time.

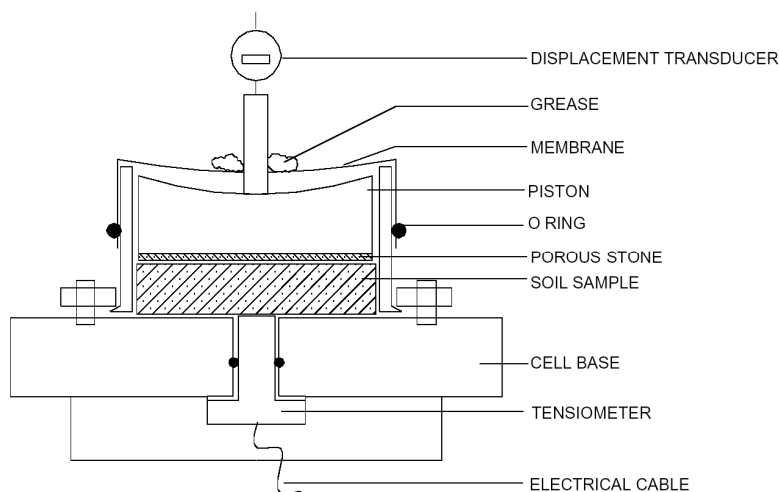


Figure 1. HCT measurement inside an oedometer cell (Delage *et al.* 2007)

As described in Munoz-Castelblanco *et al.* (2011), the wetting process was carried out by carefully removing the oedometer piston and by dropping, with a syringe, small drops of water over a filter paper placed above the sample so as to avoid any disturbance due to the water dropping. The drying process was performed by allowing free sample evaporation in laboratory conditions with no piston on the sample. Once the desired water content was reached (as indicated by the balance measurement) the piston was placed back and water equilibration was waited for during 1 hour. As shown in Figure 1, a membrane isolating the sample in the ring and the piston from the atmosphere was also placed so as to avoid evaporation during the equilibration period.

In order to analyse the microstructure changes during the drying and wetting processes, small rectangular-shape bars of loess of maximum size 2 cm were carefully trimmed by cutting them from the specimen in the oedometer cell at different times corresponding to various water contents under a known suction. Since the 1.9 cm diameter HCT is located in the sample centre, samples were taken from the annular space between the tensiometer and the 70 cm diameter metallic ring. At each sample extraction, the resulting hole was filled with paraffin wax in order to avoid any evaporation and cavitation of the tensiometer. Weight changes induced by the sample extraction and the paraffin addition were carefully monitored by using the precision balance. It appeared that the values of suction and water content did not change during this procedure. Prior to being freeze-dried, the extracted small samples were immediately protected with paraffin wax and plastic film to avoid water content changes due to evaporation.

To ensure the best possible preservation of the microstructure during dehydration, samples were freeze dried (Tovey and Wong 1973, Gillott 1973, Delage *et al.* 1982). To ensure instantaneous freezing, the small sticks of loess were plunged in liquid nitrogen (- 196°C) that was frozen down to its cooling point (- 210°C) by applying negative pressure to nitrogen prior to sample immersion (Delage *et al.* 2006). In such conditions, the heat quantity brought by the small soil sticks when plunged into nitrogen is not enough to heat nitrogen up to its boiling point and water transfer occurs in liquid phase. It is hence not slowed down by nitrogen bubbling like when directly plunging sample into liquid nitrogen. The heat transfer during freezing is instantaneous and generates amorphous ice with no volume expansion (Delage and Pellerin 1984).

SEM observations were carried out on surfaces that were obtained by fracturing the frozen soil sticks prior to placing them under vacuum in the freeze dryer apparatus. In such condition, the observation surface is not defined by any weakness plane of the wet soil microstructure and no deformation occurs when fracturing (Delage *et al.* 1982). The observation surface is plane indeed, well defined and it does cross the various levels of microstructure, allowing better observation.

Tests results

The hydraulic path followed here (Figure 2) started by a drying phase from the natural water content $w = 14.4\%$ (point 1, initial suction 40 kPa, $S_r = 0.46$) to $w = 10.7\%$ (point 2, $s_i = 84$ kPa, $S_r = 0.34$). It was followed by two drying points at water contents $w = 9.9\%$ (point 3, $s_i = 150$ kPa, $S_r = 0.30$) and $w = 8.0\%$ (point 4, suction 613 kPa, $S_r = 0.25$). In order to avoid HCT cavitation (maximum suction capacity 1 MPa), a wetting path was then followed from point 4 to point 5, (suction 195 kPa, $S_r = 0.25$). Actually, one can observe that in spite of a significant suction release, there is no significant change in water content between points 4 and 5. This is typical of scanning branches when passing from a main drying branch to a main wetting branch while mobilising hysteretic effects. Further wetting was performed at water contents $w = 9.9\%$ (point 6, $s_i = 94$ kPa, $S_r = 0.31$), $w = 14.4\%$ (point 7, $s_i = 34$ kPa, $S_r = 0.46$), $w = 20.0\%$ (point 8, $s_i = 14$ kPa, $S_r = 0.62$) and at $w = 27.0\%$ at a zero suction value (point 9, $S_r = 0.84$). A last point was afterwards obtained by drying the sample at water content $w = 20.0\%$ (point 10, $s_i = 23$ kPa, $S_r = 0.62$). Given that negligible volume changes were observed during the drying and wetting stages, the curve of Figure 2 are also plotted in terms of the degree of saturation.

The intact initial cumulative mercury intrusion and extrusion PSD curves ($w = 14\%$, $s = 40$ kPa) are presented in Figure 3 together with that obtained from the samples along the drying path at $w = 11\%$ ($s = 84$ kPa), $w = 10\%$ ($s = 150$ kPa) and $w = 8\%$ ($s = 613$ kPa). Also plotted in the graph is the total void ratio of 0.84. The intact curve, already described in Muñoz-Castelblanco *et al.* (2011) is characterised by a well sorted PSD curve around an average entrance diameter of 8 μm characterised by the inflection point of the curve. This average diameter value is in good accordance with the inter-grains pores that are observed in the SEM photo of the intact loess presented in Figure 4 that shows a dominant proportion of subangular silt grains with diameters of several tens of micrometers. The figure also shows that the clay fraction is not regularly scattered among the grains. Whereas some grains are quite clean,

some others appear to be strongly linked together by clay aggregations that seem to be firmly stuck to the grains. The figure also shows a “grain/clay aggregate” made up of various grains completely embedded in a clay matrix. Clay aggregations locally fill the inter-grains porosity.

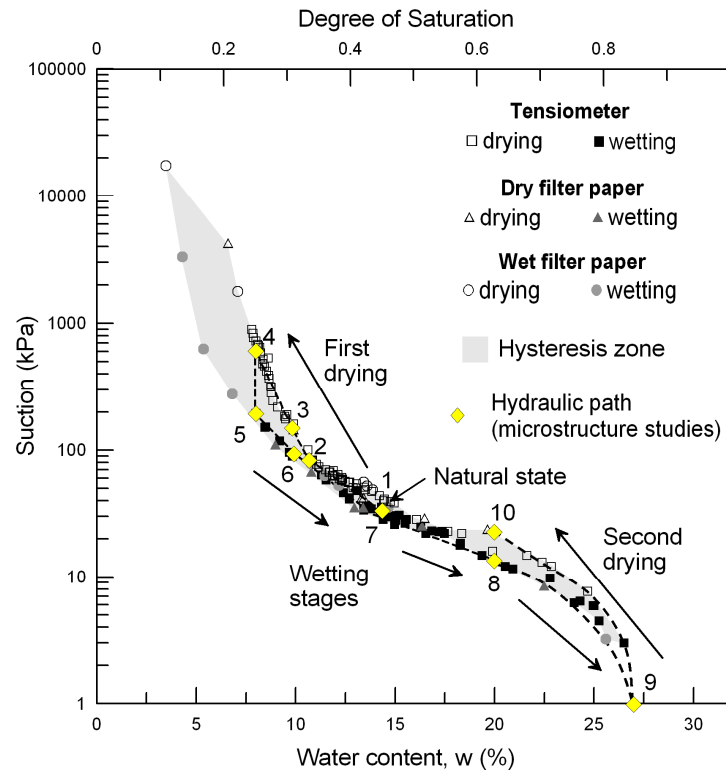


Figure 2. Water retention curve of Bapaume loess (Muñoz-Castelblanco *et al* 2011). Microstructure analysis was carried out in diamond points 1 to 10.

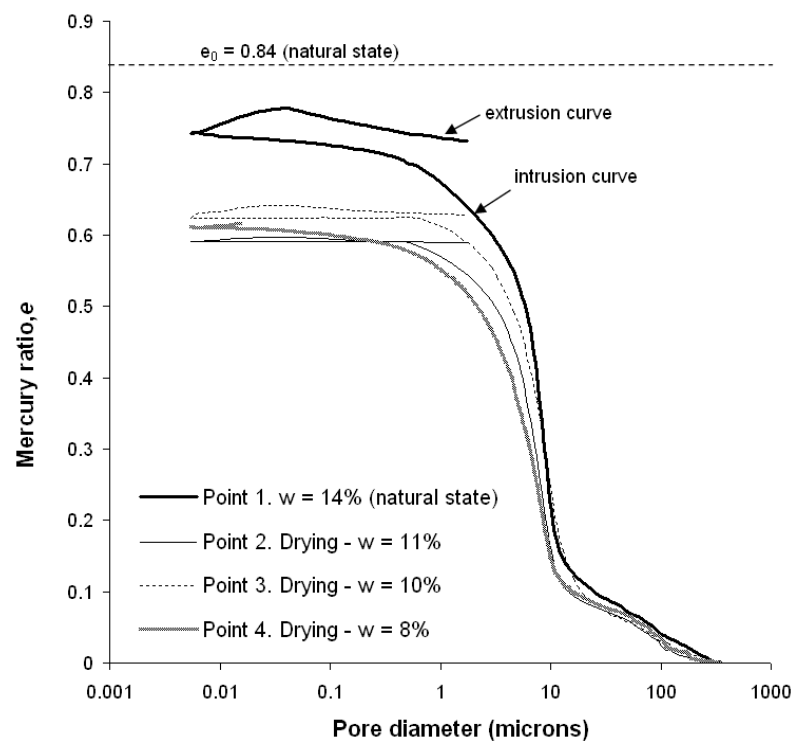


Figure 3. Intrusion and extrusion cumulated PSD curves during drying stages.

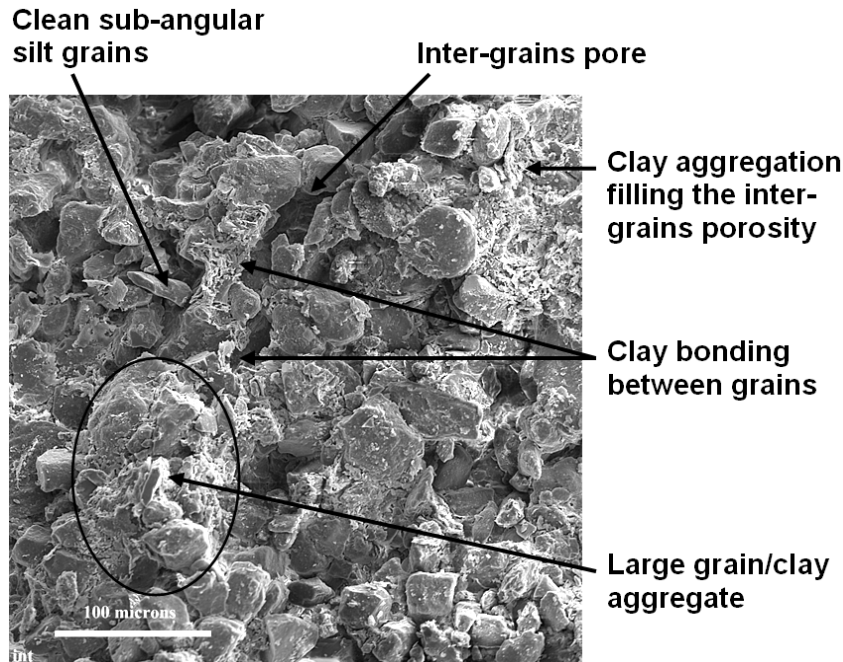


Figure 4. SEM observations of the Bapaume loess at the natural hydric state ($w = 14.4\%$)

A poorly graded linear section is observed in the large pores area with entrance pore diameters between $363 \mu\text{m}$ and $16 \mu\text{m}$. These quite large pore represent 12% of the total void ratio, i.e. 6.8% of the total porosity. This large porosity can be compared with the collapse value of 4% obtained under a vertical stress (19 kPa) close to the in-situ one (16 kPa) by soaking a loess sample from the natural water content $w = 14.4\%$ (Muñoz-Castelblanco *et al.* submitted). As previously described, a larger collapse of 7.5% was observed on the same loess when soaking from a drier state ($w = 11\%$) under a vertical stress of 200 kPa.

A first observation is that the large pore section is very slightly affected by the drying phase between 14 and 8% with no significant change in the PSD curve. This is not surprising since the initial degree of saturation is equal to 0.46. As commented in Muñoz-Castelblanco *et al.* (2011), under the hypothesis of having water located in the small pores, this pore population is already dry and hence not affected by further drying occurring in small pores.

Another common characteristic of the samples submitted to drying from the initial intact state is that the amount of intruded porosity is significantly decreased to the same value, with a total unintruded porosity of 28% in the three dried samples irrespective of the water content. The intruded porosity that initially represents 88% of the total porosity at initial state decreases to 70% when the water content is reduced. All curves show that there is very few pores with diameters smaller than $0.6 \mu\text{m}$ compared with a cumulated pore volume of 5% in

the intact sample (note that the flat sections of the curves of samples 2 and 3 ($w = 11$ and 10%) below 0.6 μm are probably an artefact of the MIP experiment that was apparently not able to detect such a tiny intruded volume). The response at $w = 8\%$ seems more realistic. After drying, the reduction of the intruded porosity and the very small porosity detected below 0.6 μm is linked to the shrinkage of the clay platelets. In other words, the larger inter-platelets distance existing in hydrated platelets that allowed for some intrusion at diameter smaller than 0.6 μm have been reduced by drying and shrinkage, resulting in a larger unintruded porosity.

In Figure 5, the cumulative mercury intrusion and extrusion curves of the samples along the main wetting branches at $w = 8\%$ ($s = 195 \text{ kPa}$), 10% ($s = 94 \text{ kPa}$), 20% ($s = 14 \text{ kPa}$) and 27% ($s = 1 \text{ kPa}$) are presented together with the curve at 20% ($s = 23 \text{ kPa}$) after drying. The dry largest pores (diameter larger than 10 μm) remain intact as previously. It is interesting to observe that after releasing suction (from 613 to 195 kPa) and starting the wetting path from the point at 8%, the mercury intruded porosity came back to higher values closer to that of the initial state (with an exception in the case of the curve at $w = 27\%$ due to a technical problem at a pressure at which the curves present a discontinuity that is not representative of any pore distribution – it seems that here the mercury pressure went on increasing with no detection of any mercury intrusion thus underestimating the total intruded porosity). This trend is related to the subsequent swelling allowed by suction release during wetting. The reversible response in terms of intruded porosity observed along the drying – wetting path from the initial state is typical of swelling clay minerals and probably related to the smectite fraction detected in the illite-smectite stratified clay minerals.

In Figure 6, the evolution of the density functions of the pore size distribution curves of the Bapaume loess upon drying and wetting obtained from mercury intrusion are plotted. The density functions calculated from the extrusion curves is also presented.

A predominant entrance pore diameter of about 8 μm corresponding to the inter-grains pores is observed (note that the 4.9, 4.7 and 3.7 μm peaks observed in the Figure at points 1, 7 and 8 are due to some dysfunctions of the porosimeter). This value does not significantly change along the drying-wetting path, confirming that water changes have little effect on the loess granular skeleton and, consequently, on macroscopic volume changes. The corresponding inter-grains pores can be seen in the SEM photos also presented on the right of the Figure (band length is 5 μm). Another population of very large pores observed around 100 μm is not sensitive to change in water contents either.

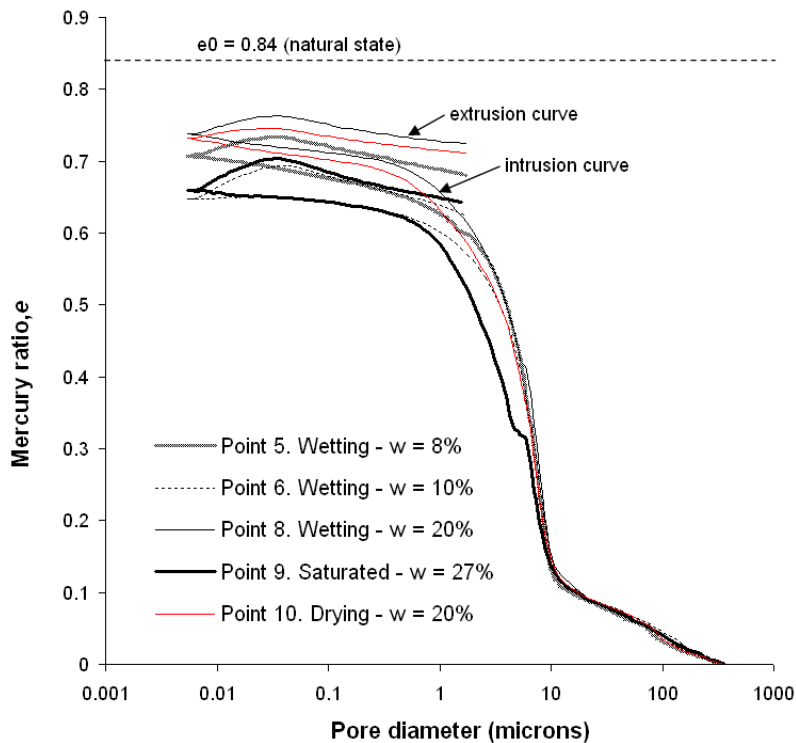


Figure 5. Intrusion and extrusion cumulated PSD curves during wetting stages.

The extrusion curves show the existence of pores in which mercury is not trapped, with a mean diameter of about $0.01 \mu\text{m}$ that is possibly related with the plane spaces between clay platelets and the inter-platelets distance. Note that extrusion progressively decreases while drying from 14% to 11 and 10%, to almost disappear at the driest point at 8%. This probably indicates the progressive shrinking of the clay platelets at small sizes that could no longer be intruded by mercury. It is interesting to observe that the suction release at 8% between points 4 and 5 correspond to the reappearance of extrusion, indicating some swelling allowed at the platelet level by the suction release. It is however not fully evident to understand how this occurred at constant (or very slightly increasing) water content. This is anyway a trend that is typical of the hysteresis.

The shaded areas below the pore size density functions of Figure 6 correspond to the water content of the various samples. They were determined from the cumulative pore volume by assuming that water was preferentially located in the smallest pores due to the combined effects of clay-water interaction and capillarity. Examination of these areas show that the inter-grains pores are partially saturated at $w = 14\%$, almost dry at 11 and 10% and completely dry at 8%. They are wetted again when following the wetting path at 20%. Note also that at 27%, the largest pores above $10 \mu\text{m}$ are not filled by water.

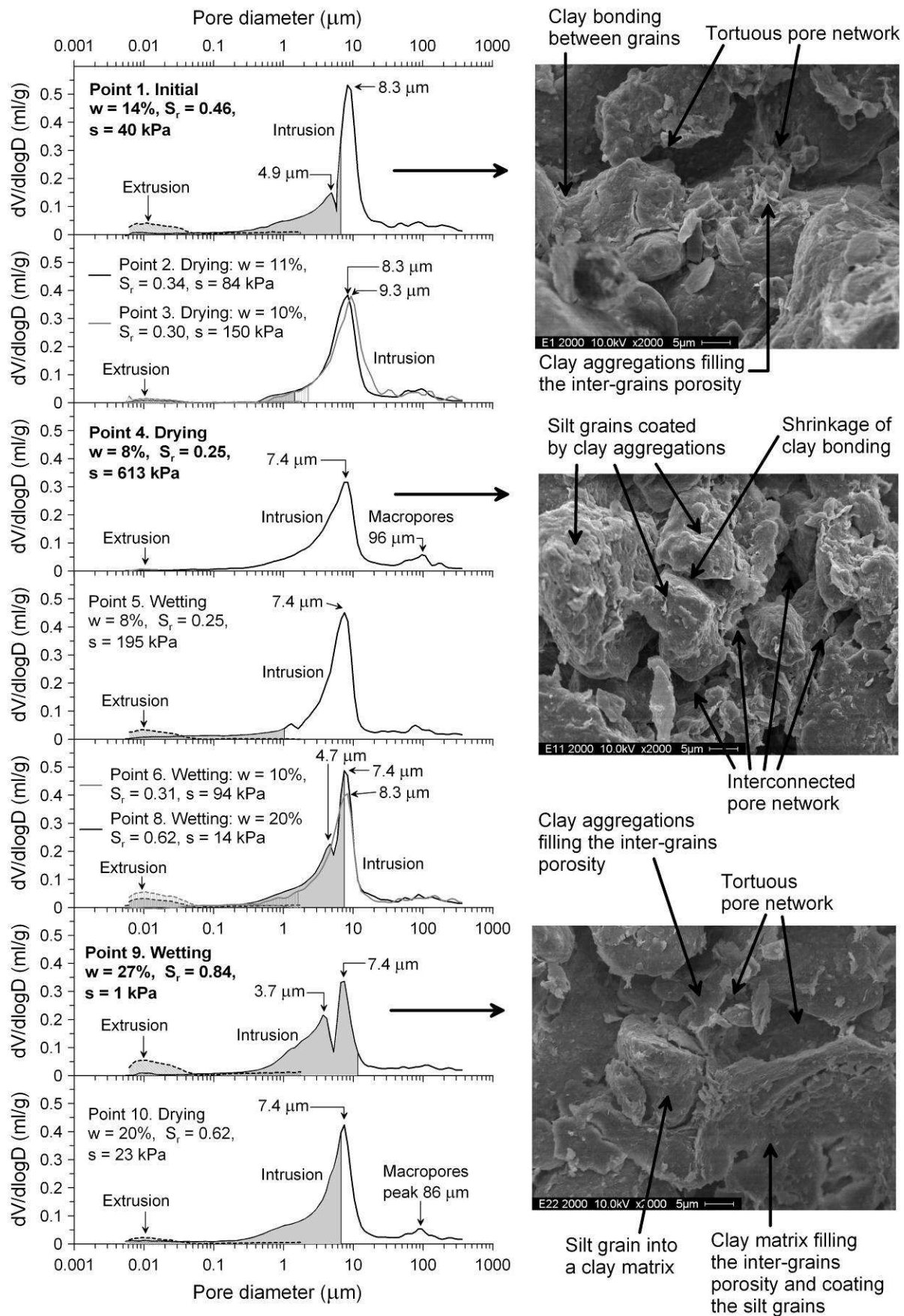


Figure 6. Evolution of microstructure of loess during drying and wetting stages

Examination of the upper SEM micro-photographs in Figure 6 (Point 1, natural in-situ state at $w = 14.4\%$), shows the presence of hydrated clay aggregations between silt grains that might increase the tortuosity of the pore network. The figure also shows the detail of a “grain/clay aggregate” made up of various grains embedded in the clay matrix.

The central photography corresponds to point 4 after drying at the smallest water content $w = 8\%$. The predominant presence of the silt grains is enhanced by the shrinking of the clay aggregations and the coating of the clay platelets along the grains, as already observed on the compacted Jossigny silt by Delage *et al.* (1996) and on the same loess by Muñoz-Castelblanco *et al.* (2011). The clay fraction also presents a jagged aspect that is typical of dry clay platelets. It is likely that clay shrinkage and silt particle coating, in particular at the inter-grains contacts, is prone to strengthen inter-grains bonding and increase the resistance of the areas containing enough clay fraction. This effect should be less in the zones with less clay fraction in which grains appear to be clean, that probably constitute the weaker zones of the loess in which failure locally starts.

The photo of the dry sample at 8% show more clearly the silt grains with diameters varying from 10 μm to 30 μm while the inter-grains pore sizes vary from about 3 μm to 10 μm , in agreement with the pore size distribution obtained from MIP. The large pores observed also illustrate the open micro-fabric of the loess, in relation with its collapse susceptibility.

The bottom photograph corresponds to the saturated state ($w = 27\%$, point 8). Clay particles no longer exhibit the jagged appearance that they exhibited in the above photo (point 4) in the dry state at $w = 8\%$ and also, in a lesser extend at $w = 14\%$ (point 1). As already observed in the Jossigny silt compacted wet of optimum (Delage *et al.* 1996), the clay fraction appears to be much more present in terms of volume, due to clay hydration and swelling. In the photo of Figure 6, the silt grains appear to be embedded in a clay matrix. Note however that, due to the heterogeneous distribution of the clay fraction among the grain skeleton, this is a local phenomenon since the PSD curve still clearly detects the presence of the inter-grains pores that, in this case, are full of water.

The structure changes along the drying and wetting paths have hence been explained based on the behaviour of a loose but non deformable grain skeleton (at least under no stress applied) among which some changes occur due to the swelling-shrinkage behaviour of a 16% clay fraction that is heterogeneously distributed among the grain skeleton. Grain coating also occurs

at dry states. The swelling shrinkage behaviour of the clay fraction is linked to the presence of some stratified illite smectite minerals. In clayey zones, the hydrated clay fraction may turn into a matrix embedding the grains.

The observed density peaks at pore sizes of about $100 \mu\text{m}$ correspond to the presence of very large pores that are highlighted in the SEM photographs in Figure 7. These pores are quite present either at initial water content (Figure 7b) or along the drying path at $w = 8.0\%$ (Figure 7a). Note that, as shown in Figure 6, these very large pores are not saturated by water at $w = 27\%$. Although some of them are detected by MIP, it is possible that many comparable large pores are trapped.

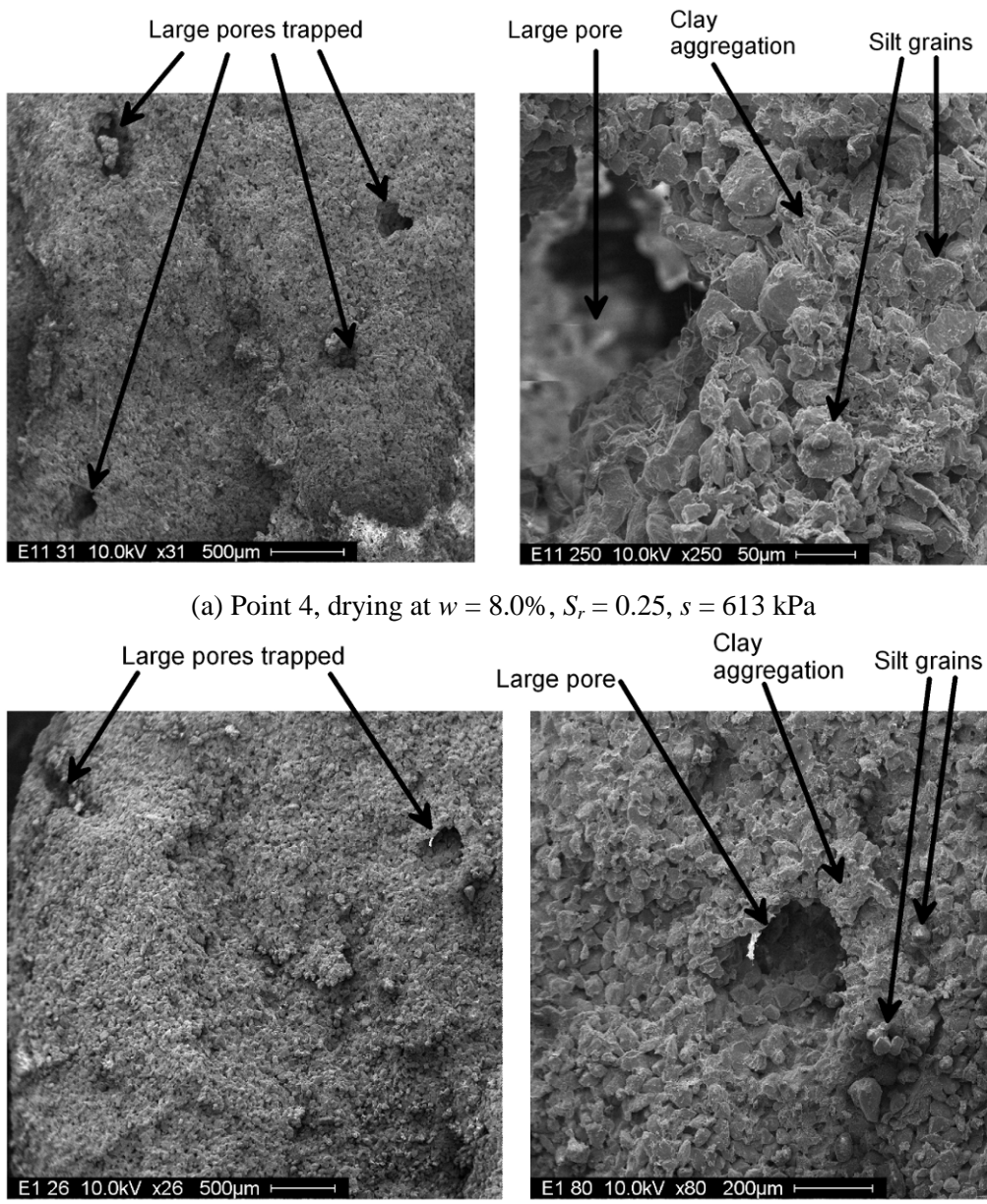


Figure 7. SEM observations of the Bapaume loess. Analysis of large pores

Discussion

The main branches of the water retention curve of Bapaume loess obtained by Muñoz-Castelblanco *et al* (2011) are presented in Figure 8. A number of researchers (Purcell 1949, Regab *et al.* 1982, Prapaharan *et al.* 1985, Aung *et al.* 2001) have previously attempted to predict water retention curves from mercury intrusion porosimetry (MIP) data. Following the same approach, three retention curves, obtained using the Laplace law and MIP data, are also presented in Figure 8. These curves correspond to the loess specimens observed at water contents $w = 8.0\%$ (drying, point 4), $w = 14.4\%$ (initial state, point 1) and $w = 27.0\%$ (saturated, point 9).

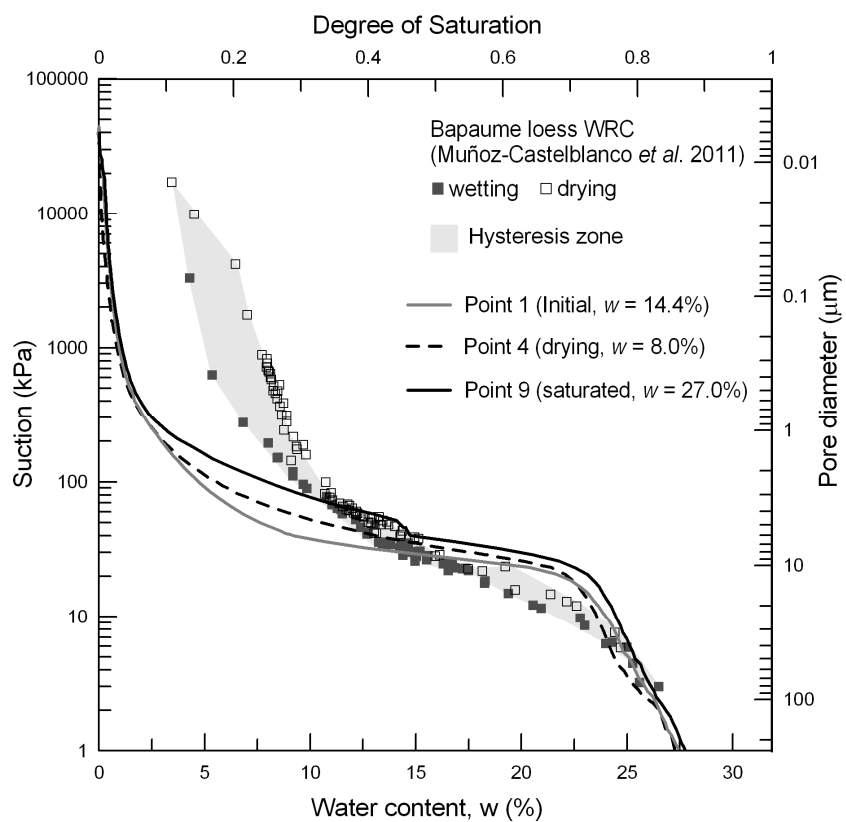


Figure 8. Retention curves from MIP porosimetry data

As proposed by Scheidegger (1957), retention curves may be estimated using MIP data by assuming that the soil can be represented as a bundle of capillary tubes of cylindrical shape with no connection between them. However, the pore network of natural soils is a complex system of irregular pores of randomly distributed different sizes. In order to obtain a water retention curve from the pore size distribution, some aspects must be considered:

1. Under the hypothesis of having water located in the smallest pores due to both capillary action and water adsorption on clay particles, all pores located in pores with a diameter (8

μm) smaller than that corresponding to the natural water content ($w = 14.4\%$) should be saturated whereas pores of higher diameter should be dry (see PSD curve of point 1 in Figure 6). Referring to SEM observations, this means that the largest porosity between clean grains should be dry whereas the clay aggregations should be water saturated. Then, the almost satisfactory correspondence observed on the right side of the drying curve concerns capillary effects in a dry granular assembly, compatible with observations in dry samples or sandstones.

2. On the left side of the natural water content, the water retention curves derived from the three MIP retention curves in Figure 8 indicate, at a given suction value, a significantly smaller water content than the real one, in relation with the water-clay interactions that allow for a larger water storage in the clay fraction at the suction considered. As an example, the PSD derived curves indicate a water content close to $w = 1\%$ under a suction of 1 MPa compared to the real water content $w = 7.5\%$. The strong effect of water adsorption on clay particles (with a 16% clay fraction) is compatible with the $w = 3.5\%$ water content that the soil is able to retain at a suction as high as 20 MPa (driest point obtained with the wet filter paper).
3. A difference between the three PSD-derived retention curves (respectively obtained at $w = 14.4\%$ at initial state (1), $w = 8\%$ after drying (4), and $w = 27\%$ after saturation) is observed in Figure 8. The curves at initial state and after drying (points 1 and 4) along the main drainage path correspond to a larger mean entrance pore diameter than the curve at saturated state ($w = 27\%$). This trend is related to the swelling-shrinkage behaviour of the clay aggregations that reduces the inter-grains pore sizes during wetting stages, whereas pore size increases during drying due to clay aggregations' shrinkage. Then, during drying at a given water content value, the water transfer is done through a wetted structure, affected by the volume increase of pores within the swelled clay aggregations. Conversely, during wetting, water transfer is done through a dry pore network modified by the clay shrinkage phenomena. Then, the analysis of drying stages must be done based on microstructure observations during wetting stages, and conversely for the wetting stages.

The experimental water retention curve shows a residual water content of $w = 3.5\%$ ($S_r = 0.11$) at a suction of 17.3 MPa. This value is related to the water adsorbed into the clay fraction (16%) that is composed of kaolinite, illite-smectite and smectite minerals. According

to Mitchell and Soga (2005), water is strongly attracted to clay particle surfaces, and the resulting interactions may influence the water properties up to distances of several tens of Ångströms. The clay – water interaction properties, including hydrogen bonding, cation hydration, attraction by osmosis, dipole orientation in an electric field and attraction by London dispersion forces, tend to decrease with distance from particle surfaces, and surface interaction effects may be significant up to distances of about 100 Å (Low 1987). If all the water in a clay is assumed to be spread uniformly over the available surface area A_s , then the average thickness, t , of the water films on the particle surfaces would be (Mitchell and Soga 2005):

$$t = w / (\rho_w A_s)$$

in which ρ_w is the density of the water. The specific surface area of kaolinite is about 10 to 30 m²/g of dry clay, that of illite is about of 65 to 100 m²/g, and, that of smectite is about of 50 to 840 m²/g. Considering a thickness of the bonded water film of about 100 Å, this would correspond to water contents of about 800% in a fully expanded pure smectite and 15% in a pure kaolinite (Mitchel and Soga 2005). As the clay fraction of loess is about 16%, bonded water on clay aggregations would represent adsorbed water contents from 2.4% (kaolinite) to 128% (fully expanded smectite). The observed adsorbed water content is about 3.5% confirms the predominance of kaolin within the clay fraction.

These facts may also explain other phenomena such as the observed inflection point in the water retention curve at w = 10% or the high hysteresis at water contents lower than 10%.

Multiscale modelling of the water retention curve

From the previous comments, it appears that an enriched description of the porous network of natural soils is required to obtain a more realistic modelling of their retention properties. This has been achieved in the present study by extending a model proposed by Rojas and Rojas (2005) to simulate the water retention curve of Bapaume loess. The previous analysis of the loess microstructure sets the bases of the modelling approach. According to these authors, the Dual Site-Bond Model (DSBM) consists in a simplified statistical description of the pore network. This latter is comprised of two types of void elements: the *sites* or cavities and the *bonds* or throats. The sites are surrounded by C bonds, where C corresponds to their connectivity. This model is characterized by four properties: a) the heterogeneity in void size,

which means that both sites and bonds entities should have their own size distribution functions; b) the size correlation between pore elements indicating that there should exist a statistical correlation between neighboring pore entities; c) some geometrical restrictions existing between pore elements ensuring that any interpenetration between adjacent bonds converging to a given site is forbidden; and d) non-uniform site connectivity traducing the fact that the number of throats surrounding a cavity can change from site to site. The model is based on the definition of the following functions and conditions:

- the density functions for sites $F_S(R)$ and bonds $F_B(R)$, where R represents the pore size;
- the probability (or number fractions) of a site $S(R)$ and of a bond $B(R)$ that can be written:

$$S(R) = \int_0^R F_S(R) dR ; \text{ and } B(R) = \int_0^R F_B(R) dR ;$$

- the density function for sites $F_S(R)$ would be located towards higher average R values than $F_B(R)$, that implies the restriction $S(R) > B(R)$;
- it is needed to avoid the intersection between two orthogonal adjacent bonds of radii R_{Bi} and R_{Bj} when they meet at a site R_S , which writes as:

$$\sqrt{R_{Bi}^2 + R_{Bj}^2} \leq R_S .$$

From the description of the pore network into two pore size density functions, Rojas and Rojas (2005) proposed the description of wetting and drying processes in porous media. The drying boundary curve is obtained by considering *domain complexions* for bonds and sites under drying. For bonds, L_{BD} represents the probability that a bond remains connected to the liquid phase during a drying process to a capillary pressure corresponding to the actual critical radius R_c . The conditions required for a bond to remain liquid-filled can be stated as: a) water cannot be drained when the bond is smaller or equal to the critical radius R_c ; this condition corresponds to the probability $B(R_c)$; and b) water can be drained from the bond when its size is bigger than the critical probability $(1 - B(R_c))$, however it remains saturated if air cannot invade any of two adjacent sites and their $C-1$ adjacent bonds $[L_{BC}]^{C-1}(1 - S(R_c))^2$. The probability for a bond to remain water-filled during drying results from the addition of conditions a) and b) and can be written as:

$$L_{BD} = B(R_c) + (1 - B(R_c)) [L_{BD}]^{C-1} (1 - S(R_c))^2$$

For sites during drying, the probability L_{SD} of a site to remain liquid-filled requires the following conditions: a) water cannot be drained when the site is smaller or equal to the critical radius R_c ; this condition is represented by the probability $S(R_c)$; b) gas should be able to invade the site, so, it should be larger than the critical size ($1 - S(R_c)$); and c) at least one of the C contiguous sites surrounding the site in question should be liquid-filled (L_{SD}) and bonds that joint them are also liquid-filled. Therefore, L_{SD} results from the addition of condition a) to the product of conditions b) and c) and can be written as:

$$L_{SD} = S(R_c) + (1 - S(R_c)) [1 - (1 - L_{SD})(1 - B(R_c))]^C$$

The overall degree of saturation of the pore network during drying processes can be obtained by dividing the addition of the volumes of water from sites and bonds by the volume of voids, in the form:

$$S_{WD} = \frac{V_S L_{SD} + V_B L_{BD}}{V_V}$$

where the volume of voids V_V results from the addition of the overall volumes of sites and bonds.

The domain complexion for bonds during wetting is based on two principles: a) the liquid can get through the bond because it is smaller than the critical size ($B(R_c)$); but b) if it can get through the bond, it is needed to consider if liquid can get through the contiguous site ($S(R_c)$) (and to all remaining bonds meeting this site) or cannot ($1 - S(R_c)$). Therefore, the probability of a bond getting liquid-filled during a wetting process results of subtracting the condition b) from the condition a) and b) and can be written as:

$$L_{BI} = B(R_c) \left\{ 1 - \left[1 - S(R_c) + S(R_c)(1 - L_{BI})^{C-1} \right]^p \right\}$$

For sites during wetting, there are two conditions: a) water can get through the considered site because it is smaller or at least equal to the critical size, ($S(R_c)$); and b) at the same time, it is necessary that at least one of the C contiguous sites be full of water (L_{SI}), then the linking bond is also invaded. This can be written as:

$$L_{SI} = \left[1 - (1 - L_{SI} B(R_c))^C \right] S(R_c)$$

Finally, the degree of saturation during wetting processes of the pore network can be expressed as:

$$S_{WI} = \frac{V_S L_{SI} + V_B L_{BI}}{V_V}$$

Based on this model, a coupled analysis of the loess microstructure and of its water retention curve is proposed. Rojas and Rojas (2005) consider that the density functions for sites and bonds can be represented by normal logarithmic distributions as it has been observed on different soils by Garcia-Bengochea *et al.* (1979), Delage *et al.* (1996) and Simms and Yanful (2001) among others. It is proposed to establish the density functions from the mean size and the standard deviation obtained from experimental PSD curves. Mercury intrusion porosimetry is mainly a drying process (Prapaharan *et al.* 1985, Delage *et al.* 1995, Romero 1999, Aung *et al.* 2001) and gives the distribution of entrance pore sizes, related to throats or *bonds*. Mercury extrusion is a wetting process giving the trapped pore sizes, cavities or *sites*.

As seen in Figure 6, extrusion curves for the overall pore size range are not available. This process was stopped at 0.7 MPa (i.e. pore diameter 1.75 μm) at the end of the high pressure cycle. The experimental setting consisted on the application of two cycles of low (0.003 – 0.7 MPa) and high (0.7 – 227 MPa) pressure. In order to identify the distributions of bonds and sites, a first approach was conducted using the obtained mercury intrusion PSD data. The density function of bonds was determined from the PSD intrusion curve of point 9 (wetting, $w = 27\%$), according to the analysis of Figure 8. In the same way, the density function for sites was estimated from the PSD intrusion curve of point 1 (initial state, $w = 14\%$). Even if both PSD curves correspond to mercury intrusion processes, the PSD of point 8 (wetting, $w = 27\%$) is characterised by a smaller mean pore diameter (4.6 μm) in comparison with the larger mean pore diameter (8 μm) of the PSD of point 1 (initial state, $w = 14.4\%$). Then, bonds can be represented by the smaller entrance pores during wetting (due to swelling), and sites by the bigger entrance pores at the initial state.

Results of this initial approach are presented in Figure 9. The curve accounts for a residual water content of 3.5% related to the water adsorbed on the clay fraction. The model well describes a hysteresis gap between the drying and wetting boundary curves. However, these curves are far from the observed experimental response, especially for water contents lower than 10%. Actually, the assumption of the existence of a unique mean size contradicts the

microstructure analysis that showed the coexistence of trapped large pores, inter-grains pores, pores within clay aggregations, and spaces between clay platelets (observed by mercury extrusion).

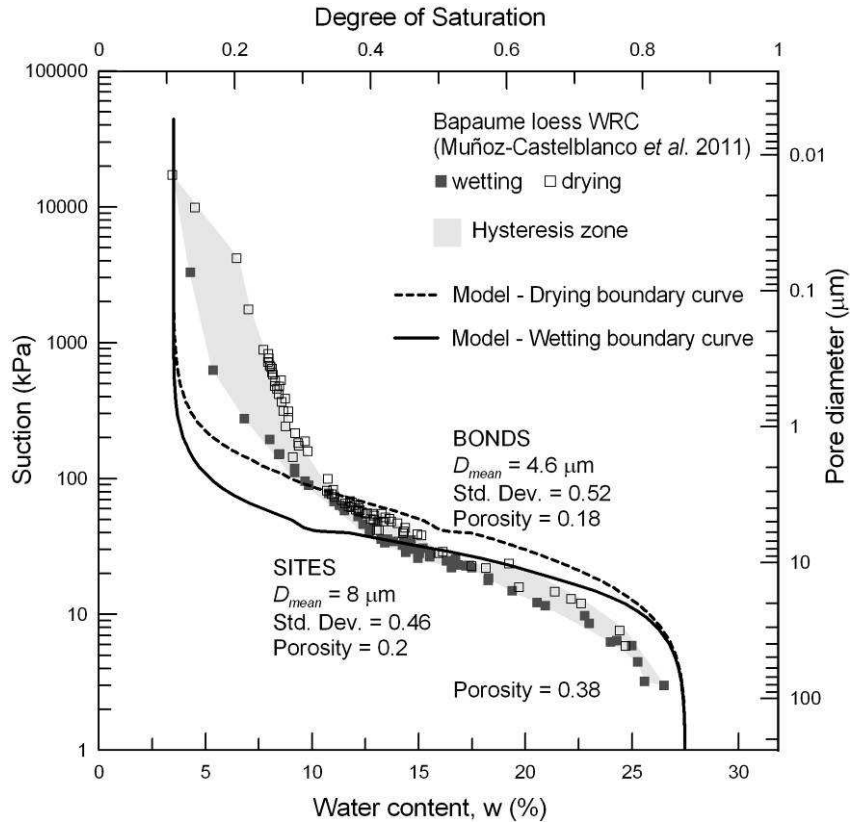


Figure 9. Retention curves from the original Dual Site-Bond Model

As a consequence, an extension of this model is now proposed. It consists in separating the overall pore network into four levels of microstructure: a volume associated to spaces between clay platelets (Figure 10), pores within clay aggregations (Figure 11), pores between silt grains (Figure 12), and large pores (Figure 13). The density functions are analysed by the dual bond-site model using two normal logarithmic PSD curves (for bonds and sites) for each domain. For the volume related to spaces between clay platelets, the density function for sites is obtained from the mercury extrusion curve presented in Figure 10. Density function for bonds is determined by the mercury intrusion curve. Bonds must be smaller than sites following the model's principles. Density functions were obtained separately for drying and wetting processes to account for the clay particles' volume changes during these processes. Data to obtain the drying side of the water retention curve were determined from the PSD curve of point 5 (wetting, $w = 8\%$), according to the analysis of Figure 8. Conversely, data to obtain the wetting side were determined from the PSD curve of point 2 (drying, $w = 11\%$).

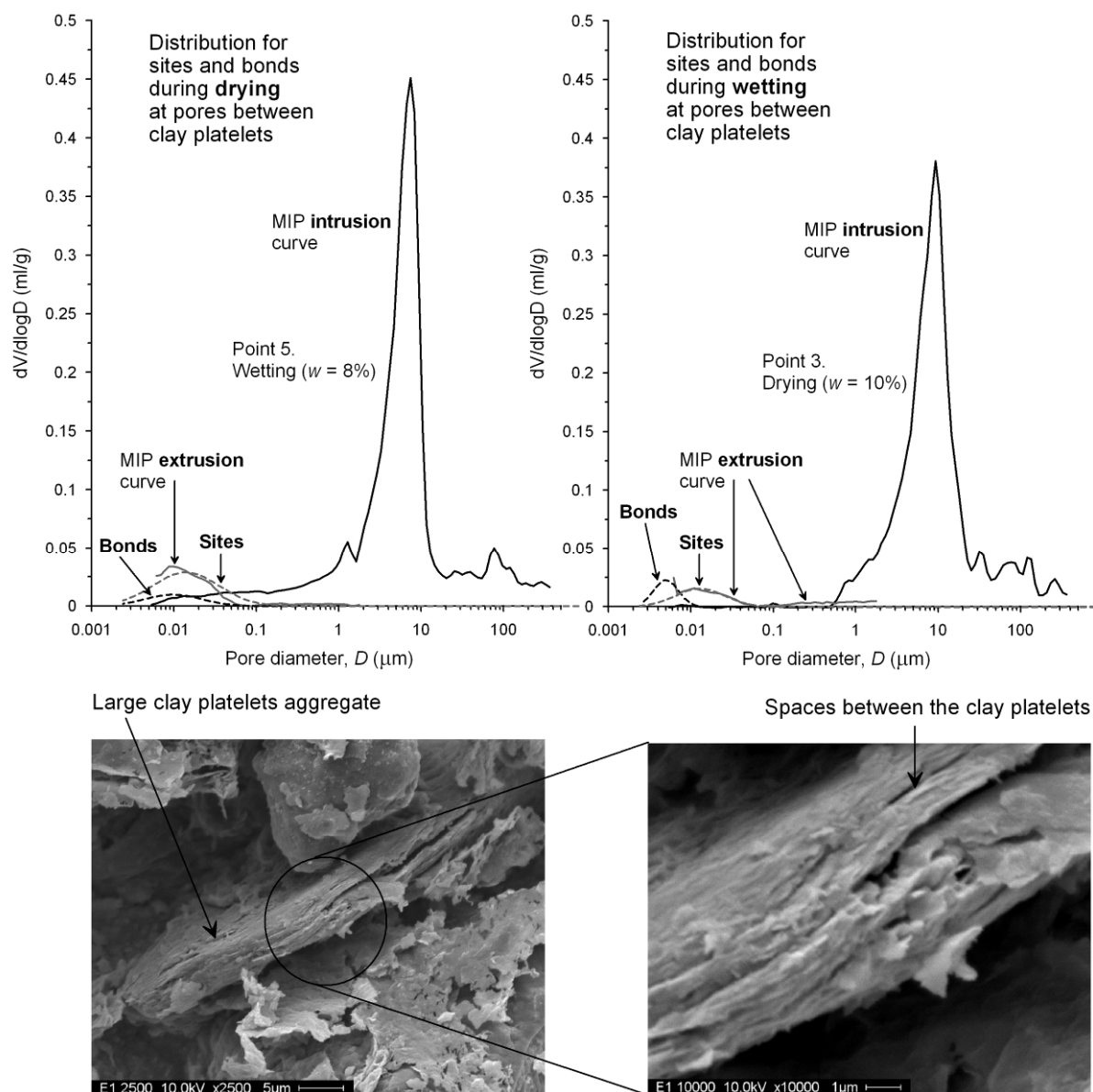


Figure 10. Proposed PSD curves for the spaces between clay platelets. Modified Dual Site-Bond Model

The separation between density functions for wetting and drying was also applied to the analysis of pores within clay aggregations (see Figure 11). For both the inter-grains pores and macropores this distinction was not made, assuming a rigid grain-skeleton. As the extrusion process only concerns the spaces between clay platelets, the other density functions for sites were obtained by analysing together the PSD intrusion curves and the MEB photographs. The parameters of the used PSD curves are presented in Table 2.

The obtained drying and wetting boundary curves from the extended model are presented in Figure 14. A residual water content of 2% is assumed in order to scale the curve to the experimental data at high suctions. This water content corresponds to the relatively high potential of clays to adsorb water as previously discussed in this document.

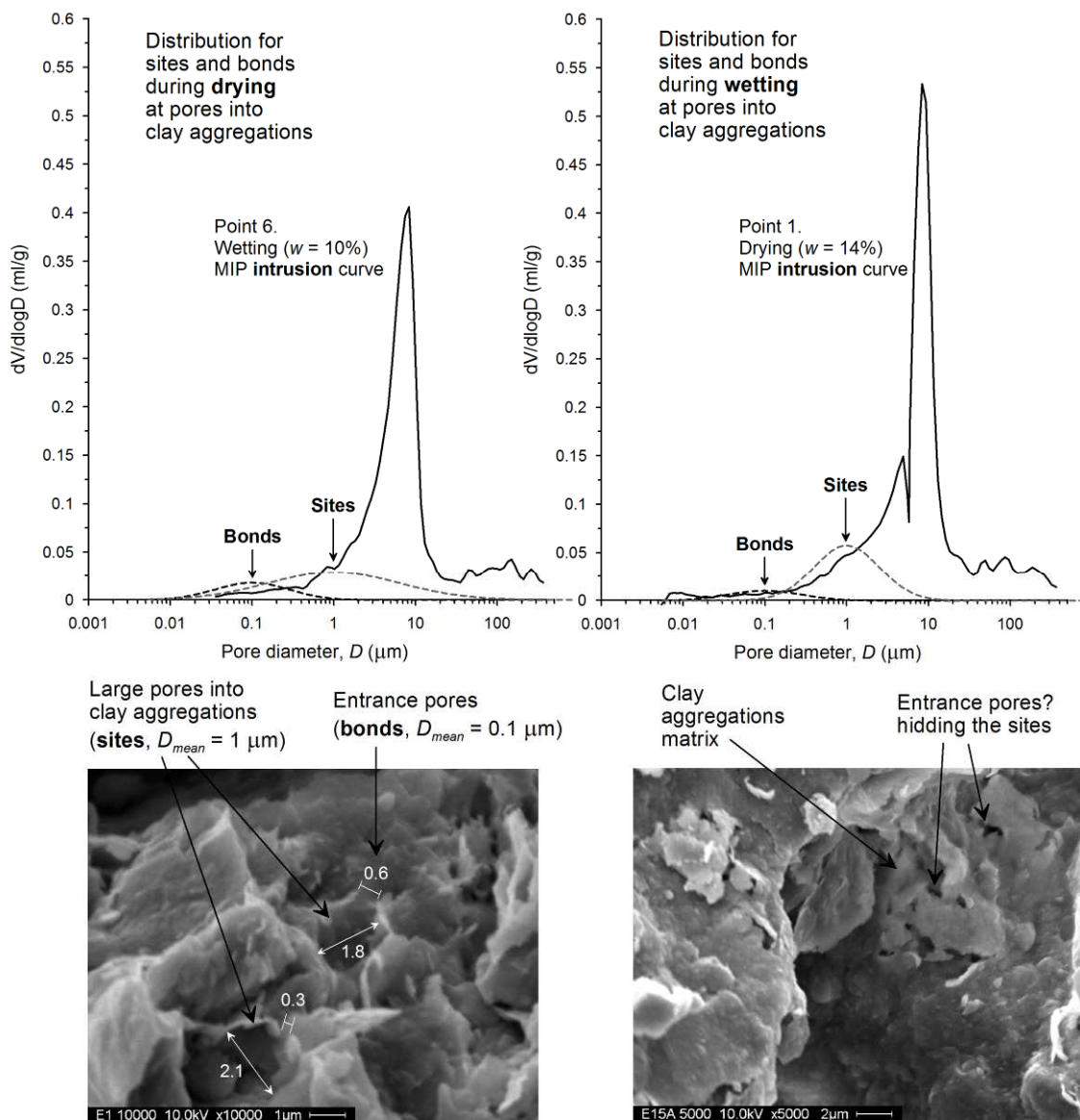


Figure 11. Proposed PSD curves to pores within clay aggregations. Modified Dual Site-Bond Model

The pore sizes of bonds and sites at each microstructure level are presented in Figure 14. It shows that the inter-grains pores located around the silt grains skeleton control the main drainage portion for water contents ranging from $w = 25\%$ to $w = 10\%$, corresponding to suctions from about 10 kPa to 80 kPa. Large pores control the drainage at high degrees of saturation. Pores existing within clay aggregations control the drainage from water content $w = 10\%$ to $w = 5\%$, corresponding to suctions from 80 kPa to 4 MPa. The potential of swelling and shrinking of clay aggregations is possibly the main cause of the important hysteretic effects at these water contents. This fact is well captured by the model. Finally, both elements, the spaces between clay platelets and the adsorbed water bounded to them, are responsible for the retention behaviour at high suctions (> 4 MPa).

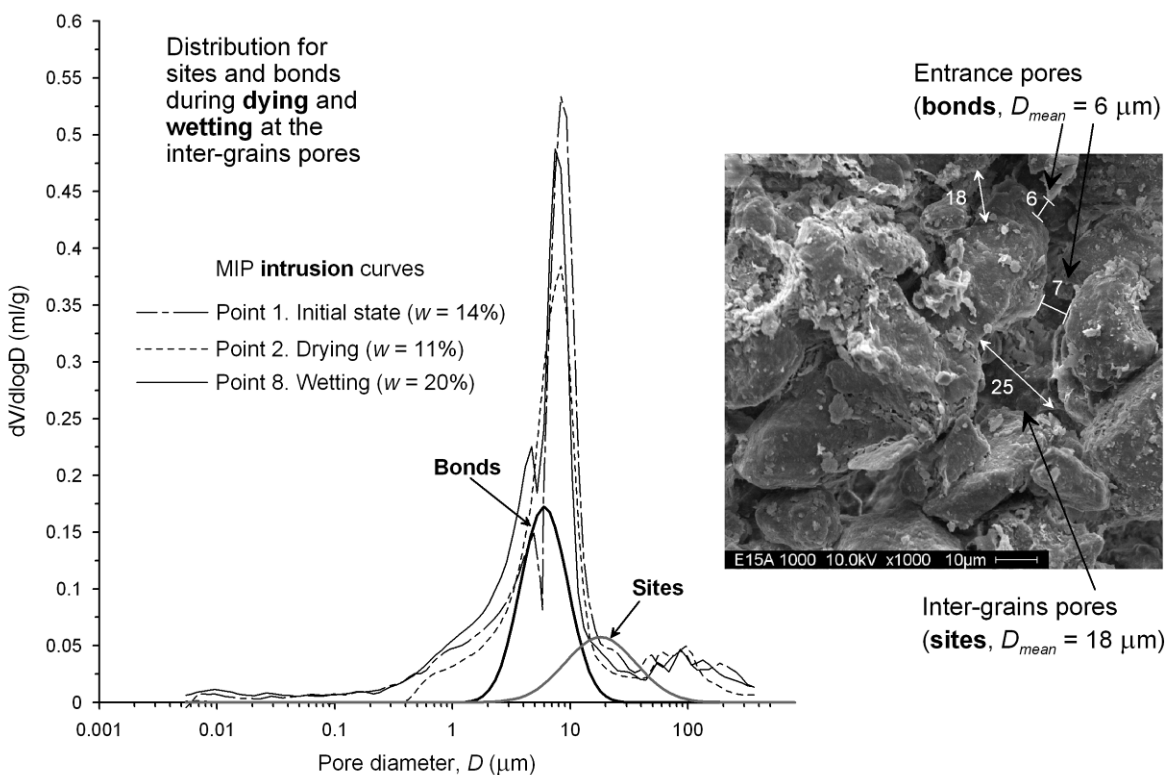


Figure 12. Proposed PSD curves to the inter-grains pores. Modified Dual Site-Bond Model

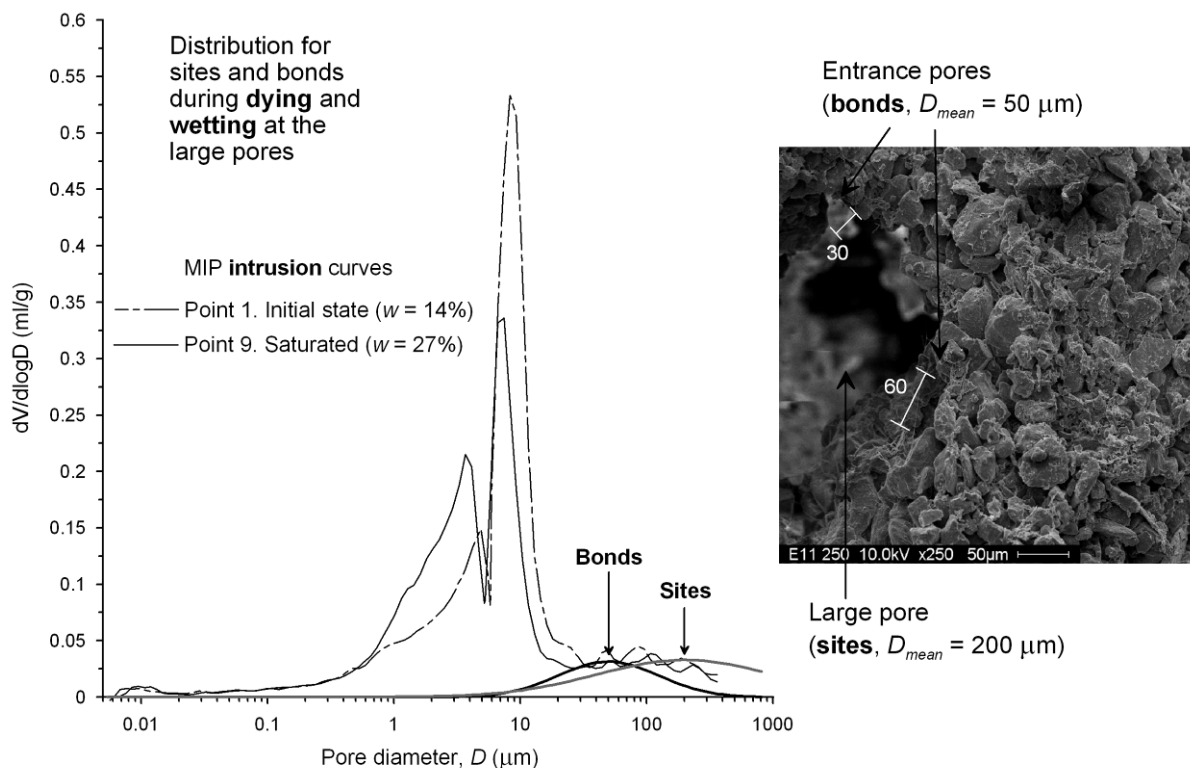


Figure 13. Proposed PSD curves to large pores. Modified Dual Site-Bond Model

Domain	Process	Bonds			Sites			Porosity at each level
		Mean pore diameter (μm)	Standard deviation (log D)	Porosity V_B	Mean pore diameter (μm)	Standard deviation (log D)	Porosity V_S	
Spaces between clay platelets	Drying	0.010	0.35	0.01	0.014	0.40	0.03	0.04
	Wetting	0.005	0.15	0.01	0.013	0.30	0.01	0.02
Pores within clay aggregations	Drying	0.1	0.45	0.02	1	0.8	0.06	0.08
	Wetting	0.1	0.45	0.01	1	0.4	0.06	0.07
Inter-grains pores	Both	6	0.2	0.09	18	0.4	0.04	0.13
Large pores	Both	50	0.4	0.03	200	0.7	0.05	0.08
Porosity (without adsorbed water)							Drying	0.32
							Wetting	0.30

Table 2. Proposed parameters for the Dual Site-Bond Model

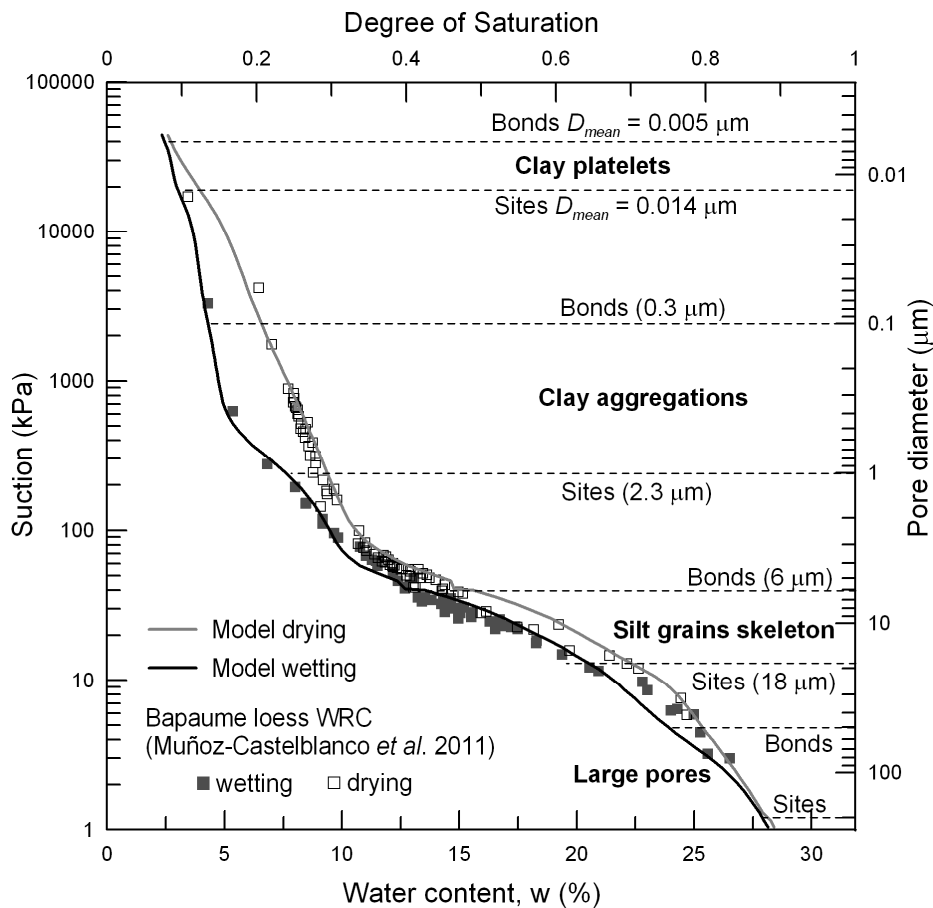


Figure 14. Drying and wetting curves from the modified Dual Site-Bond Model

Conclusions

An analysis of the water retention properties of the Bapaume loess determined by Muñoz-Castelblanco *et al.* (2011) is proposed by means of a detailed microstructure study carried out

by using mercury intrusion porosimetry (MIP) and scanning electron microscopy (SEM). Microstructure observations were carried out at 9 different points along a drying-wetting cycle.

Microstructure observations revealed a porous space composed of four different levels of porosity: large pores with mean pore size of about 200 µm, inter-grains pores with mean size of about 18 µm, pores within clay aggregations with mean size of about 1 µm and spaces between clay platelets. The porosimetries and SEM observations performed during drying and wetting evidenced the swelling of clay aggregations during wetting, and their shrinking during drying. These evolutions affect the retention response of the material and are associated to:

- the decrease of the mean pore size of the inter-grains pores during wetting;
- the increase of the mean pore size of pores within clay aggregations during wetting;
- the increase of trapped large pores ($D_{mean} = 200 \mu\text{m}$) during drying stages.

The retention curves that were calculated from the PSD curves by using Laplace's law did not fit well with the water retention curve of the loess, especially at water contents lower than 10%. The difference is related to different factors: the presence of water adsorbed in the clay fraction, the existence of trapped large pores, and the fact that mercury intrusion only gives the entrance pore radius, thus somewhat overestimating the porous volume associated to the estimated diameter.

In order to account for the complex organization of the porous structure of the loess, the Dual Site-Bond Model proposed by Rojas and Rojas (2005) was used to model the water retention curve. The approach consisting in separating the pore network into sites (or cavities) and bonds (or throats) was initially used with a mixed degree of success. An extension of the model to multiscale pore populations accounting for the cumulative effects of the different levels of porosity was then proposed based on the previous analysis of the loess microstructure. The main drying and wetting branches of the water retention curve obtained with this approach agreed well with the experimental data. Results confirmed the coexistence of four porosity domains (spaces between clay platelets, clay aggregations porosity, inter-grains pores and large pores) that control the retention behaviour of the loess. Further applications of this approach could be used with other soils characterized by a multi-modal pore size distribution.

Acknowledgments

The present study is part of the first author PhD work. It was supported by the European Alβan Program of high level scholarships for Latin America, scholarship N° E07D402297CO, through grants to Mr. J. Muñoz. The support of the French Railways Company SNCF is also acknowledged.

References

- Antoine P. (2002). Les loess en France et dans le Nord-Ouest européen. *Revue Française de Géotechnique* **99**. 3-21.
- Antoine P., Cattt. J. et Sommè J. (2003). The Loess and Coversands of Northern France and Southern England. *Journal of Quaternary Science* **18**. 309-318.
- Askarinejad A., Casini F., Kienzler P. and Springman S.M. (2011). Comparison between the in situ and laboratory water retention curves for a silty sand. In *Proc. 5th Int. Conf. on Unsaturated Soils*, Barcelona, CRC Press. 423-428.
- Aung K.K., Rahardjo H., Leong E.C. and Toll D.G. (2001). Relationship between porosimetry measurement and soil-water characteristic curve for an unsaturated residual soil. *Geotechnical and Geological Engineering* **19**. 401-416.
- Cui Y.J., Delage P., Durand F., Schlosser F. et Wojnarowicz M. (1995). Comportement mécanique des loess sur le tracé du TGV Nord. *XIème Conférence Européenne de Mécanique des Sols et des Travaux de Fondations*, Copenhague, vol. 7. 45-50.
- Cui Y.J., Marcial M., Terpereau J.M., Delage P., Antoine P., Marchadier G. et Ye W.M. (2004). A geological and geotechnical characterisation of the loess of Northern France. *A.W. Skempton Memorial Conference*, vol. 1. 417-428.
- Cui Y.J., Tang A., Mantho A. and De Laure E. (2008). Monitoring Field Soil Suction Using a Miniature Tensiometer. *Geotechnical Testing Journal* **31** (1). 95-100.
- Croney D. et Coleman J.D. (1954). Soil structure in relation to soil suction (pF). *J. Soil Sci.* **5**. 75–84.
- Dane J.H. and Wierenga P.J. (1975). Effect of hysteresis on the prediction of infiltration, redistribution and drainage of water in a layered soil. *J. Hydrol.* **25**. 229-242.
- Delage P., Audiguier M., Cui Y.J. and Deveughele M. (1995). Propriétés de rétention d'eau et microstructure de différents géomatériaux. *XIème Conférence Européenne de Mécanique des Sols et des Travaux de Fondations*, Copenhague, Vol. 3, 43-48.
- Delage P., Audiguier M., Cui Y.J. and Howat M.D. (1996). Microstructure of a compacted silt. *Can. Geotch. J.* **33**. 150-158.
- Delage P., Cui Y.J. and Antoine P. (2005). Geotechnical Problems related with Loess deposits in Northern France. *Proceedings of International Conference on Problematic Soils*. 517-540.
- Delage P., Le T.T., Tang A.M., Cui Y.J. and Li X.L. (2007). Suction effects in deep Boom clay block samples. *Géotechnique* **57** (1). 239-244.
- Delage P., Marcial D, Cui Y J and Ruiz X. (2006). Ageing effects in a compacted bentonite: a microstructure approach. *Géotechnique* **56** (5), 291-304.
- Delage P. et Pellerin F.M. (1984). Influence de la lyophilisation sur la structure d'une argile sensible du Québec. *Clay Minerals* **19**. 151-160.

- Delage P., Tessier D. and Marcel-Audiguier M. (1982). Use of the Cryoscan apparatus for observation of freeze-fractured planes of a sensitive Quebec clay in scanning electron microscopy. *Canadian Geotechnical Journal* 19 (1). 111-114.
- Everet D.H. (1967). The solid-gas interface. (Ed. by Edisson Flood), *Dekker*, New York **II**. 1005-1010.
- Garcia-Bengochea I., Lovell C.W. and Altschaeffl A.G. (1979). Pore distribution and permeability of silt clays. *J. Geotech. Engrg. Div.* **105**. 839-856.
- Gillott J.E. (1973). Methods of sample preparation for microstructurel analysis of soil. In *Soil Microscopy, Proceedings of the 4th International Working-Meeting on Soil Micromorphology*, ed. G.K Rutherford, Kingston. 143-164.
- Haines W.B. (1929). The hysteresis effect in capillary properties and the mode of moisture distribution associated therewith. *J. Agric. Science* **20** (7). 33-52.
- Hanks R.J., Klute A. and Bresler D.F. (1969). A numeric method for estimating infiltration, redistribution, drainage and evaporation of water from soil. *Water Resour. Res.* **5**. 1064-1069.
- Hillel, D. (1971). Soil and water: Physical principles and processes. *Academic*, New York
- Hogarth W.L., Hopmans J., Parlange J.-Y. and Haverkamp R. (1988). Application of a simple soil-water hysteresis model. *J. Hydrol.* **98**. 21-29.
- Jennings J.E. et Knight K. (1957). The additional settlement of foundation due to collapse of sandy soils on wetting. *Proc. 4th ICSMFE* **1**. 316-319.
- Karam J.P., Cui Y.J., Tang A.M., Terpereau J.M. et Marchadier G. (2009). Experimental study on the cyclic resistance of a natural loess from Northern France. *Soils and Foundations* **49** (3). 421-429.
- Kawai K., Kato S. and Karube D. (2000). The model of water retention curve considering effects of void ratio. *Proc. Asian Conf. Unsaturated Soils*. 329-334.
- Knight K. (1963). The origin and occurrence of collapsing soils. *Proc. 3rd Reg. African CSMFE* **1**. 127-130.
- Konyai S., Sriboonlue V., Trelo-ges V. and Muangson N. (2006). Hysteresis of water retention curve of saline soil. In *Proceedings of the Fourth International Conference on Unsaturated Soils*, Carefree, ASCE. 1394-1404.
- Le T.T., Delage P., Cui Y.J., Tang A.M., Lima A., Romero E., Gens A. and Li X.L. (2008). Water retention properties of Boom Clay: A comparison between different experimental techniques. In *Proc. 1st Eur. Conf. on Unsaturated Soils*, Durham, CRC Press. 229-234.
- Low P.F. (1987). Structural component of the swelling pressure of clay. *Langmuir* Vol. 3. 18-25.
- Manthro A. (2005). Echanges sol – atmosphère: application à la sécheresse. PhD thesis. *École Nationale des Ponts et Chaussées*. Paris.
- Mitchell J.K. and Soga K. (2005). Fundamentals of Soil Behavior. *John Wiley & Sons, ltd.*, 3th edition.
- Muñoz-Castelblanco J.A., Delage P., Pereira J.M., Cui Y.J. Some aspects of the compression and collapse behaviour of an unsaturated natural loess. Submitted to *Géotechnique Letters* in Jan 2011.
- Muñoz-Castelblanco J.A., Pereira J.M., Delage P. Cui Y.J. (2011). The water retention properties of a natural unsaturated loess from Northern France. *Géotechnique*, accepted to publication.

-
- Nimmo J.R. (1992). Semi-empirical model of soil water hysteresis. *Soil Sci. Soc. Am J.* **56**. 1723-1730.
- Pécsi M. (1990). Loess is not just the accumulation of dust. *Quaternary International* **7/8**. 1-21.
- Pham H.Q., Fredlund D.G., and Barbour S. L. (2003). A practical hysteresis model for the soil-water characteristic curve for soils with negligible volume change. *Géotechnique* **53**. 293-298.
- Prapaharan S., Altschaeffl A. and Dempsey B.J. (1985). Moisture curve of compacted clay: mercury intrusion method. *Journal of geotechnical Engineering*, **111** (9). 1139-1142.
- Purcell W.R. (1949). Capillary pressures, their measurement using mercury and the calculation of permeability therefrom. In *Petroleum transactions, IME*, **186**. 39-48.
- Regab R., Feyen J. and Hillel D. (1982). Effect of the method for determining pore size distribution on prediction of the hydraulic conductivity function and of infiltration. *Science Society of America, Proceeding* **12**. 141-145.
- Ridley A. and Burland J. (1993). A new instrument for the measurement of soil moisture suction. *Géotechnique* **43** (2). 321 – 324.
- Rojas E. and Rojas F. (2005). Modelling hysteresis of the soil-water characteristic curve. *Soils and Foundations* **45** (3). 135-145.
- Romero E. (1999). Characterisation and thermo-hydro-mechanical behaviour of unsaturated Boom clay: an experimental study. PhD thesis. *Universitat Politècnica de Catalunya*. Barcelone.
- Scheidegger A.E. (1957). The physics of flow through porous media. *University of Toronto Press*.
- Simms P.H. and Yanful E.K. (2001). Measurement and estimation of pore shrinkage and pore distribution in a clayey till during soil-water characteristic curve tests. *Canadian Geotechnical Journal* **38** (4). 741–754.
- Tovey N.K. and Wong K.Y. (1973). The preparation of soils and other geological materials for the scanning electron microscope. *Proceedings of the International Symposium on Soil Structure*, Gothenburg, Sweden. 176-183.
- Vázquez M., Durand P. and Justo J.L. (2011). Soil-Water Characteristic Curve (SWCC) and volumetric deformation law for a plastic clay under high suction. In *Proc. 5th Int. Conf. on Unsaturated Soils*, Barcelona, CRC Press. 509-512.
- Yang C., Cui Y.J., Pereira J.M. et Huang M.S. (2008). A constitutive model for unsaturated cemented soils under cyclic loading. *Computers and Geotechnics* **35**(6). 853-859.

Chapitre 3. Dispositifs expérimentaux

Table de matière

3.1	Introduction	111
3.2	Mesure de la teneur en eau: Nouvelle sonde de résistivité électrique.....	113
	Article 3. Measurement of the water content of a natural unsaturated loess by a new resistivity probe	115
	Introduction	115
	Elements of electrical resistivity in soils.....	116
	Material and experimental setup	118
	Experimental investigation on natural unsaturated loess	121
	Analysis and discussion of the resistivity data.....	123
	Conclusions	127
3.3	Dispositif triaxial pour les sols non saturés : mesure locale de la déformation, la succion et la teneur en eau.....	131
	Article 4. Triaxial testing of a natural unsaturated loess with complete local monitoring.....	133
	Introduction	133
	Tested loess	134
	Triaxial apparatus	136
	Testing procedures and results	146
	Discussion	153
	Conclusions	154

3.1 Introduction

Un nouvel appareil triaxial a été conçu pour tester le comportement hydromécanique du lœss en condition non saturée. Il est doté des mesures locales de succion, teneur en eau et déplacement à mi-hauteur de l'éprouvette triaxiale. Une sonde permettant de mesurer les variations de la teneur en eau dans le sol a été développée. Celle-ci est basée sur une mesure de résistivité électrique, dont la valeur est sensible aux changements d'humidité du sol. Cet ensemble de capteurs a été utilisé pour suivre au niveau local la variation des grandeurs hydromécaniques au cours des différents chemins de sollicitation.

Après les travaux précurseurs de Bishop et Donald (1961), un grand nombre de dispositifs triaxiaux a été conçu par différents auteurs afin de caractériser le comportement mécanique des sols non saturés. Ce genre de dispositifs est souvent équipé de systèmes de contrôle de la succion comme la technique de translation d'axes (Bishop et Donald 1961, Maâtouk *et al.* 1995, Wheeler et Sivakumar 1995, Romero 1999, Hoyos et Macari 2001, Aversa et Nicotera 2002, Barrera 2002, Matsuoka *et al.* 2002, Cabarkapa et Cuccovillo 2006, Padilla *et al.* 2006, Rojas *et al.* 2008, Xu *et al.* 2008), la méthode de contrôle par phase vapeur (e.g. Blatz et Graham 2000, Chávez *et al.* 2009) ou la technique osmotique (e.g. Cui et Delage 1996). Bien que les chercheurs optent souvent pour un contrôle de la succion, il existe des dispositifs triaxiaux qui utilisent la *mesure* de la succion à l'aide de tensiomètres (Colmenares et Ridley 2002, Meilani *et al.* 2002, Jotisankasa *et al.* 2007) ou de psychromètres (Verbrugge 1978, Tang *et al.* 2002, Thom *et al.* 2008). Dans ce travail, un tensiomètre de haute capacité (500 kPa) a été utilisé afin de mesurer la succion pendant l'essai. Ce tensiomètre, de petite dimension (5,7 mm de diamètre), avait été développé auparavant par Chiu *et al.* (2002) et utilisé au cours d'une campagne d'essais en centrifugeuse.

Pour les sols non saturés, tout changement du degré de saturation est associé aux changements du volume et de la teneur en eau du sol. Etant donné qu'on mesure localement les déplacements à l'aide de capteurs de type Effet Hall, il était préférable de mesurer aussi localement la teneur en eau. Ainsi, il fallait une mesure indirecte de la teneur en eau à l'aide d'un capteur approprié aux conditions de mise en place de l'éprouvette de sol dans la cellule triaxiale. D'après différents auteurs (McCarter 1984, Fukue *et al.* 1999, Chen *et al.* 2007, Michot *et al.* 2001), il existe une forte relation entre la variation de la teneur en eau et la valeur de la résistivité électrique du sol. Selon ces auteurs, le courant électrique se propage plutôt par la phase d'eau présente dans le volume poreux du sol, qu'à travers les particules solides. Sur la base de ces éléments, on a développé une sonde de résistivité électrique adaptée à la mesure indirecte de la teneur en eau de l'éprouvette triaxiale. Cette sonde, très légère, de 11 mm de diamètre, a été spécialement conçue pour l'installer facilement à mi-hauteur de l'éprouvette.

Dans ce chapitre, on dédie la *première partie* à la description de la nouvelle sonde de résistivité électrique ainsi qu'à l'analyse de la relation entre la résistivité et la teneur en eau du sol. Les résultats des étalonnages de la sonde et les études complémentaires font partie d'un article soumis au numéro spécial "*Symposium on Innovations in Characterizing the Mechanical and Hydrological Properties of Unsaturated Soils*" de la revue *Geotechnical*

Testing Journal. Ce numéro est dédié aux derniers avancements dans la caractérisation des propriétés hydromécaniques des sols non saturés. Ainsi, cette première partie est composée de cet article dans sa version en anglais.

La *deuxième partie* comporte la description des spécificités du nouveau dispositif triaxial conçu pour tester des sols non saturés. Cette description ainsi que les étalonnages des capteurs et les résultats de trois tests triaxiaux préliminaires ont été inclus dans un article soumis à la revue *Géotechnique*. De la même manière que dans la première partie, la deuxième partie comporte le texte de cet article dans sa version en anglais.

3.2 Mesure de la teneur en eau: Nouvelle sonde de résistivité électrique

Les méthodes de mesure indirecte de la teneur en eau du sol ont été largement développées dans les dernières décennies, spécialement dans les domaines de la géologie et de l'agriculture. Parmi les méthodes existantes, la mesure basée sur la résistivité électrique est un moyen simple pour caractériser l'humidité du sol en se fondant sur la forte relation entre la quantité d'eau et la résistivité du sol. Dans ce travail, on propose une nouvelle sonde de résistivité afin de mesurer les variations locales de la teneur en eau d'échantillons de lœss soumis au cours d'essais triaxiaux. La sonde est installée à mi-hauteur de l'éprouvette triaxiale ; une description détaillée de son utilisation dans le dispositif triaxial sera donnée dans la prochaine section de ce chapitre.

La sonde proposée est un système composé par deux paires d'électrodes, inspiré de la sonde de résistivité de surface développée par Maryniak *et al.* (2003). Elle induit un courant électrique à travers le sol à proximité du contact entre la sonde et l'échantillon. Afin d'obtenir une courbe d'étalonnage, de nombreuses mesures de l'évolution de la résistivité avec la teneur en eau volumique ont été réalisées sur des échantillons du lœss provenant de deux profondeurs différentes.

On a utilisé deux modèles théoriques liant la résistivité à la teneur en eau (Archie 1942, Fukue *et al.* 1999) afin d'analyser les résultats obtenus. On a observé une déviation importante de la courbe de résistivité modélisée par la loi d'Archie par rapport aux données expérimentales (obtenues avec la nouvelle sonde), surtout à des degrés de saturation faibles. Ce comportement semble être lié à la fraction argileuse et aux changements de la microstructure

pendant les processus de séchage. La courbe calculée par le model de Fukue *et al.* montre une meilleure correspondance avec les données expérimentales. Ce fait s'explique car le modèle de Fukue *et al.* tient compte de la variation d'un coefficient de *structure F* qui change avec le degré de saturation, spécialement à des teneurs en eau inférieures à une valeur *critique* associée à la microstructure. L'existence d'une telle valeur suggère que le phénomène de conduction électrique peut être séparé en deux régimes distincts : le transfert par l'eau présente dans les pores inter-agrégats, où la phase d'eau est *continue*; et, la conduction par un réseau *majoritairement discontinu*, composé par l'eau présente dans les pores à l'intérieur des agrégats argileux.

Il est ensuite proposé une discussion sur les possibles relations entre cette courbe d'étalonnage entre la résistivité électrique et la teneur en eau volumique et la courbe de rétention d'eau présentée dans le chapitre précédent et publiée par Muñoz-Castelblanco *et al.* (2011). A partir de ces analyses, on a confirmé que la résistivité électrique est principalement associée à la quantité d'eau dans le sol. Les résultats expérimentaux ne montrent pas d'effets d'hystéresis dans la courbe de résistivité, même si on a observé un phénomène d'hystéresis dans les propriétés de rétention d'eau du lœss.

Cette étude montre aussi que des variations de l'indice de vides initial n'ont que peu d'influence dans la courbe de résistivité en fonction de la teneur en eau. Finalement, les résultats présentés dans cette section prouvent la capacité des sondes de résistivité pour mesurer la teneur en eau dans le sol.

Muñoz-Castelblanco, J., Pereira, J.M., Delage, P. & Cui Y.J. (2011). Submitted to *Geotechnical Testing Journal*

Special issue: *Symposium on Innovations in Characterizing the Mechanical and Hydrological Properties of Unsaturated Soils*

Measurement of the water content of a natural unsaturated loess by a new resistivity probe

J. A. Muñoz-Castelblanco^{*}, J. M. Pereira^{*}, P. Delage^{*} and Y. J. Cui^{*}

Non-destructive methods to measure water content of soils have been extensively developed in the last decades, especially in geologic and agricultural sciences. Among the existing methods, measurement based on the electrical resistivity is a simple and reliable technique to characterize soil moisture based on the strong relationship between water amount and resistivity of soil. A new electrical resistivity probe was developed and used in this study allowing monitoring of local water content variations during triaxial loadings. This probe consists of a two-pair electrodes' set inspired from the concept of concentric and surface probe developed by Maryniak *et al.* (2003). It induces an electrical current through the soil at the vicinity of the probe's contact with the specimen. Experimental data of the resistivity variation with the degree of saturation were obtained by means of this sensor for specimens of a natural unsaturated loess from Northern France. Two theoretical models of resistivity were used to analyze the obtained data. On the basis of the experimental data obtained in this study and the water retention properties of the considered loess (Muñoz-Castelblanco *et al.* 2011), a discussion about special features of the relationships between electrical resistivity, water content and suction is made.

KEYWORDS: soil electrical resistivity; unsaturated soil; loess; resistivity probe; water retention properties; suction

Introduction

A number of studies have shown the relevance of using electrical resistivity to determine the water content of unsaturated soils (Gupta and Hanks 1972, Rhoades *et al.* 1976, 1977, Fowles 1980, McCarter 1984, Roberts and Schwartz 1985, Gorman 1988, Kalinski and Kelly 1993, Fukue *et al.* 1999, Michot *et al.* 2001, Robain *et al.* 2001, Samouëlian *et al.* 2003, Chen *et al.* 2007, Han *et al.* 2009). These studies showed that at low water contents resistivity decreases rapidly with increasing water content. The rate of decrease generally reduces at high water contents (McCarter 1984).

However, the resistivity of a soil does not depend solely on the water content. Other geotechnical parameters like soil density, void ratio, clay fraction, soil structure also have

* Ecole des Ponts ParisTech, Laboratoire Navier – CERMES, Université Paris-Est

significant influence. According to Fukue *et al.* (1999), the resistivity of soils depends on soil characteristics such as the degree of saturation; the electrical resistivity of the pore fluid; the porosity; the shape, size and distribution of solid particles; the diffuse double layer characteristics and the ion concentration and distribution in the diffuse double layer and pore water.

For unsaturated soils, the resistivity widely changes with the water content. The discontinuity of the pore water phase is associated with a domain where the resistivity changes are very sensitive to changes in water content (Fukue *et al.* 1999). This is particularly the case for low porosity and low water contents. It is worth noting that such a trend is observed for the water retention curve of soils containing an important clay fraction. After Romero and Vaunat (2000), the water retention curve of compacted soils exhibit two distinct domains corresponding to intra-aggregate water and inter-aggregate water and that are associated with high and low suction values, respectively.

This paper is aimed at describing the electrical response of a natural unsaturated loess submitted to changes of water content. The obtained results in terms of soil porosity and degree of saturation are then analysed by means of two literature models. A discussion about the links between resistivity data and water retention properties of this loess is finally made.

Elements of electrical resistivity in soils

When considering electrical conduction in soil science (McCarter 1984, Kalinski and Kelly 1993, Fukue *et al.* 1999, Robain *et al.* 2001, Samouëlian *et al.* 2003, Chen *et al.* 2007), soil is depicted as a multiphase material composed of solids, air and water. The electrical resistivity of the assembly of these three phases is analyzed by considering the effect of each phase considered as parallel resistors. The apparent electrical resistance of the soil depends on the solid, air and water electrical resistance values, denoted as R_s , R_a and R_w , respectively. It reads as follows (e.g. Chen *et al.* 2007):

$$R = \left(R_s^{-1} + R_a^{-1} + R_w^{-1} \right)^{-1} \quad (1)$$

The electrical resistance R (the relation between voltage V and current intensity I) is expressed in ohms ($1\Omega = 1V / 1A$). When an electrical current is imposed to a soil specimen by a simple system of two electrodes (anode-cathode), the electrical resistivity ρ can be estimated by the product between the electrical resistance and a geometric coefficient k associated with the size

and arrangement of electrodes. The electrical resistivity equals the inverse of the electrical conductivity and is expressed in ohms-meter (Ωm).

In granular soils, the electrical conductance within solids is assumed to be negligible whereas in clays the effect of water bonded to clay platelets (adsorbed water) leads to a decrease in electrical resistance (Samouëlian *et al.* 2003). On the contrary, air is considered as an electrical insulator (Samouëlian *et al.* 2003) and its electrical conductance is usually neglected. Since the water electrical conductivity is several orders of magnitude higher than that of solid or air phases, the soil apparent electrical resistivity is largely dependent on the amount and continuity of water in the porous space. As an illustration, the electrical resistivity of dry sands is about $10^5 \Omega\text{m}$ whereas it is around $10 \Omega\text{m}$ in saturated sands (Fukue *et al.* 1999).

Robain *et al.* (2001) associated the soil electrical resistivity with soil structure, indicating that low and high resistivity values are related to macro and micro pores respectively. Electrical resistivity decreases with the increase of the amount of available water. Within macro-pores, low resistivity values are associated with water molecules that are more accessible to the electrical current than within micro-pores. Since the soil water distribution is highly dependent on the pore size distribution, electrical resistivity is affected by the soil structure.

The electrical resistivity of a soil aggregate highly depends on its microstructure. This results from the tremendous contrast in resistivity between free water (2 to $100 \Omega\text{m}$) and silicates that are almost non conductive materials with huge resistivity (10^{10} to $10^{14} \Omega\text{m}$). As a consequence, an electrical current will almost totally flow through the pore water within the aggregates. Pore microstructure thus dictates the path of electric currents (Guéguen and Palciauskas 1994).

In the absence of detailed information about pore microstructure, a simple empirical relation between electrical resistivity and porosity was proposed by Archie (1942). It states that the ratio of the saturated resistivity ρ_0 to the free water resistivity ρ_w can be associated with porosity by an empirical exponent a corresponding to a given material. Archie's law, as shown in expression (2), was initially proposed to estimate the resistivity of saturated materials.

$$\frac{\rho_0}{\rho_w} = (n)^{-a} \quad (2)$$

Archie's second law is also empirical and takes into account the effect of the degree of saturation S_r on the electrical resistivity ρ of unsaturated materials (Guéguen and Palciauskas 1994). The saturation exponent b is approximately constant for a given porous medium and a given system of fluids.

$$\frac{\rho}{\rho_0} = (S_r)^{-b} \quad (3)$$

Fukue *et al.* (1999) proposed a more sophisticated model accounting for the combined effects of the serial and parallel transmission of the electric current in the three phases (air, water and solids). They introduced a structural coefficient F to account for the contributions to the total electric current of both the parallel flow (related to $1 - F$ and mainly occurring in water) and the serial one (related to F and mainly influenced by the insulating properties of solids and air). They proposed that the electric resistivity through a cylinder of radius r be read as:

$$\frac{\rho_0}{\rho_w} = \frac{1}{n} \pi r \left(\frac{1}{1 - F_{sat}} \right) \quad (4)$$

$$\Gamma_{sat} = \frac{\rho_w}{(1 - F_{sat})} \quad (5)$$

$$\frac{\rho}{\rho_0} = \frac{1}{S_r} \left(\frac{1 - F_{sat}}{1 - F} \right) \quad (6)$$

in which F_{sat} is the structural factor in saturated conditions and F is varying with the degree of saturation. According to Fukue *et al.* (1999), Γ_{sat} can be used as a measure of the quality of sampling of intact soils. The F factor has the dimension of a length and depends on the structure of the soil, the arrangement of particles, the shape of particles, etc. In unsaturated clays, Fukue *et al.* (1999) observed that, F depended on the water content and pore distribution. The sensitivity of the resistivity to soil moisture changes becomes important when the water content becomes lower than a value termed as "critical" water content. This value can be seen as the threshold value below which the water phase becomes discontinuous.

Material and experimental setup

In this work, electrical resistivity measurements were performed on a natural unsaturated loess sample from a site near the village of Bapaume in Northern France. These loess deposits were formed under periglacial conditions, during the Quaternary period, as the consequence of the aeolian transport of silty sediments. These conditions gave to the loess a relative homogeneity, a low plasticity, a high porosity and an open structure that explain its

susceptibility to collapse (Cui *et al.* 2004, Delage *et al.* 2005, Cui *et al.* 2007, Yang *et al.* 2008, Karam *et al.* 2009). The main geotechnical properties of the loess are summarized in Table 1. Cylindrical specimens of diameter 70 mm and height 17.5 mm were carefully trimmed from intact blocks that were extracted at different depths of a 5m deep excavation.

Sample depth	1 m	3.3 m
Natural water content w (%)	14.0	17.9
Natural void ratio e	0.84	0.60
Dry unit mass ρ_d (Mg/m^3)	1.45	1.67
Natural degree of saturation S_r (%)	46	80
Natural suction (HTC) (kPa)	40	48
Clay fraction (% $< 2 \mu\text{m}$)	16	25
Plastic limit w_p	19	21
Liquid limit w_l	28	30
Plasticity index I_p	9	9
Carbonate content (%)	6	5
In situ total vertical stress σ'_{v0} (kPa)	15.47	35.57

Table 1. Geotechnical properties of the Bapaume loess at two different depths.

A small sized electrical resistivity probe was developed to measure the electrical resistivity under water content variations. It was inspired from the concept of the concentric surface probe developed by Maryniak *et al.* (2003). The probe is composed of four circular electrodes of diameter 1.5 mm disposed in a squared-grid scheme as presented in Figure 1. Figure 2 shows how the resistivity probe is fixed on top of the soil specimen. The system is composed of a precision balance to measure the water mass changes, a metallic mould to house the soil specimen, a plastic cover disk to avoid evaporation during measurement and the resistivity probe fixed to the cover disk. The contact between the probe and the soil is ensured by a fine wet layer of loess slurry placed on the probe.

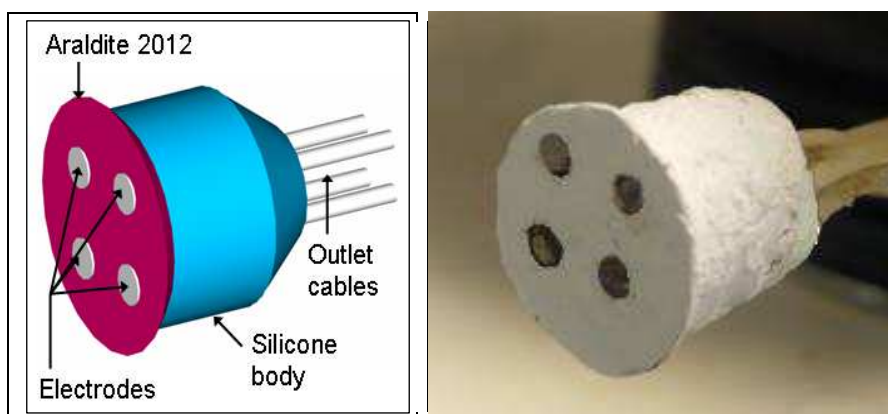


Figure 1. Home-made resistivity probe

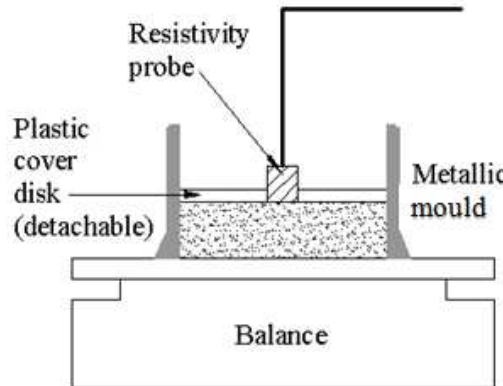


Figure 2. Experimental setup

The diameter of the resistivity probe is 11 mm and the distance between the electrodes is 6 mm. A hydrophobic and dielectric matrix must be used to accommodate the electrodes in order to properly isolate the four electrodes and forbid any direct current line between them. To this end, an epoxy resin (Araldite 2012) was used.

A representation of the electrodes' disposition is presented in Figure 3. Two input electrodes are connected to a voltage source of 10 V. The current passes through the soil (characterized by its electrical resistance R_s) and two output electrodes receive the output signal. For a circuit in parallel:

$$\frac{1}{R} = \frac{1}{R_{s1}} + \frac{1}{R_{s2}} \quad (7)$$

giving $R_s = 2R$ since $R_{s1} = R_{s2} = R_s$.

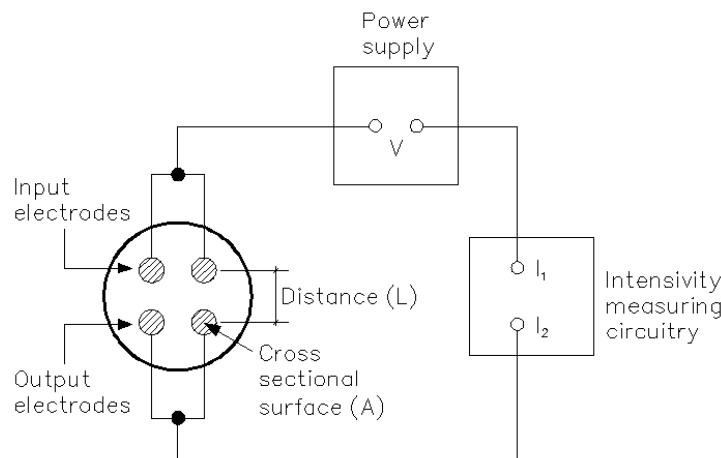


Figure 3. Electric resistivity device with four electrodes.

The shape of the current lines between the input and output electrodes are related to the geometry and boundary of the problem. Then, the electrical resistivity of soil is given as:

$$\rho = \frac{R_s A_e}{L} \quad (8)$$

where R_s is the measured soil electric resistance, A_e is the smallest electrode surface and L is the shorter distance between each pair of electrodes.

Experimental investigation on natural unsaturated loess

Experimental measurements were performed to characterize the relationship between the water content and the soil resistivity. Five loess specimens of height 17.5 mm and diameter 70 mm were subjected to controlled wetting and drying processes while measuring the electrical resistivity. Three specimens from 1m depth ($e = 0.84$) and two others from 3.3 m depth ($e = 0.60$) were tested. One additional loess specimen from 1m depth was tested at a void ratio of 0.72 in order to study the influence of porosity on the resistivity response. This sample was previously compressed in an oedometer from the natural void ratio $e = 0.84$ to $e = 0.72$ at an axial strain rate of 1.7 microns per minute. Compression was performed at the natural water content ($w = 14.4\%$).

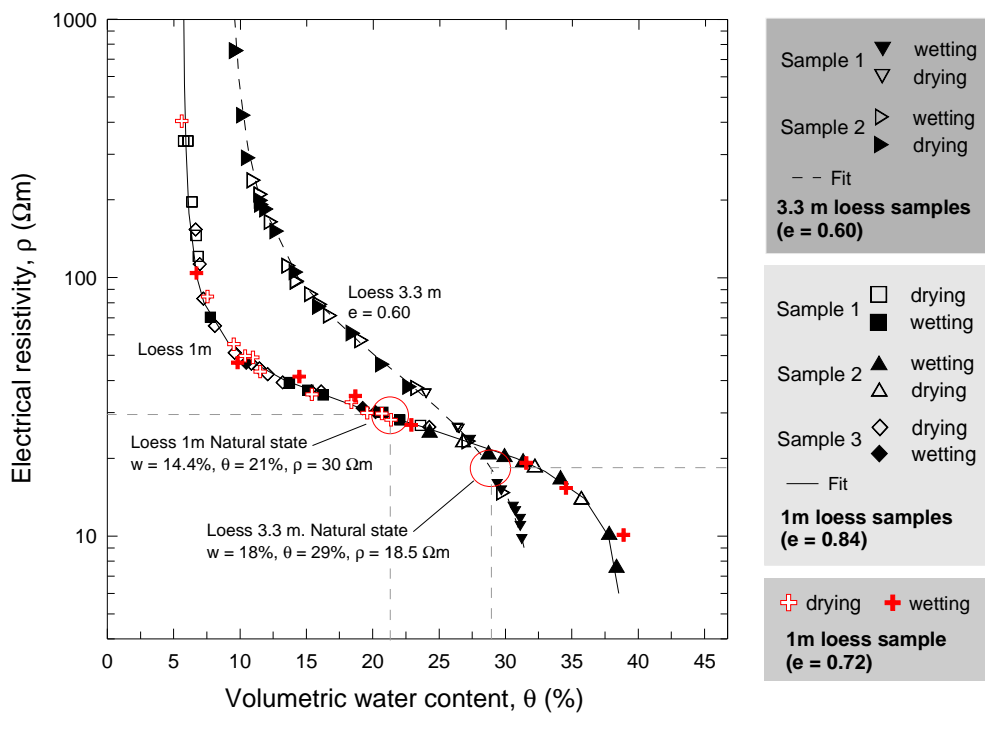
Water content decreases were achieved by free drying the sample in the laboratory for periods of time comprised between 10 and 24 hours. Wetting was achieved by carefully adding small quantities of water to the soil sample. To do so, two pieces of filter paper were placed on top and bottom of the sample and water drops were uniformly distributed over the surface by using a syringe. To ensure water content homogeneity in both drying and wetting cases, samples have been afterwards set to rest for one day. Water content changes at equilibrium were controlled by weighing to an accuracy of 1/1000 g.

Figure 4(a) shows the data obtained in all the samples along both the wetting and drying paths. The relationship between the electrical resistivity and the volumetric water content θ is presented in a semi-log plot. At each depth, a fairly good compatibility between the data from the different samples is observed along both the wetting and drying paths. The obtained results are also plotted against degree of saturation in Figure 4(b).

The sample extracted at 1 m depth and characterized by a natural void ratio $e = 0.84$ exhibits a soil resistivity increase from $7 \Omega\text{m}$ to $350 \Omega\text{m}$ when the volumetric water content decreases from 39.0% to 6.0% (gravimetric water content w decreasing from 27.5% to 4.0% respectively). The slope of the curve indicates that a reasonable estimation of the water

content from electrical resistivity can be made at volumetric water content values higher than $\theta = 7.0\%$ ($w > 5.0\%$). For a drier sample with $w < 5.0\%$, the resistivity rapidly reaches values higher than $100 \Omega\text{m}$ and the changes become too tiny to have a good accuracy in water content. A strong similarity was observed between resistivity data at $e = 0.84$ and $e = 0.72$. In general, resistivity is slightly higher for the densest sample with $e = 0.72$, especially at degrees of saturation higher than 0.7 (see Figure 4(b)). However, this apparent difference is almost negligible if data are plotted in terms of volumetric water content θ .

The resistivity curve of the 3.3 m depth specimens appears steeper than that of the 1 m depth samples, allowing a better determination of the water content that can satisfactorily be made between $\theta = 13.0\%$ and $\theta = 29.0\%$ in volumetric water content (gravimetric water contents between $w = 8.0\%$ and $w = 19.0\%$ respectively). The samples from the two depths have approximately the same plastic characteristics ($w_p = 19\%$, $w_L = 28\%$ at 1m and $w_p = 19\%$, $w_L = 28\%$ at 3.3 m depth, see Table 1) but the deepest samples have a smaller void ratio and a higher initial degree of saturation ($e = 0.60$ at 3.3 m compared to 0.84 at 1 m; $S_r = 0.72$ at 3.3 m compared to 0.46 at 1 m). This explains the smaller initial resistivity (at natural state) of the deepest sample ($20 \Omega\text{m}$ compared to $30 \Omega\text{m}$ at 1 m) in which a larger proportion of the pore volume is full of water.



(a)

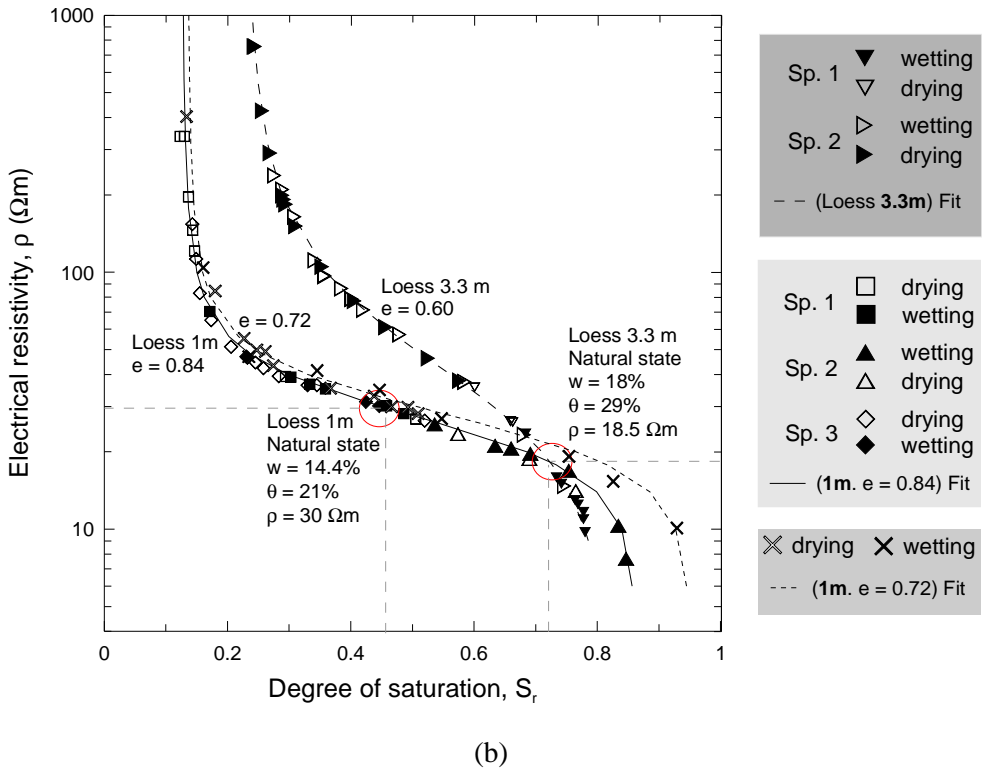


Figure 4. Resistivity data for loess at 1m depth ($e = 0.84$ and $e = 0.72$) and 3.3 m depth. Electric resistivity versus (a) volumetric water content (b) degree of saturation.

The point corresponding to the soil resistivity at natural water content of the 1m depth samples ($\rho = 30 \Omega\text{m}$ at $w = 14.4\%$) is also represented in Figure 4. The Figure shows that water content can be reasonably well estimated from the resistivity measurement with an accuracy of 1 point between $\theta = 7.0\%$ and $\theta = 34.0\%$ (corresponding to a water content range from $w = 5.0\%$ to $w = 24.0\%$ in samples at $e = 0.84$) and between $w = 4\%$ and $w = 23\%$ for samples at $e = 0.72$. The resistivity of the two 3.3 m deep specimens varies between $9 \Omega\text{m}$ and $750 \Omega\text{m}$, corresponding to a change in volumetric water content θ from 31.0% to 10.0% (w between 19.0% and 6.0% respectively). Quite a good agreement between the data from both samples is also observed.

Analysis and discussion of the resistivity data

The data from both soils are presented in a ρ/ρ_0 versus S_r plot in Figure 5 and compared to Archie's second law and to the model proposed by Fukue *et al.* (1999). In this work, the resistivity of distilled water ρ_w was estimated to $3.5 \Omega\text{m}$ compared to the 2 to $100 \Omega\text{m}$ range given for natural fresh water by Palacky (1987). The saturated soil resistivity ρ_0 is equal to $10.3 \Omega\text{m}$ for the 1m depth sample with $e = 0.84$, equal to $10.1 \Omega\text{m}$ for 1m loess sample with e

$= 0.72$ and equal to $9.8 \Omega m$ for the 3.3 m loess specimens. These comparable resistivity values under saturated conditions show that the initial porosity has little effect.

Curves obtained from Archie's law agree reasonably well with the experimental data at degrees of saturation higher than $S_r = 0.15$ for the 1m specimens and higher than $S_r = 0.30$ for the 3.3 m specimens. Given their concave shape, Fukue's curves seem to better agree with experimental data than Archie's law, especially in the domains where a larger deviation from Archie's law is observed for both samples. F_{sat} values (see Equation (6)) are 0.98 m for the 1m loess and 0.99 m for the 3.3 m loess, corresponding to Γ_{sat} values of 305Ω and 366Ω respectively. No physical meaning is associated with the soil parameter F_{sat} . Fukue *et al.* (1999) claim that parameter Γ_{sat} is an indicator of the soil state and that Γ_{sat} values near or higher than 300Ω indicate that specimens are undisturbed. The values of Γ_{sat} obtained here are consistent with the good intact state of specimens that were extracted from blocks. This confirms the quality of the extraction and sampling procedures used.

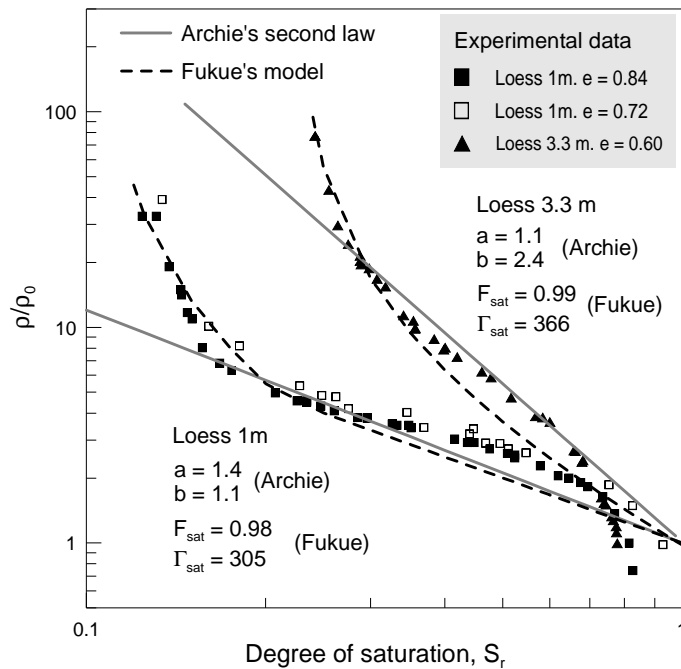


Figure 5. Resistivity data. Comparison with the Archie's second law expression and the Fukue's model

The relationship between the resistivity and the degree of saturation (Figure 5) shows that resistivity is extremely high for the lowest degrees of saturation and very low for the highest ones. The relationship also presents an abrupt drop in resistivity at $S_r = 0.15$ ($w = 5\%$, $e = 0.84$ and $w = 4\%$, $e = 0.72$) at 1m depth and at $S_r = 0.30$ ($w = 7.4\%$) at 3.3m depth. This may result from the continuity/discontinuity of pore water in the clay fraction (Fukue *et al.* 1999).

Beyond this critical degree of saturation, the resistivity seems to be stable and correctly described by the Archie's second law.

Using expression (6) and according to Fukue's model, the saturated ($1-F_{\text{sat}}$) and unsaturated ($1-F$) structural characteristics can now be compared, as done in Figure 6. The two void ratios studied for samples from 1m depth show similar trends in Figure 6(a). It shows that for volumetric water contents higher than $\theta = 7.5\%$ ($w = 5\%$ at $e = 0.84$ and $w = 4\%$ at $e = 0.72$) the ratio $(1-F_{\text{sat}})/(1-F)$ is close to unity. This indicates that the pore water is located within the inter-particle pores and that the electrical flow occurs through a continuous pore water network. According to Fukue *et al.* (1999), the smallest water content with a ratio of unity is defined as "the adsorbed water content". For water contents lower than this critical value, the ratio $(1-F_{\text{sat}})/(1-F)$ seems to increases sharply with water content decrease, as shown in Figure 6(a). At this stage, water is no longer a continuous phase and is adsorbed within the intra-aggregate space.

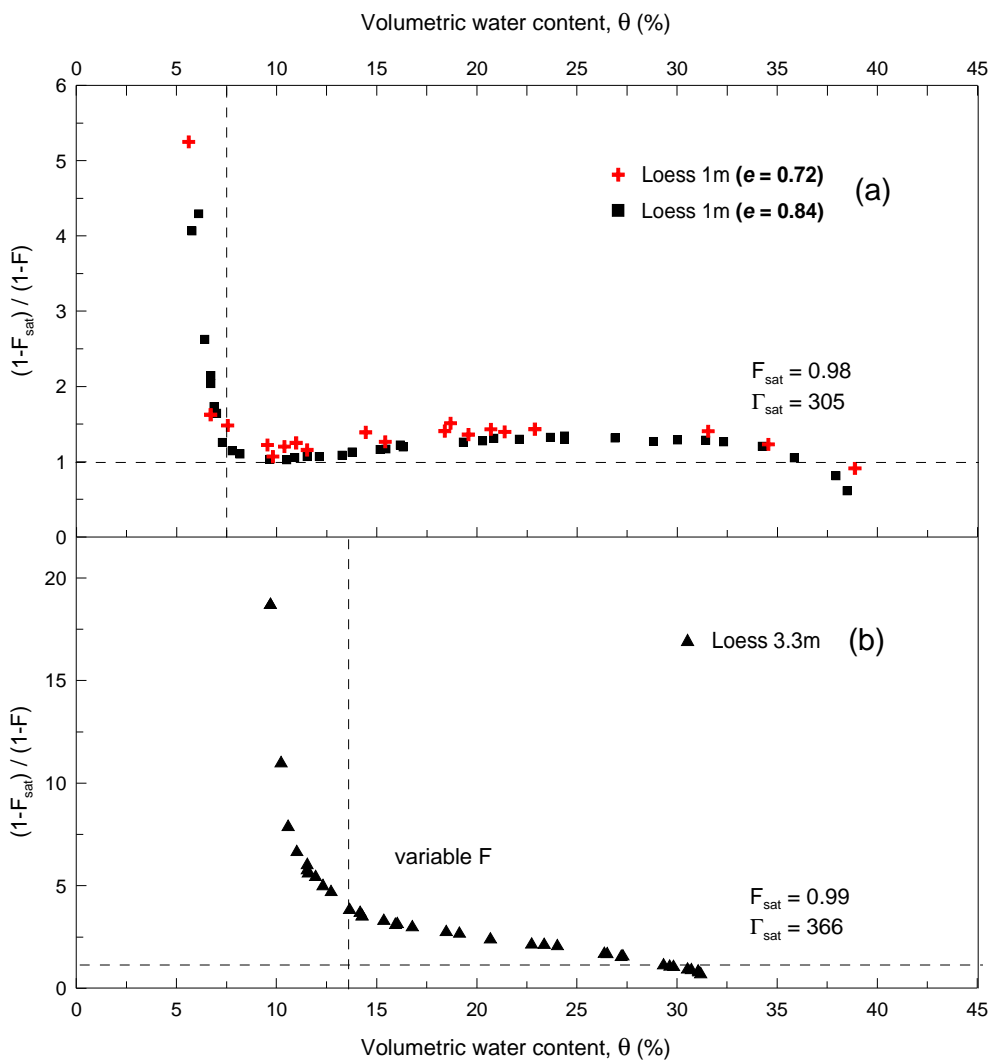


Figure 6. Comparison of the structural factors for loess specimens (Fukue's model)

The trend in the resistivity of the loess at low water contents do not match the usual observations in clays where the resistivity tends to increase more slowly with decreasing degree of saturation at low water contents, where most of the water is adsorbed. This can be interpreted from a microstructure point of view: as observed by Delage *et al.* (1996) in an aeolian silt of same origin, the clay aggregates tend to coat the silt grains and to separate from each other upon drying. This behavior could explain the appearance of the discontinuity of the water phase thus ending in a continuous increase of resistivity.

Figure 6(b) shows the same results for the 3.3m deep samples. The situation is largely different from that of the 1m deep specimens. The ratio $(1-F_{\text{sat}})/(1-F)$ is equal to unity only at water contents higher than 18% ($S_r = 0.72$). This limit coincides with the natural water content of 17.9%. Figure 6(b) shows a smooth increase of the ratio $(1-F_{\text{sat}})/(1-F)$ from 1 at $\theta = 29.0\%$ ($w = 18.0\%$) to 5 at $\theta = 13.8\%$ ($w = 7.4\%$), followed by a sharp increase at $\theta < 13.8\%$. The variations of the ratio $(1-F_{\text{sat}})/(1-F)$ when volumetric water contents vary between $\theta = 13.8\%$ and $\theta = 29.0\%$ could be the effect of an heterogeneous distribution of the clay fraction (25%) associated with a discontinuous distribution of pore water and the lower void ratio ($e = 0.60$) of 3.3m depth ($e = 0.84$ of 1 m depth). The high resistivity values observed at volumetric water contents lower than $\theta = 13.8\%$ seem to be related to a water phase mainly located within the intra-aggregate pores. In Figure 5, Fukue's model was fitted at degrees of saturation lower than 0.20 (loess 1m) and 0.30 (loess 3.3m) to the experimental data by varying the F value as a function of saturation degree. In those ranges, it is observed that F exponentially increases with the decrease of degree of saturation.

Figure 7 plots in the same graph the resistivity against water content and the water retention curve. The experimental water retention curve of the 1m sample obtained by Muñoz-Castelblanco *et al.* (2011) was used. This curve corresponds to the natural void ratio $e = 0.84$. The characterization of the water retention properties of 3.3 m loess was performed by using the filter paper method. Both water retention curves were obtained by performing wetting and drying paths on a testing system similar to that employed in the electrical resistivity measurements. The resistivity ratio ρ/ρ_0 (left y-axis) and suction (right y-axis) are represented on logarithmic scale whereas the water content (upper x-axis) and the degree of saturation (lower x-axis) are presented on linear scale.

As seen in Figure 7, the water retention curve of the 1m sample exhibits a hydraulic hysteresis. This hysteresis may be associated with the open structure of this loess. The 3.3m

loess specimens do not present an observable hysteresis and all paths are located on an almost unique relation between suction and water content. Figure 7 shows that the 1m deep sample presents lower suction values than the 3.3m deep sample at the same range of water content. This is due to the lower porosity of the 3.3m deep sample.

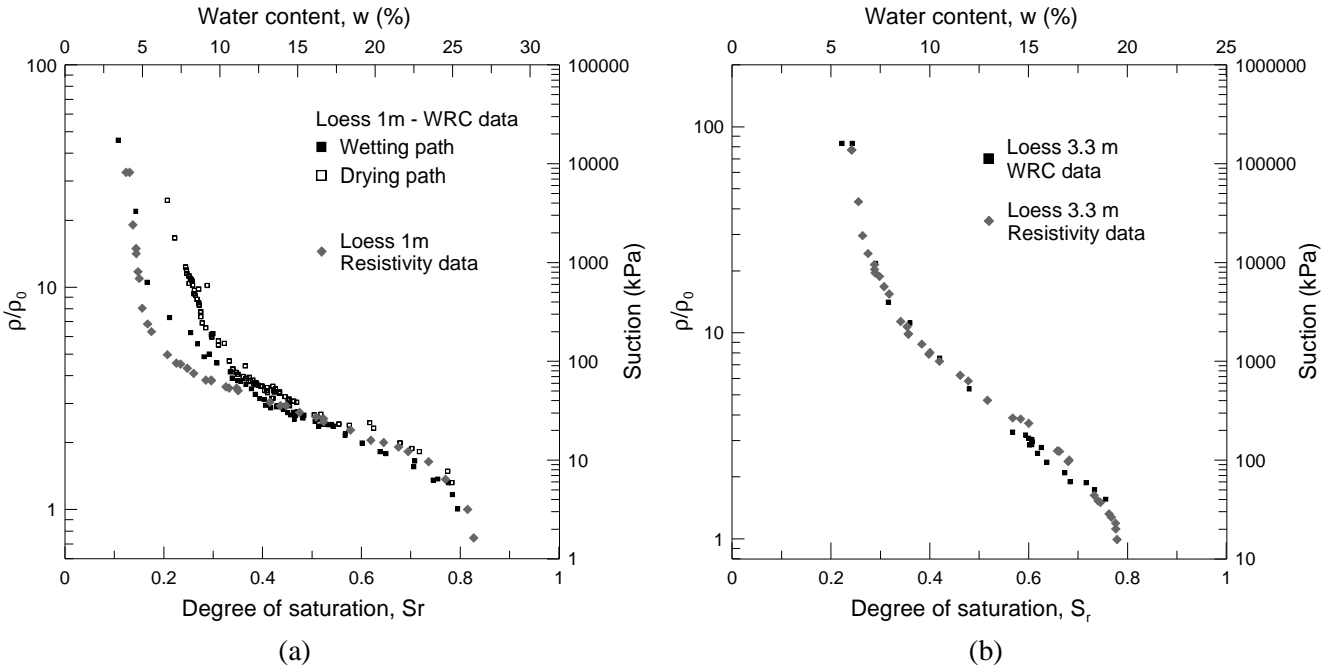


Figure 7. Comparison between water retention curves and resistivity data

Resistivity and water retention curves plotted against water content or degree of saturation show similar trends. An important remark regarding the potential use of electrical resistivity measurement as an estimation of soil moisture concerns the hydric hysteresis. Actually, even if the water retention curve of the 1m depth loess presents an hysteretic behavior, this is not the case for its resistivity data. This is due to the fact that resistivity is mainly related to the amount of water and not to its energetic potential.

Conclusions

The electrical resistivity of a natural unsaturated loess from Northern France was measured under various water contents. A deviation from Archie's law was observed at low degrees of saturation. This observation is linked to the clay fraction of the loess and to possible changes in the loess microstructure during drying. The curve obtained by using Fukue's model agrees well with experimental data at low degrees of saturation because this model accounts for the variation of a structural factor F with the degree of saturation, especially at water contents lower than a "critical" threshold related to the microstructure. This critical value suggests that the electrical conduction behavior can be divided into at least two regimes: the first one

related to the inter-aggregate pores in which the water phase is continuous and the second one corresponding to the intra-aggregate pores where the water phase is disconnected due to the empty pore space between the aggregates.

Electrical resistivity results were discussed with reference to the water retention properties of the loess. It has been confirmed that the electrical resistivity is mainly related to the amount of water. The change in resistivity during a drying-wetting cycle did not show any hysteresis, even if the water retention curve exhibited a hysteresis.

This study also showed that the influence of porosity changes on the resistivity – soil moisture curve may be neglected. Finally, the results presented in this work support the ability of resistivity probes to measure water content of soils.

Acknowledgments

The present study is part of the first author PhD work. It was supported by the European Alþan Program of high level scholarships for Latin America, scholarship N° E07D402297CO, through grants to Mr. J. Muñoz. The support of the French Railways Company SNCF is also acknowledged.

References

- Archie G.E. (1942). The electrical resistivity log as an aid in determining some reservoir characteristics. *Trans. AM. Inst. Min. Metall. Pet. Eng.* **146**. 54-62.
- Chen L., Yin Z. and Zhang P. (2007). Relationship of Resistivity with Water Content and Fissures of Unsaturated Expansive Soils. *Journal of China University of Mining & Technology* **17** (4). 537-540.
- Cui Y.J., Marcial M., Terpereau J.M., Delage P., Antoine P., Marchadier G. and Ye W.M. (2004). A geological and geotechnical characterisation of the loess of Northern France. *A.W. Skempton Memorial Conference*, vol. **1**. 417-428.
- Cui Y.J., Tang A.M., Marcial D., Terpereau J-M, Marchadier G. and Boulay X. (2007). Use of a differential pressure transducer for the monitoring of soil volume change in cyclic triaxial test on unsaturated soils. *Geotechnical Testing Journal* **30** (3). 227-233.
- Delage P., Audiguier M., Cui Y.J. & Howat M.D. (1996). Microstructure of a compacted silt. *Canadian Geotechnical Journal* **33** (1). 150-158.
- Delage P., Cui Y.J. and Antoine P. (2005). Geotechnical Problems related with Loess deposits in Northern France. *Proceedings of International Conference on Problematic Soils*. 517-540.
- Fowles D. (1980). Soil Resistivity Measurements. Report prepared by the *Ductile Iron Pipe Research Institute*, Oak Brook, US.
- Fukue M., Minato T., Horibe H. and Taya N. (1999). The micro-structures of clay given by resistivity measurements. *Engineering Geology* **54**. 43–53.

- Gorman T.G. (1988). Relationships Between Specific Retention, Permeability, and Formation factor. Master's thesis. *Department of Civil Engineering, University of Nebraska-Lincoln*.
- Guéguen Y. and Palciauskas V. (1994). Introduction to the Physics of Rocks. *Princeton University Press.*, Princeton, New Jersey. 294p.
- Gupta S.C. and Hanks R.J. (1972). Influence of Water Content on Electrical Conductivity of the Soil. *Soil Sci. Soc. Am. J.* **36**. 855-857.
- Han M., Youssef E., Rosenberg M., Fleury M. and Levitz P. (2009). Deviation from Archie's law in partially saturated porous media: Wetting film versus disconnectedness of conducting phase. *Physical Review E, the American Physical Society* **79**. 031127-1-11.
- Kalinski R. and Kelly W. (1993). Estimating Water Content of Soils from Electrical Resistivity. *Geotechnical Testing Journal* **16** (3). 323-329.
- Karam J.P., Cui Y.J., Tang A.M., Terpereau J-M and Marchadier G. (2009). Experimental study on the cyclic resistance of a natural loess from Northern France. *Soils and Foundations* **49** (3). 421-429.
- Maryniak W., Uehara T. and Noras M. (2003). Surface Resistivity and Surface Resistance Measurements Using a Concentric Ring Probe Technique. *TREK, INC. Trek Application Note Number 1005*.
- McCarter W.J. (1984). Electrical resistivity characteristics of compacted clays. *Geotechnique*. **34** (2). 263-267.
- Michot D., Dorigny A. and Benderitter Y. (2001). Mise en évidence par résistivité électrique des écoulements préférentiels et de l'assèchement par le maïs d'un CALCISOL de Beauce irrigué. *C. R. Acad. Sci. Paris, Sciences de la Terre et des planètes / Earth and Planetary Sciences* **332**. 29-36.
- Muñoz-Castelblanco J.A., Pereira J.M., Delage P. and Cui Y.J. (2011). Suction measurements on a natural unsaturated soil: A reappraisal of the filter paper method. In *Proc. 5th Int. Conf. on Unsaturated Soils*, Barcelona, CRC Press. 707-712.
- Palacky G.J. (1987). Resistivity Characteristics of Geologic Targets. In *Electrolagmetic Methods in Applied Geophysics*, vol. 1 (ed. M.N. Nabighian). Series: Investigations in Geophysics, vol. 3, Soc. of Expl. Geophys., Tulsa, Okla.
- Rhoades J.D., Kaddah M.T., Halvorson A.D. and Prather R.J. (1977). Establishing Soil Electrical Conductivity-Salinity Calibrations Using Four-Electrode cells Containing Undisturbed Soil Cores. *Soil Science* **123** (3). 137-141.
- Rhoades J.D., Raats P.A.C. and Prather R.J. (1976). Effects of Liquid-phase Electrical Conductivity, Water Content, and Surface Conductivity on Bulk Soil Electrical Conductivity. *Soil Sci. Soc. Am. J.* **40**. 651-655.
- Robain H., Bellier G., Camerlynck C. and Vergnaut D. (2001). Relation entre résistivité et teneur en eau. Importance des caractéristiques granulométriques, minéralogiques et rhéologiques des sols. *Proceedings of the Third Conference of GEOFCAN*, Paris, France, September 25–26. 101–105.
- Roberts J.N. and Schwartz L.M. (1985). Grain consolidation and electrical conductivity in porous media. *Physical Review B, the American Physical Society* **31** (9). 5990.
- Romero E. and Vaunat J. (2000). Retention curves of deformable clays. Proc. International Workshop On Unsaturated Soils: Experimental Evidence And Theoretical Approaches, Balkema. 91 – 106.
- Samouëlian A., Cousin I., Richard G., Tabbagh A. and Bruand A. (2003). Electrical resistivity imaging for detecting soil cracking at the centimetric scale. *Soil Sci. Soc. Am. J.* **67**. 1319-1326.

Yang C., Cui Y.J., Pereira J.M. and Huang M.S. (2008). A constitutive model for unsaturated cemented soils under cyclic loading. *Computers and Geotechnics* **35**(6). 853-859.

3.3 Dispositif triaxial pour les sols non saturés : mesure locale de la déformation, la succion et la teneur en eau

Afin d'assurer le suivi complet de l'état d'un échantillon de sol non saturé pendant de chargement triaxial, on a développé un système permettant la mesure locale de la teneur en eau, de la succion et des déformations axiale et radiale. Ces mesures sont faites avec des capteurs spéciaux installés à mi-hauteur de l'éprouvette triaxiale. On mesure la succion à l'aide d'un tensiomètre de haute capacité (500 kPa) développé au laboratoire UR Navier – CERMES. Le suivi des déplacements locaux est fait avec des capteurs du type Effet Hall. La teneur en eau est mesurée avec la sonde de résistivité électrique, développée dans ce travail et décrite dans la partie précédente. On a obtenu les courbes d'étalonnage de résistivité électrique en fonction de la teneur en eau pour des échantillons de lœss provenant de deux profondeurs différentes (1 et 3,3 m). Les résultats des étalonnages montrent la bonne précision et fiabilité des mesures de teneur en eau avec cette technique.

Afin de tester le système, on a effectué des essais triaxiaux sur des échantillons de lœss extraits à 1m et 3,3 m de profondeur. On a réalisé de tests de cisaillement sous contrainte de confinement constante et égale à la condition de contrainte in-situ. Ces premiers essais ont montré la bonne qualité des résultats et la précision et la fiabilité du dispositif. Les résultats ont donné un aperçu préliminaire du comportement du lœss de Bapaume intact. Il est à noter que ce type d'essais, avec un ensemble relativement complet de mesures locales, sur un matériau intact non saturé est encore peu étudié dans la littérature. Il apparaît que l'application des contraintes de cisaillement, à contrainte de confinement constante et à teneur en eau et volume constants, induit des changements modérés de la succion pendant le test. Le bruit observé dans la variation de la teneur en eau peut être négligé car il est inférieur à la précision de mesure de la sonde de résistivité. La mesure de la teneur en eau pendant 15 heures, sur un échantillon de lœss isolé de variations externes, a montre que la précision de la sonde est de $w = \pm 0.3\%$. Les mesures réalisées avec les capteurs locaux sont en bonne correspondance avec les mesures globales, réalisées aux états initiaux et finaux, de la teneur en eau, de la succion et du volume.

Les échantillons de lœss extraits à 3,3 m sont plus rigides et plus résistants que les échantillons extraits à 1m de profondeur. Bien qu'elles soient faibles, les variations de la

suction semblent être couplées aux variations globales de la teneur en eau : si la teneur en eau diminue, la succion augmente, et vice-versa.

Muñoz-Castelblanco, J., Delage, P., Pereira, J.M. & Cui Y.J. Submitted to *Géotechnique*

Triaxial testing of a natural unsaturated loess with complete local monitoring

J. A. Muñoz-Castelblanco*, P. Delage*, J. M. Pereira* and Y. J. Cui*

To provide a complete local monitoring of the state of an unsaturated soil sample during triaxial testing, a local water content measurement device was adapted to a triaxial device comprising the measurement of local displacements (Hall effect transducers) and suction (High capacity transducer). Water content was locally monitored by means of a local resistivity probe. The water content/resistivity calibration curves of an intact natural unsaturated loess from Northern France extracted by block sampling at two depths (1 and 3.3 m) were carefully determined, showing good precision and repeatability. The validity of two models giving the resistivity of unsaturated soils with respect to their water content was examined.

The first triaxial tests carried out with this device at low stresses in the range of in-situ stresses showed good quality results and provided some preliminary behaviour characteristics of a natural unsaturated soil, a type of material rarely tested up to now in the literature. It appeared that the application of a shear stress at constant water content and volume induced some suction changes. Also, the yield stresses appeared to be significantly higher than the in-situ stresses, confirming the combined effect of partial saturation and structure in the response of the unsaturated loess investigated.

KEYWORDS: unsaturated soil; loess; local monitoring; suction; resistivity; triaxial testing

Introduction

Following the pioneering work of Bishop and Donald (1961), various suction controlled triaxial devices have been developed to test unsaturated soils (Table 1). Most systems are based on the axis translation technique whereas the osmotic technique (Delage *et al.* 1987, Cui and Delage 1996) and the vapour control technique (Blatz and Graham 2000, Chávez *et al.* 2009) have also been used. Triaxial devices with internal suction measurement have also been developed by using psychrometers (Verbrugge 1978, Tang *et al.* 2002 and Thom *et al.* 2008) or high capacity tensiometers (Colmenares and Ridley 2002, Meilani *et al.* 2002 and Jotisankasa *et al.* 2007).

In unsaturated soils, the changes in degree of saturation are derived from the changes in both sample volume and water content. Local strain measurements in unsaturated triaxial soil testing should hence preferably be coupled with local measurements of the changes in water content. In this paper, a new system in which local measurements include local strains,

* Ecole des Ponts ParisTech, Laboratoire Navier – CERMES, Université Paris-Est

suction and water content is presented and used to study the behaviour of an unsaturated natural loess from Northern France.

Author	Soil volume changes (Devices)	Suction (control and/or measurement)	Observations
Bishop ad Donald (1961)	Internal cylinder full of mercury	Axis translation (control). Air pressure applied on top	
Maâtouk <i>et al.</i> 1995	Vertical external deflectometer and lateral strain monitoring device	Axis translation (control). Air pressure applied through a hole at specimen mid-height.	-
Wheeler and Sivakumar 1995	Double cell system	Axis translation (control)	-
Cui and Delage 1996	Double cell system	Osmotic technique (control)	-
Hoyos and Macari 2001	True triaxial strain system	Axis translation (control)	True triaxial device
Barrera 2002	Local strain measurement. Global measurement of volume change and water content	Axis translation (control)	
Aversa and Nicotera 2002	Double cell system	Axis translation (control)	Water content measurement with double walled burettes system
Matsuoka <i>et al.</i> 2002	True triaxial strain system	Axis translation (control)	-
Sivakumar <i>et al.</i> 2006	Twin-cell stress path apparatus	-	-
Cabarkapa and Cuccovillo 2006	LVDT, Radial strain belt	Axis translation (control)	-
Padilla <i>et al.</i> 2006	Double cell system	Axis translation (control)	-
Cui <i>et al.</i> 2007	Double cell system	-	Cyclic loading at different water content levels
Jotisankasa <i>et al.</i> 2007	Local axial strain devices and radial strain belt	Two suction probes at two heights of the specimen (measurement)	Drying and wetting paths under loading
Rojas <i>et al.</i> 2008	Double cell system	Axis translation (control)	-
Thom <i>et al.</i> 2008	Hall Effect transducers	Thermocouple psychrometer (measurement)	-
Xu <i>et al.</i> 2008	Hall Effect transducers	Axis translation (control)	-
Blatz and Graham 2000		Relative humidity	
Chávez <i>et al.</i> 2009	Double cell system / LVDT and DDT transducers	Relative humidity control (vapour transfert)	-

Table 1. Triaxial systems to test unsaturated soils

Tested loess

The soil tested is an intact natural loess from Northern France. In this area, loess deposits were formed under periglacial conditions during the Quaternary period by the aeolian

transport of silt particles eroded by a constant North West wind (Antoine 2002, 2003), resulting in loess deposits characterized by a relative homogeneity, a low plasticity, a high porosity and an loose microstructure. These features explain the loess susceptibility to collapse when exposed to intense rainfall or accidental water leaking (Cui *et al.* 2004, Delage *et al.*, 2005, Yang *et al.*, 2008).

High quality specimens were trimmed from intact cubic block samples (300 mm side) extracted at 1m and 3.3 m depths. The geotechnical properties of the samples are presented in Table 2 and the grain size distribution curves are showed in Figure 1. Both samples, classified as CL in Casagrande's classification, have a relatively low clay fraction and the same low plasticity index (9). The dominant clay minerals are kaolinite, illite and interstratified illite-smectite (Karam 2006). The carbonate content values are close (6% at 1m and 5% at 3.3 m). Due to higher void ratio and lower degree of saturation, the 1 m depth sample exhibits a collapse potential slightly higher than that of the 3.3 m deep sample.

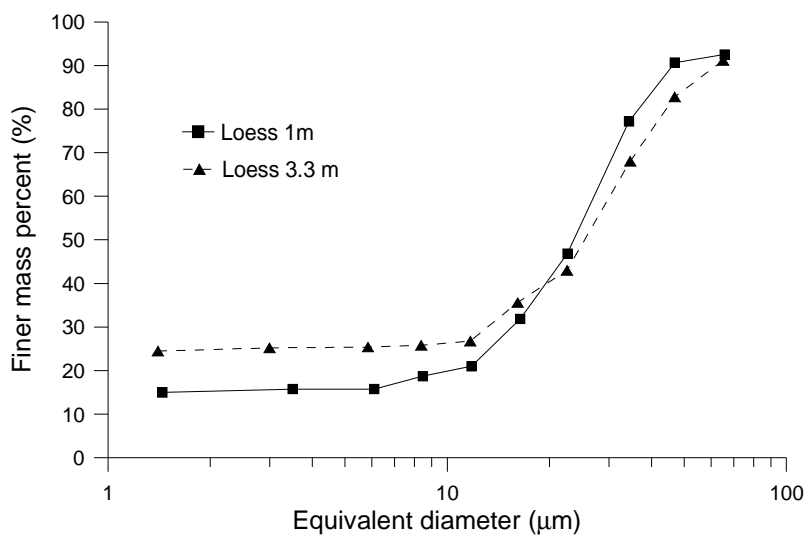


Figure 1. Grain size distribution of Bapaume loess samples from 1 and 3.3 m depths

Sample depth	1 m	3.3 m Test 1	3.3 m Test 2
Natural water content w (%)	14.0	17.9	17.0
Natural void ratio e	0.84	0.60	0.60
Dry unit mass ρ_d (Mg/m ³)	1.45	1.67	1.67
Natural degree of saturation S_r (%)	46	80	76
Natural suction (HTC) (kPa)	40	48	49
Clay fraction (% < 2 μm)	16	25	25
Plastic limit w_p	19	21	21
Liquid limit w_l	28	30	30

Sample depth	1 m	3.3 m Test 1	3.3 m Test 2
Plasticity index I_p	9	9	9
Carbonate content (%)	6	5	5
In situ total vertical stress σ'_{v0} (kPa)	15.47	35.57	35.57
Collapse (%) under σ'_{v0}	7.5	6.3	6.3

Table 2. Geotechnical characteristics of the Bapaume loess

Triaxial apparatus

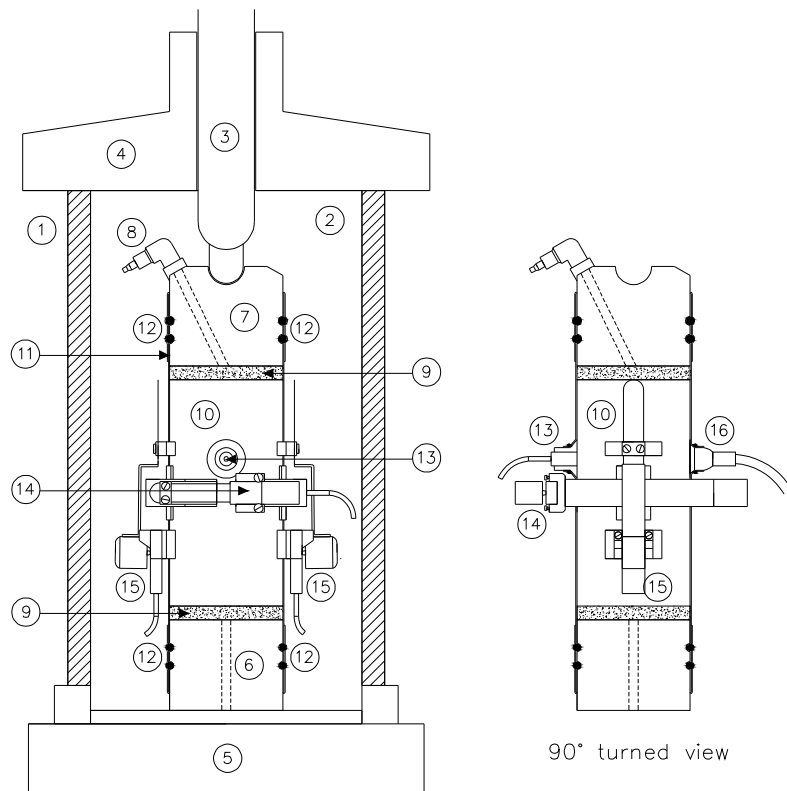
The triaxial cell developed (in Figure 2) was designed to accommodate samples of 50 mm diameter and 100 mm height so as to achieve better precision in local measurements. Hall Effect radial and axial displacement transducers (GDS) were used and the axial displacement was also measured by using an external LVDT transducer. Local suction was measured at the sample mid-height by using a miniature 500 kPa high capacity tensiometer of diameter 5 mm (Chiu *et al.* 2002). Water content was monitored by using a specially designed electrical resistivity probe of diameter 11 mm.

An overall view of the device is presented in Figure 3. Air pressure (maximum value 1 MPa), is regulated by a computer-controlled electro-valve (7). An air-liquid interface cell (9) is used to transmit the air pressure to the fluid. The fluid pressure is measured by using a pressure gauge (5) of 500 kPa capacity. The shear load is applied by a strain-controlled press (1) and measured by an external load sensor of 5 kN capacity (4). The cell base (Figure 4) accommodates the connection wires of the different immersed sensors. The cell chamber consists of a Perspex cylinder and of top and bottom plates. The top plate houses a valve to apply the confining pressure (Figure 3).

Local measurement of the suction

A home-made high capacity miniature tensiometer (HCT) previously designed for centrifuge testing (Chiu *et al.* 2002) was used to measure suction at sample mid-height (Meilani *et al.* 2002, Colmenares and Ridley 2002). As seen in Figure 5, the HCT (Ridley and Burland 1993) is an integral strain gauge tensiometer (Tarantino 2004, Delage *et al.* 2008) of diameter 6.4 mm in which strain gauges are glued to a metallic diaphragm with a thin water reservoir of 0.1 mm thickness. A porous high air entry value ceramic disk (500 kPa) of diameter 5.7 mm and height 1.6 mm (Druck PDCR-81 ceramic disk) is stuck to the system. The HCT allows

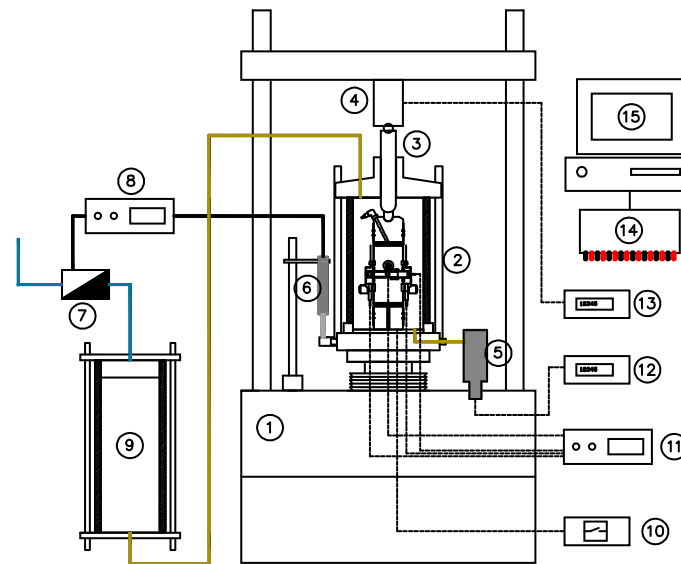
suction measurements between 0 to 400 kPa. As suggested by Tarantino and Mongiovi (2001), the HCT was first saturated at a pressure higher than the air entry value of the ceramic porous stone (700 kPa) to get rid of any air trapped in the system. The tensiometer was also resubmitted to a water pressure of 700 kPa after each cavitation. Performing cycles of cavitation-saturation improves the tensiometer performance (Tarantino and Mongiovi 2001, Chiu *et al.* 2002, Mantho 2005).



1. Perspex cylinder
2. Cell chamber (1 MPa)
3. Loading piston
4. Top plate
5. Cell base
6. Lower cap
7. Top cap
8. Top drainage
9. Porous stone
10. Soil specimen
11. Latex membrane
12. o-rings
13. Tensiometer
14. Radial strain transducer (Hall Effect)
15. Axial strain transducer (Hall Effect)
16. Resistivity probe

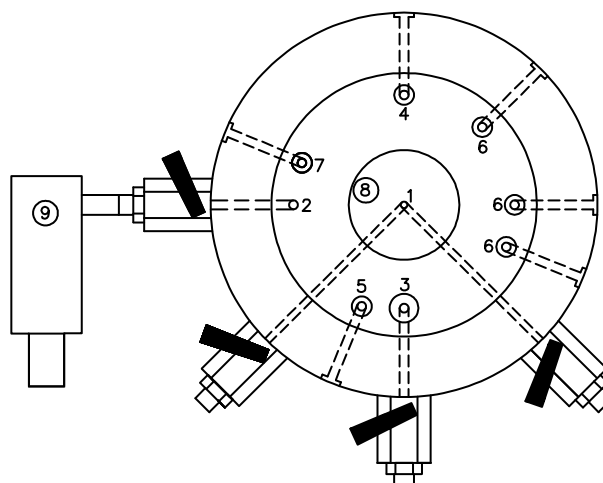


Figure 2. Modified triaxial cell



1. Triaxial press
2. Triaxial cell
3. Loading piston
4. Load sensor
5. Cell pressure sensor
6. Axial displacement LVDT
7. Servovalve
8. Voltage source (24V) : Servovalve, LVDT.
9. Cell pressure exchange (air – silicone oil)
10. Electric current relay
11. Voltage source (10V) : Tensiometer, hall effect sensors
12. Regulator: cell pressure sensor
13. Regulator: load sensor
14. Acquisition card
15. PC

Figure 3. Triaxial system



1. Low specimen drainage connection (2 ways)
2. Cell pressure sensor connection
3. Top specimen drainage connection
4. Tensiometer line
5. Not used
6. Hall effect transducer line
7. Resistivity probe line
8. Soil specimen metallic base
9. Cell pressure sensor

Figure 4. Triaxial cell base

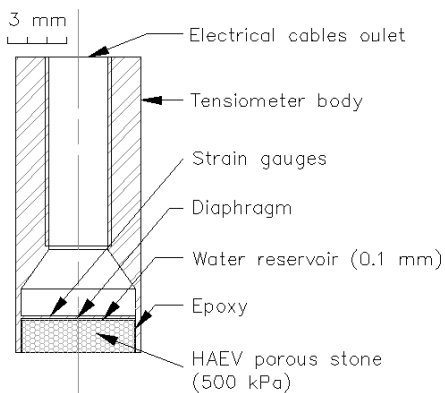


Figure 5. CERMES high capacity miniature tensiometer (Chiu *et al.* 2002)

As seen later in Figure 7 (left), the HCT was placed in contact with the soil specimen by means of a holding system composed of a rubber grommet, O-rings and silicone past to ensure sealing with the membrane. A thin layer of slurry made from the tested soil was placed on the tensiometer surface to improve the contact with the sample and to avoid early cavitation. An elastic band was also placed around the soil specimen to adjust the tensiometer - grommet set.

Local Measurement of the water content

To investigate in the laboratory the relationship between water content and electrical resistivity, Gupta and Hanks (1972) and Rhoades *et al.* (1976) tested compacted specimens by using circular four-probe resistivity cells, a device also utilized by Kalinski and Kelly (1993). Other resistivity measurements were made by Fowles (1980) on compacted specimens, McCarter (1984) on remoulded clays, Fukue *et al.* (1999) on remoulded and natural clays and Chen *et al.* (2007) on expansive soils. As quoted by Kalinski and Kelly (1993), the resistivity of saturated soils depends on the particle size distribution, mineralogy, specific clay surface, porosity, pore size distribution, connectivity of pores, water content, salt concentration and temperature.

In unsaturated soils, the electrical resistance depends on that of the solid phase R_s , of air R_a and of water R_w . Whereas the air phase is an electrical insulator, water has a significantly higher electrical conductivity than solids and the electrical current flows through it. In clay soil, the electrical charges located at the surface of the clay particles lead to greater electrical conductivity (corresponding lower resistivity) than in coarse-textured soils because of the magnitude of the specific surface (Fukue *et al.* 1999). This reduction in electrical resistivity

seems however negligible in low specific surface area systems ($S_s < 50 \text{ m}^2/\text{g}$, Fukue *et al.* 1999) and should not be significant in the loess studied here.

Archie (1942) proposed a simple empirical model relating in saturated soils the soil electrical resistivity ρ , that of the pore water ρ_w to the porosity n :

$$\frac{\rho}{\rho_w} = (n)^{-a} \quad (1)$$

This law was modified for unsaturated soils by introducing the degree of saturation S_r as follows (Guéguen and Palciauskas 1994):

$$\frac{\rho}{\rho_w} = (n)^{-a} (S_r)^{-b} \quad (2)$$

where a and b are experimental parameters.

Fukue *et al.* (1999) proposed a more sophisticated model accounting for the combined effects of the serial and parallel transmission of the electric current in the three phases (air, water and solids). They defined a structural coefficient F to separate the parallel flux (related to $1 - F$ and mainly occurring in water) and the serial one (related to F and influenced by the insulating properties of solids and air) giving the following expression of the electric resistivity ρ through a cylinder of radius r :

$$\rho = \frac{\pi r}{w G_s n} \Gamma ; \quad \Gamma = \frac{\rho_w}{(1-F)} \quad (3)$$

where w is the gravimetric water content, G_s is the specific solid density and n the soil porosity. The F value is a dimension of the length and depends on the structure of the soil. The Γ value can be related to the soil state.

In this work, a small sized electric resistivity probe (11 mm in diameter) was developed to measure the water content at the mid-height of the specimen. It was inspired from the concept of concentric and surface probe developed by Maryniak *et al.* (2003). The probe is composed by four circular electrodes of diameter 1.5 mm disposed in a squared-grid (inter electrodes distance of 6 mm) as presented in Figure 6. A hydrophobic and dielectric matrix (Araldite 2012 epoxy resin) was used to accommodate the electrodes with proper electric isolation). Figure 7 shows how the resistivity probe is fixed on the triaxial sample opposite to the suction probe.

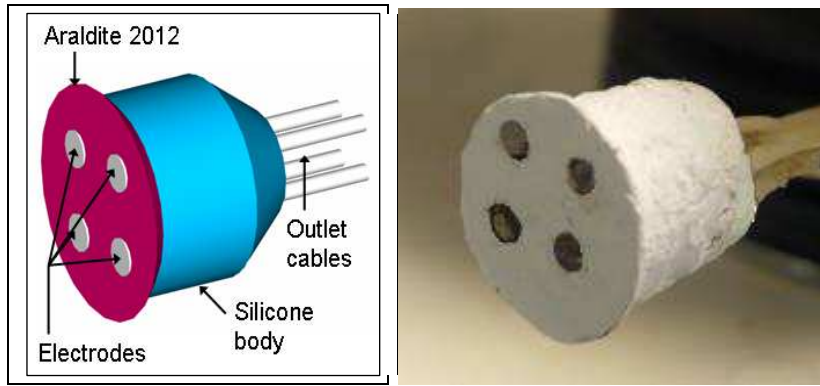


Figure 6. Cermes resistivity probe



Figure 7. Triaxial specimen. Lateral view. Holding system for the tensiometer (left) and the resistivity probe (right)

The electrodes' connection is presented in Figure 8. Two input electrodes are supplied by a voltage source of 10 V. The current passes through the soil (characterized by its resistance R_s) and two output electrodes receive the output signal.

In a circuit in parallel:

$$\frac{1}{R} = \frac{1}{R_{s1}} + \frac{1}{R_{s2}} \quad (4)$$

giving $R_s = 2R$ because $R_{s1} = R_{s2} = R_s$

The shape of the current lines between the input and output electrodes is related to the geometry and boundary of the problem. The electrical resistivity is given as:

$$\rho = \frac{R_s A_e}{L} \quad (5)$$

in which R_s is the measured soil electric resistance, A_e is the smallest electrode surface and L is the shorter distance between each pair of electrodes.

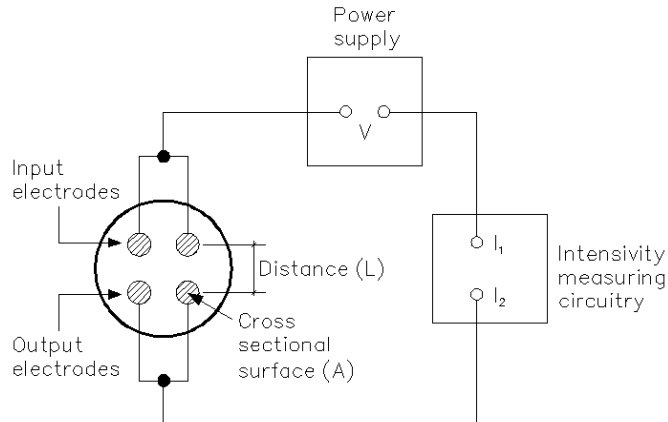


Figure 8. Electric resistivity device with four electrodes.

When an electrical signal comes out from the input electrode, an instantaneous output response is provided by the closest electrodes. Once the initial current peak appears, the electric signal decreases due to diffusion through the soil. To avoid this artefact, electric pulses were sent each 6 minutes during periods shorter than 20 s. The time spacing between the electrical pulses was determined after a calibration taking into account the time needed to disperse all the electrical charge after each pulse. This operation was needed to avoid any polarization in the soil and any effect in the tensiometer also in contact with the specimen. The time taken for half the dispersion to occur is termed the relaxation time τ and is related to characteristic frequency f_0 (Debye 1929, Mitchell and Arulanandan 1968) according to:

$$\tau = \frac{1}{2\pi f_0} \quad (6)$$

Electric dispersion causes several types of polarization in soils (Fam and Santamarina 1995): electronic, molecular, Maxwell-Wagner and macroscopic polarization, each of which has a range of characteristic frequency. The lower limit of the characteristic frequency of the macroscopic polarization is 0.001 Hz corresponding to a maximum relaxation time of 2.65 min, a value that coincides with the half period of electrical dispersion obtained experimentally (3 min).

A calibration was previously performed to characterize the relationship between the water content and the soil resistivity. Five triaxial loess specimens (three from 1m deep and 3 from 3 m deep) of height 100 mm and diameter 50 mm were submitted to controlled wetting and drying processes while measuring their electrical resistivity at mid-height with the gauge presented in Figure 6. To ensure water content homogeneity, drying was performed by allowing evaporation of the sample under laboratory conditions for periods of time comprised

between 10 and 24 hours. Homogeneous wetting was achieved by carefully adding small drops of water with a syringe to the soil sample through two pieces of filter paper placed on top and bottom. Water content changes at equilibrium were controlled by precision weighing (1/1000 g).

Figure 9 shows the calibration data obtained on both samples from 1m and 3.3 m depth along both the wetting and drying paths (whole range in a semi log plot in Figure 9a and a zoom in linear plot between 0 and 100 Ωm in Figure 9b). A fairly good compatibility between the data from the different samples is observed along both the wetting and drying paths. At 1 m depth, the soil resistivity increases from 7 Ωm to 350 Ωm when the volumetric water content θ decreases from 36 to 6 % respectively (gravimetric water content w decreasing from 25% to 4% respectively). The slope of the curve indicates that a reasonable estimation can be made with volumetric water content values higher than 7% ($w > 5\%$). For a drier sample with $w < 5\%$, the resistivity rapidly reach value higher than 100 Ωm and the changes become too tiny. Also reported in the figure is the resistivity of pure distilled water measured in the laboratory (4 Ωm to compare to the 2 - 100 Ωm range given for natural fresh water by Palacki 1987). The soil resistivity at natural water content ($\rho = 30 \Omega\text{m}$ at $w = 14.4\%$) is also represented. The figure shows that the water content can be satisfactorily estimated from resistivity measurement with a precision of 1 point between 24 and 5%. The resistivity of the two specimens tested from 3.3 m changes between 9 Ωm to 750 Ωm , corresponding to a change in θ from 31% to 9% (w between 22% and 7%). Quite a good agreement between the data from both samples is also observed. The calibration curve of the 3.3 m sample appears to be less steep than that of the 1 m sample, allowing a better determination of the water content that can satisfactorily be made between $\theta = 13\%$ and 31% (w between 8% and 22%). The samples from the two depths have approximately the same plastic characteristics ($w_p = 19 - 21$, $w_L = 28 - 30$ at 1 and 3.3 m respectively) but the deepest sample has a smaller void ratio and a higher initial degree of saturation ($e = 0.60$ at 3.3 m compared to 0.84 at 1 m; $S_r = 76 - 80$ at 3.3 m compared to 46 at 1 m). This explains the smaller initial resistivity of the deepest sample (20 Ωm compared to 30 Ωm at 1 m) in which a larger proportion of the pore volume is full of water. A deeper understanding of the differences in shape between the curves could probably be gained by considering in more detail the water retention properties of the two samples.

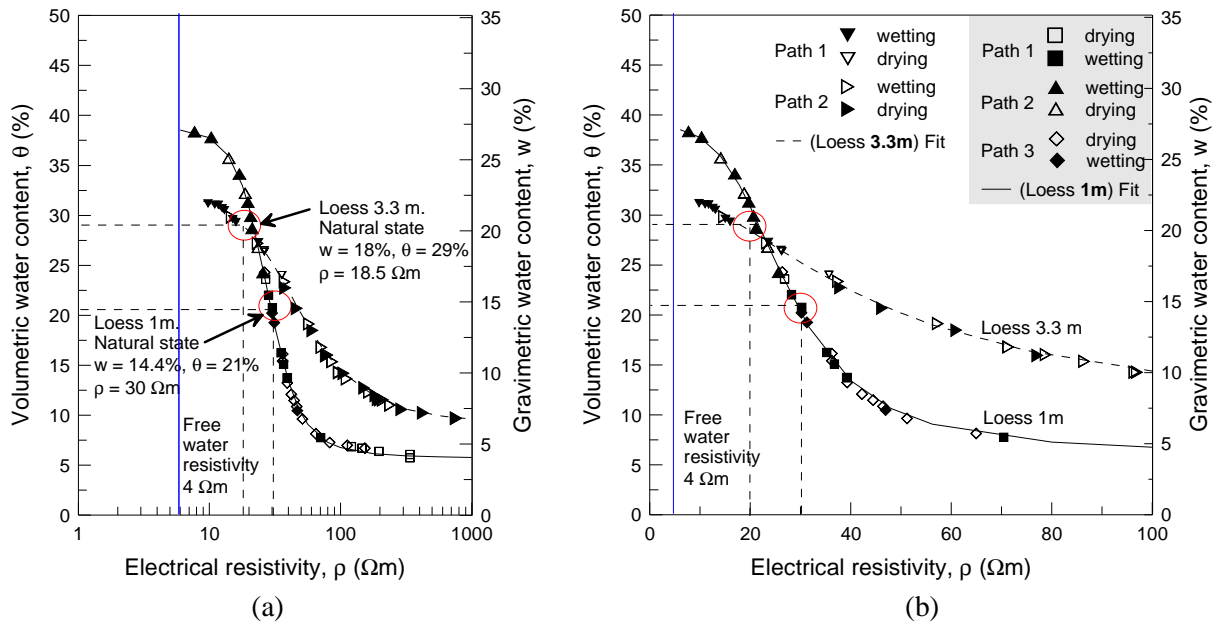


Figure 9. Calibration curves of the resistivity probe for loess at 1m depth and 3.3 m depth. Electric resistivity v.s. volumetric water content. (a) Resistivity values in log-scale. (b) Zoom in true scale

The data from both soils are also presented in a ρ/ρ_w versus S_r plot in Figure 10 and compared to the modified Archie's law and to the model proposed by Fukue *et al.* (1999). Archie's curves agree reasonably well between degrees of saturation of 15 and 70% for the 1m deep specimen and between 30 and 70% for the 3.3 m deep specimen. Given their concave shape, Fukue's curves better agree with experimental data than Archie's model, especially between degrees of saturation of 15 and 75% for the 1m depth specimens and between 25 and 50% for the 3.3 m deep specimens. F values are 0.94 m for the 1m deep specimen and 0.97 m for the 3.3 m deep specimen, corresponding to Γ values of 297 Ω and 366 Ω respectively. There are no evidence of a specific or quantitative meaning of the F value. Fukue *et al.* (1999) state that parameter Γ is an indicator of the soil state and that Γ values near to or higher than 300 Ω indicate that specimens are undisturbed. The values fitted in this study show the good quality of the extraction and sampling procedures followed.

The stability of the probe response with respect to time was checked on the 1m deep soil by using a sample of height 20 mm and diameter 70 mm (Figure 11). The overall sample water content was kept constant at 14.1% by enveloping the sample in a plastic film and a slurry layer of the same loess was put over the probe to ensure proper contact with the sample. The initial measured water content of 26.7% corresponds to that of the slurry. As seen in Figure 11 (top), the water content is observed to linearly decrease due to water transfer from the slurry into the sample with equilibration reached after 16 hours. Once the soil water content is attained, small further variations are observed (Figure 11 down) with a water content

stabilised at $14.15 \pm 0.03\%$ in good agreement with the overall water content determined by weighing. The amount of water infiltrated here from the slurry is not enough to significantly affect the sample water content. The data of Figure 11 indeed shows an excellent stability of the water content measurement.

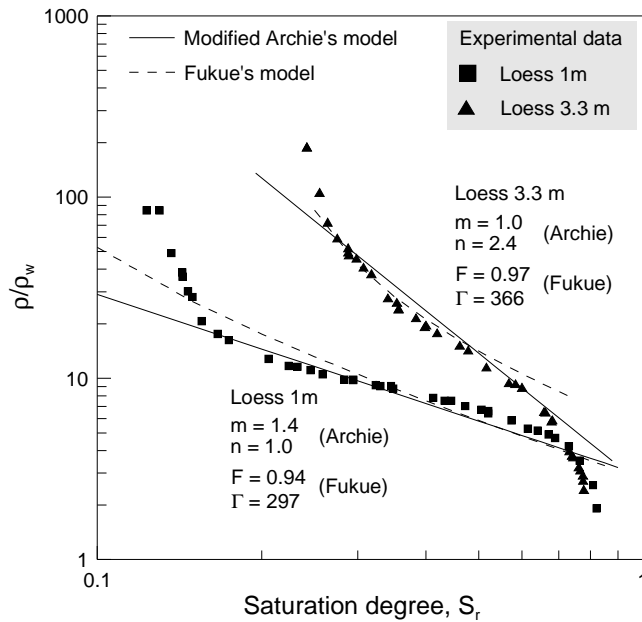


Figure 10. Resistivity data. Comparison with the modified Archie's law expression and the Fukue's model

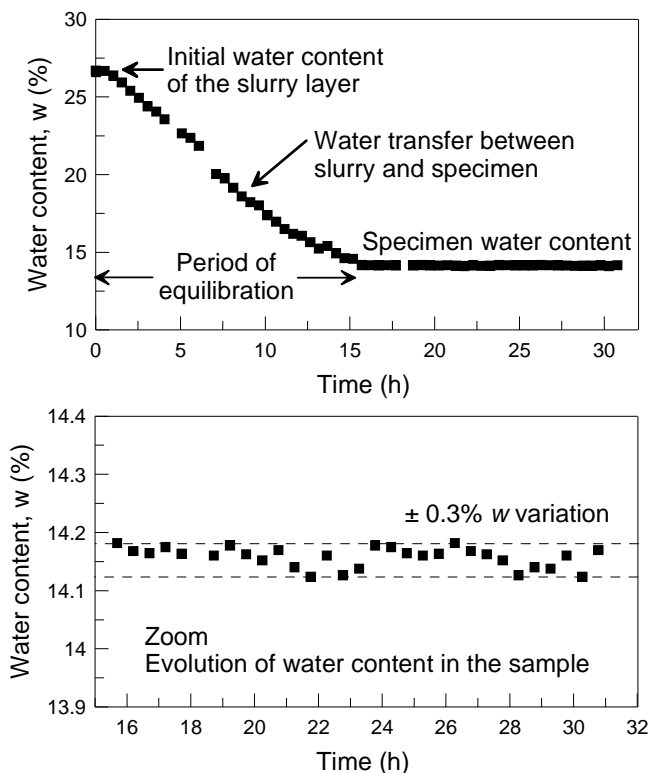


Figure 11. Response of the resistivity probe. Evolution of water content with time. Overall view (top). Zoom (bottom)

Testing procedures and results

After trimming, the dimensions and weight of each sample were taken with a precision calliper. At natural state, the water content was about 14.4% and suction around 45 kPa. To increase the water content, the samples were enveloped with filter paper and carefully sprayed. To decrease the water content, the sample was dried by simple evaporation in laboratory conditions. A subsequent period of equilibration of at least 24 hours was afterwards waited for to ensure water content homogeneity. The water retention curve of the loess was employed to estimate the amount of water to be added or subtracted in order to obtain the desired value of suction. The dimensions and weight of the sample were again measured after water addition or extraction. The sample was immediately inserted into the triaxial cell and covered with a latex membrane.

Before placing the membrane over the sample, the latex membrane was marked with a pen to localize the position of the Hall Effect transducers, of the tensiometer and of the resistivity probe. To introduce the tensiometer and the resistivity probe, two circular holes of diameter 3 mm about were made at the positions defined on the membrane.

The fixation device of both the tensiometer and the resistivity probe is presented in Figure 7. A rubber grommet was used to fix the tensiometer at the mid-height side of the sample. The shape of the resistivity probe, also located at the mid-height of the sample, was adapted to be easily sealed to the membrane. At least three layers of silicone and glue were applied to seal the grommet and the resistivity probe to the latex membrane. An O-ring was employed to tightly seal the tensiometer within the grommet and another one was used to seal the resistivity probe within the latex membrane. Several layers of glue and silicone were painted around the tensiometer and the resistivity probe holding systems to provide a safe seal. Once the tensiometer and the resistivity probe were installed, the Hall Effect local displacement transducers were fixed as previously described. The sealing of all local sensors was made with silicone in order to avoid a possible increase of the membrane stiffness. The sensors are light with a weight of 70 g partly supported by the membrane stickiness.

The cell chamber was subsequently positioned over the sample and the cell filled with silicone oil prior to place the external load and displacement sensors. The internal ducts at top and bottom of the specimen were connected to a container full of water at atmospheric pressure to avoid any evaporation from the sample. Once a test was finished, the local

instruments and the membrane were carefully dismantled so as to immediately measure the dimensions and weight of the tested sample.

Shear tests on the 3.3 m deep sample

To investigate the reliability of the device, two similar tests were conducted on two specimens trimmed from the same block extracted at 3.3 m. The transient suction equilibration phase with water exchanges between the tensiometer, the slurry and the sample is presented in Figure 12 for both samples. It lasts about 20 minutes in both cases, a period of time quite similar to that observed by Meilani *et al.* (2002) in the same conditions. Stabilisation is afterwards observed at the same suction value for both specimens ($s_0 = 50$ kPa). This shows the validity of the suction measurements and the good homogeneity of the two specimens in terms of suction.

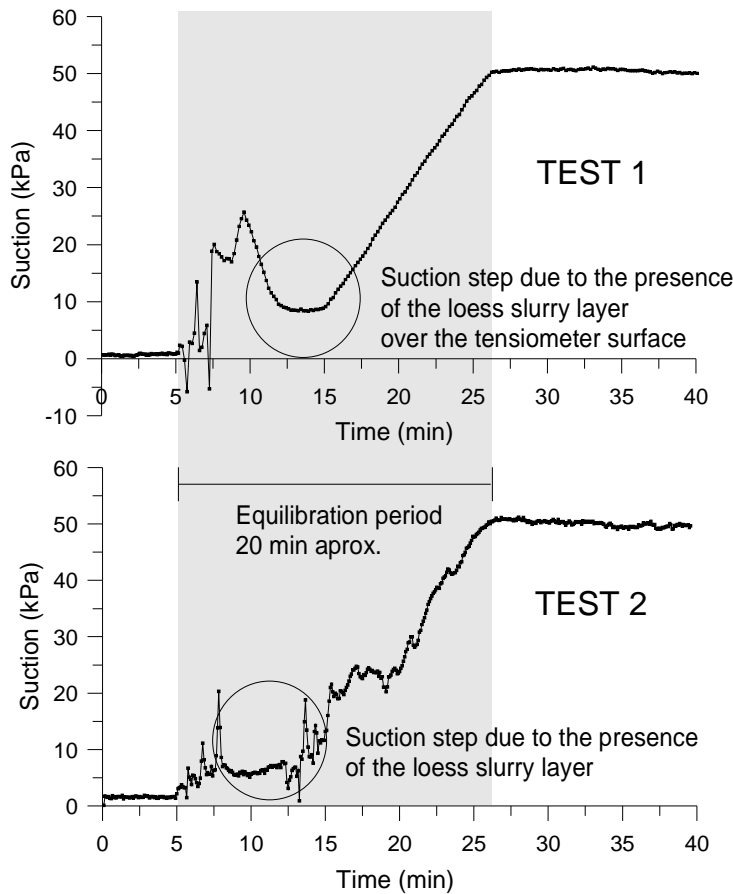


Figure 12. Suction measurement for 3.3 m loess samples during equilibration between tensiometer and sample

The data of the two triaxial tests performed are presented in Figure 13 in terms of changes in deviator stress q , volumetric ε_v and radial ε_3 strain (local measurements from the Hall effects transducers), suction s and water content w with respect to the local axial strain ε_l on the right

side of the Figure. The same data are presented with respect to the changes in net mean stress $p - u_a$ on the left side of the Figure.

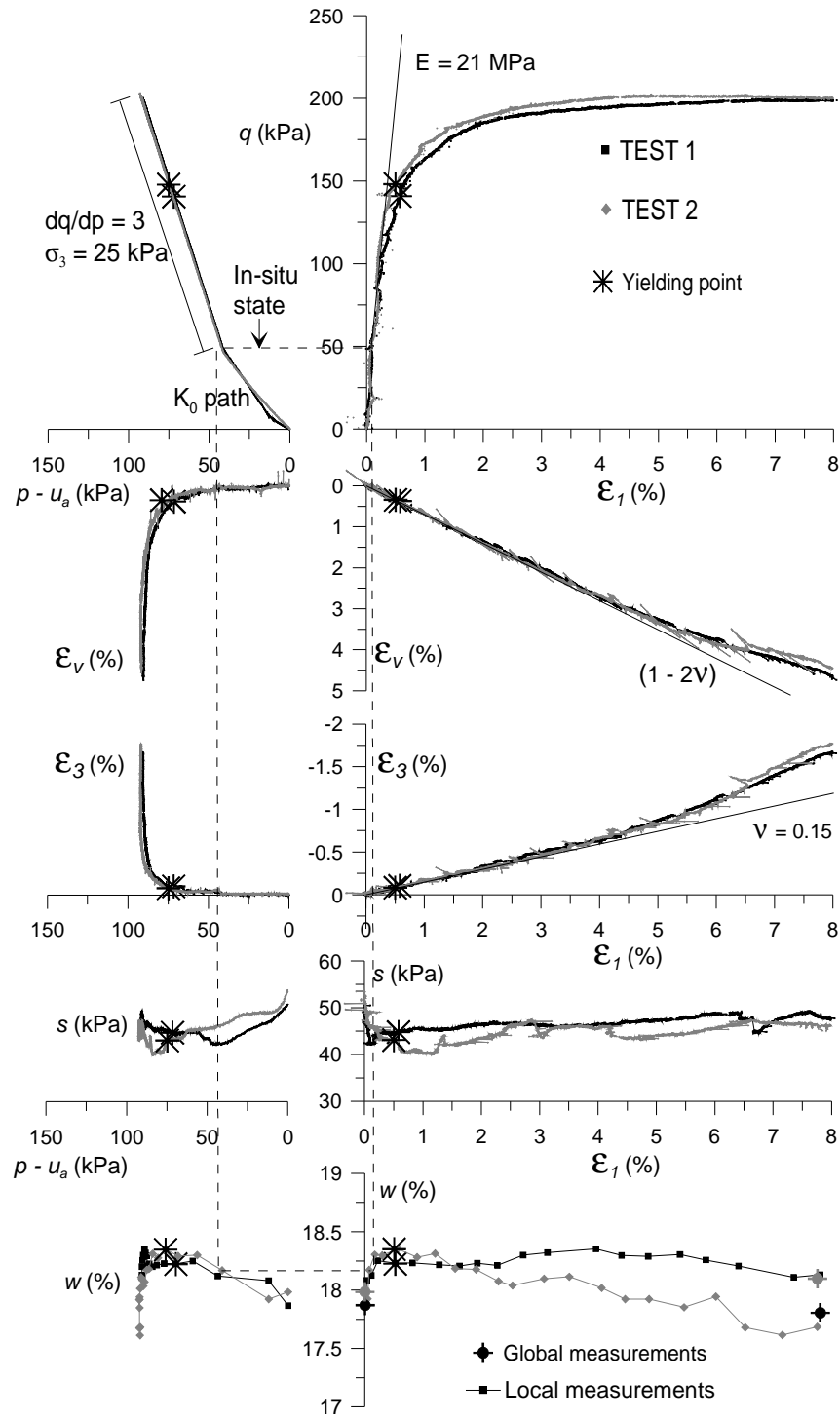


Figure 13. Triaxial tests on 3.3 m loess samples at their natural state ($w \approx 18\%$, $s \approx 50$ kPa). Both samples are from the same block

The stress path followed is indicated on the left top figure. The samples were firstly brought back to the in-situ net stress ($\sigma_v - u_a = 65$ kPa at a depth of 3.3 m with $\rho = 1.87$ Mg/m³)

through a K_0 test (no lateral stress allowed, see the $\varepsilon_3/\varepsilon_l$ versus $p - u_a$ diagram in the Figure). Note that due to the important concerns related to the validity of the effective stress in unsaturated soils, K_0 is defined here in terms of net stresses, as follows:

$$K_0 = \frac{\sigma_3 - u_a}{\sigma_l - u_a} \quad (7)$$

in which σ_l is the axial stress, σ_3 is the confining pressure and u_a the air pressure (atmospheric pressure). The test provided a value of the lateral net stress of 25 kPa corresponding to a K_0 value of 0.38. The stress paths of the two tests appear quite close in terms of q/ε_l , $\varepsilon_v/\varepsilon_l$ and $\varepsilon_3/\varepsilon_l$ plots. Note also that the volume change is quite small along the K_0 path.

A standard test with constant all round pressure ($\sigma_3 = 25$ kPa) was carried out starting from the in-situ net stress conditions. The q/ε_l stress strain curves obtained exhibit in both cases a typical shape and provide estimated yield stress values that are also reported in the other graphs. These yield stresses are close ($q = 141$ kPa and 148 kPa for Test 1 and 2 respectively), they are significantly larger than the in-situ stress state also represented in the plot. This confirms the combined effects of microstructure and suction hardening due to desaturation (Gens and Nova 1993, Cui and Delage 1996) that provide in unsaturated structured soils yield data much larger than the in-situ stress conditions. Little volume change is observed before yield whereas compressive strain is afterwards progressively developing, in accordance with the high void ratio, the low initial degree of saturation and the collapsible behaviour of the loess.

Since the in-situ stress state is far from yield, the elastic characteristics can be easily derived in the simplifying hypothesis of isotropic linear elasticity, for a triaxial test with constant confining stress. The estimated values of the Young's modulus E and Poisson ratio ν are 21 MPa and 0.15 respectively. The Poisson ratio line, drawn in the $\varepsilon_3/\varepsilon_l$ diagram of Figure 13, coincides with experimental values in the elastic range, and even further.

The local changes in water content are presented together with the initial and final global values estimated by weighing. They appear to be very small and included in the ± 0.3 points range identified in Figure 11, showing no significant change, in spite of a sudden monotonic increase in gravimetric water content at the beginning (between 17.87 and 18.25% for test 1

and between 18% and 18.3% for test 2). Again, this change might be not significant, like that observed from the global water content measurement (less than 0.11%).

The local changes in suction observed in the $s/p - u_a$ plot show an initial decrease of 9-14 kPa from the initial values (from 51 to 42 kPa and 54 to 40 for samples 1 and 2 respectively) that occurs when bringing the samples back to in-situ conditions under K_0 conditions at constant water content. The curve of test 1 exhibits a minimum suction value at in-situ conditions followed by an increase. The curve of test 2 present more changes with ε_l that are not easy to interpret. Note that a failure plane appeared in these tests.

Shear test on the 1 m deep sample

Figure 14 shows the response of the HCT during the suction equilibration period. There is a sharp increase in suction up to 29 kPa followed by a progressive equilibration within the sample after 15 minutes, a period shorter than previously. A final suction of 39 kPa is obtained. The oscillations around the average value have amplitude of ± 2 kPa. The signal giving the initial suction is satisfactorily stable along the 45 minutes period of time waited for after equilibration. Anyway, a minimal period of two hours was waited for at the beginning of each test so as to ensure full stabilization of all local measurements.

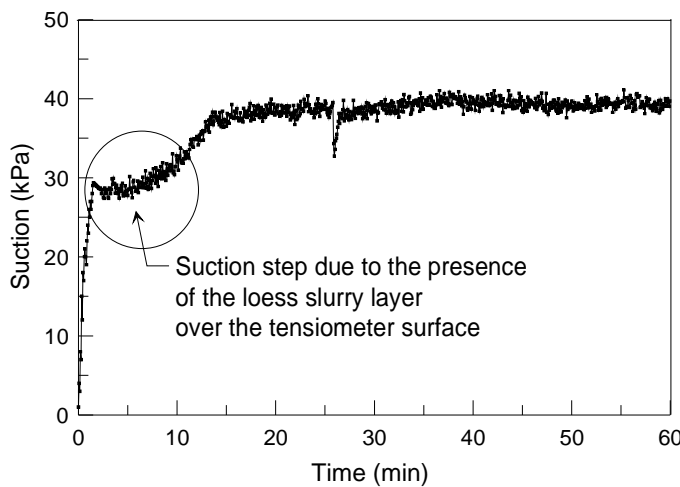


Figure 14. Suction equilibration between tensiometer and sample (1 m deep sample)

A K_0 constant rate of strain shear test with no radial stress allowed was performed. With an in-situ vertical net mean stress of 28 kPa at 1 m depth, a lateral net stress value of 8 kPa was obtained, giving a recalculated in-situ deviator stress equal to 20 kPa and a K_0 value of 0.29, lower than the 0.38 value previously obtained.

Once all readings stabilised, a test with a constant all round pressure of 8 kPa was started at a constant vertical displacement rate of 10 micrometers per minute. Figure 15a and b show the comparison between the local and global axial measurements during shearing, including a zoom at small strains (Figure 15b) where a load cycle has been carried out. Since the beginning, local measurements appear to provide smaller strain than the global one, resulting in higher sample stiffness (also observed by Damarola 1978, Costa-Filho and Vaughan 1980, Miller 1980 and Burland and Symes 1982). It seems from Figure 15b that most of the difference starts to appear at small strains, between 0 and 0.2%. Afterwards, the stress strain curves are roughly parallel (Figure 15a).

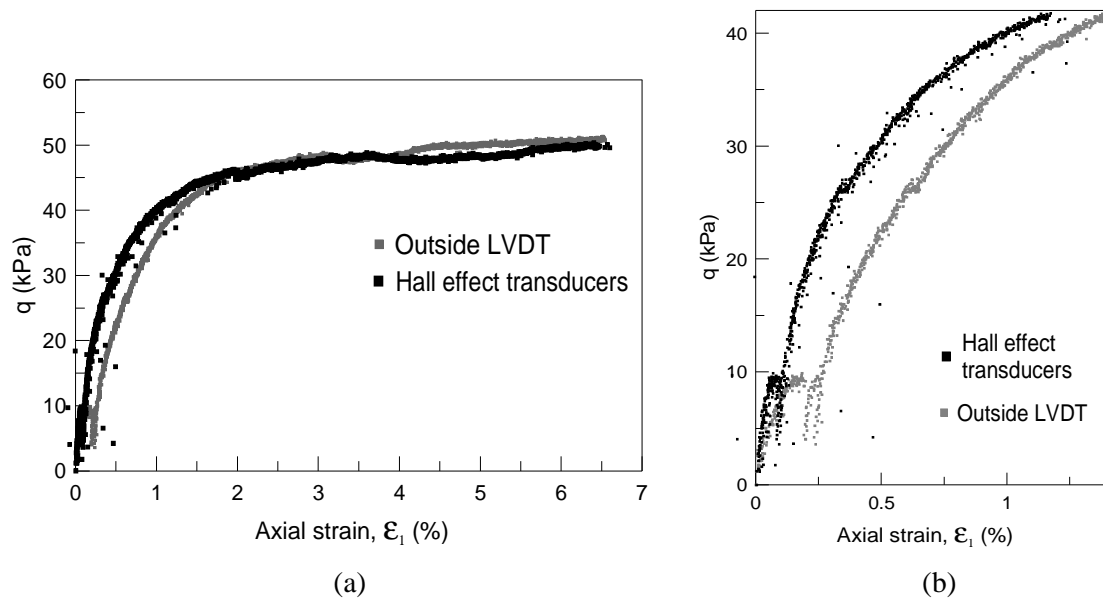


Figure 15. Comparison between outside LVDT and the local Hall Effect strain measurements. (a) 1m loess test data, (b) Zoom

The complete set of data is presented in Figure 16 in the same fashion as in Figure 13. The stress strain curve shows a typical shape with a yield stress estimated from the q/ε_1 curve and reported in the other plots. As previously, the yield stress is far above the in-situ stress state. Little volume change is observed before yield whereas compressive strain is afterwards progressively developing, in accordance with the high void ratio, the low initial degree of saturation and the collapsible behaviour of the loess. The elastic parameters calculated in the elastic zone are $E = 8.8$ MPa (taken from the stress cycle) and $\nu = 0.27$. The Young's modulus of this looser sample ($e = 0.84$) extracted at shallow depth (1 m) and tested under smaller in-situ stresses ($\sigma_3 - u_a = 8$ kPa) appears to be significantly smaller than that previously obtained at 3.3 m ($\sigma_3 - u_a = 25$ kPa) on a denser and more clayey sample ($e = 0.60$, % clay fraction equal to 16% compared to 25%).

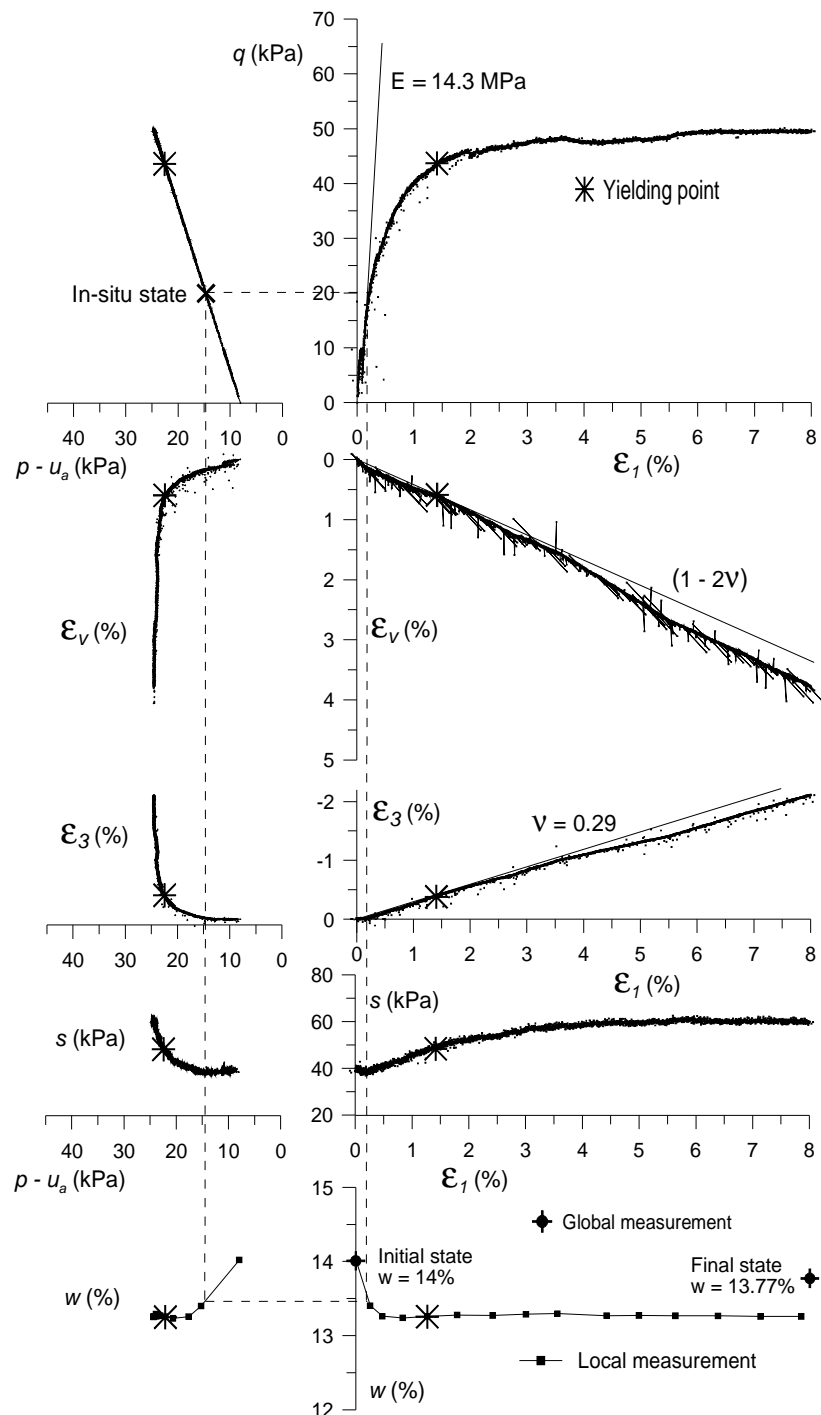


Figure 16. Triaxial tests results for 1m loess sample under constant confining pressure of 8 kPa corresponding to the natural in-situ lateral stress

The changes in water content shows a slight initial decrease in local water content from 14% to 13.1% whereas the global water content measured after the test shows a smaller change from 14 to 13.77%. These changes are to be compared to the $\pm 0.3\%$ precision observed in Figure 11. In parallel, after a slight immediate decrease, the local suction appears to progressively increase during compression from 40 kPa to 60 kPa.

Discussion

The data from the two triaxial tests on intact natural loess specimens from two depths (1 and 3.3 m), showed that the water content locally monitored by a new resistivity probe remained constant during shearing. However, some suction changes have been observed, depending on the sample tested. On the denser 3.3 m deep samples ($e = 0.60$ compared to 0.84 at 1 m) that contains a higher clay fraction (25% compared to 16% at 1 m) with a higher initial degree of saturation (76-80 % compared to 46 % at 1 m) and a higher initial suction (48 - 49 kPa compared to 40 kPa at 1 m), an initial suction decrease of about 10 kPa was observed under constant volume when putting the sample back under in-situ stress conditions ($\sigma_l - u_a = 65$ kPa, $\sigma_3 - u_a = 25$ kPa) in the elastic domain. This is apparently a new result, since the few suction changes that have been monitored during shearing (Colmenares and Ridley 2002, Meilani *et al.* 2002) have been made without any local strain measurement. This suction change at constant water content and volume could be interpreted by some reorganisation of the inter-grains menisci network induced by the application of the deviator stress. The further approximately constant value observed during shearing is similar to the data of Meilani *et al* (2002).

Further comparison can be made by plotting, as suggested by Colmenares and Ridley (2002), the changes of the normalised value of suction s/s_0 with respect to ϵ_l . (Figure 17).

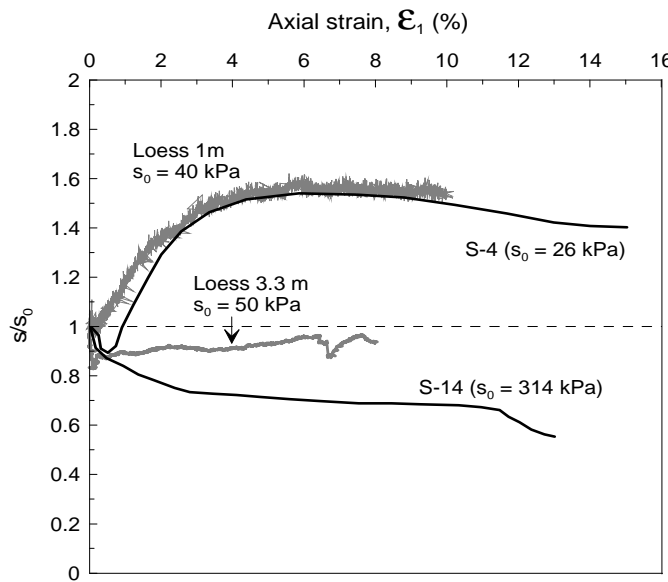


Figure 17. Comparison of suction changes with the results of unconfined compression tests on compacted silty clay of Colmenares and Ridley (2002)

The Figure that also includes the data of Colmenares and Ridley (2002) shows a good compatibility of our test at 1 m with the data of test S-4 on reconstituted artificial clayey silt samples with comparable plastic index (10.7 %), an initial suction s_0 of 26 kPa and a high initial degree of saturation (97% compared to 44% in our case). Colmenares and Ridley (2002) obtained a decrease in suction in test S-14, also represented ($s_0 = 314$ kPa, $S_{r0} = 86$ %). The response in suction of the test at 3.3 m is located above the response of test S-14. This confirms our findings that suction changes during shear depend of the characteristics of the unsaturated soil.

Conclusions

A new precision triaxial cell with complete local monitoring of the state of an unsaturated specimen was designed. Besides local strain and suction measurements, the system also includes a new home made resistivity probe for the local measurement of water content. The design and the calibration of this new device were carried out on two intact natural loess specimens and the validity of two existing resistivity models was examined.

Two sets of preliminary triaxial tests at a constant confining pressure and constant water content starting from the in-situ stress conditions were conducted on loess specimens. The tests showed a good response of all the local devices and a good repeatability. They evidenced negligible local changes in water content during shear that were coupled with some suction changes induced by the application of a deviator stress at constant volume. The two loess specimens exhibited a fragile behaviour characterized by yield values significantly higher than in-situ stress conditions, a trend typical of structured unsaturated soils. Based on the simplified hypothesis of isotropic linear elasticity, some values of the elastic parameters (Young's modulus and Poisson coefficient) were estimated. These data provide some first behaviour characteristics of an intact natural unsaturated soil. This kind of data appears to be quite rare in the literature, since most existing data concern artificial unsaturated samples.

Acknowledgments

The present study is part of the first author PhD work. It was supported by the European Alβan Program of high level scholarships for Latin America, scholarship N° E07D402297CO, through grants to Mr. J. Muñoz. The support of the French Railways Company SNCF is also acknowledged.

References

- Antoine P. (2002). Les loess en France et dans le Nord-Ouest européen. *Revue Française de Géotechnique* **99**. 3-21.
- Antoine P., Cattt. J. & Sommé J. (2003). The Loess and Coversands of Northern France and Southern England. *Journal of Quaternary Science* **18**. 309-318.
- Archie G.E. (1942). The electrical resistivity log as an aid in determining some reservoir characteristics. *Trans. AM. Inst. Min. Metall. Pet. Eng.* **146**. 54-62.
- Aversa S. and Nicotera M.V. (2002). A Triaxial and Oedometer Apparatus for Testing Unsaturated Soils. *Geotechnical Testing Journal* **25** (1). 3-15.
- Barrera M. (2002). Estudio experimental del comportamiento hidro-mecánico de suelos colapsables. PhD thesis. *Universitat Politècnica de Catalunya*. Barcelona.
- Bishop A.W. and Donald I.B. (1961). The experimental study of partly saturated soil in the triaxial apparatus. *Proc. 5th Int. Conf. on Soil Mechanics and Found. Eng.*, vol. 1, Paris. 13-21.
- Blatz J. and Graham J. (2000). A system for controlled suction in triaxial tests. *Géotechnique* **50** (4). 465-469.
- Burland J.B. and Symes M. (1982). A simple axial displacement gauge for use in the triaxial apparatus. *Géotechnique* **32** (1). 62-65.
- Cabarkapa Z. and Cuccovillo T. (2006). Automated Triaxial Apparatus for Testing Unsaturated Soils. *Geotechnical Testing Journal* **29** (1). 21-29.
- Chávez C., Romero E. and Alonso E.E. (2009). A Rockfill Triaxial Cell with Suction Control. *Geotechnical Testing Journal* **32** (3). 219-231.
- Chen L., Yin Z. and Zhang P. (2007). Relationship of Resistivity with Water Content and Fissures of Unsaturated Expansive Soils. *Journal of China University of Mining & Technology* **17** (4). 537-540.
- Chiu C.F., Cui Y.J., Haza E., De Laure E., Favraud C. and Thériot N. (2002). Experimental study of pollutant transport in an unsaturated compacted silt on centrifuge: second test. *Ecole Nationale des Ponts et Chaussées (Paris) – Laboratoire Centrale des Ponts et Chaussées (Nantes)*. France.
- Colmenares J.E. and Ridley A.M. (2002). Stress-strain and strength relationships for a reconstituted clayey silt. *Proceedings of the Third International Conference on Unsaturated Soils. Unsat 2002*, vol. **2**. Jucá J.F.T., de Campos T.M.P. and Marinho F.A.M. (eds.), Balkema Publishers, The Netherlands. 481-484.
- Costa-Filho L.F. and Vaughan P.R. (1980). Discussion on A computer model for the analysis of ground movements in London clay, by B. Simpson, N.J. O'Riordan and D.D. Croft. *Géotechnique* **30** (3). 336-339.
- Cui Y.J. and Delage P. (1996). Yielding and plastic behaviour of an unsaturated compacted silt. *Géotechnique* **46** (2). 291-311.
- Cui Y.J., Marcial M., Terpereau J.M., Delage P., Antoine P., Marchadier G. and Ye W.M. (2004). A geological and geotechnical characterisation of the loess of Northern France. *A.W. Skempton Memorial Conference*, vol. 1. 417-428.
- Cui Y.J., Tang A., Marcial D., Terpereau J., Marchadier G. and Boulay X. (2007). Use of a Differential Pressure Transducer for the Monitoring of Soil Volume Change in Cyclic Triaxial Test on Unsaturated Soils. *Geotechnical Testing Journal* **30** (3). 227-233.
- Damarola O. (1978). The influence of stress history on the deformation of a sand. *PhD Thesis, University of London*.

- Debye P. (1929). Polar Molecules. New York, reprinted by *Dover Publications Inc.*
- Delage P., Suraj de Silva G.P.R. and De Laure E. (1987). Un nouvel appareil triaxial pour les sols non saturés. *IXème Conf. Eur. Mécanique des Sols et Travaux de Fondations* 1, Dublin, Balkema, Rotterdam. 26-28.
- Delage P., Cui Y.J. and Antoine P. (2005). Geotechnical Problems related with Loess deposits in Northern France. *Proceedings of International Conference on Problematic Soils*. 517-540.
- Delage P., Romero E. and Tarantino S. (2008). Recent developments in the techniques of controlling and measuring suction in unsaturated soils. *Keynote Lecture, Proc. 1st Eur. Conf. on Unsaturated Soils*, Durham, CRC Press. 33-52.
- Fam M. and Santamarina C. (1995). Study of geoprocesses with complementary mechanical and electromagnetic wave measurements in an oedometer. *Geotechnical testing Journal* 18 (3). 307-314.
- Fowles D. (1980). Soil Resistivity Measurements. Report prepared by the *Ductile Iron Pipe Research Institute*, Oak Brook, US.
- Fukue M., Minato T., Horibe H. and Taya N. (1999). The micro-structures of clay given by resistivity measurements. *Engineering Geology* 54. 43–53.
- Gens A. and Nova R. (1993). Conceptual bases for a constitutive model for bonded soils and weak rocks. *Proc. Int. Symp. On Hard Soils – Soft Rocks*, Athens. 485-494.
- Guéguen Y. and Palciauskas V. (1994). Introduction to the Physics of Rocks. *Princeton University Press*. Princeton, New Jersey. 294p.
- Gupta S.C. and Hanks R.J. (1972). Influence of Water Content on Electrical Conductivity of the Soil. *Soil Sci. Soc. Am. J.* 36. 855-857.
- Hoyos L.R. and Macari E.J. (2001). Development of a Stress/Suction-Controlled True Triaxial Testing Device for Unsaturated Soils. *Geotechnical Testing Journal* 24 (1). 5-13.
- Jotisankasa A., Coop M. and Ridley A. (2007). The Development of a Suction Control System for a Triaxial Apparatus. *Geotechnical Testing Journal* 30 (1). 69-75.
- Kalinski R. and Kelly W. (1993). Estimating Water Content of Soils from Electrical Resistivity. *Geotechnical Testing Journal* 16 (3). 323-329.
- Karam J.P. (2006). Etude de la rhéologie des loess du Nord de la France. Application à l'évaluation de leur risque de liquéfaction. PhD thesis. École Nationale des Ponts et Chaussées. Paris.
- McCarter W.J. (1984). Electrical resistivity characteristics of compacted clays. *Geotechnique*. 34 (2). 263-267.
- Maâtouk A., Leroueil S. and La Rochelle P. (1995). Yielding and critical state of a collapsible unsaturated silty soil. *Geotechnique* 45 (3). 465-477.
- Manthro A. (2005). Echanges sol – atmosphère: application à la sécheresse. PhD thesis. École Nationale des Ponts et Chaussées. Paris.
- Maryniak W., Uehara T. and Noras M. (2003). Surface Resistivity and Surface Resistance Measurements Using a Concentric Ring Probe Technique. *TREK, INC. Trek Application Note Number 1005*.
- Matsuoka H., Sun D., Kogane A., Fukuzawa N. and Ichihara W. (2002). Stress-strain behaviour of unsaturated soil in true triaxial tests. *Canadian Geotechnical Journal* 39 (3). 608-619.
- Meilani I., Rahardjo H., Leong E.C., and Fredlund D.G. (2002). Mini suction probe for matric suction measurements. *Canadian Geotechnical Journal* 39. 1427-1432.

- Miller C.J. (1980). The laboratory determination of the small strain behaviour for Lias clay, and its significance to settlement analysis. *MSc Thesis, University of London*.
- Mitchell J.K. and Arulanandan K. (1968). Electrical dispersion in relation to soil structure. *Journal of the Soil Mechanics and Foundations Division* **94** (2). 447-471.
- Padilla J.M., Houston W.N., Lawrence C.A., Fredlund D.G., Houston S.L. and Perez N.P. (2006). An automated triaxial testing device for unsaturated soils. *Geotechnical Special Publication 147 Proceedings of the Fourth International Conference on Unsaturated Soils*. 1775-1786.
- Palacky G.J. (1987). Resistivity Characteristics of Geologic Targets. In *Electrolagmetic Methods in Applied Geophysics*, vol. **1** (ed. M.N. Nabighian). Series: Investigations in Geophysics, vol. 3, Soc. of Expl. Geophys., Tulsa, Okla.
- Rhoades J.D., Raats P.A.C. and Prather R.J. (1976). Effects of Liquid-phase Electrical Conductivity, Water Content, and Surface Conductivity on Bulk Soil Electrical Conductivity. *Soil Sci. Soc. Am. J.* **40**. 651-655.
- Ridley A. and Burland J. (1993). A new instrument for the measurement of soil moisture suction. *Géotechnique* **43** (2). 321 – 324.
- Rojas J.C., Mancuso C., Vinale F.A. (2008). Modified triaxial apparatus to reduce testing time: Equipment and preliminary results. *1st European Conference on Unsaturated Soils*, Jul. 2-04, 2008, Durham, England. 103-109.
- Sivakumar R., Sivakumar V., Blatz J. and Vimalan J. (2006). Twin-Cell Stress Path Apparatus for Testing Unsaturated Soils. *Geotechnical Testing Journal* **29** (2). 175-179.
- Tang G.X., Graham J., Blatz J., Gray M. and Rajapakse R.K.N.D. (2002). Suctions, stresses and strengths in unsaturated sand-bentonite. *Engineering Geology* **64**, Issue: 2-3. 147-156.
- Tarantino A. (2004). Direct measurement of soil water tension. *Unsaturated Soils*, Jucá, de Campos & Marinho (eds). Swets & Zeitlinger, Lisse, ISBN 90 5809 371 9.
- Tarantino A. and Mongiovì L. (2001). Experimental procedures and cavitation mechanisms in tensiometer measurements. *Geotechnical and Geological Engineering* **19**. 189-210.
- Thom R., Sivakumar V., Brown J. and Hughes D. (2008). A Simple Triaxial System for Evaluating the Performance of Unsaturated Soils Under Repeated Loading. *Geotechnical Testing Journal* **31** (2). 107-114.
- Verbrugge J.C. 1978. Emploi d'une méthode psychrométrique dans des essais triaxiaux sur un limon remanié non saturé. *Can. Geotech. J.* **15**(4): 501-509 (1978)
- Wheeler S.J. and Sivakumar V. (1995). An elasto-plastic critical state framework for unsaturated soil. *Géotechnique* **45** (1). 35-53.
- Xu J., Ng C.W.W. and Yung S.Y. (2008). Drying and wetting effects on shear wave velocity of an unsaturated soil. . *1st European Conference on Unsaturated Soils*, Jul. 2-04, 2008, Durham, England. 525-530.
- Yang C., Cui Y.J., Pereira J.M. & Huang M.S. (2008). A constitutive model for unsaturated cemented soils under cyclic loading. *Computers and Geotechnics* **35** (6). 853-859.

Chapitre 4. Comportement hydromécanique

Table de matière

4.1	Introduction	158
4.2	Caractérisation de la compressibilité et du phénomène d'effondrement	159
	Some aspects of the compression and collapse behaviour of an unsaturated natural loess	161
	Abstract	161
	Introduction	161
	Experimental programme	162
	Time dependent behaviour	164
	Collapse behaviour	166
	Discussion	168
	Conclusions	169
4.3	Caractérisation du comportement hydromécanique du Loess de Bapaume	172
	Hydromechanical behaviour of a natural unsaturated loess	174
	Introduction	174
	Material and experimental setup	176
	Experimental results	180
	Effects of moisture changes on the mechanical behaviour	190
	Impact of loading on microstructure and on water retention properties	197
	Conclusions	201

4.1 Introduction

Les développements récents dans la compréhension du comportement hydromécanique des sols non saturés ont été concentrés sur la modélisation constitutive (Alonso *et al.* 1990, Wheeler et Sivakumar 1995, Wheeler 1996, Barbour 1998, Jommi 2000, Vaunat *et al.* 2000, Gallipoli *et al.* 2003, Wheeler *et al.* 2003, Tarantino 2007, entre autres) et sur la caractérisation expérimentale, spécialement sur des échantillons compactés ou reconstitués (Maatouk *et al.* 1995, sur un limon compacté du Québec ; Cui et Delage 1996, sur le limon de Jossigny compacté ; Romero et Vaunat 2000, sur une argile compactée ; Cunningham *et al.* 2003, sur une argile limoneuse reconstitué ; Tarantino and De Col 2008, sur une argile compactée ; Jotisankasa *et al.* 2009, sur une argile limoneuse compactée). Les couplages

hydromécaniques incluent la dépendance du comportement mécanique (déformabilité et propriétés à la rupture) vis-à-vis des propriétés de rétention d'eau et vice-versa.

Ce chapitre est divisé en deux parties. Une *première partie* étudie le phénomène d'effondrement (suite au remouillage sous chargement constant) à partir d'essais oedométriques avec suivi de la succion par un tensiomètre de haute capacité. Les résultats montrent l'effet des variations de la vitesse de déformation et du remouillage à deux contraintes nettes verticales différentes. Ces résultats font partie d'un article accepté de publication au journal *Géotechnique Letters*.

Une *deuxième partie* se concentre sur les résultats d'essais triaxiaux à trois teneurs en eau différentes. On a appliqué trois types de chemins de contrainte : une compression isotrope, une compression anisotrope K_0 et un cisaillement à confinement constant. Des observations supplémentaires, dont des courbes de rétention d'eau à deux porosités différentes et des observations microstructurales, aident à la compréhension des couplages hydromécaniques caractérisant le comportement du lœss. Ces analyses ont été rédigées sous la forme d'un article en anglais, prêt à être soumis dans un journal international.

4.2 Caractérisation de la compressibilité et du phénomène d'effondrement

Dans cette section, on présente l'étude de la susceptibilité à l'effondrement du Lœss de Bapaume à partir de différents essais. On a utilisé deux méthodes de chargement pour les essais oedométriques : un chargement par paliers et un chargement à vitesse de déplacement contrôlée. Le programme expérimental inclut des essais de double oedomètre où le remouillage a été effectué sous deux contraintes verticales différentes (19 kPa et 200 kPa). La contrainte la plus faible est proche de la contrainte verticale totale in-situ, 16 kPa. Ces tests ont été faits afin d'analyser l'influence de la contrainte appliquée sur l'importance de l'effondrement. L'effondrement observé sous la contrainte verticale de 200 kPa est inférieur à celui observé à faible contrainte. Cela suggère l'existence d'une valeur d'effondrement maximal à faibles contraintes. Les tests où l'on a fait varier la vitesse de déplacement ont montré une compressibilité qui augmente et une contrainte de plastification qui diminue avec l'incrément de la vitesse de déplacement. Ceci nécessite probablement de la réalisation

d'études supplémentaires car, selon différents auteurs (par exemple Leroueil et Marques 2006), le comportement visco-élastoplastique des sols fins présente une augmentation de la contrainte de plastification avec l'incrément de la vitesse de déplacement. Les résultats ont été analysés à l'aide d'observations microstructurales.

Muñoz-Castelblanco, J., Delage, P., Pereira, J.M. & Cui Y.J. (2011). *Géotechnique Letters* (Accepted for publication)

Some aspects of the compression and collapse behaviour of an unsaturated natural loess

J. Muñoz-Castelblanco, P. Delage, J.M. Pereira, Y.J. Cui

Ecole des ponts ParisTech, CERMES/Navier, Université Paris-Est

Abstract

The compression and collapse behaviour of a natural unsaturated loess from Northern France was investigated by running a series of constant rate of strain oedometric compression tests (together with some step loading tests) while monitoring suction by means of a high capacity tensiometer. The reasonably constant suction measured during constant water compression tests was linked to the collapse of the largest dry pores. A time dependent behaviour was also observed, with different responses obtained at different strain rates. In a standard fashion, collapse tests appeared to bring the representative point from the constant water content curve to the zero suction compression curve, evidencing the existence of a maximum collapse stress. Data were qualitatively interpreted by using the LC curve concept from the Barcelona Basic Model. Changes in the LC curve inclinations could account for the existence of a maximum collapse value.

Keywords: natural loess, collapse, unsaturated, suction, loading collapse, time dependent.

Introduction

Some problems related to the collapsibility of loess deposits in Northern France (Antoine *et al.* 2003) in areas crossed by the “TGV Nord” high speed train line have been described in Cui *et al.* (2004). As seen in Figure 1, impressive sinkholes were observed during the construction period when loess layers that were previously protected from rain by an upper superficial illuviated clayey layer were exposed to climatic effects (drying and raining).

Following Jennings and Knight (1957), soil collapse has been investigated either by using the double oedometer technique or by performing soaking tests under constant stress. The developments carried out in the past decades in the mechanics of unsaturated soils allow a

better understanding of collapse thanks to a relevant theoretical framework (BBM model, LC curve, Alonso *et al.* 1987, 1990) and to advanced techniques of either controlling (e.g. Maâtouk *et al.* 1995) or measuring suction (e.g. Jotisankasa *et al.* 2007) in collapsible samples. To date, these approaches were mainly applied to reconstituted collapsible soils. This work is devoted to the behaviour of a natural aeolian loess, investigated by running constant water content oedometer compression tests with suction measurements. Results were interpreted by using the LC curve concept developed within the BBM model.



Figure 1. Collapse behaviour in shallow layers of loess directly exposed to climatic actions

Experimental programme

Tests were performed on good quality samples trimmed from a block that was manually extracted at a depth of 1 m in October 2007 during a rather cool, dry and sunny autumn. As seen in Table 1, the loess has a 9% plasticity index and contains 6% carbonate, a component known to provide inter-particles bonding (“Loess is not just the accumulation of dust”, Pécsi 1990). Its water retention properties have been investigated in details in Muñoz-Castelblanco *et al.* (2011).

Sample depth	1 m		
Natural water content w (%)	14.4	Clay fraction (% < 2 μm)	16
Natural void ratio e	0.84	Plastic limit w_p	19
Dry unit mass ρ_d (Mg/m^3)	1.45	Liquid limit w_l	28
Natural degree of saturation S_r	0.46	Plasticity index I_p	9
Natural suction (HTC) (kPa)	40	Carbonate content (%)	6

Table 1. Geotechnical characteristics of the Bapaume loess

A series of oedometric compression tests (Table 2) in which, like in Jotisankasa *et al.* (2007), suction changes were monitored by using an in-house constructed high capacity tensiometer (HCT) located at the base of the sample (Figure 2), was carried out.

Test	Description	Initial state				Final state			
		e_i	s_i (kPa)	w_i (%)	S_{ri}	e_f	s_f (kPa)	w_f (%)	S_{rf}
SL001	Natural state	0.85	46.7	14.6	0.46	0.59	41.3	14.5	0.65
SL002	Saturated	0.85	46.3	14.3	0.45	0.55	-2.5	20.8	1.01
SL003	Natural state, collapse/soaking under $\sigma_v = 205$ kPa	0.85	41.2	14.4	0.45	0.53	0.2	19.7	0.99
SL004	Collapse / soaking under σ_v = 19 kPa	0.85	47.0	14.6	0.46	0.58	3.3	22.3	1.03
CRS01	Natural state 0.003%/min	0.84	45	14.4	0.46	0.66	29	14.3	0.59
CRS02	Natural state 0.010%/min	0.84	39	14.4	0.46	0.62	33	14.6	0.64
CRS03	Natural state 0.059%/min	0.84	40	14.9	0.48	0.61	35	14.5	0.63
CRS05	Saturated, 0.010%/min	0.84	38	14.4	0.48	0.59	-2.2	22.9	1.04

Table 2. Experimental program (SL: Step Loading test, CRS : Constant Rate of Strain test)

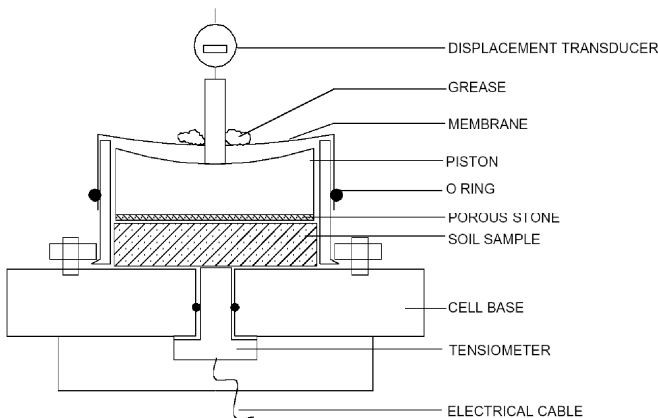


Figure 2. HCT measurement inside an oedometer cell (Delage et al. 2007)

Oedometer testing was selected in a purpose of simplicity (K_0 tests in the triaxial apparatus would have been preferable to get rid of the friction effects along the ring that may overestimate the specimen's mechanical response). Most tests were performed at constant water content starting from the natural unsaturated state (w_i between 14.3% and 14.9%) with initial suctions s_i between 38 and 47 kPa (Table 2). Evaporation was prevented by isolating the sample from laboratory atmosphere with a plastic film as indicated in the Figure. In one of the tests, the sample was soaked at very low stress (1.5 kPa) prior to compression by carefully

pouring water through the annular gap between the piston and the ring. Water infiltrated the soil through the porous disk and filter paper placed on top of the sample (Figure 2).

Compression of the soaked sample provided the “saturated” reference compression curve. Constant water content tests were made to compare the unsaturated compression behaviour (with preserved natural structure) with the saturated one, like in the double oedometer test. As noted by Tarantino and De Col (2008), constant rate of strain (CRS) compression tests are preferable when monitoring suction changes. This was done here together with standard 24 h long step loading tests (with suction and displacement rates finally equal to 2 kPa/h and 27 µm/h respectively).

Time dependent behaviour

The response of the CRS tests carried out at rates of 0.003, 0.010 and 0.059 %/mn are presented in Figure 3 in both linear and semi-log plot of the vertical net stress ($\sigma_v - u_a$, where u_a is the air pressure), together with the responses in suction. Given the low values of the degree of saturation (Table 1), the air phase is continuous and the pore air pressure is equal to the atmospheric pressure that prevails in the upper porous stone, giving $u_a = 0$ at all times.

Compared to compacted soils that keep the memory of the compaction stress (Cui and Delage 1996, Maâtouk *et al.* 1995, Jotisankasa *et al.* 2007), the response observed here in a natural soil at all rates is not strictly elasto-plastic and exhibit a less apparent yield stress in the semi-log plot. Indeed, yield is not due to any previous maximum supported stress, given the aeolian origin of the soil. As in structured soils, it is linked to a loose structure and to inter-particle bonding. The various available methods of determining gross yield are known to provide different values. In a purpose of simplification, gross yield was determined here at the intersection of two lines fitted on the pseudo-elastic and plastic section of the compression curve respectively.

Figure 3 shows that the response of the CRS tests is time dependent, in particular in terms of (visco)-plastic compressibility as illustrated by the slope of the curve (λ_{oedo}) in the post-yield regime, that shows that the unsaturated loess appears to be stiffer at smaller strain rates. The ordering of yield stresses with respect to strain rate is less clear, in particular between tests CRS01 (0.003%, 87 kPa) and CRS02 (0.010%, 97 kPa), due to the sensitivity of the determined yield with respect to the lines drawn. The distinction with the fastest test CRS03

(0.059%, 64 kPa, that corresponds well with the step loading test SL001) is more apparent, with a smaller yield at faster rate. This trend, different from what is observed in saturated fine grained soils and/or sands, should obviously be confirmed by further investigation. The smallest yield stress and highest compressibility of the step loading test could come from the dramatic impact of instantaneous loading on a porous metastable unsaturated structure (step loading is better adapted in saturated samples). The reason why tests SL001 and CRS03 correspond so nicely is not straightforward.

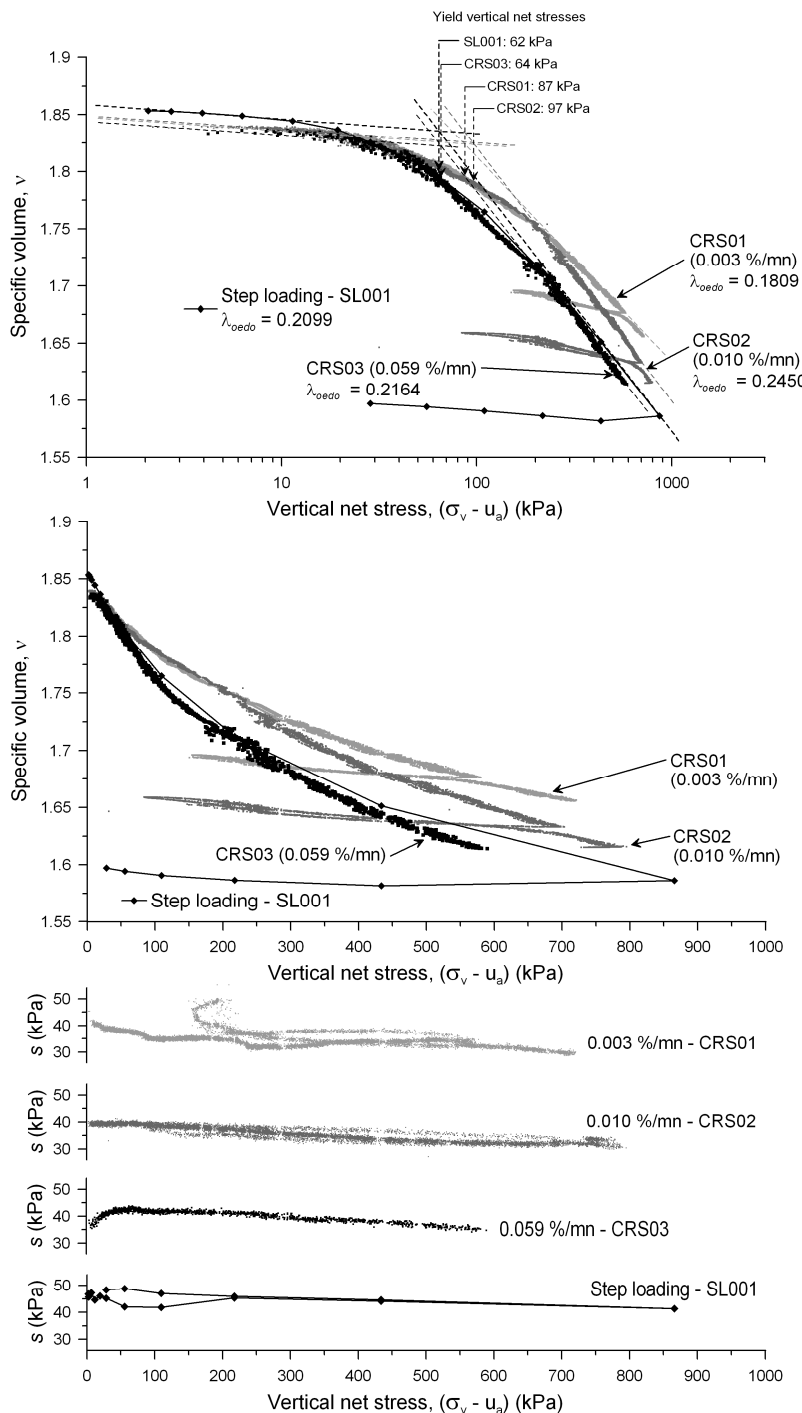


Figure 3. The effect of strain rate in the response at constant water content.

The responses in suction are fairly comparable at 0.003 and 0.010%/mn with a progressive decrease from the initial value (40 kPa) to 32 kPa. They are fairly reversible at 0.010%/mn, whereas larger suction variations are observed at 0.003 %/mn (CRS01, CRS04). At higher rate (0.059 %/mn) and with the step loading procedure, the responses are different with a rapid initial increase followed by a progressive decrease that ends at a comparable suction value.

Collapse behaviour

All the initial states of the samples tested in Figure 4 have the same initial void ratio (0.85), showing fairly good homogeneity within the block.

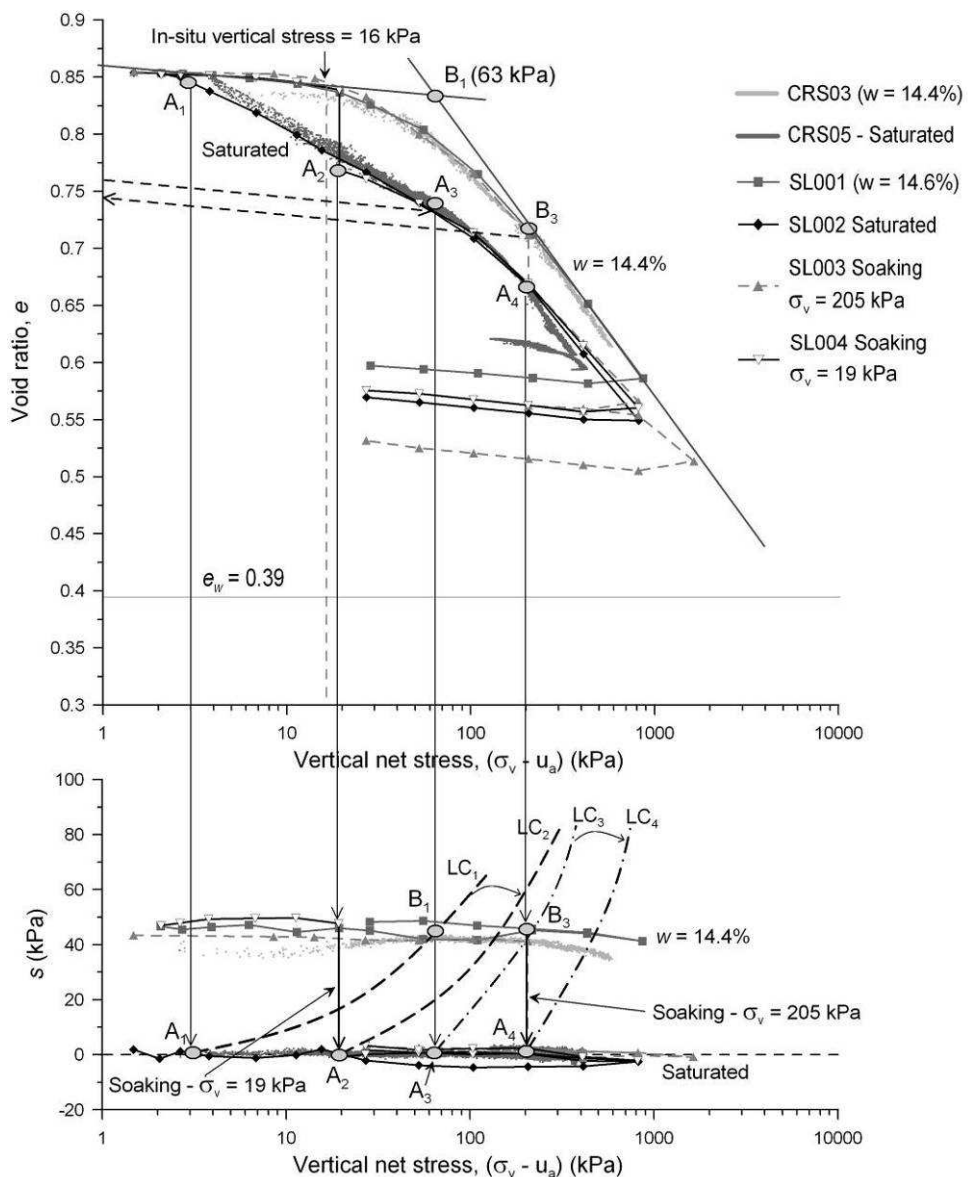


Figure 4. Collapse and compression tests performed

Tests include:

- The SL001 step loading test at constant initial water content (14.6%) that presents excellent correspondence with test CRS03 ($0.059\%/\text{mn}$, $w = 14.4\%$);
- The SL002 step loading test of a sample previously soaked under 1.5 kPa (no collapse) that presents excellent correspondence with test CRS05 carried out after soaking under 3 kPa (no collapse);
- The SL003 step loading collapse test (soaking at 205 kPa, 2.3% collapse) that presents excellent correspondence with test CRS03 before collapse and with tests SL002 and CRS05 after collapse;
- The SL004 step loading test with soaking at 19 kPa (close to the 16 kPa in-situ stress, 3.8% collapse) that presents excellent correspondence with test CRS03 before collapse and good correspondence with tests SL002 and CRS05 after collapse, confirming the (well known) validity of Jennings and Knight's approach.

The responses in suction are reasonably constant in all tests. As a result, comparable suction decreases occurred during both collapses at 205 and 19 kPa. Constant suction during compression was observed by some authors in samples compacted dry of optimum (e.g. Tarantino and De Col 2009) but not in all cases (Jotisankasa et al. 2007).

Various observations can be made from Figure 4:

- There is excellent correspondence between all tests, showing the good quality and homogeneity of the samples tested and of the experimental procedures;
- All rebound curves are comparable, confirming the independence of the BBM κ parameter (slope of the curve in the elastic range) with respect to suction, a trend also observed by Jotisankasa et al. 2007 in a artificial collapsible soil;
- Irreversible strain appears to develop from low stress in tests at zero suction (CRS05, SL002), reducing the yield stress to about 3 kPa;
- Accordingly, the mutual positions of the constant water content and zero suction curves evidence above 3 kPa the progressive development of collapse (an irreversible strain) up to a maximum under 30 kPa. Below 30 kPa, the unsaturated sample is less compressible than the saturated one (in agreement with the BBM model). Above, it becomes more compressible, as observed by Wheeler and Sivakumar (1995). The constant water content curve progressively joins the zero suction line, with an intersection probably located

between 1000 and 2000 kPa. The existence of a maximum collapse has been integrated in some constitutive models (e.g. Josa *et al.* 1992 and Georgiadis *et al.* 2008);

- The collapse strain at 19 kPa (3.8%) is larger than that at 205 kPa (2.3%). Indeed, 19 kPa is located below yielding (63 kPa) whereas a compressive plastic strain of about 10% developed prior to the plastic collapse strain of 2.3%;
- The changes in collapse with vertical stress are illustrated in Figure 5 that clearly shows the maximum collapse at 30 kPa.

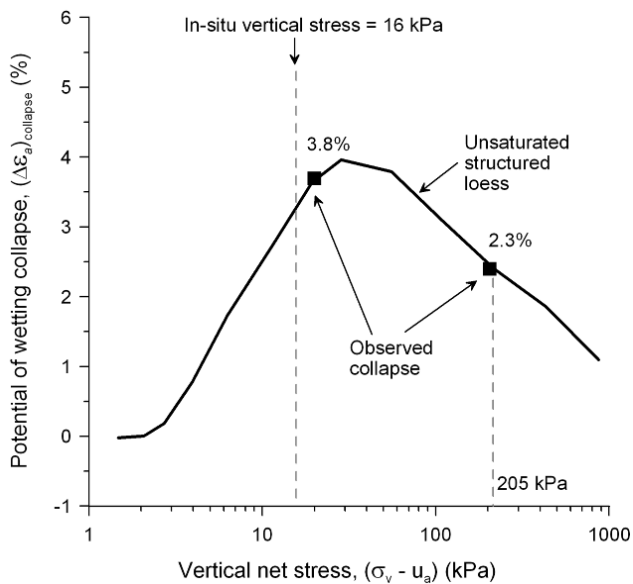


Figure 5. Potential of collapse due to wetting

Discussion

The small suction changes observed during compression can be related to the low saturation state of the samples with degrees of saturation increasing from 47% to 62 % (Table 2). Based on Laplace's capillary law and under the approximate hypothesis of cylindrical pores, a 40 kPa suction corresponds to a pore diameter of 7.5 μm , which means that larger pores should be dry. Given that the loess pore size distribution curve (not shown here for brevity, see Munoz-Castelblanco 2011) shows that 6.8% of the pore volume corresponds to larger inter-grains pores with diameter between 16 and 363 μm , it is believed that compression occurs by the breakdown of these larger and weaker dry pores with little effect on smaller water saturated pores that govern suction changes (Delage 2009).

At any stress, collapse brings the representative point from the constant water compression curve down to the "saturated" compression curve. Note however, as shown in Figure 4 (in

which both the constant saturated void ratio – $e_w = 0.39$), that collapse is far from erasing all the initially dry porosity.

A qualitative interpretation in terms of change in LC curves with the mobilization of either plastic compression or plastic collapse is proposed in Figure 4 in a $s/\log(\sigma_v - u_a)$ plot. The initial LC₁ curve represented in the Figure is fully determined by the two yield points at zero suction (A₁) and at $s \approx 40$ kPa (B₁, $\sigma_v - u_a = 63$ kPa). According to the BBM model, soaking under 19 kPa starts in the elastic region and should first induce a slight elastic swelling (not observed here). As drawn in Figure 4, the vertical soaking path curve then reaches the LC₁ curve and plastic collapse corresponds to the moving of point A₁ to A₂ and of curve LC₁ to LC₂. Plastic compression at constant water content to 205 kPa moves LC₁ to a LC₃ curve. LC₃ is defined by B₃ ($s \approx 40$ kPa, $\sigma_v - u_a = 205$ kPa) and A₃. The position of A₃ is estimated by (virtually) unloading the sample (using the known κ parameter), soaking it (with a small rebound defined by an estimated κ_s parameter) and compressing it elastically up to the yield defined by the intersection with the saturated compression curve (62 kPa). Indeed, the LC₃ curve appears to have a smaller inclination than LC₂ illustrating a smaller potential collapse (Alonso et al. 1987). LC₃ is afterwards moved to LC₄ during plastic collapse (A₃ moves to A₄) with also a smaller estimated inclination.

Conclusions

Up to date experimental techniques (including collapse tests with suction monitoring) and qualitative constitutive modelling of unsaturated soils have been used in the investigation of the collapse behaviour of a natural aeolian loess from Northern France. Compared to existing data on reconstituted collapsible soils, the following set of conclusions can be drawn for a natural soil:

- Suction measurements showed that constant water content compression tests occurred at a fairly constant suction (even at yielding). This is explained by the compression induced collapse of the largest dry pores of the loess, with little effect on the smaller hydrated pores that control suction changes;
- Given the aeolian origin of the loess, yield is not related to any previous applied stress but to the bonding due to carbonate re-precipitation between the grains, resulting in less apparent yield values compared to compacted soils;

- The response of the loess to compression is time dependent. Whereas the trend governing the changes in yield stress with strain rate is not very clear and needs further investigation, the plastic compression parameter λ appears to be time dependent unlike in saturated fine grained soils that are generally characterised by an isotach-type viscous response;
- A maximum collapse is observed at a vertical net stress of 30 kPa;
- The volume change behaviour has been qualitatively interpreted by means of the LC curve concept, the inclination of which varied to account for the existence of a maximum collapse;
- The magnitude of collapse is known to increase with higher suction. This is the case during dry periods, in particular like in Figure 1 when the layer of collapsible loess has been directly exposed to atmosphere and does experience evaporation. As a result, the magnitude of the collapse observed in the photo could be significantly higher than that measured here.

References

- Alonso E., Gens A. and Hight A. (1987). Special problems soils. General Report, *Proc. 9th European Conference on Soil Mechanics and Foundation Engineering*, Dublin 3, Balkema. 1087-1146.
- Alonso E., Gens A. et Josa A. (1990). A constitutive model for partially saturated soils. *Géotechnique* 40 (3). 405-430.
- Antoine P., Catt J. and Sommè J. (2003). The Loess and Coversands of Northern France and Southern England. *Journal of Quaternary Science* 18. 309-318.
- Cui Y.J. and Delage P. (1996). Yielding and plastic behaviour of an unsaturated compacted silt. *Géotechnique* 46 (2). 291-311.
- Cui Y.J., Marcial M., Terpereau J.M., Delage P., Antoine P., Marchadier G. and Ye W.M. (2004). A geological and geotechnical characterisation of the loess of Northern France. *A.W. Skempton Memorial Conference*, vol. 1. 417-428.
- Delage P., Le T.T., Tang A.M., Cui Y.J., Li X.L. 2007. Suction effects in deep Boom clay block samples. *Géotechnique* 57 (1), 239-244.
- Delage P. (2009). Compaction behaviour of clay: discussion. *Géotechnique* 59 (1). 75-76.
- Georgiadis K., Potts D.M. and Zdravkovic L. (2008). An improved constitutive model for unsaturated and saturated soils. In *Unsaturated Soils : Advances in Geo-Engineering*, Proc. of the 1st European Conference on Unsaturated Soils, Durham, UK, CRC Press. 581-588.
- Jennings J.E. and Knight K. (1957). The additional settlement of foundation due to collapse of sandy soils on wetting. *Proc. 4th International Conference on Soil Mechanics and Foundation Engineering* 1. 316-319.
- Josa A., Balmaceda A., Gens A. and Alonso E.E. (1992). An elasto-plastic model for partially saturated soils exhibiting a maximum of collapse. *Proceedings of 3rd International Conference on Computational Plasticity*, Barcelona, vol. 1. 815–826.
- Jotisankasa A., Ridley A. and Coop A. (2007). Collapse behavior of a compacted silty clay in the suction-monitored oedometer apparatus, *Journal of Geotechnical and Geoenvironmental Engineering*, ASCE. 867-877.

-
- Maâtouk A., Leroueil S. and La Rochelle P. (1995). Yielding and critical state of a collapsible unsaturated silty soil. *Geotechnique* **45** (3). 465-477.
- Muñoz-Castelblanco J., Pereira J.M., Delage P. and Cui Y.J. (2011). The water retention properties of a natural unsaturated loess from Northern France. *Géotechnique*, accepted for publication.
- Muñoz-Castelblanco J. (2011). Comportement hydromécanique d'un lœss naturel non saturé. Thèse de doctorat, *Ecole des Ponts ParisTech*, Paris, France.
- Pécsi M. (1990). Loess is not just the accumulation of dust. *Quaternary International* 7/8. 1-21.
- Tarantino A. and De Col E. (2008). Compaction behaviour of clay. *Géotechnique* **58** (3). 199-213.
- Wheeler S.J. and Sivakumar V. (1995). An elasto-plastic critical framework for unsaturated soil. *Géotechnique* **45** (1). 35-53.

4.3 Caractérisation du comportement hydromécanique du Loess de Bapaume

Cette dernière section présente les résultats des essais triaxiaux à différentes teneurs en eau et à des chemins de contraintes divers (compression isotrope, compression K_0 anisotrope, cisaillement triaxial à confinement constant). Elle propose aussi des couplages des propriétés mécaniques (comportement à de déformations faibles, comportement à la rupture, compressibilité après la rupture) avec les caractéristiques hydrauliques (courbe de rétention d'eau) du lœss. Une analyse de ces couplages à partir du rôle de la microstructure est également proposée.

D'après les analyses réalisées, le lœss est un dépôt éolien naturel caractérisé par une structure composée d'un arrangement métastable de grains de limon dont l'espace poreux est rempli d'agrégats argileux ayant un potentiel important de changement de volume. Ces caractéristiques donnent à ce matériau des propriétés hydromécaniques particulières telles que :

- une compressibilité qui augmente avec la succion ;
- un risque d'effondrement assez important lorsque l'on remouille sous chargement anisotrope;
- une augmentation de la rigidité du lœss avec la succion à de déformations faibles (associée à l'état non-saturé des agrégats argileux) ;
- un comportement de plus en plus dilatant au fur et à mesure que la succion augmente ;
- une hystérésis hydraulique importante à l'état intact initial et à des teneurs en eau faibles. Ce phénomène est lié aux changements de volume des agrégats argileux lors des cycles de séchage – remouillage. L'hystérésis est fortement réduite si on soumet le sol à un chargement mécanique. On peut supposer que l'application de charges externes endommage les agrégats argileux, ces derniers étant les principaux responsables de l'hystérésis (on a aussi observé un peu d'hystérésis à de hautes teneurs en eau, associée aux effets capillaires dans les pores entre les grains de limon);
- un comportement en général isotrope associé à la forme ellipsoïdale des surfaces de charge obtenues, lesquelles sont similaires à celle proposée dans le modèle Cam-Clay pour les sols saturés. D'ailleurs, on a observé une différence entre la forme des surfaces

de charge et les incrément des déformations plastiques. Ceci est lié à une loi d'écoulement plastique non-associé.

Muñoz-Castelblanco, J., Delage, P., Pereira, J.M. & Cui Y.J.

Hydromechanical behaviour of a natural unsaturated loess

J. A. Muñoz-Castelblanco*, P. Delage*, J. M. Pereira* and Y. J. Cui*

A comprehensive experimental study has been carried out to investigate the couplings of the compressibility and yielding behaviour with the water retention properties of an unsaturated collapsible natural loess from the area of Bapaume (Northern France). Hydromechanical couplings of the Bapaume loess behaviour were analyzed by means of triaxial tests conducted on a novel apparatus providing a complete local monitoring of strains, suction and water content. Scanning electron microscope observations of the microstructure were also performed before and after triaxial testing. The test results are interpreted on the basis of the effects of moisture changes on the mechanical behaviour and of the impact of mechanical loading on the water retention properties. The analysis of the role of the microstructure of loess on its coupled hydromechanical behaviour shows the main effect of the swelling-shrinking potential behaviour of the clay aggregations that partially fill the pore network of an open and metastable arrangement of silt grains. Further constitutive modeling should account these microstructure features with a non-standard compressibility behaviour, a collapse sensibility and an overall structure-dependent hydromechanical behaviour.

KEYWORDS: Loess; hydromechanical couplings; microstructure; hysteresis; non-standard material

Introduction

Research on the hydromechanical behaviour of unsaturated soils have been concentrated on the constitutive modelling of the coupling of hydromechanical properties (e.g. Alonso *et al.* 1990, Wheeler and Sivakumar 1995, Wheeler 1996, Barbour 1998, Jommi 2000, Vaunat *et al.* 2000, Gallipoli *et al.* 2003, Wheeler *et al.* 2003, Tarantino 2007) and on the experimental characterisation of this behaviour, especially on compacted and reconstituted soil samples (e.g. Maâtouk *et al.* 1995 on an unsaturated loose compacted silt from Québec, Cui and Delage 1996 on a unsaturated compacted Jossigny silt, Romero and Vaunat 2000 on a compacted clay, Cunningham *et al.* 2003 on a reconstituted unsaturated silty-clay, Tarantino and De Col 2008 on a compacted clay, Jotisankasa *et al.* 2009 on a compacted silty-clay). Coupling includes the dependence of yielding and compressibility on water retention properties and vice versa.

However, there is little experimental evidence on the effect of hydro-mechanical couplings on the behaviour of natural soils. Natural soils in unsaturated conditions are yet very common around the World, especially in tropical, arid and semi-arid regions (Dudley 1970). There is a

* Ecole des Ponts ParisTech, Laboratoire Navier – CERMES, Université Paris-Est

large variety of problematic soils that may be encountered in the field, such as high plasticity swelling clays (high potential to swell and shrink due to wetting and drying, respectively), alluvial deposits (collapse potential due to metastable structure), colluvial soils and also aeolian soils, like loesses, that are characterized by a metastable structure prone to collapse due to wetting.

Widespread aeolian loess deposits are located in Northern France (Antoine *et al.* 2003, Cui *et al.* 2004, Delage *et al.* 2005). In most areas, they are naturally unsaturated and characterized by satisfactory geotechnical properties with no particular problematic behaviour. In some areas however, some layers of loess are characterized by a significant calcareous content, a high porosity and a low plasticity. These features lead to a metastable structure that is strengthened by suction when the soil is partially saturated. A loss of stability of the structure may appear upon wetting which leads to relatively large volumetric deformations due to the collapse of the open structure of the soil. This collapse behaviour of loose unsaturated soils has been observed and described by many authors including Barden *et al.* (1973), Yudhbir (1982), Alonso *et al.* (1987), Cui *et al.* (2004), Delage *et al.* (2005), Hormdee (2008), Punrattanasin (2008), Yuan and Wang (2009).

This paper presents an experimental campaign devoted to the characterisation of the constitutive hydromechanical behaviour of an intact loess. Loess samples have been extracted from a site close to the city of Bapaume (France). The collapse susceptibility of the loess has been already investigated by different authors (Cui *et al.* 1995, 2004, Delage *et al.* 2005, Karam 2006, Yang *et al.* 2008, Karam *et al.* 2009) in relation with some stability problems (due to water infiltration) detected on the loess foundation deposits of the high speed train line linking Paris to Brussels (LGV Nord). The loess water retention properties have been investigated in detail in Muñoz-Castelblanco *et al.* (2011b) in relation with microstructure features.

A series of constant water content triaxial tests was performed in a newly developed triaxial device for unsaturated soils (Muñoz-Castelblanco *et al.* 2011a) at three values of water content, i.e. close to saturation ($w = 27\%$), at initial natural water content ($w = 14.4\%$) and in a drier state ($w = 10\%$). The specimens were loaded following three different stress paths: isotropic compression, K_0 anisotropic compression and shear loading. The new system allows a complete local monitoring of the state of the unsaturated soil sample during testing thanks to the combined use of a new local resistivity probe for water content measurement, of Hall

Effect transducers to measure the local displacements and of an in-house constructed high capacity tensiometer to measure suction (Manthro 2005, Cui *et al.* 2008).

In order to analyse the impact of mechanical loading on the water retention properties, the water retention curve (Muñoz-Castelblanco *et al.* 2011b) of the intact material ($e_0 = 0.85$) was compared to the retention curve of a denser specimen that was obtained by oedometer compression under the natural hydric state ($w = 14.4\%$, $s = 40$ kPa) down to a lower void ratio $e_0 = 0.65$.

Material and experimental setup

Bapaume loess

The soil studied is an intact unsaturated loess extracted from a deposit located in an area near to the city of Bapaume (Northern France). These loess deposits were formed during the Quaternary period under periglacial conditions from the aeolian transport of silt particles eroded by a constant North West wind (Antoine 2002, Antoine *et al.* 2003). The loess is characterized by a relative homogeneity, a low plasticity, a high porosity, a carbonate fraction of 6% and an open structure that explains its susceptibility to collapse when saturated (Cui *et al.* 2004, Delage *et al.* 2005, Yang *et al.* 2008, Karam *et al.* 2009, Muñoz-Castelblanco *et al.* 2011a,b).

Intact loess blocks were manually extracted from a 5 m deep excavation in cubic boxes of 300 mm side and immediately protected by paraffin coating and with a plastic film to avoid evaporation. The void ratio at natural state is about 0.85, the natural water content is 14.4% and the initial degree of saturation is 44%. The plastic properties are quite low ($I_p = 9$, $w_p = 37\%$, $w_l = 28\%$) and the Casagrande classification of the loess is CL. The water retention properties of the loess have been investigated in detail in Muñoz-Castelblanco *et al.* (2011b) in relation to its microstructure. The sand, silt and clay fractions are equal to 2, 82 and 16% respectively. The dominant clay minerals are kaolinite, illite and interstratified illite-smectite (Cui et Marcial 2003). The loess contains 6% of carbonates, a component known to provide some bonding between particles due to the alteration of primary carbonates ($MgCO_3$ or $CaCO_3$) followed by re-precipitation (“Loess is not just the accumulation of dust”, as quoted by Pécsi 1990).

Triaxial apparatus

The employed apparatus incorporates local measurement sensors of displacement, water content and suction, installed at the midheight of the triaxial sample. Axial and radial strains are locally measured using a set of Hall-Effect sensors. Local suction is measured by using a miniature 500 kPa high capacity tensiometer of diameter 5 mm (Chiu *et al.* 2002). Water content is monitored by using a home-designed electrical resistivity probe of diameter 11 mm. This new device is described in detail in Muñoz-Castelblanco *et al.* (2011c).

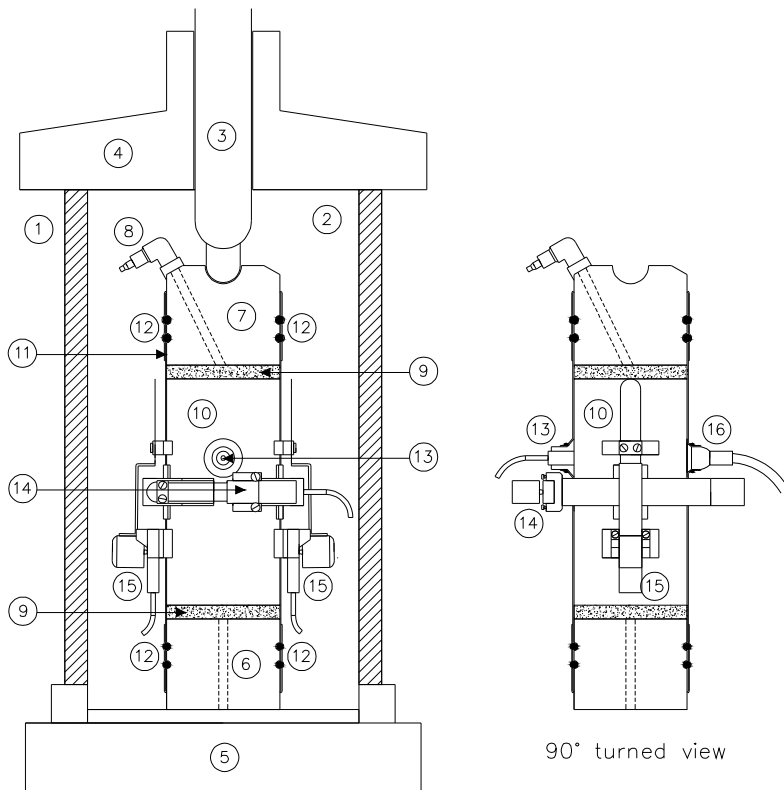
An overall view of the device is presented in Figure 1. Air pressure (maximum value 1 MPa), is regulated by a computer-controlled electro-valve (7). An air-liquid interface cell (9) is used to transmit the air pressure to the fluid. The fluid pressure is measured using a pressure gauge (5) of 500 kPa capacity. The shear load is applied by a strain-controlled press (1) and measured by an external load sensor of 5 kN capacity (4). The cell base accommodates the connection wires of the different immersed sensors. The cell chamber consists of a Perspex cylinder and of top and bottom plates. The top plate houses a valve to apply the confining pressure (Figure 1).

Testing programme and procedure

One isotropic compression, one K_0 compression and one triaxial shear test were performed on saturated loess specimens. The isotropic compression test was performed at a rate of 0.6 kPa per minute after consolidating and saturating the specimen under isotropic conditions. The samples used in the K_0 compression and the triaxial shear tests were previously consolidated at natural state up to the in-situ stress ($\sigma_v = 17$ kPa and $\sigma_h = 8$ kPa) by a drained K_0 compression path (CAD) where lateral strain was controlled, close to zero ($\varepsilon_r = \pm 0.0035\%$). The samples were then saturated under in-situ stress state by applying a water pressure head of 50 cm (5 kPa). After these different stages, one specimen was submitted to a drained triaxial shear (CID) test and the other was loaded following the K_0 path.

To study the compressibility and yield behaviour of the unsaturated loess, two isotropic and two K_0 compression tests were performed at water contents of 14% and 10% respectively. The main characteristics of the tests are given in Table 1 and Table 2. To study the influence of the suction on shear behaviour, two drained triaxial shear (CID) tests were performed at water contents of 14.4% and 10.5%. The shear tests were performed under a confining stress of 8

kPa corresponding to the horizontal in situ stress. The main characteristics of these tests are given in Table 3.



- 17. Perspex cylinder
- 18. Cell chamber (1 MPa)
- 19. Loading piston
- 20. Top plate
- 21. Cell base
- 22. Lower cap
- 23. Top cap
- 24. Top drainage
- 25. Porous stone
- 26. Soil specimen
- 27. Latex membrane
- 28. o-rings
- 29. Tensiometer
- 30. Radial strain transducer (Hall Effect)
- 31. Axial strain transducer (Hall Effect)
- 32. Resistivity probe



Figure 1. Modified triaxial cell

The specimens were trimmed from intact blocks (natural initial state $w = 14.4\%$, $S_r = 44\%$ suction $s = 40$ kPa). The initial void ratio varied between 0.82 and 0.85, corresponding to small variations in the initial porosity between 45% and 46% respectively and illustrating a relatively homogeneity in the block. To achieve a water content value of 10%, samples were

submitted to controlled evaporation under laboratory conditions for a period of time of about 15 hours. Once the target water content was reached, the specimen was placed into the triaxial cell and the local displacement sensors, the high capacity tensiometer and the resistivity probe were placed at mid-height. Complete equilibration of suction and water content was monitored and measurements showed that stabilisation was reached within a maximum of 6 hours. The equilibrated measured suctions at $w = 14.4\%$ and $w = 10.5\%$ were 40 kPa and 100 kPa respectively.

Test	w_0 (%)	e_0	$\nu = I+e_0$	s_0 (kPa)	$(p - u_a)_y$ (kPa)	e_{yield}	w_{yield} (%)	s_{yield} (kPa)	$\lambda(s)$	κ
CI-SAT	25.5	0.84	1.84	0.9	53*	0.84	25.6	1.5	0.096	0.020
CI-14%	14.2	0.85	1.85	44.7	147	0.83	14.4	40.6	0.150	0.007
CI-10%	10.5	0.84	1.84	101.2	227	0.83	11.2	98.5	0.125	0.004

* The mean yield net stress correspond to $(p - u_w)_y$ for the saturated test

Table 1. Isotropic compression tests data

Test	w_0 (%)	$I+e_0$	s_0 (kPa)	$(p - u_a)_y$ (kPa)	e_{yield}	w_{yield} (%)	s_{yield} (kPa)	$\lambda(s)$	k	K_0
CK ₀ -SAT	25.0	1.84	0	26*	0.77	24.8	-0.5	0.156	0.076	0.50
CK ₀ -14%	14.3	1.83	44.0	82	0.76	15.6	43.1	0.194	0.033	0.46
CK ₀ -10%	10.6	1.84	107.3	137	0.81	10.9	93.3	0.241	0.009	0.45

* The mean yield net stress correspond to $(p - u_w)_y$ for the saturated test

Table 2. K_0 compression tests data

Test	w_0 (%)	e_0	s_0 (kPa)	E (MPa)	ν	q_y (kPa)	$(p - u_a)_y$ (kPa)	e_{yield}	w_{yield} (%)	s_{yield} (kPa)
S-SAT	25.9	0.84	0.3	3.6	0.21	13	13*	0.81	26.1	0
S-14%	14.0	0.84	38.6	9	0.22	38	21	0.83	13.2	43.7
S-10%	10.6	0.84	98.1	28	0.21	114	46	0.83	10.2	94.2

* The mean yield net stress correspond to $(p - u_w)_y$ for the saturated test

Table 3. Triaxial shear tests data. $(\sigma_3 - u_a) = 8$ kPa when unsaturated; $(\sigma_3 - u_w) = 8$ kPa when saturated.

The K_0 compression test were carried out by increasing the cell pressure at a changing rate comprised between 0.3 kPa to 1 kPa per minute in order to maintain the lateral strain equal to zero. An axial strain rate of 0.010 %/mn (corresponding to a speed of 10 $\mu\text{m}/\text{mn}$) was used in the triaxial shear tests.,

The volume of each specimen was carefully determined just after specimen preparation and at the end of the test by using a precision calliper. Volume changes were also measured by monitoring the axial and radial strains at the midheight of the specimen. A good agreement between results from both methods was observed. A good correspondence of water content values was also observed between an external measure performed by weighing at the final state after testing and the measurements given by the electrical resistivity probe.

The stress variables considered in the analysis are the net mean stress ($p - u_a$), the deviatoric stress q and suction $s = (u_a - u_w)$, in which u_a and u_w are the air and water pressures respectively, $p = (\sigma_l - 2\sigma_3)/3$ and $q = (\sigma_l - \sigma_3)$ with σ_l and σ_3 being the axial and radial stress respectively.

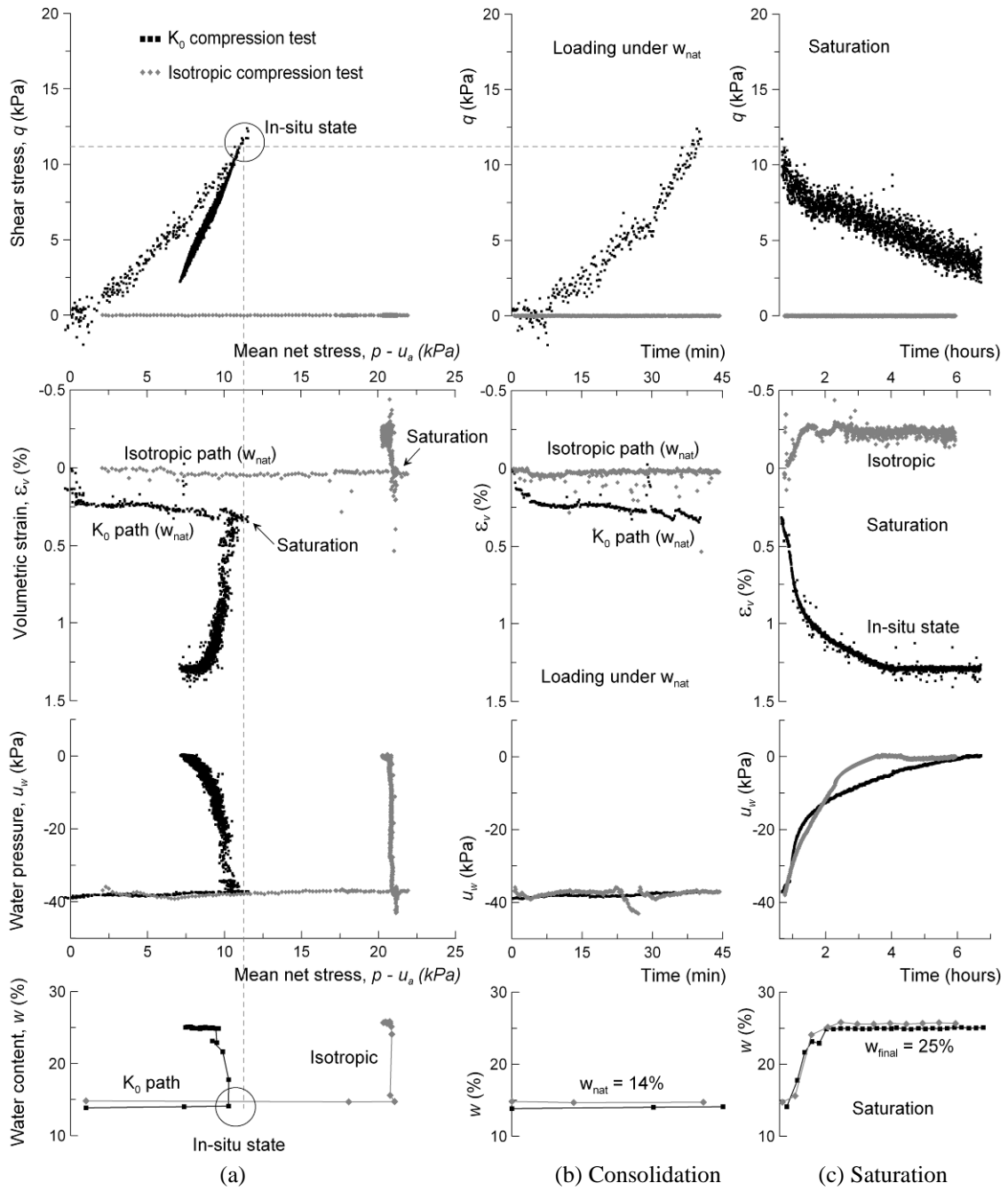
Experimental results

Stress-strain behaviour in the saturated state

The initial stages of consolidation and saturation of the isotropic (CI-SAT) and K_0 compression tests are presented in Figure 2.

In test CI-SAT (gray points in Figure 2), the specimen was initially isotropically consolidated under its natural state ($w = 14.4\%$ and $s = 40$ kPa) up to a confining pressure of 20 kPa. During this stage, represented as a function of time in Figure 2(b), no significant volume change was observed. The sample was then saturated under 20 kPa by applying a back-pressure of 10 kPa at the bottom of the sample while connecting the top valve to a water reservoir under atmospheric pressure. Figure 2(c) shows the observed swelling of $\varepsilon_{vf} = -0.25\%$ that is coupled with a suction decrease from $s = 37.6$ kPa to zero and a water content increase from 14.7% to 25.8%. A Skempton coefficient $B = 0.97$ was obtained, showing good saturation.

The K_0 anisotropic compression tests (CK $_0$ -SAT, black points in Figure 2) were carried out by submitting the specimens at natural state ($w = 14.4\%$ and $s = 40$ kPa) to a K_0 compression path (Figure 2b) until the in situ stress state corresponding to $\sigma_v - u_a = 17$ kPa and $\sigma_h - u_a = 8$ kPa ($p - u_a = 11$ kPa). A compression strain of 0.3% was observed when bringing the specimens back to in-situ stress state. Specimen saturation was then performed (Figure 2c) by applying a water head of 50 cm (5 kPa) at the base of the sample while keeping the confining stress constant at 8 kPa. During saturation, suction decreased from $u_w = 37$ kPa to zero, water content increased from 14% to 25.1% and the shear stress decreased significantly from 10 kPa to 3 kPa with a compression strain of about 1%. This compression response under a final mean net stress of 6 kPa significantly differs from the swelling deformation previously observed during saturation under a final effective isotropic mean net stress of 10 kPa. This compression, related to collapse under wetting, shows the drastic effect of the initial shear stress component (9 kPa).

Figure 2. Consolidation - saturation processes. Isotropic and K_0 compression tests

Data obtained during the isotropic (CI-SAT) and K_0 -anisotropic (CK₀-SAT) compression tests on the saturated loess are presented together in Figure 3. A plastic compressibility parameter [$\lambda(s=0) = -\Delta(1+e)/\Delta \log p'$] of 0.096 was calculated from the data of test CI-SAT in the post-yield range. A yield stress $p'_y = 53$ kPa can be determined by using Casagrande's method. The explanation of such a high value (to compare to the in-situ stress state and given the swelling observed under saturation) is not easy to figure out.

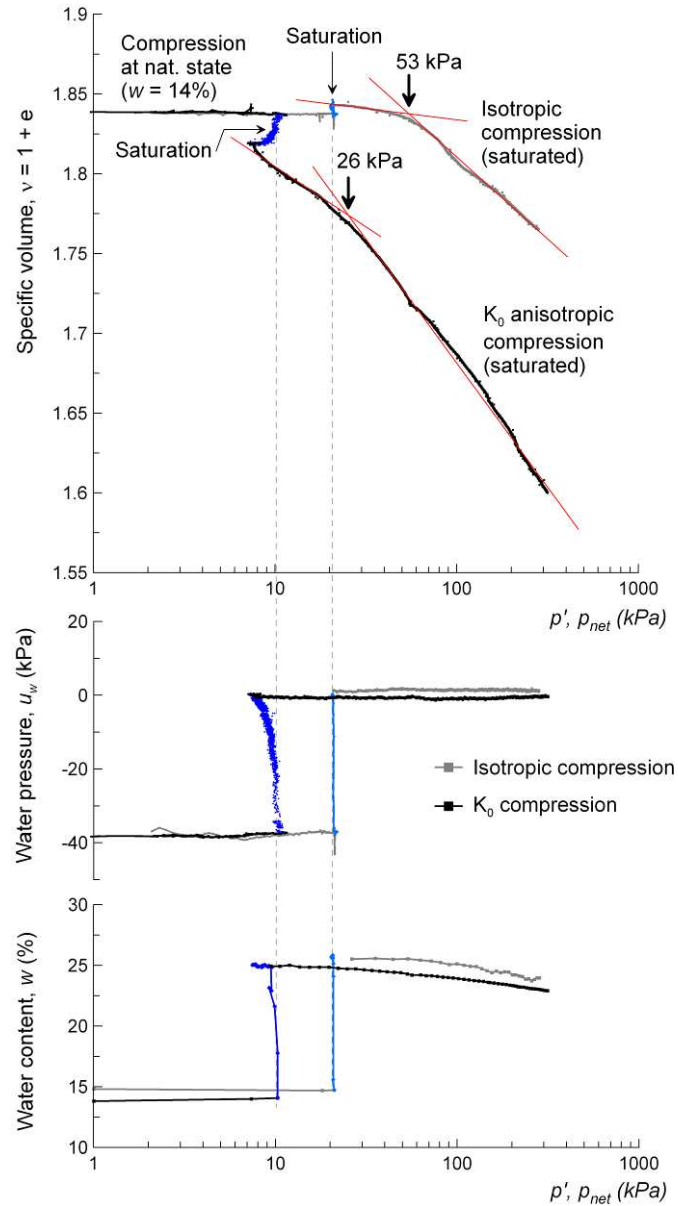


Figure 3. Isotropic and K_0 compression tests on saturated loess

The data of test CK₀-SAT shows a compressibility parameter $\lambda(s=0)$ of 0.156 after saturation, higher than that of test CI-SAT. A yield stress $p'_y = 26$ kPa was observed.

Isotropic compression tests

Figure 4 and Table 1 present the results of the isotropic constant water content compression tests performed at $w_0 = 14.2\%$ (test CI-14%) and $w_0 = 10.5\%$ (CI-10%) that are compared with the data of test CI-SAT. All specimens have comparable initial void ratios of about 0.85.

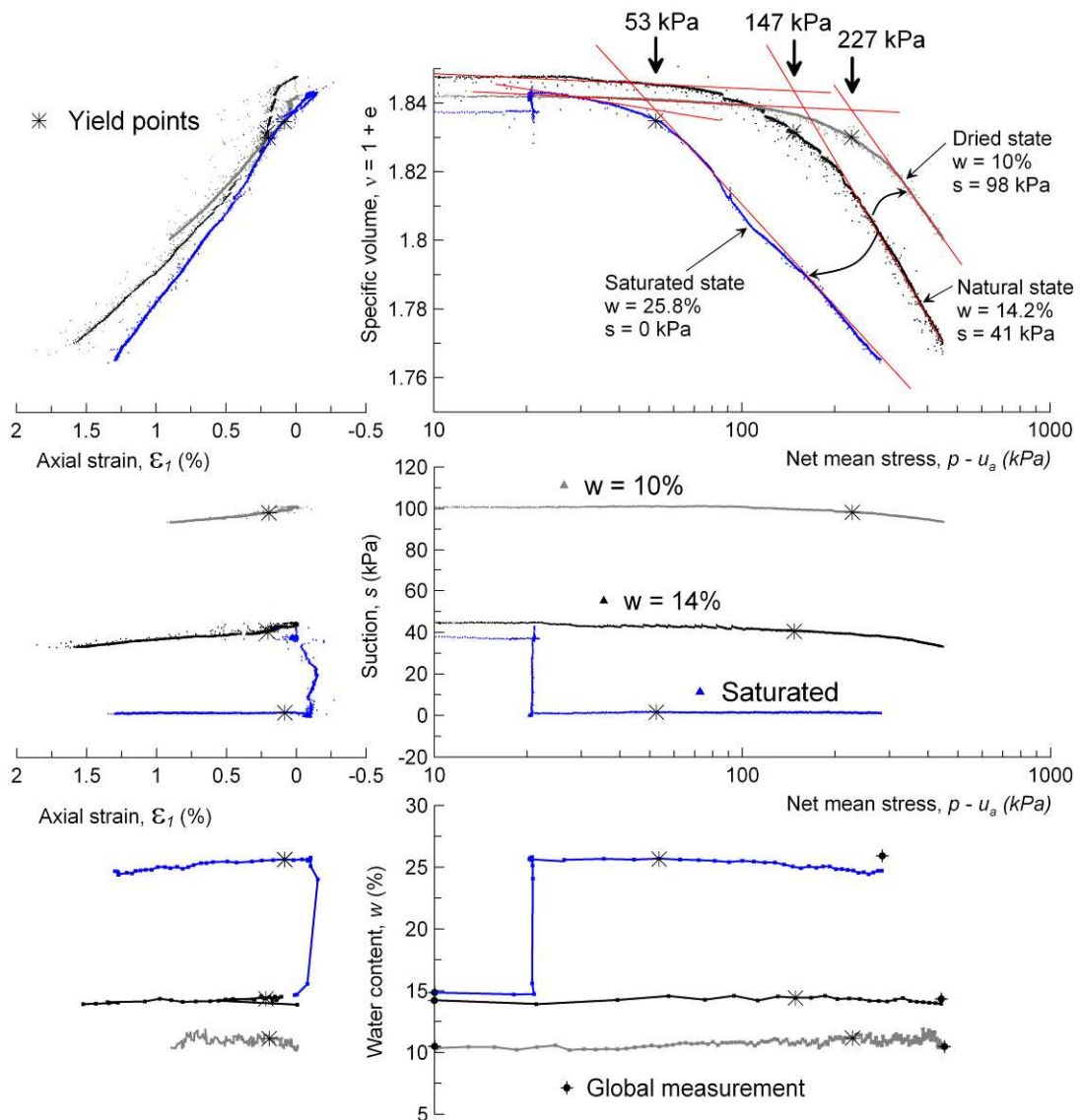


Figure 4. Isotropic compression test results on specimens at different initial water content values

The following observations can be drawn from the Figure:

- In agreement with a well established feature of unsaturated soils captured in the BBM model (Alonso *et al.* 1987, 1990), the isotropic yield stress increases with increased suction from $(p - u_a)_y = 53 \text{ kPa}$ at zero suction to $(p - u_a)_y = 147 \text{ kPa}$ at $s = 41 \text{ kPa}$ (natural state at 14.2%) and to $(p - u_a)_y = 227 \text{ kPa}$ at $s = 98 \text{ kPa}$ (dried state at 10%); these values allow the determination of the LC curve of the loess that will be further commented later on;
- The plastic compressibility parameter $\lambda(s)$, equal to 0.150 at initial natural state ($w = 14.2\%$, $s = 41 \text{ kPa}$) decreases to 0.125 when the sample is dried at $w = 10\%$ ($s = 98 \text{ kPa}$), in accordance with the BBM model; conversely, $\lambda(s)$ decreases to 0.096 when the sample is initially saturated (Table 1);

-
- The elastic swelling parameter $\kappa = -\Delta(1+e)/\Delta \log(p - u_a)$ obtained in the pre-yield range is $\kappa = 0.007$ in the initial state, $\kappa = 0.020$ after saturation and it decreases to $\kappa = 0.004$ after drying ($s = 98$ kPa);
 - Extending the double oedometer approach (Jennings and Knight 1957) to isotropic stress conditions, one can observe in Figure 4 that the magnitude of collapse significantly increases when the sample is dried from $w = 14.2\%$ to 10% . The observed values of maximum collapse are equal to $\varepsilon_v = 1.5\%$ and $\varepsilon_v = 3.0\%$ respectively and take place under isotropic stresses of 132 kPa and 332 kPa respectively.

Figure 4 also shows the changes in suction with both mean net stress ($p - u_a$) and axial strain ε_l during the isotropic compression. Suction does not change in the pre-yield range but it slightly decreases in the post-yield range from 44.7 kPa to 33.2 kPa in test CI-14%, and from 101.2 kPa to 93.6 kPa in test CI-10%, coupled with slight increases in degree of saturation ($\Delta S_r = 3\%$ in test CI-14% and $\Delta S_r = 5\%$ in test CI-10%). The comparison with global measurements validates the low changes monitored in water contents in the unsaturated tests. Quite low variations of water content were observed during the zero-suction test CI-SAT. Under the hypothesis of no volume change at the intact state, a degree of saturation of 1 theoretically corresponds to a water content of $w = 31.8\%$. Since the initial degree of saturation is lower ($S_{ri} = 0.81$), it is very probable that the sample is not fully saturated when put under zero suction by infiltrating liquid water. As quoted in Muñoz-Castelblanco *et al.* (2011b), total saturation of intact loess specimens ($e = 0.85$) seems to be not possible when soaking at low external pressure (i.e. atmospheric pressure). As a consequence, since the final degree of saturation after loading is 0.86 (i.e. $e_f = 0.77$), the water content could remain merely constant during mechanical loading as in the other unsaturated tests. This is actually what is observed in Figure 4.

K₀ compression tests

The K_0 compression testing programme carried out is summarized in Table 2. K_0 stress paths, were carried out under a constant axial strain rate of 0.010 %/mn by controlling the confining pressure so as to ensure a no lateral strain condition. Observation of the Table shows that drying does not significantly affect the K_0 value that slightly decreases from 0.46 to 0.45 when drying the sample (with $K_0 = (\sigma_3 - u_a)/(\sigma_l - u_a)$) whereas it increases to 0.5 after saturation (with $K_0 = (\sigma_3 - u_w)/(\sigma_l - u_w)$).

Figure 5 shows the results obtained from the specimens at natural initial water content ($w_0 = 14.3\%$, $s_0 = 44 \text{ kPa}$, test CK₀-14%), after drying at $w_0 = 10.6\%$ ($s_0 = 107.3 \text{ kPa}$, test CK₀-10%) and after saturation ($w_0 = 25\%$, $s_0 = 0 \text{ kPa}$, test CK₀-SAT). Saturation, performed by wetting the sample under K_0 conditions exhibited a $\varepsilon_v = 1.0\%$ collapse strain, opposite to the $\varepsilon_v = -0.25\%$ swelling that was observed in isotropic conditions (see Figure 3). The difference might be due to the slight shear component acting under K_0 conditions.

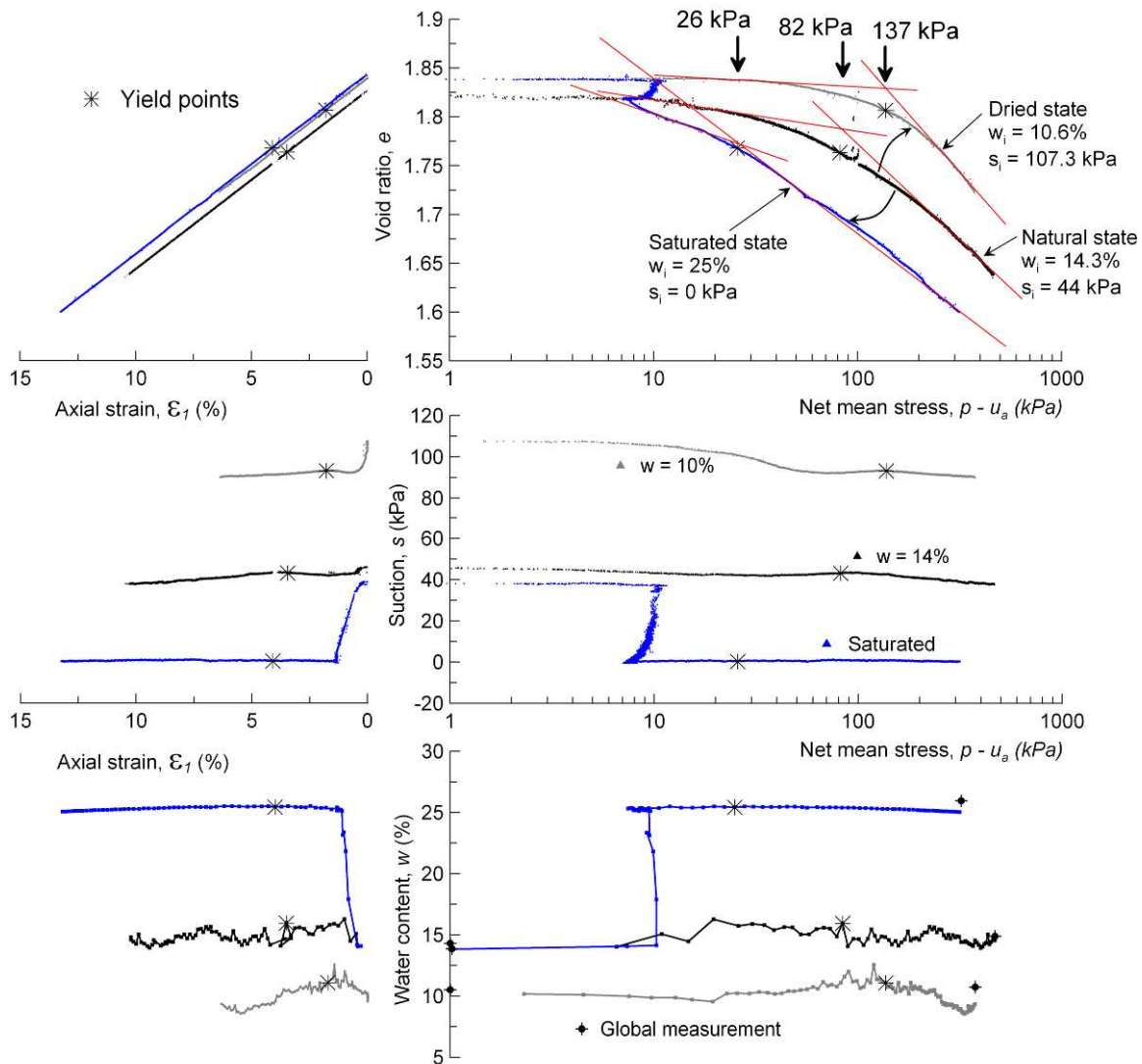


Figure 5. K_0 anisotropic compression test results on specimens at different initial water content values

The following observations can be drawn from the Figure:

- As under isotropic compression, yield values are well classified with respect to suction: the yield value under K_0 conditions at natural state is equal to 82 kPa, significantly smaller than that obtained from isotropic compression (147 kPa). It decreases to $(p - u_a)_y = 26 \text{ kPa}$ after sample saturation (compared to 53 kPa under isotropic stress) and increases to $(p -$

$u_a)_y = 137$ kPa when dried at 10.6% (compared to 227 kPa under isotropic stress). These values provide a further determination of the elastic limit surface in the $(q, p - u_a, s)$ space that crosses the $(s, p - u_a)$ plane through the LC curve;

- The plastic compressibility parameter $\lambda_{K_0}(s)$ slightly decreases when saturating the specimen from $\lambda_{K_0}(42$ kPa) = 0.194 to $\lambda_{K_0}(0)$ = 0.156, making the saturated specimen slightly less compressible than in initial unsaturated conditions; conversely, $\lambda_{K_0}(s)$ slightly increases with $\lambda_{K_0}(93$ kPa) = 0.241 when drying the specimen at 10.6 % at a suction of 107.3 kPa. These two observations do not follow the common volumetric behaviour feature of unsaturated soils as described by the BBM model (note that the so-called λ_{K_0} parameter is not a constitutive parameter, since it illustrates the response of the soil to a boundary problem. This is even more true given that K_0 depends on suction, as seen in Table 2 although it would appear reasonable to consider it independent in a constitutive law to simplify. Indeed, λ_{K_0} should be calculated from the constitutive law that should account for the variations in volume changes due to the K_0 proportion of shear stress involved during plastic flow);
- $\lambda_{K_0}(s)$ values are significantly higher than the $\lambda(s)$ values (isotropic compression) and they don't change in the same way. The difference is due to the shear component of the stress state in K_0 conditions, the importance of which has already been noted when soaking the sample under both isotropic and K_0 conditions. This sensitivity is thought to be related to the loose collapsible loess structure, the stability of which is known to be highly affected by local shear stresses (Burland 1956).
- In the pre-yield range, the compressibility parameter κ_{K_0} decreases with increased suction: $\kappa_{K_0} = 0.033$ ($s = 42$ kPa) and $\kappa_{K_0} = 0.009$ ($s = 93$ kPa) with higher values than in isotropic tests. In ideal isotropic elastic media, the shear component has no effect on volume changes and κ_{K_0} should be equal to κ values (a reasonable hypothesis in modelling). However, since elastic and plastic deformation are not separated in natural soils (as seen in particular here on the compression curves of saturated samples), it is probable that the phenomenon described above also intervenes at small strains;
- Given the changes in plastic volume changes observed under K_0 conditions, the dependency of collapse strains with respect to the stress applied is somewhat different when compared to isotropic collapse, again enhancing the important effect of the shear component acting in K_0 conditions (a situation in which most experimental collapse investigation are made). As observed in Figure 6, the magnitude of collapse also increases

when the sample is dried from $w = 14.2\%$ to 10% for the K_0 conditions. The observed values of maximum collapse are equal to $\varepsilon_v = 4.1\%$ and $\varepsilon_v = 7.7\%$ respectively and take place under mean net stresses of 68 kPa and 150 kPa respectively.

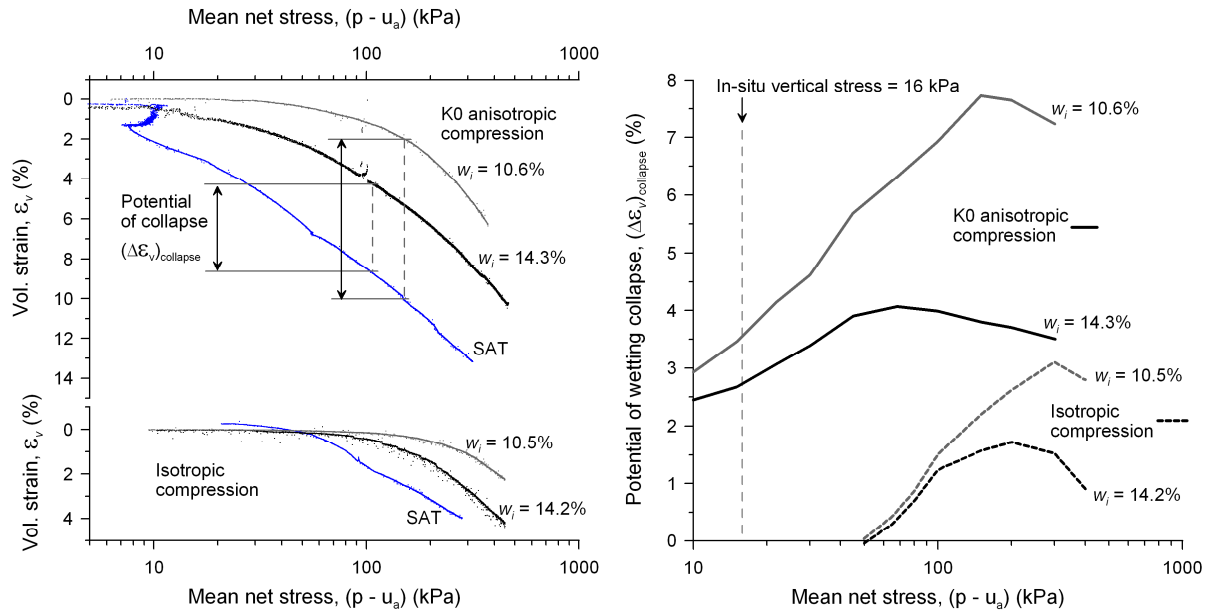


Figure 6. Potential of collapse due to wetting

Figure 5 also shows the suction variations with mean net stress ($p - u_a$) and axial strain ε_l during K_0 anisotropic compression tests. Suction slightly decreases from 44 kPa to 38 kPa during the post-yield range at initial state (test CK₀-14%). A suction decrease, from 107 kPa to 90 kPa , was also observed in test CK₀-10% during the pre-yield range ($p - u_a$ from 10 to 50 kPa). The observed water content variations are quite low ($\pm 0.5\%$ in test CK₀-SAT, $\pm 0.5\%$ in test CK₀-14% and $\pm 0.8\%$ in test CK₀-10%), compared to the water content sensor precision equal to $\pm 0.3\%$.

Drained Shear Triaxial Tests

The drained shear triaxial (CID) test programme conducted with a constant confining pressure of 8 kPa is summarized in Table 3 and results of the tests S-14 (initial state), S-SAT (saturated) and S-10% (dried at 10%) are given in Figure 7. Soaking was performed under constant in-situ stress ($\sigma_l - u_a = 16.4 \text{ kPa}$, $\sigma_3 - u_a = 8.3 \text{ kPa}$) resulting in a high axial strain ($\varepsilon_a = 1.3\%$) and a $(\Delta\varepsilon_v) = 1.3\%$ collapse contraction that completely released the deviatoric stress, evidencing gain the important effect of shear on collapse volume changes.

Compared to the initial natural state, saturation significantly decreased the stiffness and resistance of the specimen whereas drying significantly strengthened it. In the tests at initial

water content (S-14%) and saturated state (S-SAT), failure occurred by bulging without apparent localized shear planes whereas a shear plane was observed on the dried sample (S-10%) at $w_0 = 10.6\%$ hence exhibiting a more fragile behaviour (see Figure 8). All volume change curves show continuous contraction.

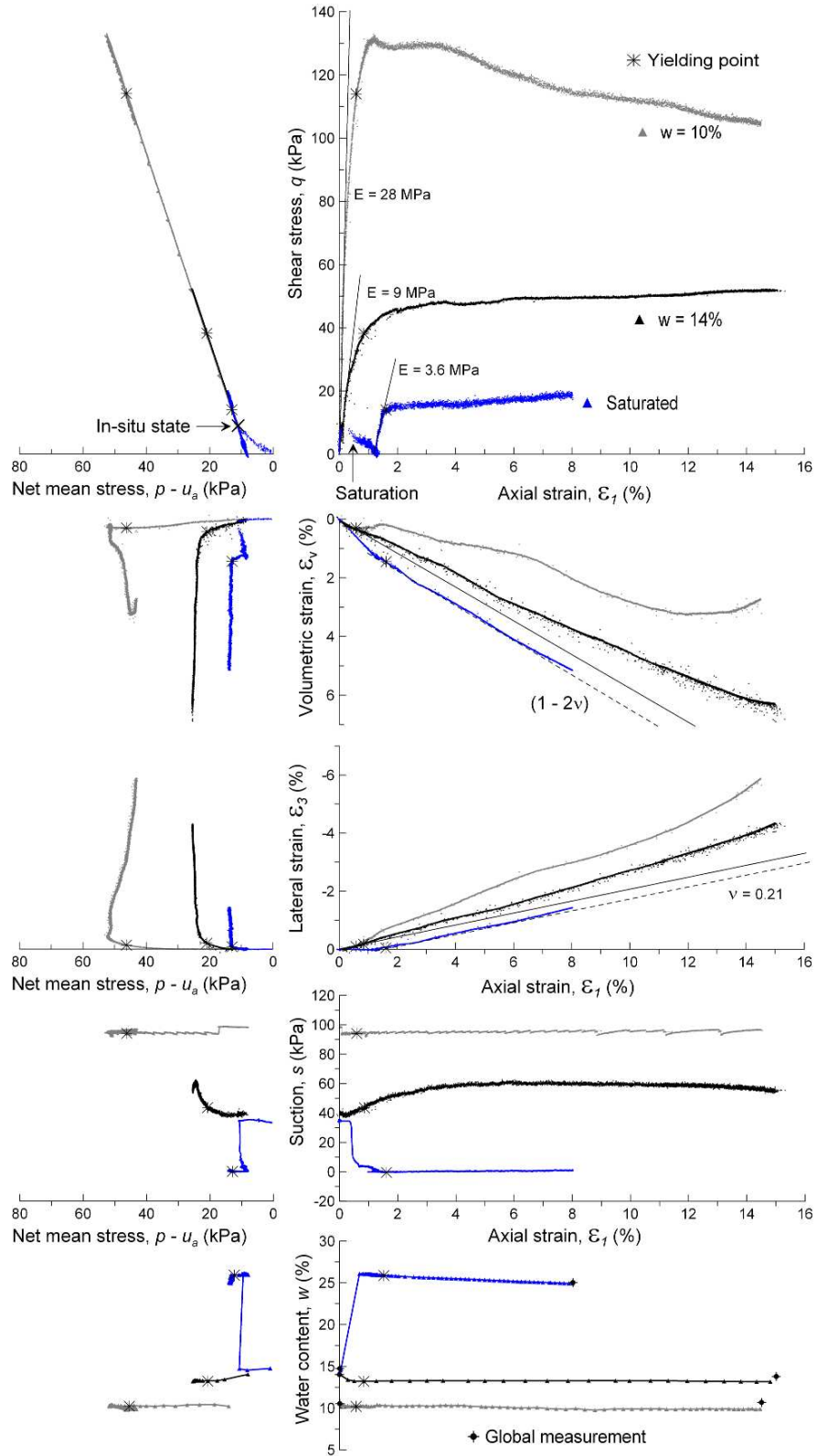


Figure 7. Shear triaxial test results on specimens at different initial water content values



Figure 8. Shear plane in the shear triaxial test at water content of 10.6%

In the drier sample, there is apparently a contraction-dilation transition phase in the volumetric response at small axial strains, prior to the onset of localisation. The development of dilatancy at higher suction has been observed on a compacted silt by Cui and Delage (1996) and discussed by Pereira *et al.* (2005). Contraction afterwards again occurs when ε_a becomes larger than 1.6%. Actually, both the volumetric and shear responses at larger axial strain rather reflect the behaviour of the two half-samples sliding along the shear plane and are no longer considered as being representative of a continuous sample.

In the samples at $w = 14.0$ and 25.9% (saturated) in which no failure plane was observed, there is no critical state attained in spite of having a fairly constant shear stress. In both cases, continuous shearing kept on contracting the specimen at a constant rate up to around 5%, again emphasising the effects of shear on sample contraction.

Elastic behaviour was observed after saturation in test S-SAT from $\varepsilon_a = 1.3\%$ to $\varepsilon_a = 1.5\%$, with a Young's modulus of 3.6 MPa and a yield stress $q_y = 13$ kPa at $\varepsilon_a = 1.6\%$. At initial state, (S-14%, $w = 14\%$, $s_0 = 39$ kPa), the stress – strain curve shows a pseudo-elastic behaviour up to an axial strain $\varepsilon_l = 0.7\%$ before yielding at $q_y = 38$ kPa. In the sample dried at 10% (S-10, $s_0 = 99$ kPa), yielding is observed at $q_y = 114$ kPa ($\varepsilon_a = 0.6\%$) before a peak in the stress – strain curve at $q = 132$ kPa ($\varepsilon_l = 1.2\%$). The Young's moduli E change in a typical manner, with a decrease from 9 ($w = 14\%$, $s = 39$ kPa) to 3.6 MPa upon saturation ($w = 26.3\%$) and an increase up to 28 MPa upon drying at 10% while the Poisson coefficients ν stays equal to 0.21 in all cases, independently of the suction changes.

At the saturated state, the $\varepsilon_v/\varepsilon_a$ curve is almost parallel to the line $(1 - 2\nu)$ corresponding to elastic behaviour.

The changes in suction with respect to both axial strain and mean net stress are also presented in Figure 7. At initial state (S-14%), after an initial decrease below 0.3%, suction increases from 38 kPa to 60 kPa between 0.3 and 6% to afterwards decrease to a final value of 52 kPa. Conversely, suction remains almost constant in the dried sample (S-10%). The local resistivity gauge confirms that water content is also almost constant during all tests. The constant response in suction in the dry sample is compatible with the results obtained in compression in samples compacted dry of Optimum (Li 1995, Gens *et al.* 1995, Romero 1999, Tarantino and De Col 2008). In dry compacted soils, compression is known to affect the arrangement of aggregates that are broken and brought together in a denser state, while suction, which is governed by intra-aggregates phenomena, is not affected and remains constant inside the aggregates. In the case of the Bapaume loess, as shown by Muñoz-Castelblanco *et al.* (2011b), the distribution of the clay fraction within the loess granular skeleton is not homogeneous, with, at low water contents, some areas of clean and dry grains and other areas where clay aggregations are surrounding and enveloping the grains. It is thought that in drier conditions, the macroscopic response is more governed by the response of the dry inter-grains skeleton with little effect on the drier and stiffer clay fraction. Note however that this interpretation only holds before strain localisation ($\varepsilon_a < 1.5\%$). It is not surprising, at higher axial strain, that the relative movements of the two half specimens along the shear plane has no effect on suction.

Effects of moisture changes on the mechanical behaviour

Yielding behaviour

The yield points from all the tests are plotted together in the $q/(p - u_a)$ plane together with the extrapolated yield loci at constant suctions (exact measured values indicated at each point) and the plastic strains directions in Figure 9. All yield loci have an ellipsoidal shape similar to a modified Cam-Clay type one with the K_0 line crossing it close to the ellipse apex. The symmetry of the yield curve along the $p - u_a$ axis evidences a structural isotropy. Yield points from isotropic tests are located in the $(p - u_a, s)$ plane and define the LC curve whereas those from K_0 tests are positioned with a K_0 inclination while those from constant σ_3 shear tests are located along the $(p = q/3 + \sigma_3)$ lines at each suction. Two additional yields points were

plotted, corresponding to a p_{net} -constant path and a q constant path, both started from the in-situ stress state and performed at the natural hydric state ($w = 14.4\%$, $s = 44 \text{ kPa}$).

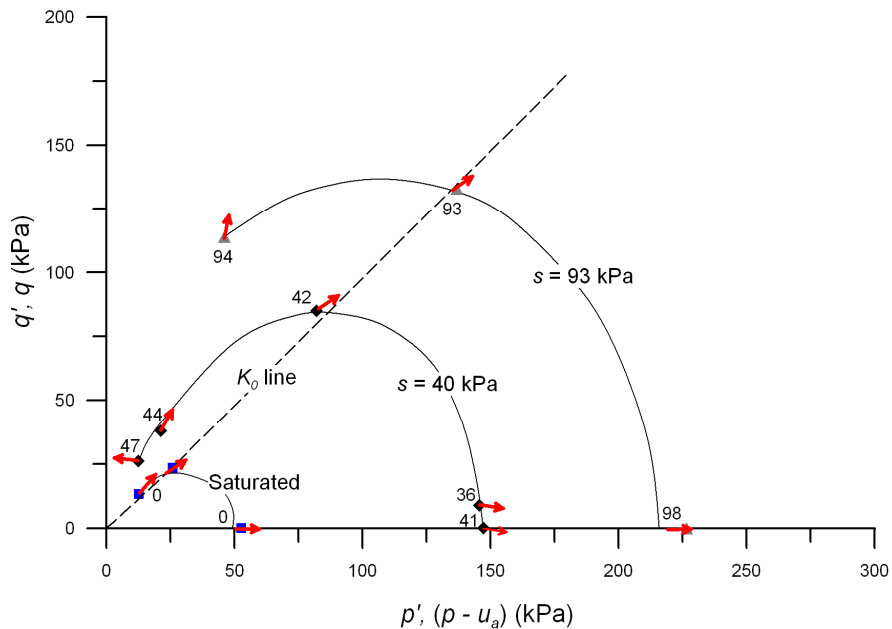


Figure 9. Experimental determination of yield curves at different suctions. Experimental suction values at yield in kPa are indicated on the side of each yield-data point

The changes in mean yield net stress $(p - u_a)_y$ with respect to suction and deviatoric stress q are shown in Figure 10 for each test in a 3D diagram $(q, p - u_a, u_a - u_w)$. The evolution of the yield mean net stress with suction for the isotropic tests has the standard convex shape of the loading collapse (LC) yield curve of the Barcelona Basic Model (BBM, Alonso *et al.* 1987, 1990). The 3D presentation allows an extension of the LC curve in the $q, (p - u_a), (u_a - u_w)$ space of the yield points obtained at the K_0 compression and the shear triaxial tests. The projections of these yield points on the $(p - u_a, s)$ plane show a convex shape of the projected K_0 yield curve, whereas a concave shape is observed for the shear yield points that evidences the effect of the deviatoric stress.

The modified Cam-Clay type yield locus of Figure 9 is symmetrical with respect to the $p - u_a$ axis and differs from the inclined ones obtained on unsaturated anisotropically (statically) compacted soils by Cui and Delage (1996) on a silt of the same aeolian origin and by Jotisankasa *et al.* (2009) on an unsaturated compacted silty clay. It is comparable to the yield locus of an isotropically compacted clay presented in Wheeler and Karube (1996) and to that of a natural unsaturated residual degrade sandstone by Machado and Vilar (2003). Rock degradation hence appears to be an isotropic process that does not induce any anisotropy.

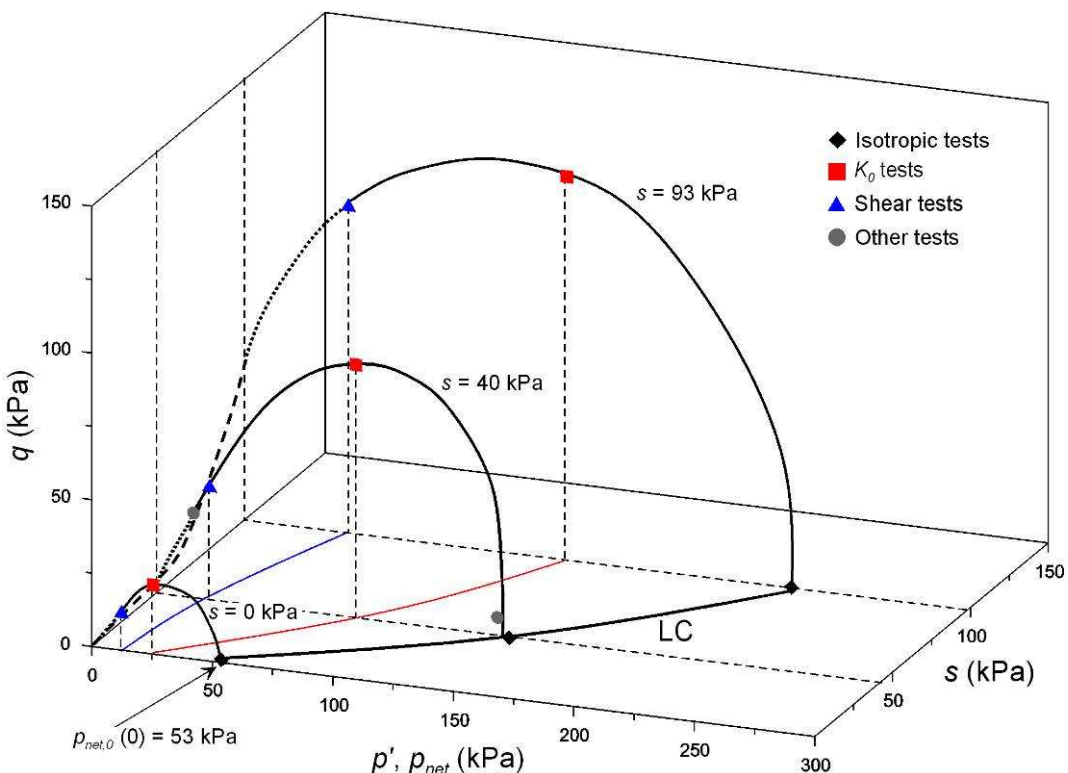


Figure 10. Evolution of yield mean net stress with suction and deviatoric stress

The isotropy observed in Figure 9, that is scarcely observed in intact natural soils, is thought to be due to the fact that loess is not a sedimentary deposit comparable to sands or clays sedimented in marine or lacustrine environments: loess has been transported and deposited by wind, not in a vertical direction that could favour sub-horizontal inter-grains contact and with no significant overburden supported after deposition (actually, a transverse isotropy could be suspected along a plane perpendicular to the wind direction - West-North West in the case of Northern France - but its identification would require a precise orientation of the extracted block). Also, the subsequent recrystallisation of calcite as a bonding agent is likely to be an isotropic process not influenced neither by gravity nor by the wind direction.

Except during isotropic compression, plastic strains are not perpendicular to the yield curve evidencing a non associated plastic flow that seems to generally have the same direction as the stress inclination. The expansion of the yield surface with increased suction illustrates the “suction-hardening” effect proposed by Alonso *et al.* (1990) and also observed on some natural soils (e.g. Machado and Vilar 2003, in a residual soil from Brazil).

In Figure 7, the brittle response observed in the stress-strain curve at suction 93 kPa (constant $\sigma_3 = 8$ kPa) can be related to an increase in the apparent “cohesion” related to the intersection of the yield locus with the q -axis (Figure 9). The shape of the yield loci shows that a smaller

cohesion would be obtained at natural state ($s = 40$ kPa) whereas it seems that no (or a quite small) cohesion would be observed at saturated state

Loess compressibility

The “compressibility parameter” $\lambda_{K_0}(s)$ obtained from the K_0 anisotropic compression tests in the post-yield range increases with suction whereas the isotropic compressibility parameter $\lambda(s)$ is higher at natural state ($w = 14\%$) compared to both the saturated and the drier states ($w = 10\%$) (Figure 11). According to Matyas and Radhakrishna (1968), Abelev and Abelev (1979), Alonso *et al.* (1987), Wheeler and Sivakumar (1995), Cui and Delage (1996) (among others) suction stiffens the soil. in agreement with the observed decrease of $\lambda(s)$ between 40 kPa and 93 kPa and in disagreement with, on the one hand, the increase in $\lambda(s)$ between the saturated and the natural ($s = 40$ kPa) states and, on the other hand, with the compressibility increase with suction in the K_0 compression tests.

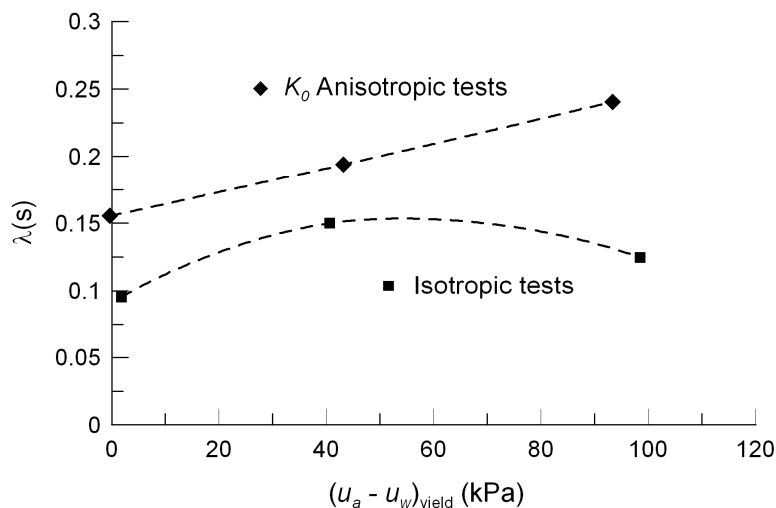


Figure 11. Variation of $\lambda(s)$ and $\lambda_{K_0}(s)$ with suction in isotropic and K_0 anisotropic compression tests

In the data obtained by Jennings and Burland (1962) on air-dried soils, the slope of the compression lines is more or less constant whereas it increases with suction in the data by Sivakumar and Wheeler (2000) on compacted soils. This feature, that was associated to collapse susceptibility by Maâtouk *et al.* (1995), is indeed observed here in the Bapaume loess, in relation with a loose and metastable structure (Cui *et al.* 2004, Delage *et al.* 2005, Yang *et al.* 2008, Karam *et al.* 2009, Muñoz-Castelblanco *et al.* 2011a,b).

Collapse behaviour

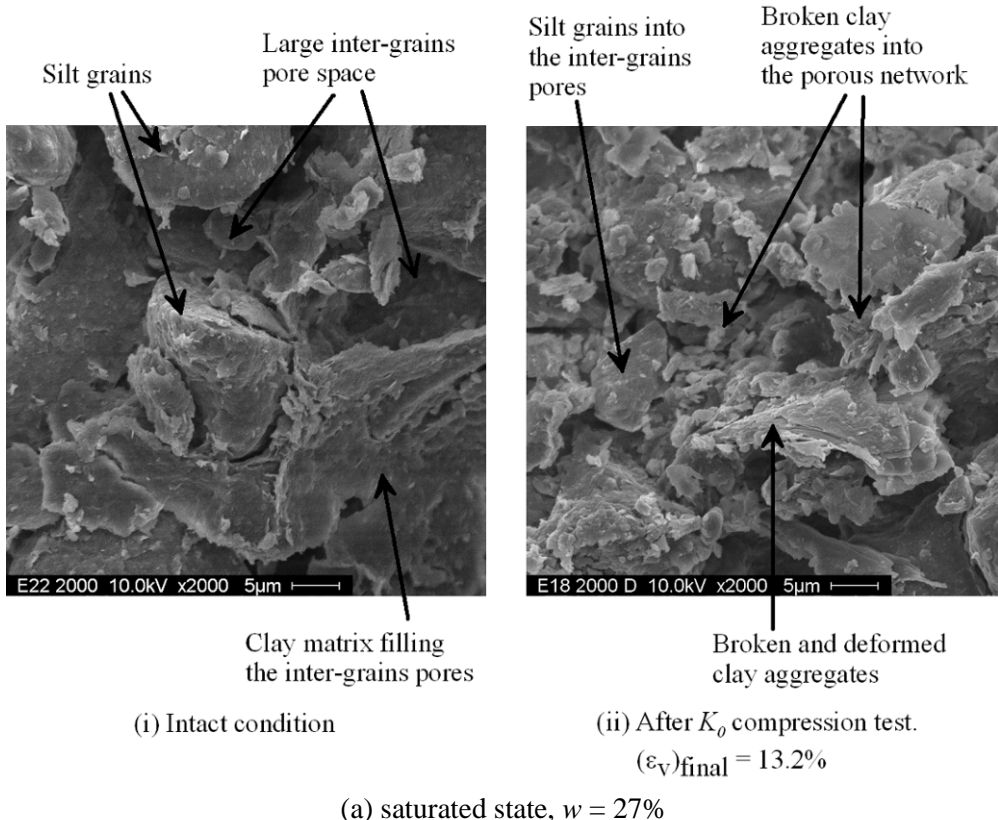
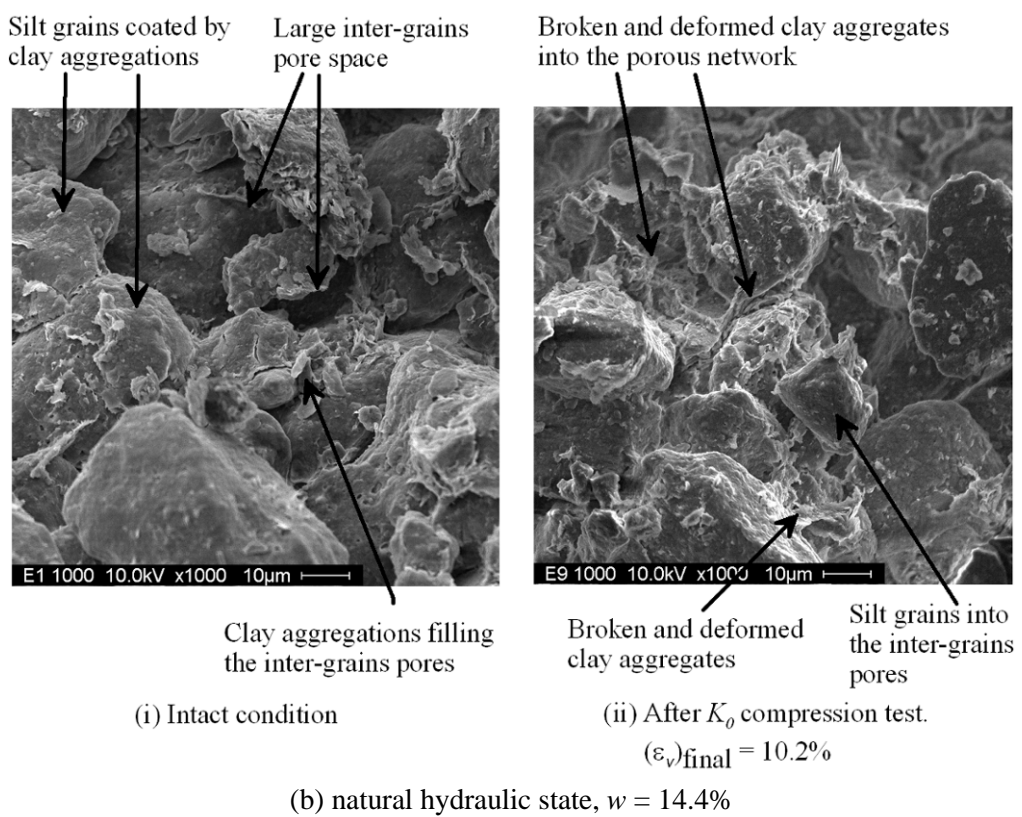
A collapse upon wetting under in-situ stress state was observed in the K_0 tests (Figure 2). Compression at the constant natural water content ($w = 14.4\%$, $S_r = 0.46$) affects a loose and dry assembly of silt grains bonded together by either hydrated clay aggregations links or recrystallised carbonate bonds (Pecsi 1991, Muñoz-Castelblanco *et al.* 2011b), that are sensitive to changes in water content, given that both the compressibility and the amplitude of collapse change with water content. In the same loess deposit, double oedometer tests carried out on intact unsaturated loess samples at different initial suctions (Cui *et al.* 2004, Delage *et al.* 2005) and more recent microstructure investigations (Muñoz-Castelblanco *et al.* 2011b) showed that collapse at $w = 14.4\%$ occurred in some large dry pores between clean grains.

Extrapolating the concepts of the Sensitivity framework (Cotecchia and Chandler 2000, Baudet and Stallebrass 2004) to unsaturated soils, the progressive convergence of the constant water content compression curve towards the saturated one observed in the K_0 compression tests (Figure 3), corresponds to the progressive structure degradation by the mechanical collapse of the largest pores. As commented before, a more complete structure degradation is achieved by soaking under constant stress with the curve joining the saturated one. Figure 3 would be fruitfully completed by the compression curve of a reconstituted loess but the first experimental attempts in this direction were not successful. The respective position of the saturated and reconstituted curves would certainly be an interesting complementary information with respect to structure considerations.

Role of microstructure in the mechanical behaviour

According to the microstructure analysis performed by Muñoz-Castelblanco *et al.* (2011b), the Bapaume loess is characterized by a loose assembly of silt grains of mean size 30 μm with an heterogeneous scattering of the clay fraction (clay aggregations composed of kaolinite and smectite-illite) among the grains skeleton and at the inter-grains contact. In Figure 12, SEM observations of the loess microstructure before and after the K_0 triaxial test are presented. Observations were performed at three hydric states, i.e. close to saturation ($w = 27\%$), at natural state ($w = 14.4\%$) and in the drier state ($w = 10\%$). In Figure 12a, the microstructure (i) of the saturated specimen ($w = 27\%$) shows an open arrangement of silt grains with large inter-grains pores filled by hydrated and swollen clay aggregations. The K_0 compressed microstructure at a maximum mean net stress of 313 kPa (ii) presents a denser arrangement of

silt grains with deformed and broken clay aggregations into smaller inter-grains pores. In this case, mechanical loading causes a decrease of the pore sizes and the plastic deformation of clay aggregates that are very probably saturated.

(a) saturated state, $w = 27\%$ (b) natural hydraulic state, $w = 14.4\%$

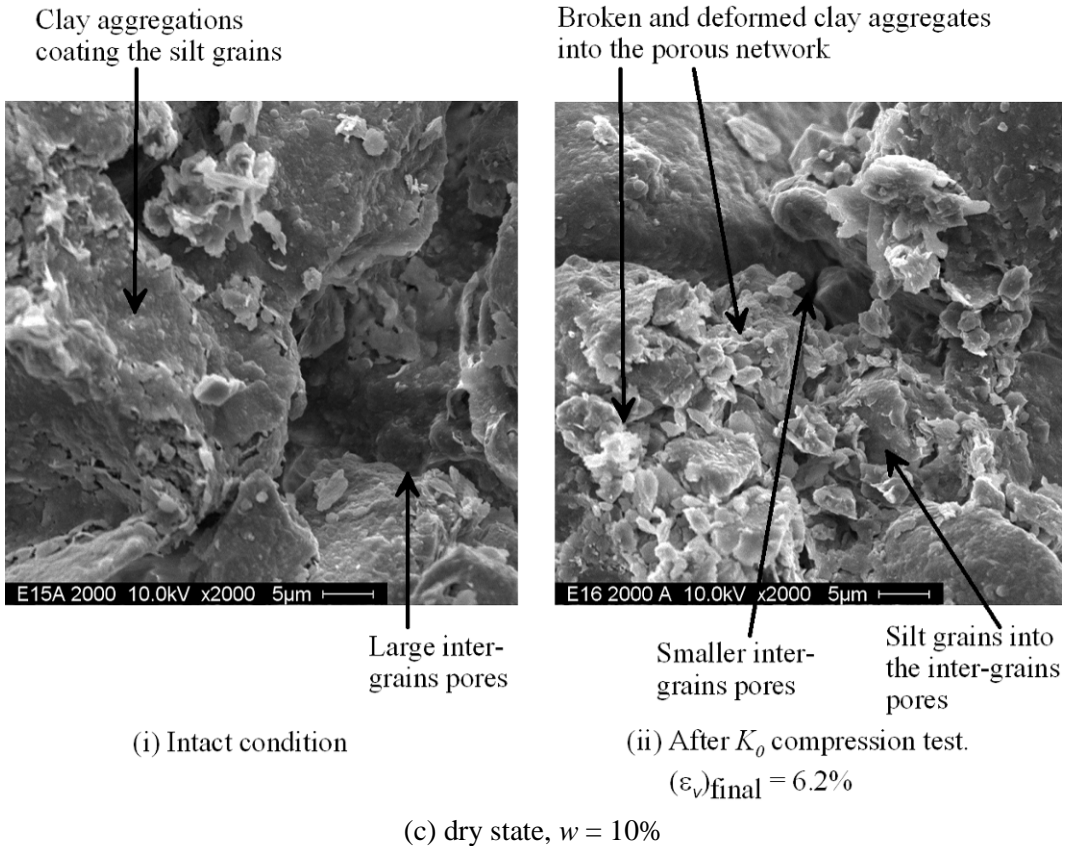


Figure 12. SEM observations in the loess microstructure before and after loading

At the natural water content ($w = 14.4\%$), the K_0 compression generates a denser organization of silt grains with deformed clay aggregations filling the inter-grains pores (Figure 12b). In this condition, clay aggregations, assumed to initially be and remain saturated (which appears to be a reasonable hypothesis at a 40 kPa suction in aggregates made up of kaolinite and stratified illite-smectite minerals), seem to have been plastically deformed. At the drier state ($w = 10\%$), the intact microstructure (i) in Figure 12c is composed by an open arrangement of silt grains coated by shrunk clay aggregates with a jagged aspect typical of dry clays (Delage *et al.* 1996). Compression induces the breaking of clay aggregations and a reduction of the pore size (Figure 12c (ii)).

The mechanical behaviour during the drained triaxial shear tests performed at constant confining mean net stress $p - u_a = 8$ kPa (starting from the in-situ stress state, Figure 7) is now analyzed with reference to microstructure changes. At saturated state, in which the stress – strain curve (Figure 7) shows a ductile behaviour, both the intergranular pores and the clay aggregations (Figure 12a) are saturated, resulting in a loose structure where only the effects of friction between particles and particles organization seem to control the mechanical response. At natural state ($w = 14.4\%$, $s = 40$ kPa, $S_r = 0.46$), the stress – strain curve (Figure 7) also

presents a ductile behaviour with a higher Young modulus (9 MPa compared to 3.6 MPa in the saturated state). In this case, only the clay aggregations are saturated (according to the combined analysis of microstructure and water retention properties of loess, see Munoz-Castelblanco *et al.* 2011b) leading to a metastable structure; the silt grains can mutually slide one along another during shearing.

Impact of loading on microstructure and on water retention properties

In Figure 13, the relationship between matrix suction and the water ratio e_w (comparable to the degree of saturation) along the main wetting and drying paths have been plotted at two different void ratios. The water ratio e_w ($e_w = V_w / V_s$ in which V_w is the volume of water and V_s the volume of solids, with $-\delta e_w = -G_s \delta w$ in which G_s is the specific mass of solid grains) has been selected as the volumetric state variable associated with matrix suction, based on the definition of stress and work conjugate strain variables in unsaturated soils (Edgar 1993, Wheeler and Sivakumar 1995, Housby 1997, Dangla *et al.* 1997, Romero and Vaunat 2000). In the same way, the volumetric state variable void ratio $-\delta e$ is associated with the stress variable. Suction values are also plotted in function of the degree of saturation in order to normalize the water retention response at both void ratios.

Further insight into the effects of the loading paths followed on the water retention behaviour of the loess can be done by plotting the suction and water content measurements obtained during the tests in a water retention diagram (suction changes with respect to changes in water ratio / degree of saturation), as shown in Figure 13 for the isotropic compression tests. To complete the analysis, a water retention curve obtained on the same loess at a void ratio of 0.65 by means of the techniques presented in Munoz-Castelblanco (2011b) has also been plotted.

In test CI-SAT, the path corresponding to the wetting process under an isotropic load of 20 kPa goes from the natural state $e_w = 0.38$ ($w = 14.2\%$, $s = 35$ kPa) to a water ratio close to 0.7 ($w = 25.6\%$, $s = 0.4$ kPa) with a swelling volumetric strain of -0.25% ($\Delta e = -0.0023$). At the end of the isotropic loading path up to 283 kPa, the water ratio decreased down to $e_w = 0.63$ ($w = 24.0\%$, $s = 1$ kPa), corresponding to a final void ratio of 0.77. At natural state ($e_w = 0.38$, $w = 14.2\%$), water ratio is almost constant during isotropic loading with only a small decrease in suction. At the dried state ($e_w = 0.27$, $w = 10.5\%$, $s = 101$ kPa), suction is almost constant

during loading with some small variations in water content that could be possibly be due to some noise in the electrical signal given by the resistivity probe.

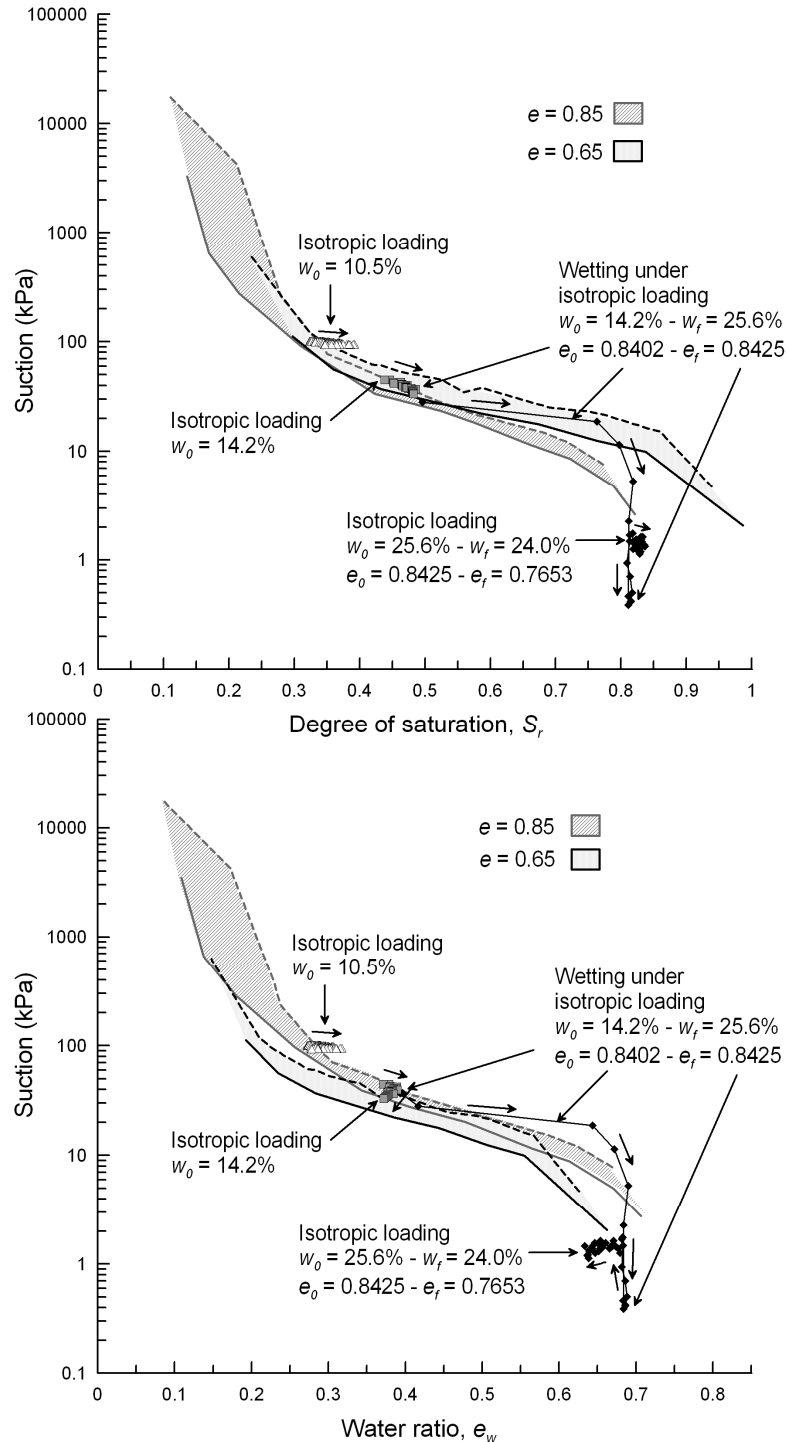


Figure 13. Hydraulic paths during the isotropic compression triaxial tests

In Figure 14, the hydraulic paths obtained during the K_0 anisotropic compression tests are presented. In test CK₀-SAT, wetting under in-situ K_0 conditions ($\sigma_v - u_a = 17$ kPa, $\sigma_h - u_a = 8$ kPa) induced a collapse of about 1.6% ($\Delta e = 0.03$) and water ratio afterwards decreased to $e_w = 0.62$ ($w = 22.9\%$) at the end of loading with a degree of saturation close to 1. At the final

point ($e_f = 0.60$), the representative point goes below the water retention curve at $e = 0.85$ to reach a point located on the water retention curve of a denser specimen at $e_0 = 0.65$). For the natural ($w_0 = 14.2\%$) and the dry ($w_0 = 10.5\%$) states, the hydric paths also tend to reach the low porosity retention curve with a reduction in the suction at the end of loading. The final void ratios are $e_f = 0.64$ for loading at the natural state ($w_0 = 14.2\%$), and $e_f = 0.72$ for loading at the dry state ($w_0 = 10.5\%$).

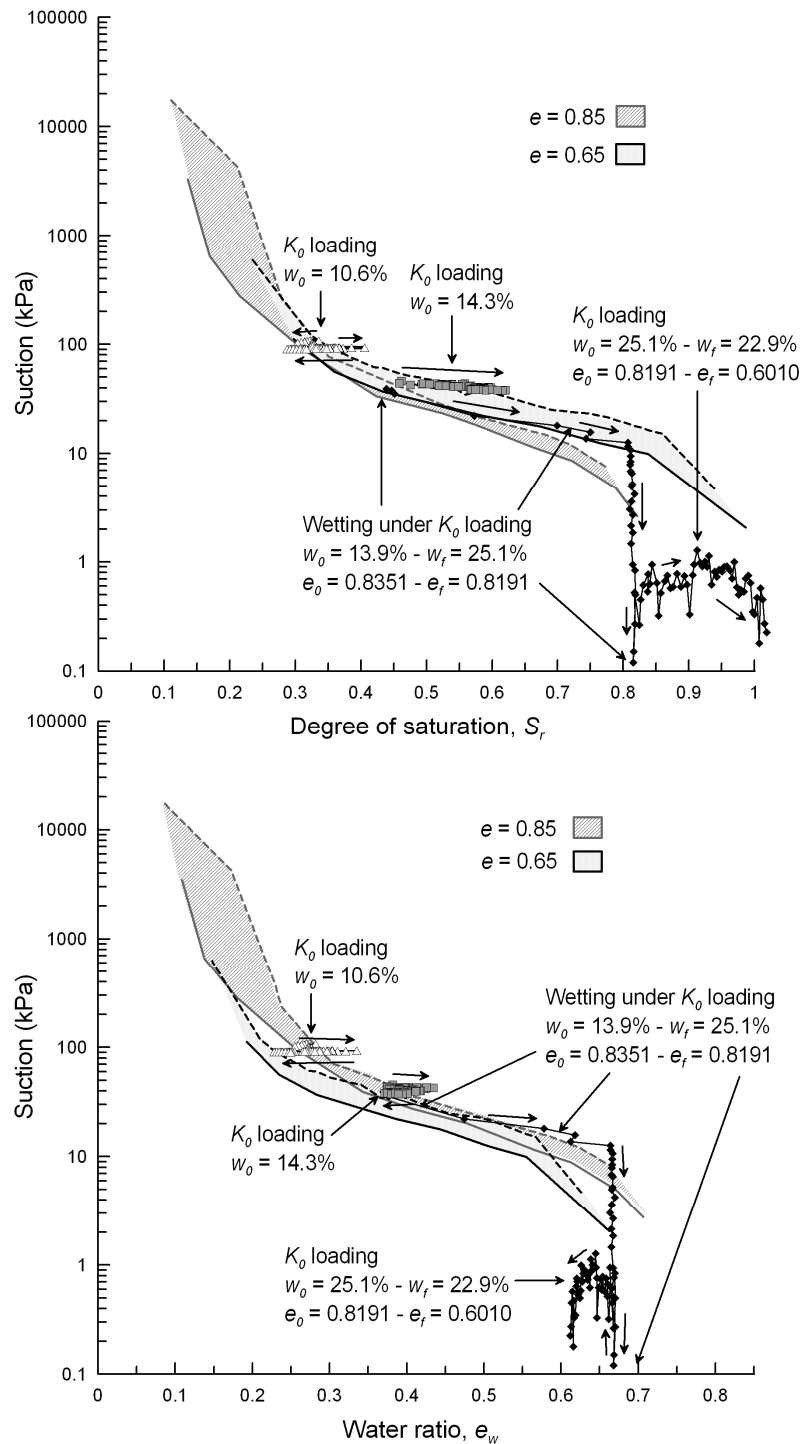


Figure 14. Hydraulic paths during the K_0 anisotropic compression triaxial tests

Finally, in Figure 15, the hydraulic paths obtained during the triaxial shear tests are plotted. Water ratio values are almost constant during loading.

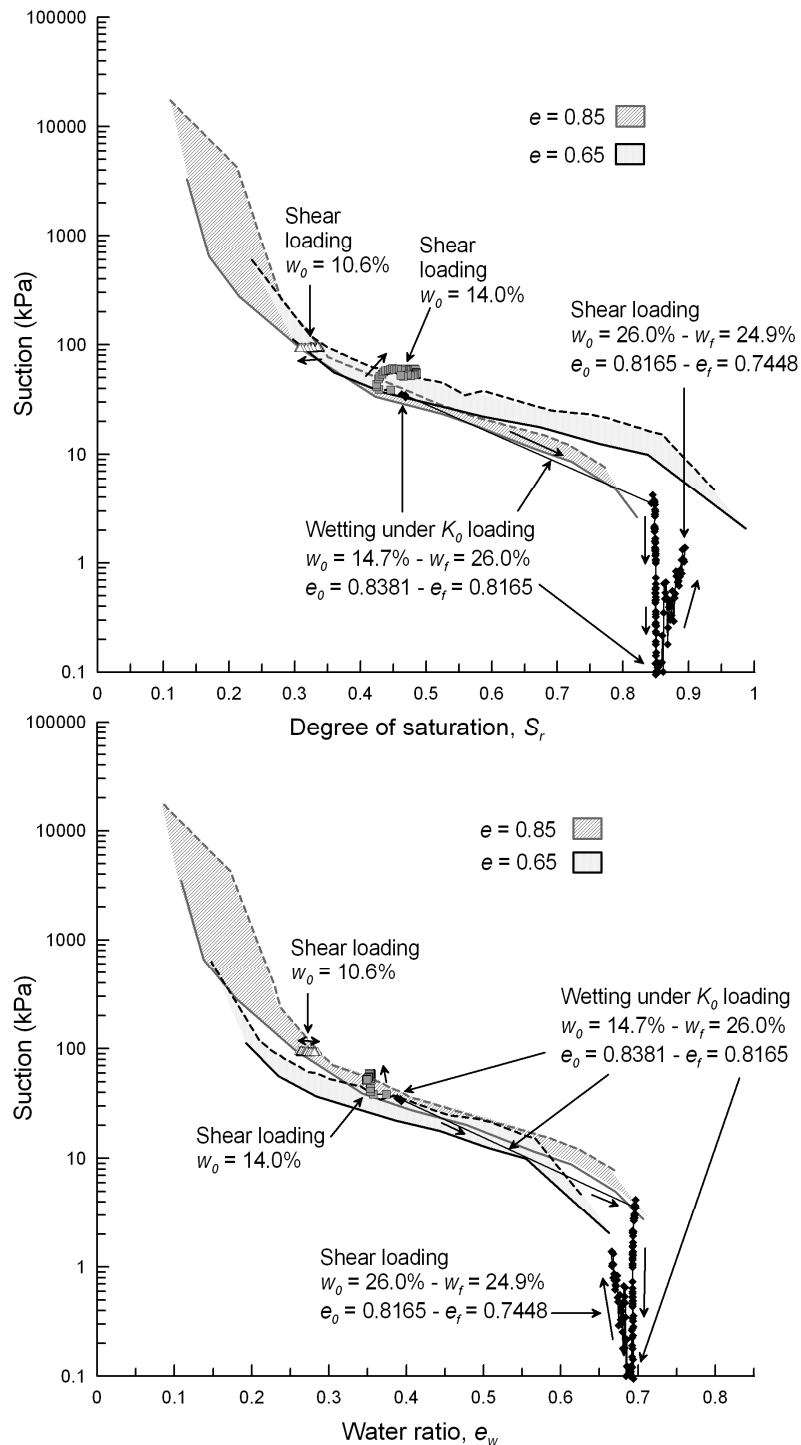


Figure 15. Hydraulic paths during the shear triaxial tests

Suction increases during triaxial shearing at the natural hydraulic state ($w_0 = 14.0\%$) while the sample contracts ($\varepsilon_v = 4.4\%$). A similar behaviour was observed by Colmenares and Ridley (2002) in unconfined compression tests on reconstituted artificial clayey silt samples. They obtained an increase in suction in test S-4 ($S_r = 97.1\%$, $s_0 = 26$ kPa) of about $s/s_0 = 1.6$,

comparable to the suction increase observed here during triaxial shearing at natural state ($w_0 = 14.0\%$, $S_r = 46\%$, $s_0 = 40$ kPa), equal to $s/s_0 = 1.5$. It seems necessary to invoke strong deviatoric effects in the reorganisation of the inter-grains menisci network to interpret this unexpected increase in suction while the sample contracts at constant water content (giving rise to an increase in the degree of saturation).

Conclusions

A new triaxial apparatus with complete local monitoring of the state variables of an unsaturated soil (strains, suction and water content) was used to carry out an experimental program on an unsaturated natural collapsible loess from Northern France. The effects of moisture changes on the mechanical behaviour was analyzed through isotropic and K_0 compression tests together with shear tests at three water contents. The compressibility index from K_0 compression tests tended to increase with increased suction, contrary to the standard suction stiffening effect of unsaturated soils captured in the BBM model. Conversely, yield stresses were observed to increase with suction, while the compression curves tended to converge towards the saturated compression curve at high stresses, a feature to relate to the progressive degradation of the loess's unsaturated structure during compression.

The loess exhibited an isotropic behaviour illustrated by the symmetrical shape of the yield curves that appeared to be reasonably comparable to that of the modified Cam-clay model with non associated plastic flow. Suction induced an expansion of the yield surface related to the suction-hardening effect. Suction also leads to increasing dilatancy, associated to the suction hardening of the clay bonding between silt grains, which confers to the soil a brittle behaviour at low water content states and a failure along a distinct shear plane.

Collapse upon wetting was identified when the loess specimen was soaked under a K_0 anisotropic stress state close to the in-situ stress condition. Wetting under an isotropic stress close to the in-situ horizontal stress (8 kPa) leads to a smooth swelling of the specimen.

The microstructure of the Bapaume loess changes with moisture changes, affecting its mechanic response. This soil is composed by an arrangement of silt grains with some inter-grains pores filled by heterogeneously distributed clay aggregates. Trapped macropores are also observed in the SEM observations. At dry conditions, clay aggregates tend to shrink due leading to an increase in soil stiffness due to suction hardening. At the natural hydric state, the

combined analysis of the water retention properties and microstructure shows that clay aggregations tend to remain almost saturated whereas inter-grains pores are still unsaturated. This leads to a ductile behaviour related to the low resistance to loading of the saturated clay aggregates between the silt grains. At states close to saturation both the clay aggregations and the inter-grains pores are water-filled resulting in a ductile behaviour.

Mechanical loading has an impact on the water retention properties of the loess. The presence of clay aggregations, with some potential of swelling-shrinkage into some of the inter-grains pores is one of the reasons of the hysteretic response of the intact loess, especially at low water contents. Microscopic observations at natural water content shows that a K_0 compression loading induces the plastic deformation and breaking of the clay aggregations, leading to a reduction of the swelling – shrinking potential of clay aggregations and to a decrease of the hysteretic potential of clay aggregates at low water contents. The collapse of the large pores is also clearly visible at high water contents.

Further analysis of the hydromechanical couplings on the loess can be oriented to develop the constitutive modeling of its structure-dependent behaviour. It should take into account the key role of the swelling – shrinkage potential of the clay aggregates filling part of the pore network of an open and metastable arrangement of silt grains. Features as the non-standard compressibility behaviour, the collapse sensibility and the microstructure evolution with moisture changes should be also further analyzed.

Acknowledgments

The present study is part of the first author PhD work. It was supported by a grant provided by the European Alþan Program of high level scholarships for Latin America (scholarship N° E07D402297CO) completed by a financial support of the French Railways Company SNCF. Both organisations are gratefully acknowledged.

References

- Abelev Y.M. and Abelev M.Y. (1979). Bases de l'élaboration des projets et de la construction sur les sols loessiques affaissables. Translated from Russian into French by J.P. Magnan (1986). Paris: Lavoisier, Tech. et Doc.
- Alonso E., Gens A. et Hight D.W. (1987). Special problem soils. *General Report. 9th European Conference on Soil Mechanics*, Dublin, vol. 3.
- Alonso E., Gens A. and Josa, A. (1990). A constitutive model for partially saturated soils. *Géotechnique* 40 (3). 405-430.
- Antoine P. (2002). Les loess en France et dans le Nord-Ouest européen. *Revue Française de Géotechnique* 99. 3-21.

- Antoine P., Catt J. and Somm   J. (2003). The Loess and Coversands of Northern France and Southern England. *Journal of Quaternary Science* 18. 309-318.

Barbour S.L. (1998) Ninetheenth Canadian geotechnical Colloquium: The soil-water characteristics curve – A historical perspective. *Can. Geotech. J.* 35. 873-894. Baudet B. and Stallebrass S. (2004). A constitutive model for structured clays. *G  otechnique* 54 (4). 269–278.

Barden L., Mc Gown A. et Collins K. (1973). The collapse mechanism in partly saturated soil. *Eng. Geol.* 7. 49-60.

Baudet B. and Stallebrass S. (2004). A constitutive model for structured clays. *G  otechnique* 54 (4). 269–278.

Burland J.B. (1956). Some aspects of the mechanical behaviour of partly saturated soils. In: *Moisture Equilibria and Moisture Changes in Soils Beneath Covered Areas, A Symposium in Print* (Aitchison, G.D. Ed), 270-278, Sidney, Australia, Butterworths..

Chiu C.F., Cui Y.J., Haza E., De Laure E., Favraud C. and Th  riot N. (2002). Experimental study of pollutant transport in an unsaturated compacted silt on centrifuge: second test. *Ecole Nationale des Ponts et Chauss  es (Paris) – Laboratoire Centrale des Ponts et Chauss  es (Nantes)*. France.

Colmenares J.E. and Ridley A.M. (2002). Stress-strain and strength relationships for a reconstituted clayey silt. *Proceedings of the Third International Conference on Unsaturated Soils. Unsat 2002*, vol. 2. Juc   J.F.T., de Campos T.M.P. and Marinho F.A.M. (eds.), Balkema Publishers, The Netherlands. 481-484.

Cotecchia F. and Chandler R.J. (2000). A general framework for the mechanical behaviour of clays. *G  otechnique* 50 (4). 431-447.

Cui Y.J. and Delage P. (1996). Yielding and plastic behaviour of an unsaturated compacted silt. *Geotechnique* 46 (2). 291-311.

Cui Y.J., Delage P., Durand F., Schlosser F. et Wojnarowicz M. (1995). Comportement m  canique des loess sur le trac   du TGV Nord. *XI  me Conf  rence Europ  enne de M  canique des Sols et des Travaux de Fondations*, Copenhague, vol. 7. 45-50.

Cui Y.J. et Marcial D. (2003). Etude de comportement des limons non satur  s soumis aux vibrations ferroviaires (Lot1). *Rapport SNCF*. 47 pages.

Cui Y.J., Marcial M., Terpereau J.M., Delage P., Antoine P., Marchadier G. and Ye W.M. (2004). A geological and geotechnical characterisation of the loess of Northern France. *A.W. Skempton Memorial Conference*, vol. 1. 417-428.

Cui Y.J., Tang A., Mantho A. and De Laure E. (2008). Monitoring Field Soil Suction Using a Miniature Tensiometer. *Geotechnical Testing Journal* 31 (1). 95-100.

Cunningham M.R., Ridley A.M., Dineen K. and Burland J.B. (2003). The mechanical behaviour of a reconstituted unsaturated silty clay. *G  otechnique* 53 (2). 183-194.

Dangla P., Malinsky L. and Coussy O. (1997). Plasticity and imbibition-drainage curves for unsaturated soils: A unified approach. *Proc. 6th Int. Symp. on Numerical Models in Geomechanics*, Montreal, 141–146.

Delage P., Audiguier M., Cui Y.J. and Howat M.D. (1996). Microstructure of a compacted silt. *Can. Geotech. J.* 33. 150-158.

Delage P., Cui Y.J. and Antoine P. (2005). Geotechnical Problems related with Loess deposits in Northern France. *Proceedings of International Conference on Problematic Soils*. 517-540.

Dudley J.H. (1970). Review of collapsing soils. *J. Soil Mech. Fdn Engng, Am. Sot. Civ. Engrs* 96, SM3. 925-947.

- Edgar T.V. (1993). One and three dimensional, three phase deformation in soil. In *Unsaturated Soils, ASCE Geotechnical Special Publication No. 39*. 139–150.
- Gallipoli D., Gens A., Sharma R. and Vaunat J. (2003). An elasto-plastic model for unsaturated soil incorporating the effects of suction and degree of saturation on mechanical behaviour. *Géotechnique* 53 (1). 123-136.
- Gens A., Alonso E.E., Suriol J., and Lloret A. (1995). Effect of structure on the volumetric behavior of a compacted soil. In *Unsaturated Soils: Proc. 1st Int. Conf. on Unsaturated Soils / UNSAT 95*, Paris. 83-88.
- Hormdee D. (2008). Investigation on Collapse Potential of Loess Soil. *Proceedings of the 18th International Offshore and Polar Engineering Conference*, Vol. 2. Fontaine E., Uchida K., Chung J.S. et Moshagen H. (Eds.). 579-583.
- Houlsby G.T. (1997). The work input to an unsaturated granular material. *Géotechnique* 47 (1). 193–196.
- Jennings J.E. and Burland J.B. (1962). Limitations to the use of effective stress in partly saturated soils. *Géotechnique* 12 (2). 125-144.
- Jennings J.E. and Knight K. (1957). The additional settlement of foundation due to collapse of sandy soils on wetting. *Proc. 4th ICSMFE* 1. 316-319.
- Jommi C. (2000). Remarks on the constitutive modelling of unsaturated soils. In *Experimental Evidence and Theoretical Approaches in Unsaturated Soils*, (eds. Tarantino et Mancuso), Balkema, Rotterdam. 139-153.
- Jotisankasa A., Coop M. and Ridley A. (2009). The mechanical behaviour of an unsaturated compacted silty clay. *Géotechnique* 59 (5). 415-428
- Karam J.P. (2006). Etude de la rhéologie des loess du Nord de la France. Application à l'évaluation de leur risque de liquéfaction. PhD thesis. *École Nationale des Ponts et Chaussées*. Paris.
- Karam J.P., Cui Y.J., Tang A.M., Terpereau J.M. et Marchadier G. (2009). Experimental study on the cyclic resistance of a natural loess from Northern France. *Soils and Foundations* 49 (3). 421-429.
- Li Z.M. (1995). Compressibility and collapsibility of compacted unsaturated loessial soils. *Proc. 1st Int. Conf. Unsaturated soils UNSAT'95* 1. Balkema, Paris. 139-144.
- Maâtouk A., Leroueil S. and La Rochelle P. (1995). Yielding and critical state of a collapsible unsaturated silty soil. *Geotechnique* 45 (3). 465-477.
- Machado S.L. and Vilar O.M. (2003). Geotechnical characteristics of an unsaturated soil deposit at São Carlos - Brazil. In *Characterisation and engineering properties of natural soils* (ed. T.S. Tan, K.K. Phoon, D.W. Hight and S. Leroueil), vol. 2, Balkema, The Netherlands. 1305 – 1321.
- Manthro A. (2005). Echanges sol – atmosphère: application à la sécheresse. PhD thesis. *École Nationale des Ponts et Chaussées*. Paris.
- Matyas E.L. and Radhakrisna H.S. (1968). Volume change characteristics of partially saturated soils. *Géotechnique* 18 (4). 432-448.
- Muñoz-Castelblanco J., Delage P., Pereira J.M., and Cui Y.J. (2011a). Some aspects of the compression and collapse behaviour of an unsaturated natural loess. Submitted to *Géotechnique Letters*, decision in progress.
- Muñoz-Castelblanco J., Pereira J.M., Delage P. and Cui Y.J. (2011b). The water retention properties of a natural unsaturated loess from Northern France. *Géotechnique*, accepted for publication.

- Muñoz-Castelblanco J., Pereira J.M., Delage P. and Cui Y.J. (2011c). Measurement of the water content of a natural unsaturated loess by a new resistivity probe. Submitted to *Symposium on Innovations in Characterizing the Mechanical and Hydrological Properties of Unsaturated Soils*", *Geotechnical Testing Journal*, editorial evaluation.
- Pécsi M. (1990). Loess is not just the accumulation of dust. *Quaternary International* 7/8. 1-21.
- Pereira J.M., Wong H., Dubujet P. and Dangla P. (2005) Adaptation of existing behaviour models to unsaturated states: Application to CJS model. *Int. J. Numer. Anal. Meth. Geomech.* 29 (11). 1127-1155
- Punrattanasin P. (2008). The capacity of improved Khon Kaen Loess as a road construction material. *1st International Conference on Transportation Geotechnics*, Nottingham, England, Aug. 25-27, 2008. Publié dans: *Advances in Transportation Geotechnics*, Ellis E., Yu H.S., McDowell G. Dawson A. et Thom N. (eds.). 535-540.
- Romero E. (1999). Characterisation and thermo-hydro-mechanical behaviour of unsaturated Boom clay: an experimental study. PhD thesis. *Universitat Politècnica de Catalunya*. Barcelone.
- Romero E. and Vaunat J. (2000). Retention curves of deformable clays. In *Experimental Evidence and Theoretical Approaches in Unsaturated Soils*, (eds. Tarantino et Mancuso), Balkema, Rotterdam. 91-106.
- Sivakumar V. and Wheeler S.J. (2000). Influence of compaction procedure on the mechanical behaviour of an unsaturated compacted clay. Part 1: Wetting and isotropic compression. *Géotechnique* 50 (4). 359-368.
- Tarantino A. (2007). A possible critical state framework for unsaturated compacted soils. *Géotechnique* 57 (4). 385-389.
- Tarantino A. and De Col E. (2008). Compaction behaviour of clay. *Géotechnique* 58 (3). 199-213.
- Vaunat J., Romero E. et Jommi C. (2000). An elastoplastic hydro-mechanical model for unsaturated soils. In *Experimental Evidence and Theoretical Approaches in Unsaturated Soils*, (eds. Tarantino et Mancuso), Balkema, Rotterdam. 121-138.
- Wheeler S.J. (1996). Inclusion of specific water volume within an elastoplastic model for unsaturated soil. *Can. Geotech. J.* 33. 33-42.
- Wheeler S.J. et Karube B. (1996). Constitutive modelling. In *Unsaturated Soils*, A.A. Bakelma Rotterdam, number 3. Wheeler S.J. and Sivakumar V. (1992). Development and application of a critical state model for unsaturated soil. In *Predictive soil mechanics* (eds. G.T. Houlsby & N. Schofield), London: Thomas Telford. 709-728.
- Wheeler S.J. and Sivakumar V. (1995). An elasto-plastic critical framework for unsaturated soil. *Géotechnique* 45 (1). 35-53.
- Wheeler S.J., Sharma R. and Buisson M. (2003). Coupling of hydraulic hysteresis and stress-strain behaviour in unsaturated soils. *Géotechnique* 53 (1). 41-54.
- Yang C., Cui Y.J., Pereira J.M. and Huang M.S. (2008). A constitutive model for unsaturated cemented soils under cyclic loading. *Computers and Geotechnics* 35(6). 853-859.
- Yuan Z.X. et Wang L.M. (2009). Collapsibility and seismic settlement of loess. *Engineering Geology* 105 (1)-(2). 119-123.
- Yudhbir (1982). Collapsing behaviour of residual soils. Proc. *7th Southeast Asian Geotech. Conf., Hong-Kong* 1. 915-930.

Conclusion Générale

Ce travail, de caractère essentiellement expérimental, est consacré à l'étude du comportement hydro-mécanique d'un loess non saturé naturel intact provenant de la région de Bapaume (Nord de la France), en relation avec ses propriétés de rétention d'eau et sa microstructure. Il vise à combler le manque de données existant sur les sols non saturés naturels, sachant que la majorité des études publiées concerne des sols non saturés compactés ou reconstitués. Il s'inscrit dans le cadre de recherches développées au CERMES en relation avec la SNCF et RFF suite à des problèmes de tassement de terrain sous les fondations des voies ferrées dans des zones où le TGV traverse des dépôts de loess effondrable. Les investigations ont été menées sur des échantillons de bonne qualité prélevés manuellement sous forme de blocs dans une excavation proche de la ligne nord du TGV. Ce loess est naturellement non saturé du fait de la présence d'une couche végétale de surface reposant sur une couche argileuse presque imperméable, résultat des processus d'illuviation et de précipitation des carbonates.

Suite à une analyse bibliographique dédiée au comportement des sols non saturés et au phénomène d'effondrement, le travail a successivement abordé la caractérisation détaillée des propriétés de rétention d'eau en relation avec une analyse fine de la microstructure à l'aide de la porosimétrie au mercure et de la microscopie électronique à balayage et l'étude du comportement hydromécanique, principalement faite à l'aide d'un appareil triaxial permettant la caractérisation locale complète du matériau non saturé.

L'étude de la microstructure a montré que le loess est caractérisé par une structure poreuse constituée d'un squelette lâche de grain de diamètre moyen 30 microns (dont 70% de quartz) au sein duquel la fraction argileuse (15 – 18% : smectite, vermiculite, kaolinite avec une faible proportion d'illite et de chlorite) est inégalement répartie, dans des zones où les agrégations argileuses peuvent enrober plusieurs grains. Une porosité inter-grains bien classée représentant 65% de la porosité globale autour d'un diamètre moyen d'accès de 8 µm est identifiée en porosimétrie au mercure. Il existe une famille de pores de grande dimensions (entre 40 µm et 363 µm) toujours désaturés et insensibles aux changements de teneur en eau.

La courbe de rétention d'eau du loess de Bapaume, déterminée par l'usage conjoint du tensiomètre à haute capacité et de la méthode du papier filtre (dont l'utilisation avec un papier

filtre initialement humide selon une approche distincte de celle recommandée par l'ASTM a fait l'objet d'une étude détaillée), présente une forme particulière avec deux boucles d'hystérésis situées de part et d'autre d'une zone réversible autour de la teneur en eau naturelle. L'hypothèse que cette gamme de teneur en eau corresponde à la fluctuation saisonnière des teneurs en eau a été émise, elle demanderait bien sûr à être vérifiée par des mesures de teneur en eau in-situ. Les très faibles variations de volume engendrées par les changements de teneur en eau (à contrainte nulle) montrent que le squelette granulaire est stable et peu influencé par ces changements. Des identifications porosimétriques à plusieurs niveaux de teneur en eau ont permis de préciser davantage l'évolution de la microstructure avec les changements de teneur en eau. A la teneur en eau naturelle, la porosité intergranulaire est partiellement emplie d'eau, une grande partie des pores est à l'état sec et la courbe de rétention obéit aux lois de la capillarité. L'effet prédominant des interactions eau-argile sur la rétention d'eau se fait sentir quand la succion augmente, et on observe une diminution avec le séchage de la porosité accessible au mercure, montrant une forte rétraction locale des agrégations argileuses reliée à la proportion d'interstratifiés illite-smectites (qu'il est difficile de quantifier).

L'étude du comportement hydro-mécanique repose sur l'utilisation et le développement de plusieurs techniques expérimentales, qui comprennent l'utilisation, dans l'oedomètre et le triaxial, d'un tensiomètre de haute capacité développé au CERMES et capable de mesurer des succions entre 0 et 1 MPa. Un nouvel appareil triaxial permettant le suivi local, sur le tiers central d'éprouvettes de diamètre 50 mm et de hauteur 100 mm, de l'ensemble des variables qui caractérisent l'état d'un sol non saturé (déformation, teneur en eau et succion), a été développé. Les déformations axiale et radiale sont mesurées grâce à des capteurs à Effet Hall et les mesures locales de succion sont faites à l'aide d'un tensiomètre miniature de haute capacité (Chiu *et al.* 2002, Cui *et al.* 2008). Pour la mesure de teneur en eau, une sonde résistive a été développée. Les procédures d'étalonnage confirment la bonne précision de ces capteurs dont le temps d'équilibre dépend de l'état hydrique initial de l'échantillon. Le dispositif permet d'appliquer des trajectoires complexes de contrainte en asservissant la contrainte de confinement par d'autres mesures (force axiale, déplacements locaux, teneur en eau et succion). On peut obtenir notamment une trajectoire de compression anisotrope suivant la ligne K_0 (coefficient de pression latérale des terres au repos) en maintenant la déformation locale radiale nulle.

Une étude des propriétés d'effondrement conduite à l'oedomètre à l'aide d'essais à taux de déformation contrôlée a montré une dépendance en fonction du temps de la réponse volumique (oedométrique) du loess à teneur en eau constante, qui reste à préciser par des essais supplémentaires. L'étude confirme les éléments connus de l'effondrement des sols non saturés, avec en particulier la mise en évidence d'un maximum d'effondrement.

L'étude de la compressibilité à teneur en eau constante, menée au triaxial en conditions isotrope et K_0 sur des éprouvettes à teneur en eau naturelle ($w = 14\%$), séchées à 10% et saturées ($w = 27\%$), a montré la grande importance de la composante déviatorique en K_0 sur l'ampleur des déformations volumiques, en compression comme en remouillage (avec des valeurs de K_0 trouvées comprises entre 0,45 et 0,5). Les variations de succion sont ténues lors du cisaillement dans l'échantillon le plus sec, et elles semblent influencées, à la teneur en eau naturelle, par la composante déviatorique. On observe bien un écrouissage en succion caractérisé par la courbe LC du modèle BBM de Barcelone ; en revanche, les variations de compression en fonction de la succion ne sont pas régulièrement ordonnées comme dans le modèle, alors que celles du module d'Young le sont avec une plus grande rigidité et un comportement fragile contractant dilatant avec localisation des déformations à l'état le plus sec. Aux états naturel et saturé, le loess est continûment contractant sous une contrainte déviatorique croissante. Les surfaces de charge à plusieurs succions ont pu être déterminées dans l'espace ($q, p - u_a, s$). Leur forme symétrique par rapport à l'axe de la contrainte moyenne nette illustre un comportement isotrope relié au mode particulier de sédimentation de ces matériaux éoliens et à la recristallisation post-dépôt des minéraux calcaires primaires ; la loi d'écoulement est non associée.

Du fait des efforts consentis à l'acquisition de données expérimentales nouvelles à l'aide du dispositif original développé dans ce travail, il n'a pas été possible dans le temps imparti, de proposer un modèle élasto-plastique isotrope de comportement. La détermination d'expressions algébriques pour la surface de charge et le potentiel plastique est assez abordable, sur la base des nombreuses propositions actuellement publiées. Les changements non monotones de la compressibilité isotrope en fonction de la succion, avec l'existence du point d'effondrement maximum, ajouteraient cependant un certain degré de complexité. Le modèle élasto-plastique devrait alors permettre de retrouver l'effet de la composante déviatorique sur les variations volumique en conditions K_0 , ce qui n'est peut-être pas évident non plus. Les variations (ou non variations) observées de la teneur en eau lors de la compression ou du cisaillement ne seraient plus à prendre en compte uniquement en fonction

des variations volumiques, comme dans la plupart des modèles existants, mais également en fonction de la part déviatorique des contraintes.

Les nombreux traits de comportement hydromécanique originaux de ce loess effondrable naturel que cette étude a pu identifier ouvrent donc des perspectives de modélisation intéressantes.

Références

- Aitchison G.D. (1961). Relationship of moisture stress and effective stress functions in unsaturated soils. *Conf. Pore Pressures*, Butterworths, Lond. (1.2.3), (1.2.4).
- Aitchinson G.D. (1965a). Editeur scientifique. *Moisture equilibria and moisture changes in soils beneath covered areas. A Symposium in print, convened by Soil mechanics section, Commonwealth scientific and industrial research Organization, Australia.* 278 p. (1.2.1).
- Aitchinson G.D. (1965b). Panelist intervention. *Proc. 6th. ICSMFE 3*, Montreal. 318-321. (1.2.4).
- Aitchison G.D. et Donald I.B. (1956). Some preliminary studies of unsaturated soils. (b) Effective stresses in unsaturated soils. *Proc. 2nd Austr.-N. Zealand Conf. Soil Mech. Fdn Engng, Christchurch.* 192-199. (1.2.4), (1.2.5).
- Alonso E., Gens A. et Hight D.W. (1987). Special problem soils. *General Report. 9th European Conference on Soil Mechanics*, Dublin, vol. **3**. (1.2.1), (1.2.3), (1.2.4), (1.2.5), (1.2.6), (1.2.7), (1.2.8).
- Alonso E., Gens A. et Josa, A. (1990). A constitutive model for partially saturated soils. *Géotechnique* **40** (3). 405-430. (1.2.5), (1.2.7), (1.2.8), (4.1).
- Alonso E., Pereira J.M., Vaunat J. et Olivella S. (2010). A microstructurally based effective stress for unsaturated soils. *Géotechnique* **60** (12). 913-925. (1.2.5).
- Alonso E., Romero E., Hoffman C., Garcia-Escudero E. (2005). Expansive bentonite-sand mixtures in cyclic controlled-suction drying and wetting. *Eng. Geol.* **81** (3). 213-226. (1.2.8).
- Alonso E., Vaunat J. et Gens A. (1999). Modelling the mechanical behaviour of expansive clays. *Eng. Geol.* **54**. 173-183. (1.2.8).
- Al-Rawas A.A. et McGown A. (1999). Microstructure of omani expansive soils. *Canadian Geotechnical Journal* **36**. 272-290. (1.2.8).
- Ahmed S., Lovell C.W. et Diamond S. (1974). Pore sizes and strength of compacted clay. *Journal of the Geotechnical Engineering Division, ASCE*, **100** (GT4). 407-425. (1.2.6).
- Andersen B.J. et Borns H.W. (1997). The Ice age of World. *Scandinavian University Press*. Oslo. (1.3).
- Antoine P. (2002). Les loess en France et dans le Nord-Ouest européen. *Revue Française de Géotechnique* **99**. 3-21. (1.3), (1.3.1).
- Antoine P., Cattt. J. et Sommè J. (2003). The Loess and Coversands of Northern France and

- Southern England. *Journal of Quaternary Science* **18**. 309-318. (1.3.1).
- Archie G.E. (1942). The electrical resistivity log as an aid in determining some reservoir characteristics. *Trans. AM. Inst. Min. Metall. Pet. Eng.* **146**. 54-62. (3.2).
- ASTM International. (2003). Standard Test Method for Measurement of Soil Potential (Suction) Using Filter Paper, D 5298-03. ©ASTM International. (2.2).
- Audric T. (1973). Etude Géologique Et Géotechnique Des Limons De Plateau De La Région Parisienne. *Bulletin of Engineering Geology and the Environment* **8** (1). 49-59. (1.3.1).
- Aversa S. and Nicotera M.V. (2002). A Triaxial and Oedometer Apparatus for Testing Unsaturated Soils. *Geotechnical Testing Journal* **25** (1). 3-15. (3.1).
- Barrera M. (2002). Estudio experimental del comportamiento hidro-mecánico de suelos colapsables. PhD thesis. *Universitat Politècnica de Catalunya*. Barcelona. (3.1).
- Becze-Deack J., Langholt R. et Verrechia E.P. (1997). Small scale secondary CaCO₃ accumulations in selected sections of the European loess belt. Morphological forms, and potential for paleoenvironmental reconstruction. *Geoderma* **76**. 221-252. (1.3).
- Barbour S.L. (1998) Ninetheenth Canadian geotechnical Colloquium: The soil-water characteristics curve – A historical perspective. *Can. Geotech. J.* **35**. 873-894. (1.2.8), (4.1).
- Barden L., Madedor A.O. et Sides G.R. (1969). Volume change characteristics of unsaturated clays. *J. Soil Mech. Fdn Engng, Am. Sot. Civ. Engrs* **95**, SM1. 33-51. (1.2.5), (1.2.7), (1.4).
- Barden L., Mc Gown A. et Collins K. (1973). The collapse mechanism in partly saturated soil. *Eng. Geol.* **7**. 49-60. (1.4.1).
- Barrera M. (2002). Estudio experimental del comportamiento hidro-mecánico de suelos colapsables. *Thèse de doctorat, Universitat Politècnica de Catalunya*. Barcelone. (1.2.7).
- Bishop A.W. (1959). The principle of effective stress. *Teknisk Ukeblad*, N° **39**. 859-863. (1.2.3), (1.2.4).
- Bishop A.W., Alpan I., Blight G.E. et Donald I.B. (1960). Factors Controlling the Strength of Partly Saturated Cohesive Soils. *Proc. ASCE Research Conf. on Shear Strength of Cohesive Soils*, Boulder. 503-532. (1.2.4).
- Bishop A.W. et Blight G.E. (1963). Some aspects of effective stress in saturated and partly saturated soils. *Géotechnique* **13** (3). 177-197. (1.2.3), (1.2.4), (1.2.5).
- Bishop A.W. et Donald I.B. (1961). The experimental study of partly saturated soil in the triaxial apparatus. *Proc. 5th Int. Conf. on Soil Mechanics and Found. Eng.*, vol. **1**, Paris. 13-21. (1.2.4), (1.2.5), (3.1).

- Blatz J. and Graham J. (2000). A system for controlled suction in triaxial tests. *Géotechnique* **50** (4). 465-469. (3.1).
- Blight G.E. (1965). A study of effective stress for volume change. In *Moisture equilibria and moisture changes in soils beneath covered areas*, Sydney: Butterworths. 259-269. (1.4).
- Bolzon G., Schrefler B.A. et Zienkiewicz O.C. (1996). Elastoplastic soil constitutive laws generalized to partially saturated states. *Géotechnique* **46** (2). 279–289. (1.2.5).
- Brackley I.J. (1971). Partial collapse in unsaturated, expansive clay. *Proc. 5th. Reg. Conf. for Africa on SMFE*, **1**, Luanda. 23-30. (1.2.4).
- Buckingham E. (1907). Studies on the movement of soil moisture. *Bur. Of Soils Bull.* **38**, U.S. Dept. of Agric. Washington, D.C. (1.2.1).
- Burland J.B. (1961). The concept of effective stress in partly saturated soils. *Master of Science Thesis, Univ. of Witwatersrand*. (1.4).
- Burland J.B. (1965). Some aspects of the mechanical behaviour of partially saturated soils. In *Moisture equilibria and moisture changes beneath covered areas*, Sydney: Butterworths. 270-278. (1.2.5).
- Cabarkapa Z. and Cuccovillo T. (2006). Automated Triaxial Apparatus for Testing Unsaturated Soils. *Geotechnical Testing Journal* **29** (1). 21-29. (3.1).
- Chávez C., Romero E. and Alonso E.E. (2009). A Rockfill Triaxial Cell with Suction Control. *Geotechnical Testing Journal* **32** (3). 219-231. (3.1).
- Chen L., Yin Z. and Zhang P. (2007). Relationship of Resistivity with Water Content and Fissures of Unsaturated Expansive Soils. *Journal of China University of Mining & Technology* **17** (4). 537-540. (3.1).
- Chen Z.H., Fredlund D.G. et Gan J.K.M. (1999) Overall volume change, water volume change and yield associated with an unsaturated compacted loess. *Can. Geotech. J.* **36**. 321-329. (1.2.8).
- Chiu C.F., Cui Y.J., Haza E., De Laure E., Favraud C. and Thériot N. (2002). Experimental study of pollutant transport in an unsaturated compacted silt on centrifuge: second test. *Ecole Nationale des Ponts et Chaussées (Paris) – Laboratoire Centrale des Ponts et Chaussées (Nantes)*. France. (3.1).
- Coleman J.D. (1962). Stress strain relations for partly saturated soil. Correspondence to *Géotechnique* **12** (4). 348-350. (1.2.4), (1.2.5).
- Collins K. (1984). Characterisation of expansive soil microfabric. *Proc. 5th Int. Conf. Expansive Soils*, Adelaide. 37-41. (1.2.6).

- Collins K. et McGown A. (1974). The form and function of microfabric features in a variety of natural soils. *Géotechnique* **24** (2). 223-254. (1.2.8).
- Colmenares J.E. and Ridley A.M. (2002). Stress-strain and strength relationships for a reconstituted clayey silt. *Proceedings of the Third International Conference on Unsaturated Soils. Unsat 2002*, vol. **2**. Jucá J.F.T., de Campos T.M.P. and Marinho F.A.M. (eds.), Balkema Publishers, The Netherlands. 481-484. (3.1).
- Coussy O. (2004). Poromechanics. Chichester: Wiley. (1.2.5).
- Croney D. et Coleman J.D. (1954). Soil structure in relation to soil suction (pF). *J. Soil Sci.* **5**. 75–84. (1.2.2).
- Croney D., Coleman J.D. et Black W.P.M. (1958). The movement and distribution of water in soil in relation to highway design and performance. *Highway research Board, Special Report n°40*, Washington. (1.2.3).
- Cui Y.J. (1993). Etude du comportement d'un limon compacté non saturé et de sa modélisation dans un cadre elasto-plastique. *Thèse de doctorat, Ecoles nationale des Ponts et Chaussées*, Paris. (1.2.7).
- Cui Y.J. et Delage P. (1996). Yielding and plastic behaviour of an unsaturated compacted silt. *Geotéchnique* **46** (2). 291-311. (1.1), (1.2.7), (1.2.8), (3.1), (4.1).
- Cui Y.J., Delage P., Durand F., Schlosser F. et Wojnarowicz M. (1995). Comportement mécanique des loess sur le tracé du TGV Nord. *XIème Conférence Européenne de Mécanique des Sols et des Travaux de Fondations*, Copenhague, vol. **7**. 45-50. (1.1), (1.3.1), (1.4.1).
- Cui Y.J. et Marcial D. (2003a). Etude de comportement des limons non saturés soumis aux vibrations ferroviaires (Lot1). *Rapport SNCF*. 47 pages. (1.3.1), (1.4.1).
- Cui Y.J. et Marcial D. (2003b). Etude de comportement des limons non saturés soumis aux vibrations ferroviaires (Lot2). *Rapport SNCF*. 24 pages. . (1.3.1), (1.4.1).
- Cui Y.J., Marcial M., Terpereau J.M., Delage P., Antoine P., Marchadier G. et Ye W.M. (2004). A geological and geotechnical characterisation of the loess of Northern France. *A.W. Skempton Memorial Conference*, vol. **1**. 417-428. (1.1), (1.3.1), (1.4), (1.4.1), (1.4.2).
- Cui Y.J., Tang A., Mantho A. and De Laure E. (2008). Monitoring Field Soil Suction Using a Miniature Tensiometer. *Geotechnical Testing Journal* **31** (1). 95-100. (2.1), (2.3).
- Cunningham M.R., Ridley A.M., Dineen K. and Burland J.B. (2003). The mechanical behaviour of a reconstituted unsaturated silty clay. *Géotechnique* **53** (2). 183-194. (1.1), (4.1).

- Delage P. (2002). Experimental unsaturated soil mechanics. *Proc. 3rd Int. Conf. on Unsaturated Soils, UNSAT'2002*, (eds. Juca J.F.T., De Campos T.M.P., Marinho F.A.M.), Recife, Brazil, Balkema, **3**. 973-996. (1.2.1).
- Delage P., Audiguier M., Cui Y.J. and Howat M.D. (1996). Microstructure of a compacted silt. *Can. Geotech. J.* **33**. 150-158. (1.2.6), (1.2.8).
- Delage, P. et Cui, Y. (2000a). L'eau dans les sols non saturés. *C 301, Traite Construction*, vol. **C2**. (1.2.1).
- Delage, P. et Cui, Y. (2000b). Comportement mécanique des sols non saturés. *C 302, Traite Construction*, vol. **C2**. (1.2.3), (1.2.4), (1.2.5), (1.2.7).
- Delage P., Cui Y.J. et Antoine P. (2005). Geotechnical Problems related with Loess deposits in Northern France. *Proceedings of International Conference on Problematic Soils*. 517-540. (1.1), (1.3), (1.3.1), (1.4), (1.4.1), (1.4.2).
- Delage P. et Graham J. (1995). Mechanical behaviour of unsaturated soils : Understanding the behaviour of unsaturated soils requires conceptual models. *Proc; 1st Conf. On Unsaturated Soils*, Paris, Rotterdam, Balkema. 1223-1256. (1.2.7).
- Delage P. et Lefebvre G. (1984). Study of the structure of a sensitive Champlain clay and of its evolution during consolidation. *Canadian Geotechnical Journal* **21** (1). 21-35. (1.2.8).
- Delage P., Romero E. et Tarantino S. (2008). Recent developments in the techniques of controlling and measuring suction in unsaturated soils. Keynote Lecture, *Proc. 1st Eur. Conf. on Unsaturated Soils*, Durham, CRC Press. 33-52. (1.2.1).
- Delage P., Suraj de Silva G.P.R. et De Laure E. (1987). Un nouvel appareil triaxial pour les sols non saturés. *Proc. 9th European Conf. Soil Mech. Fdn Engng*, Dublin, **1**. 25-28. (1.2.7).
- Denisov N.Y. (1951). Mechanical properties of loess and loams (en russe). Gosstroizdat, Moscou. 136p. (1.4.1).
- Donald I.B. (1960). Discussion-Proceedings of Conference on pore pressure and suction in soils. Butterworth, London. (1.2.4).
- Dudley J.H. (1970). Review of collapsing soils. *J. Soil Mech. Fdn Engng, Am. Sot. Civ. Engrs* **96**, SM3. 925-947. (1.1), (1.2.7), (1.4), (1.4.2).
- Ehlers W., Graf T. et Ammann M. (2004). Deformation and localization analysis of partially saturated soil. *Comput. Methods Appl. Mech. Engng* **193** (27–29). 2885–2910. (1.2.5).
- El Nimr A., Al Faysi S. Et Hamadto M. (1995). Regulations to control rising ground water impacts on eastern Riyadh buildings and infrastructures. *Proc. 1st Int. Conf. Unsaturated soils UNSAT'95* **2**. Balkema, Paris. 967-972. (1.4.1).

- Engel J., Schanz T., et Lauer, C. (2004). State parameters for unsaturated soils, basic empirical concepts. *Proc. Int. Conf. From Experimental Evidence towards Numerical Modeling of Unsaturated Soils*, Weimar, Germany, 2003 (ed. T. Schanz), Berlin: Springer, Vol. 2. 125-138. (1.2.1), (1.2.3).
- Erol O.A. et El-Ruwaih I.A. (1982). Collapse behaviour of desert loess. *Proc. 4th Cong. IAEG* 1. 443- 448. (1.4).
- Escario V. et Juca J.F.T. (1989). Strength and deformation of partially saturated soils. In *Proceeding of the 12th International Conference on Soil Mechanics and Foundation Engineering*, Rio de Janeiro, 13–18 August 1989, A.A. Balkema, Rotterdam, the Netherlands. 43–46.. (1.2.1), (1.2.7).
- Escario V. et Sáez J. (1986). The shear strength of partly saturated soils. *Géotechnique* 36 (3). 453-456. (1.2.7).
- Feda J. (1966). Structural stability of subsident loess soil from Praha-Dejvice. *Engineering Geology* 1 (3). 201-219. (1.4.1).
- Fredlund D.G. et Morgenstern N.R. (1977). Stress state variables for unsaturated soils. *J. Geotech. Engng Div., Am. Soc. Civ. Engrs* 103, GT5. 447-446. (1.2.4), (1.2.5).
- Fredlund D.G., Morgensten N.R. et Widger R.S. (1978). The shear strength of unsaturated soils. *Can. Geotech. J.* 15 (3). 313-321. (1.2.7).
- Fredlund D.G. et Rahardjo H. (1985). Theoretical context for understanding unsaturated residual soil behaviour. *Proc. Ist Int. Conf: on Geomech. in Tropical, Lateritic and Saprolitic Soils, Brasilia*, 1. 295-306. (1.2.7).
- Fredlund D.G. et Rahardjo H. (1993). Soil Mechanics for Unsaturated Soils. *John Wiley & Sons, Inc.* New York. (1.2.1), (1.2.2).
- Fukue M., Minato T., Horibe H. and Taya N. (1999). The micro-structures of clay given by resistivity measurements. *Engineering Geology* 54. 43–53. (3.1).
- Gallipoli D., Gens A., Sharma R. and Vaunat J. (2003). An elasto-plastic model for unsaturated soil incorporating the effects of suction and degree of saturation on mechanical behaviour. *Géotechnique* 53 (1). 123-136. (1.2.5), (4.1).
- Geiser F. (1999). Comportement mécanique d'un limon non saturé : étude expérimentale et modélisation constitutive. *Thèse de doctorat, EPFL*, Lausanne. (1.2.7).
- Geiser F., Laloui L. et Vulliet L. (2000). Modelling the behaviour of unsaturated silt. In *Experimental Evidence and Theoretical Approaches in Unsaturated Soils*, (eds. A. Tarantino & C. Mancuso), Rotterdam, Balkema; 155-175. (1.2.7).

- Gens A. (1995). Constitutive laws. In Modern issues in nonsaturated soils (eds A. Gens, P. Jouanna and B. A. Schrefler), Berlin: Springer. 129–158. (1.2.5).
- Gibbs H.J. et Bara J.P. (1962). Predicting surface subsidence from basic soils tests. *ASTM STP 322*. 277-283. (1.4.1).
- Gray W.G. et Schrefler B.A. (2001). Thermodynamic approach to effective stress in partially saturated porous media. *Eur. J. Mech. A Solids* **20** (4). 521–538. (1.2.5).
- Gulhati S.K. et Satija B.S. (1981). Shear strength of partially saturated soils. *Proc. 10th Int. Conf. Soil Mech. Fdn Engng, Stockholm*, **1**. 609-612. (1.2.7).
- He L.C. (1999). Evaluation of instruments for measurement of suction in unsaturated soils. *MEng Thesis, School of Civil & Structural Engineering, Nanyang technological University, Singapore*. (1.2.1).
- Ho D.Y.F. et Fredlund D.G. (1982). Increase in strength due to suction for two Hong Kong soils. *Proc. Conf: Engng and Construction in Tropical and Residual Soils, Honolulu*. 263-295. (1.2.7).
- Holtz W.G. (1948). The determination of limits for the control of placement moisture in high rolled-earth dams. *Proc. Amer. Soc. Civ. Engrs.* **48**. 1240-1248. (1.4).
- Hormdee D. (2008). Investigation on Collapse Potential of Loess Soil. *Proceedings of the 18th International Offshore and Polar Engineering Conference*, Vol. **2**. Fontaine E., Uchida K., Chung J.S. et Moshagen H. (Eds.). 579-583. (1.4.1).
- Houston S.L. (1995). Foundations and pavements on unsaturated soils – Part 1: Collapsible soils. *Proc. 1st Int. Conf. Unsaturated Soils UNSAT'95* **3**. Balkema. Paris. 1421-1439. (1.4.1).
- Hoyos L.R. et Macari E.J. (2001). Development of a Stress/Suction-Controlled True Triaxial Testing Device for Unsaturated Soils. *Geotechnical Testing Journal* **24** (1). 5-13. (3.1).
- Huang R.Q. (2008) Large-scale landslides in China: Case studies. *10th International Symposium on Landslides and Engineered Slopes*, Xian, China, Jun. 30 - Jul. 04, 2008. Publié dans: *Landslides and Engineered Slopes: From the Past to the Future*, Vols. **1** et **2**. 2037-2053. (1.4.1).
- Huergo P.J., Verbrugge J.C. et Nuyens J. (1989). Tassement d'un massif de fondation à intercalations de sols effondrables. *Proc. 12th ICSMFE* **1**, Rio de Janeiro. 611-614. (1.4.1).
- Jamagne M., Lautridou J.P. et Sommé J. (1981). Préliminaire à une synthèse sur les variations sédimentologiques des loess de la France du Nord-Ouest dans leur cadre géographique et paléogéographique. *Bull. Soc. Géologique de France* **7**, XXIII. 143-147. (1.3).

- Jennings J.E. (1961). A revised effective stress law for use in the prediction of the behaviour of unsaturated soils. *Pore Pressure and Suction in Soils*, Butterworths, Londres. 26-30. (1.2.3), (1.4).
- Jennings J.E. (1965). The theory and practice of construction on partly saturated soils as applied to South African conditions. *Engineering Effects of Moisture Changes in Soils; Concluding Proceedings International Research and Engineering Conference on Expansive Clay Soils*, Texas A & M Press. 345-363. (1.4).
- Jennings J.E. et Burland J.B. (1962). Limitations to the use of effective stress in partly saturated soils. *Géotechnique* **12** (2), 125-144. (1.2), (1.2.3), (1.2.4), (1.4).
- Jennings J.E. et Knight K. (1957). The additional settlement of foundation due to collapse of sandy soils on wetting. *Proc. 4th ICSMFE* **1**. 316-319. (1.2.4), (1.4), (1.4.1).
- Jimenez-Salas J.A. (1995). Foundations and pavements on unsaturated soils – Part 2: Swelling soils. *Proc. 1st Int. Conf. Unsaturated soils UNSAT'95* **3**. Balkema, Paris. 1441-1464. (1.4.1).
- Jommi C. (2000). Remarks on the constitutive modelling of unsaturated soils. In *Experimental Evidence and Theoretical Approaches in Unsaturated Soils*, (eds. Tarantino et Mancuso), Balkema, Rotterdam. 139-153. (1.2.5), (4.1).
- Josa A., Alonso E.E., Lloret A. et Gens, A. (1987). Stress-strain behaviour of partially saturated soils. *Proc. 9th European Conz Soil Mech. Fdn Engng, Dublin*, **2**. 561-564. (1.2.7).
- Josa A. (1988). Un modelo elastoplástico para suelos no saturados. *Thèse de doctorat, Universidad Politécnica de Cataluña*, Barcelone. (1.2.7).
- Jotisankasa A., Coop M. and Ridley A. (2007). The Development of a Suction Control System for a Triaxial Apparatus. *Geotechnical Testing Journal* **30** (1). 69-75. (1.2.8), (3.1).
- Jotisankasa A., Coop M. and Ridley A. (2009). The mechanical behaviour of an unsaturated compacted silty clay. *Géotechnique* **59** (5). 415-428. (1.1), (1.2.8), (4.1).
- Justo J.L., Delgado A. et Ruiz J. (1984). The influence of stress-path in the collapse-swelling of soils at the laboratory. *Proc. 5th Int. Conf: Expansive Soils, Adelaide*. 67-71. (1.2.7).
- Karam J.P. (2006). Etude de la rhéologie des loess du Nord de la France. Application à l'évaluation de leur risque de liquéfaction. Thèse de doctorat à l'*École Nationale des Ponts et Chaussées*. Paris. (1.1), (1.4.1).
- Karam J.P., Cui Y.J., Tang A.M., Terpereau J.M. et Marchadier G. (2009). Experimental study on the cyclic resistance of a natural loess from Northern France. *Soils and Foundations* **49** (3). 421-429. (1.1), (1.3.1), (1.4.2).

- Khalili N. et Khabbaz M.H. (1998). An effective stress based approach for shear stress strength determination of unsaturated soils. *Proc. Of the 2nd Conference on Unsaturated Soils, Unsat'98*, Beijing, vol. **1**. 78-83. (1.2.7)..
- Knight K. (1961). The collapse of structure of sandy subsoils on wetting. *Master of Science Thesis, Univ. of Witwatersrand*. (1.4).
- Knight K. (1963). The origin and occurrence of collapsing soils. *Proc. 3rd Reg. African CSMFE* **1**. 127-130. (1.4.1).
- Kohgo Y., Nakano M. et Miyazaki T. (1993). Theoretical aspects of constitutive modelling for unsaturated soils. *Soils Found.* **33** (4). 49–63. (1.2.5).
- Kropp A., McMahon D. et Houston S. (1994). Field wetting of compacted soil fill. *Proc. 1st Int. Symp. On Eng. Characteristics and properties of arid soils*. London. (1.4.1).
- Laloui L., Klubertanz G. et Vulliet L. (2003). Solid–liquid–air coupling in multiphase porous media. *Int. J. Numer. Anal. Methods Geomech.* **27** (3). 183–206. (1.2.5).
- Lambe T.W. et Whitman R.V. (1959). The role of the effective stress in the behaviour of expansive soils. *Quart. Of the Colo. Sch. Of Mines* **54** (4). 33-66. (1.2.7).
- Lautridou J.P. (1985). Le cycle périglaciaire pléistocène en Europe du Nord-Ouest et plus particulièrement en Normandie. *Centre Géomorphologie* (ed). Caen, France. 908p. (1.3).
- Leroueil S. and Marques M.E.S. (1996). Importance of strain rate and temperature effects in geotechnical engineering. In *Measuring and modeling time dependent soil behaviour, Proc. of the ASCE Convention*. 1-60. (4.2).
- Li Z.M. (1995). Compressibility and collapsibility of compacted unsaturated loessial soils. *Proc. 1st Int. Conf. Unsaturated soils UNSAT'95* **1**. Balkema, Paris. 139-144. (1.4.1).
- Loret B. et Khalibi N. (2000). A three phase model for unsaturated soils. *Int. J. Numer. Anal. Method. Geomech.* **24** (11). 983-927. (1.2.5), (1.2.8).
- Lucas C.V. *et al.* (1964). Design and construction studies of shallow land subsidence for the California aqueduct in the San Joaquin Valley. *California Department of Water Resources*, Sacramento, California. (1.4).
- Maâtouk A., Leroueil S. and La Rochelle P. (1995). Yielding and critical state of a collapsible unsaturated silty soil. *Geotechnique* **45** (3). 465-477. (1.1), (1.2.7), (1.2.8), (3.1), (4.1).
- Mahler C.F. et Diene A.A. (2007). Tensiometer development for high suction analysis in laboratory lysimeters. In *Experimental Unsaturated Soil Mechanics* (ed. T. Schanz). 103-115. (1.2.1).
- Manthro A. (2005). Echanges sol – atmosphère: application à la sécheresse. PhD thesis. *École Nationale des Ponts et Chaussées*. Paris. (2.1), (2.3).

- Marinho F.A.M., Take A. et Tarantino A. (2008). Tensiometric and axis translation techniques for suction measurement. *Geotechnical and Geological Engineering* **26** (6). 615-631. (1.2.1).
- Maryniak W., Uehara T. and Noras M. (2003). Surface Resistivity and Surface Resistance Measurements Using a Concentric Ring Probe Technique. *TREK, INC.* Trek Application Note Number 1005. (3.2).
- Maswoswe J. (1985). Stress path for a compacted soil during collapse due to wetting. Thèse de doctorat, *Imperial College, London.* (1.2.7), (1.4).
- Matsuoka H., Sun D., Kogane A., Fukuzawa N. and Ichihara W. (2002). Stress-strain behaviour of unsaturated soil in true triaxial tests. *Canadian Geotechnical Journal* **39** (3). 608-619. (3.1).
- Matyas E.L. et Radhakrisna H.S. (1968). Volume change characteristics of partially saturated soils. *Géotechnique* **18** (4). 432-448. (1.2.5), (1.2.7), (1.4.1).
- McCarter W.J. (1984). Electrical resistivity characteristics of compacted clays. *Geotechnique*. **34** (2). 263-267. (3.1).
- McGown A. et Collins K. (1975). The microfabrics of some expansive and collapsing soils. *Proc. 5th Pan. Am. Conf. SMFE* **1**, Buenos Aires. 323-332. (1.2.6).
- Meier C., Boley C. et Zou Y. (2008). Collapse and deformation behaviour of alluvial loess soils from Afghanistan. *2nd International Workshop on Geotechnics of Soft Soils*, Sep. 3-5, 2008, Glasgow, Scotland. *Geotechnics of Soft Soils - Focus on Ground Improvement.* Karstunen M. et Leoni M. (eds.). 269-273. (1.4.1).
- Meilani I., Rahardjo H., Leong E.C., and Fredlund D.G. (2002). Mini suction probe for matric suction measurements. *Canadian Geotechnical Journal* **39**. 1427-1432. (3.1).
- Michot D., Dorigny A. and Benderitter Y. (2001). Mise en évidence par résistivité électrique des écoulements préférentiels et de l'assèchement par le maïs d'un CALCISOL de Beauce irrigué. *C. R. Acad. Sci. Paris, Sciences de la Terre et des planètes / Earth and Planetary Sciences* **332**. 29–36. (3.1).
- Mitchell J.K. et Soga K. (2005). Fundamentals of Soil Behavior. *John Wiley & Sons, ltd.*, 3th edition. (1.2.8), (1.4.1), (1.4.2).
- Modaressi A. et Abou-Bekr N. (1994). Constitutive model for unsaturated soils: validation on a silty material. *Proc. Numer. Methods Geomechan., NUMOG V* **1**. 91–96. (1.2.5).
- Mongiovi L et Tarantino A. (1998). An apparatus to investigate on the two effective stresses in unsaturated soils. *Proc. of the 2nd Conference on unsaturated Soils, Unsat'98*, Beijing, vol. **1**. 422-425. (1.2.5).

- Muñoz-Castelblanco J.A., Pereira J.M., Delage P. Cui Y.J. (2011). The water retention properties of a natural unsaturated loess from Northern France. *Géotechnique*, accepted to publication. (2.3), (3.2).
- Ng C.W.W. et Pang Y.W. (1999). Influence of stress state on soil-water characteristics and slope stability. *J. Geotech. Engrg. ASCE* **126** (2). 157-166. (1.2.8).
- Noorany I. et Stanley J. (1990). Swell and hydrocompression behaviour of compacted soils : test data. Research report, *San Diego State Univ.*, CA. (1.4.1).
- Nouaouria M.S., Guenfoud M. et Lafifi B. (2008). Engineering properties of loess in Algeria. *Engineering Geology* **99** (1)-(2). 85-90. (1.4.1).
- Nuth M. et Laloui L. (2007). Effective stress concept in unsaturated soils: Clarification and validation of a unified framework. *Int. J. Numer. Anal. Methods Geomech.* **32** (7). 771–801. (1.2.5).
- Padilla J.M., Houston W.N., Lawrence C.A., Fredlund D.G., Houston S.L. and Perez N.P. (2006). An automated triaxial testing device for unsaturated soils. *Geotechnical Special Publication 147 Proceedings of the Fourth International Conference on Unsaturated Soils*. 1775-1786. (3.1).
- Parcevaux P. (1980). Étude microscopique et macroscopique du gonflement de sols argileux. PhD thesis. *École Nationale Supérieure des Mines de Paris*. (2.2).
- Pécsi M. (1990). Loess is not just the accumulation of dust. *Quaternary International* **7/8**. 1-21. (1.3).
- Pedro G. (1976). Sols argileux et argiles. Eléments généraux en vue d'une introduction à leurs étude. *Sci. du Sol*, vol. **2**. 69-84. (1.2).
- Pereira J.M., Ta A.N., Cui Y.J., Karam J.R. et Chai H.Y. (2008). A damage model for unsaturated natural loess submitted to cyclic loading. *1st European Conference on Unsaturated Soils*, Durham, England, Jul. 2-4, 2008. Publié dans: *Unsaturated Soils: Advances in Geo-Engineering*. 647-652. (1.4.1).
- Pereira J.M., Wong H. et Dubujet P. (2003). A general framework for constitutive models adaptation to unsaturated states. In *Deformation Characteristics of Geomaterials: Proc. IS-Lyon03*, Lyon. 1269–1276. (1.2.5).
- Prikloksij V.A. (1952). Gruntovedenie (en russe). Vtoriaia Chast (Soil Science II). Gosgeolizdat, Moscow. 371p. (1.4.1).
- Punrattanasin P. (2008). The capacity of improved Khon Kaen Loess as a road construction material. *1st International Conference on Transportation Geotechnics*, Nottingham, England, Aug. 25-27, 2008. Publié dans: *Advances in Transportation Geotechnics*, Ellis E., Yu H.S., McDowell G. Dawson A. et Thom N. (eds.). 535-540. (1.4.1).

- Rampino C., Mancuso C. et Vinale F. (1999). Laboratory testing on unsaturated soil: equipment, and first experimental results. *Can. Geotech. J.* **36** (1). 1-12. (1.2.8).
- Richards L.A. (1928). The usefulness of capillary potential to soil moisture and plant investigators. *J. Agric. Res.* **37**. 719-742. (1.2.1).
- Rico A. et Del Castillo H. (1976). La ingeniería de suelos en las vías terrestres. **1**, Limusa, México. (1.2.7).
- Ridley A. et Burland J. (1995). Measurement of suction in materials which swell. *Applied Mechanics Reviews* **48** (9). 727-732. (1.2.1).
- Ridley A.M. et Wray W.K. (1996). Suction measurement: A review of current theory and practices. *Proc. 1st Int. Conf. on Unsaturated Soils UNSAT'95* **3**, Paris, Balkema, Rotterdam. 1293-1322. (1.2.1).
- Rojas E. and Rojas F. (2005). Modelling hysteresis of the soil-water characteristic curve. *Soils and Foundations* **45** (3). 135-145. (2.1), (2.3).
- Rojas J.C., Mancuso C., Vinale F.A. (2008). Modified triaxial apparatus to reduce testing time: Equipment and preliminary results. *1st European Conference on Unsaturated Soils*, Jul. 2-04, 2008, Durham, England. 103-109. (3.1).
- Romero E. (1999). Characterisation and thermo-hydro-mechanical behaviour of unsaturated Boom clay: an experimental study. *PhD thesis. Universitat Politècnica de Catalunya*. Barcelone. (1.2.8), (3.1).
- Romero E. et Vaunat J. (2000). Retention curves of deformable clays. In *Experimental Evidence and Theoretical Approaches in Unsaturated Soils*, (eds. Tarantino et Mancuso), Balkema, Rotterdam. 91-106. (1.1), (1.2.8), (4.1).
- Sanchez M., Gens A., Guimaraes L. et Olivella S. (2005). A double structure generalized plasticity model for expansive materials. *Int. J. Numer. Anal. Method. Geomech.* **29**. 751-787. (1.2.8).
- Santaguliana R. et Schrefler B.A. (2006). Enhancing the Bolzon—Schrefler—Zienkiewicz constitutive model for partially saturated soil. *Transp. Porous Media* **65** (1). 1-30. (1.2.5).
- Seed H.B. et Chan A.M. (1959). Structure and strength characteristics of compacted clays. *Journal of Soil Mechanics and Foundations Division, A.S.C.E.* **85** SM5. 87-128. (1.2.7).
- Shao S., Yu Q.G. et Long J.Y. (2007). A stress-strain relationship with soil structural parameter of collapse loess. *3rd Sino-Japan Geotechnical Symposium*, Chongqing, China, Nov. 4-7 2007. Publié dans: New Frontiers in Chinese and Japanese Geotechnics. Yao Y.P. Akagi H. et Zhang G. (Eds.). 488-500. (1.4.1).

- Sheng D., Sloan S.W., Gens A. et Smith D.W. (2003). Finite element formulation and algorithms for unsaturated soils. Part I: Theory. *Int. J. Numer. Anal. Methods Geomech.* **27** (9). 745–765. (1.2.5).
- Shmuelyan A. (1995). Uneven subsidence of the soil due to collapse. *Proc. 1st Int. Conf. Unsaturated soils UNSAT'95* 2. Balkema, Paris. 1005-1010. (1.4.1).
- Smalley I.J. (1971). “in situ” theories of loess formation and the significance of the calcium carbonate content of loess. *Earth Science Review* **7**. 67-86. (1.3).
- Stephanoff G. et Kremakov B. (1960). Building properties of Bulgarian loess soils. *Publishing office technika*. Sophia. 220p. (1.4.1).
- Tang G.X., Graham J., Blatz J., Gray M. and Rajapakse R.K.N.D. (2002). Suctions, stresses and strengths in unsaturated sand-bentonite. *Engineering Geology* **64**, Issue: 2-3. 147-156. (3.1).
- Tarantino A. (2004). Panel Lecture: Direct measurement of soil water tension. *Proc. 3rd Int. Conf. on Unsaturated Soils*, Recife, Brasil, **3**. 1005-1017. (1.2.1).
- Tarantino A. (2007). A possible critical state framework for unsaturated compacted soils. *Géotechnique* **57** (4). 385-389. (4.1).
- Tarantino A. and De Col E. (2008). Compaction behaviour of clay. *Géotechnique* **58** (3). 199-213. (1.1), (4.1).
- Tarantino A., Mongiovi L. et Bosco G. (2000). An experimental investigation on the independent isotropic stress variables for unsaturated soils. *Géotechnique* **50** (3). 275-282. (1.2.5).
- Tarantino A., Romero E. et Cui Y.J. (2008). Laboratory and field testing of unsaturated soils. Reprinted from *Geotechnical and Geological Engineering* **26** (6), 2008, Springer. (1.2.1).
- Terzaghi K. et Fröhlich O.K. (1936). Theorie der Setzung von Tonschichten. F. Deuticke, Leipwig-Wien. (1.1), (1.2.3).
- Thom R., Sivakumar V., Brown J. and Hughes D. (2008). A Simple Triaxial System for Evaluating the Performance of Unsaturated Soils Under Repeated Loading. *Geotechnical Testing Journal* **31** (2). 107-114. (3.1).
- Townend J., Reeve M.J. et Carter A. (2000). Soil and environmental analysis. Chap. 3. *Water Release Characteristic*. Marcel Dekker Inc., New York, Etats Unis. (1.2.1).
- Vanapalli S.K., Fredlund D.G. et Pufahl D.E. (1999). The influence of soils structure and stress history on the soil-water characteristics of a compacted till. *Géotechnique* **49** (2). 143-159. (1.2.8).

- Vaunat J., Romero E. et Jommi C. (2000). An elastoplastic hydro-mechanical model for unsaturated soils. In *Experimental Evidence and Theoretical Approaches in Unsaturated Soils*, (eds. Tarantino et Mancuso), Balkema, Rotterdam. 121-138. (1.2.8), (4.1).
- Verbrugge J.C. (1978). Emploi d'une méthode psychrométrique dans des essais triaxiaux sur un limon remanié non saturé. *Can. Geotech. J.* **15**(4). 501–509. (3.1).
- Wagener F. (1960). Consolidation settlement of soils under repetitive loading as experienced in road foundations. *Master of Science Thesis, Univ. of Witwatersrand.* (1.4).
- Walsh K., Houston W. et Houston S. (1993). Evaluation of in-place wetting using soil suction measurements. *J. Geotech. Eng., ASCE* **119**. 862-973. (1.4.1).
- Walthall S. et Duffy W.P. (2008). An example of the impact of loess soils on foundations and earthworks in Kazakhstan. *1st European Conference on Unsaturated Soils, Durham, England, Jul. 2-4, 2008.* Publié dans: *Unsaturated Soils: Advances in Geo-Engineering.* 973-978. (1.4.1).
- Wheeler S.J. (1996). Inclusion of specific water volume within an elastoplastic model for unsaturated soil. *Can. Geotech. J.* **33**. 33-42. (1.2.8), (4.1).
- Wheeler S.J. et Karube B. (1996). Constitutive modelling. In *Unsaturated Soils*, A.A. Bakelma Rotterdam, number **3**. 1323-1356. (1.2.3), (1.2.8).
- Wheeler S.J. et Sivakumar V. (1995). An elasto-plastic critical framework for unsaturated soil. *Géotechnique* **45** (1). 35-53. (1.2.4), (1.2.8), (3.1), (4.1).
- Wheeler S.J., Sharma R. and Buisson M. (2003). Coupling of hydraulic hysteresis and stress-strain behaviour in unsaturated soils. *Géotechnique* **53** (1). 41-54. (1.2.5), (4.1).
- Wilson S.D. (1952). Effect of compaction on soil properties. In proceedings of the Conference on *Soil Stabilization*, Massachussets institute of technology, Boston. (1.2.7).
- Xu J., Ng C.W.W. and Yung S.Y. (2008). Drying and wetting effects on shear wave velocity of an unsaturated soil. . *1st European Conference on Unsaturated Soils, Jul. 2-04, 2008, Durham, England.* 525-530. (3.1).
- Yang C., Cui Y.J., Pereira J.M. et Huang M.S. (2008). A constitutive model for unsaturated cemented soils under cyclic loading. *Computers and Geotechnics* **35**(6). 853-859. (1.1), (1.3.1), (1.4.2).
- Yong R.N., Japp R.D. et How G. (1971). Shear strength of partially saturated clays. *Proc. 4th Asian Reg. Con& Soil Mech. Fdn Engng, Bangkok* **2** (12). 183-187. (1.2.7).
- Yuan Z.X. et Wang L.M. (2009). Collapsibility and seismic settlement of loess. *Engineering Geology* **105** (1)-(2). 119-123. (1.4.1).

-
- Yudhbir (1982). Collapsing behaviour of residual soils. Proc. *7th Southeast Asian Geotech. Conf.*, Hong-Kong **1**. 915-930. (1.4).
- Yuk Gehling W.Y. (1994). Suelos expansivos: estudio experimental y aplicación de un modelo teórico. *Thèse de doctorat, Universidad Politécnica de Cataluña*, Barcelone. (1.2.7).
- Zhang X., Leong E.C. et Rahardjo H. (2001) ; evaluation of a thermal conductivity sensor for measurement of matric suction in residual soil slopes. In: *Proceedings of 14th southeast Asian geotechnical conference*, Hong Kong. 611-616. (1.2.1).